*The Geological Society of America*
*Memoir 27*

# THEORY OF PROPAGATION OF EXPLOSIVE SOUND IN SHALLOW WATER

BY
C. L. PEKERIS
Department of Applied Mathematics
The Weizmann Institute, Rehovoth, Israel

October 15, 1948
Reprinted 1963

ACKNOWLEDGMENT

This paper is based on work done in 1944 at Columbia University, Division of War Research, under contract with the Office of Scientific Research and Development.

The writer is indebted to Dr. Columbus O'D. Iselin for the assistance given by the editorial staff of the Woods Hole Oceanographic Institution in the preparation of this paper.

## CONTENTS

## ILLUSTRATIONS

### PLATES



### FIGURES

## TABLES

## ABSTRACT

A wave-theoretical interpretation is given of pressure waves generated in shallow water by explosions of charges of T.N.T. ranging from 0.5 to 300 lbs., and recorded by Ewing and Worzel. (*See* accompanying paper, *Explosion sounds in shallow water.*) The normal mode theory of propagation of sound in layered media, which was developed by the writer in 1941, was extended to cover the case of explosive sound, and the predictions of the theory about the shape and variation of amplitude in the received pressure pulse were investigated in detail. It was found that the theory predicted the existence of a series of readily identifiable new features in the pressure wave, each of which is characteristic of the depth of water and the structure of the bottom. A study of the original records, some of which are reproduced on Plates 1–11, revealed the presence of all the predicted phases. The characteristics of these phases were then measured, and the data were interpreted in terms of the structure of the bottom at the various stations. The deductions about the distribution of sound velocity in the bottoms, based on an analysis of the various features of the pressure waves, are given in Table A, and it will be seen that they agree among themselves.

The following results were obtained:

(1) A study was made of the *dominant periods* in the ground waves which are propagated along the various interfaces in the layered bottom, in order to verify the theoretical prediction that the deeper the interface (higher sound velocity) the longer should be the periods. A verification of this theoretical prediction is well illustrated in Figures 1 and 2, and to a lesser extent in Figure 3.

(2) An extensive investigation, covering an analysis of more than 40 records, was made of the dispersion in the *water wave* (which is illustrated by the third trace from the bottom on Plate 11). A technique was developed for determining from the records the speed with which each frequency in the water wave is propagated. The discovery made empirically by Ewing that this speed is a function of frequency only (*see* accompanying paper, *Explosion sounds in shallow water*) and is independent of the range was confirmed in all the records, as is shown in Figures 6–19. The shape of the *mean dispersion curve* at each station was successfully interpreted by an application of the normal mode theory in a layered liquid half-space. Theoretical dispersion curves form the background in Figures 6–19, and, with the aid of these, deductions were made about the sound-velocity distribution in the top layers of the bottom. The conclusions are given in columns 6 and 7 of Table A and in Table 1.

(3) The theory of normal modes was developed by the writer to a stage which enables one to compute the actual curve of pressure variation, as recorded by various types of receivers, due to an arbitrary explosion. A sample of such a theoretical pressure wave is shown in Figures 24A, 24, and 25.

(4) The following new features of the pressure waves were predicted by the theory of normal modes of a layered liquid half-space and were subsequently discovered and analyzed by the writer:

A) In case of a uniform bottom extending down to a depth many times the depth of water, the *ground wave should begin with a so-called limiting period* which is characteristic of the depth of water and the sound velocity in the bottom. The limiting period was identified and measured in the records taken at the Solomons Shoal station where the bottom is known to meet the requirement stated above, and the results are shown in Table 2. The value of 1.29 for $c_2/c_1$ obtained from the average observed limiting period, where $c_1$ and $c_2$ denote the sound velocities in the water and in the bottom, is slightly higher than the values deduced from the other features quoted in Table A, but this small discrepancy can be explained by the effect of the deep layers.

B) The water wave should arrive riding on a low-frequency wave called the ***rider wave***; the frequency of the rider wave just prior to the arrival of the water wave is determined by the depth of water and the distribution of sound velocity in the bottom. The rider wave was identified and its period measured on all records taken at Solo-

TABLE A.—*Deductions about the variation of sound velocity with depth in the bottom*

Based on the interpretation of the various phases in the recorded pressure waves from explosions.

$c_1$ = sound velocity in water; $c_2$ = sound velocity in a top layer of the bottom referred to as the intermediate layer; $c_3$ = sound velocity in the bottom below the intermediate layer; $\bar{H}$ = thickness of layer in the bottom for which average value of $c_2/c_1$ holds.

| Station | Depth of water H in feet | Refraction | | | Dispersion in Water Wave | | Limiting Period $c_2/c_1$ | Rider Wave $c_2/c_1$ | Airy Wave $c_2/c_1$ |
|---|---|---|---|---|---|---|---|---|---|
| | | $c_2/c_1$ | Thickness of intermediate layer in feet | $c_3/c_1$ | Average $c_2/c_1$ | $\bar{H}$ in feet | | | |
| Solomons Shoal | 52 | 1.15 | 1300 | 1.79 | 1.2 | 25 | 1.29 | 1.09 | (1.1) |
| Jacksonville Shoal | 60 | — | — | — | 1.05<br>1.1 | 30<br>80 | — | 1.17 | 1.10 |
| Jacksonville Deep | 115 | (1.14) | (1200) | 2.13 | 1.2<br>1.35 | 30<br>70 | — | — | 1.12 |
| Virgin Islands Shoal | 70 | (1.05 to 1.1) | 70 | 3.02 | 1.06<br>1.2 | 30<br>45 | — | — | 1.12 |
| Virgin Islands Deep | 140 | (1.05 to 1.1) | 150 | 3.02 | 1.05<br>1.3 | 55<br>65 | — | — | (1.05) |

nons Shoal, Jacksonville Shoal, and Jacksonville Deep. The results are set out in Tables 3–5, and the resulting conclusions about the sound velocity in the bottom are quoted in Table A. Some illustrations of the rider waves can be seen in the records reproduced on Plates 1–9.

C) The amplitude of the water wave should increase with time to a maximum value and should decrease thereafter, while the period should remain constant after the maximum is passed. The value of this period, which will be referred to as the *Airy period*, is again characteristic of the depth of water and the structure of the bottom. Values of the Airy period are given in Tables 2, 3, 5, and 6, and the interpretation of the average values is given in Table A.

D) A three-layered medium in which the thickness of the intermediate layer is only of the order of the depth of water should possess dispersion characteristics similar to those of a medium with a uniform bottom. The existence of the intermediate layer should therefore not be revealed by a secondary arrival. Theory also predicts that the amplitude of the rider wave should be relatively low in such a medium (by a factor of $\frac{1}{5}$ to $\frac{1}{10}$), while the water wave should be of normal intensity. The stations of Virgin Islands Shoal and Virgin Islands Deep which, judged by the combined evidence from the refraction data and the dispersion data in the water wave, have a veneer of mud of a thickness of the order of the depth of water covering a high-speed coral base, would be expected to fall into this class. The records taken at these stations were found to be lacking in secondary arrivals and to be devoid of rider waves, as is illustrated in Plates 8 and 9. The success of the theory in explaining the appearance of the records taken at the Virgin Islands, which were entirely different from the records taken at all the other stations, is very encouraging.

(5) Theoretically the maximum amplitude in the water wave should vary like the inverse $\frac{5}{6}$-th power of the range, whereas the observations of Ewing and Worzel indicate that in some stations the maximum amplitude varies like the inverse square of the range. We have, of course, neglected absorption and scattering, but, as I have already suggested, it would be interesting to check the experimental determination of variation of intensity with range.

(6) Our study shows that in all stations the speed of sound in the first 30 feet of the bottom is no more than about 10 per cent greater than in water. This result conforms with Ewing's finding that all bottom samples were muddy.

(7) A complete theory of propagation of sound, both of single-frequency and of the explosive type, in layered media is developed in Part II of this paper. This includes a discussion of the "ray theory" and the wave theory. One interesting theoretical result is that in case of a density discontinuity at the bottom the normal modes are not orthogonal, nor is their amplitude, in case of a point source, correctly given by standard theory of normal modes.

Another of the new results arrived at is that, when the wave length of sound is of the order of the depth of water, the *amplitude* of the pressure should decrease at large ranges like the inverse *square* of the range, as in the Lloyd Mirror Effect. The asymptotic expressions given in Eqs. (32) and (33) are strikingly verified in Figure 23, in which they are compared with values obtained by numerical integration of the integral in the exact solution.

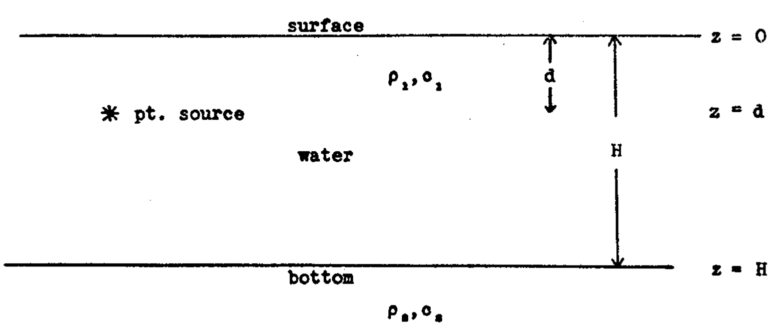


FIGURE A.—*Assumed model for a two-layered liquid half-space*

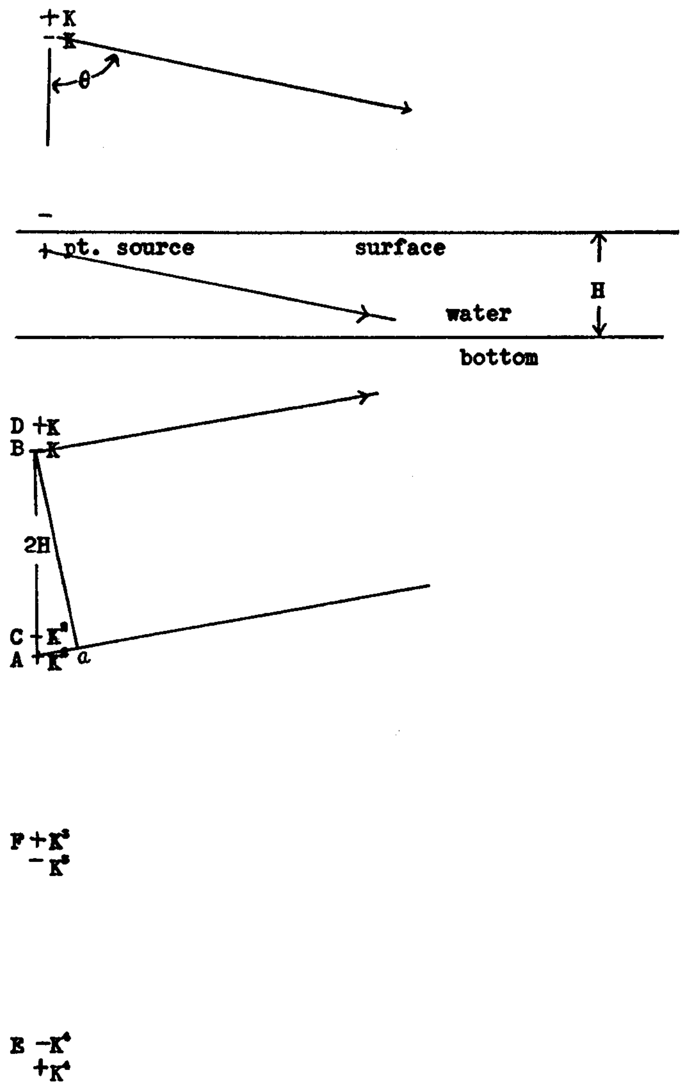


FIGURE B.—*System of images of a point source situated in shallow water*

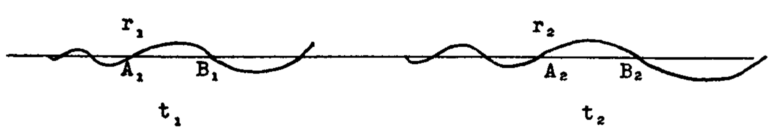


FIGURE C.—*Illustration of the difference between phase velocity and group velocity*

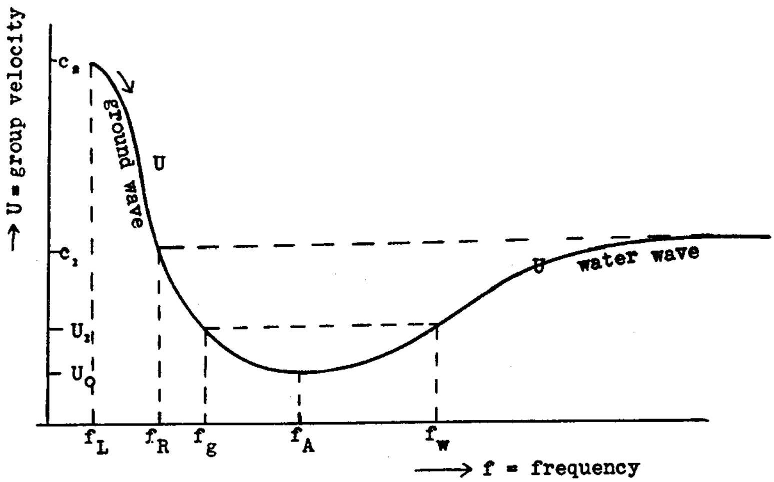


FIGURE D.—*Variation of group velocity U with frequency f in a two-layered liquid half-sapce*

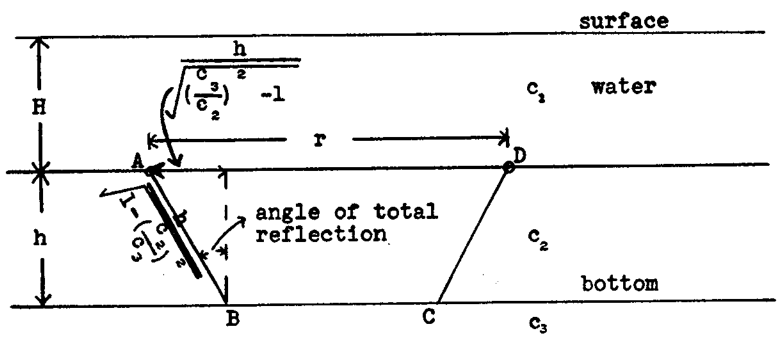


FIGURE E.—*Ray-path in case the charge and receiver are beached on the bottom*

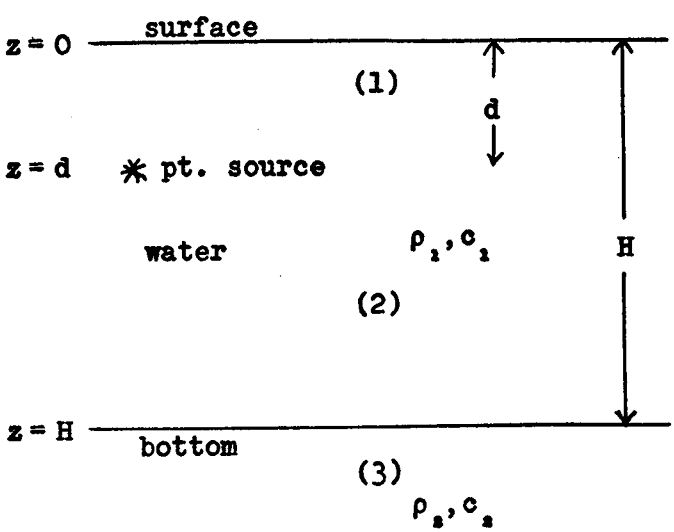


FIGURE F.—*Assumed model for a two-layered liquid half-space*

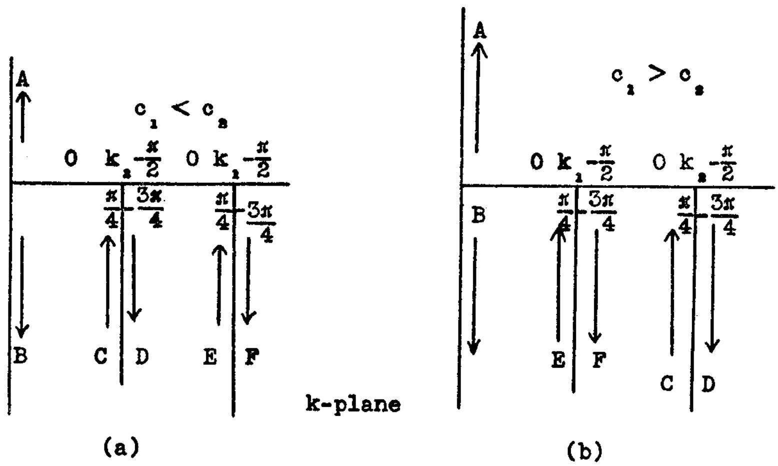


FIGURE G.—*Cuts are made in the complex k-plane along lines parallel to the negative imaginary axis and starting on the real axis at the points $k = k_1$ and $k = k_2$ respectively*

The numbers give the phases of $\beta_1 = \sqrt{k^2 - k_1^2}$ and of $\beta_2 = \sqrt{k^2 - k_2^2}$ on the real axis and on either side of the respective cut.

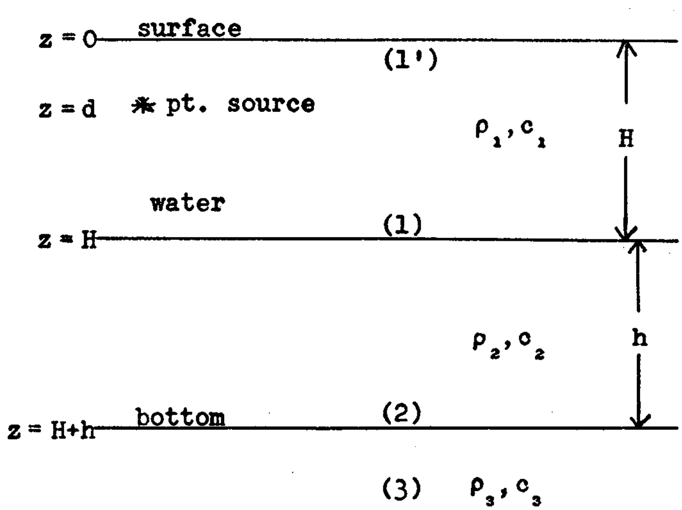


FIGURE H.—*Assumed model for a three-layered liquid half-space*

# PART I: DATA

## 1. SOME OBSERVED CHARACTERISTICS OF PRESSURE RECORDS OBTAINED AT LARGE RANGES FROM AN EXPLOSION IN SHALLOW WATER

This investigation was undertaken with the aim of providing a wave-theoretical interpretation of some interesting features of pressure records from under-water explosions observed in shallow water at large ranges by Ewing and Worzel. (*See* accompanying paper, *Explosion sounds in shallow water.*) In these experiments, charges of 0.5, 5, 25, and 300 lbs. of T.N.T. were set off either on the bottom or at mid-depth, and the resulting pressure wave was recorded at distances ranging from $\frac{1}{4}$ mile to about 12 miles for a typical station. The depth of water was 10 or 20 fathoms, so that the maximum ranges were of the order of a thousand times the depth of water.

The recording systems admitted five separate frequency bands as shown in Figures 39–44; in addition, two of these bands were recorded separately with high and low amplification. Each record therefore consisted of seven traces as shown in Plates 1–11. It will be noted that the geophone system admits a frequency band of from 10 to 100 cps; the Mark I system is sensitive to frequencies less than about 10 cps; the Mark II high-frequency system has a flat response up to about 1000 cps, which covers practically the whole range of relevant frequencies. This trace should therefore give a faithful representation of the actual pressure variation. The Mark II rectified system is peaked around 5000 cps and is therefore useful for determining the *beginning* of the water wave. On the other hand, the Mark II low-frequency system is a low-pass filter with a cut-off frequency around 150 cps. This system has proven particularly useful in the interpretation of the records.

The function of the various traces as used in the interpretation is as follows. The time break determines the instant of detonation of the shot. The geophone portrays the vertical component of velocity in the low-frequency range of 10 to 100 cps. The Mark II high-frequency trace reproduces the actual pressure variation. The Mark II rectified traces are used especially for determining the time of arrival of the "water wave" produced by the original explosion and also of the subsequent "water waves" produced by the successive expansions of the oscillating "bubble". The Mark II low-frequency traces are especially useful for analyzing the dispersion in the water wave as well as in the train of waves preceding the waterwave phase. This trace also serves to determine the arrival time of the ground wave.

We shall now discuss some of the principal characteristics of the pressure record, which form the subject of our study. Perhaps the simplest record reproduced in this paper is the one of shot No. 275 shown in Plate 9. A low-frequency disturbance commencing at .882 sec.[1] after detonation is seen on the geophone trace and the low-frequency Mark II trace (next to the bottom trace; the Mark II trace appearing third from the bottom has the same frequency characteristics but is less sensitive). At $t = 2.768$ sec., a new phase arrives and is recorded on all but the very low-frequency Mark I trace. From the Mark II trace one can see that in this phase, which

[1] The time scale on the top of the records does not commence at the instant of detonation, hence the difference between that scale and the time marks on the trace Mark II.

will be referred to as the "water wave", the first oscillations are of high frequency,, and that subsequently the frequency decreases continuously. At $t$ = 2.914 sec., a similar train of waves arrives but is somewhat weaker than the first. This is a water wave produced by the first expansion of the "bubble". The second expansion of the bubble produces a third water wave which arrives at $t$ = 3.153 sec. The wave reaching the station at $t$ = .882 sec. is the "ground wave" which has traveled through the bottom where the velocity of sound is about 2.768/.882 = 3.1 times the velocity of sound in the water.

A clearer presentation of the dispersion in the waterwave phase is given on Plates 10 and 11 by the low-sensitivity Mark II trace. It will be noted that the Mark II high-frequency trace, which should faithfully reproduce the actual pressure variation, is more complicated and less regular.

Ewing discovered empirically that the dispersion in the water wave is such that *each frequency travels with a characteristic velocity.* If this velocity be called $U(f)$ then the time of arrival of a given frequency $f$ in the water wave $T(f)$ is given by

$$r = T(f)U(f), \tag{1}$$

where $r$ denotes the range. If $T_0$ now denote the time between the detonation and the beginning of the water wave, as read off the Mark II rectified trace, then we have $r = T_0c_1$, $c_1$ denoting the sound velocity in water. It follows that

$$\frac{T - T_0}{T_0} = \frac{c_1}{U(f)} - 1 = F(f) \tag{2}$$

independently of the range. Hence plots of $(T - T_0)/T_0$ vs. $f$, made from records taken at different ranges, should fall on a universal curve characteristic of the depth of water and the nature of the bottom. That this is actually the case is shown in Figures 6–19.

The technique of determining the $U(f)$ curves, which was developed by the writer in connection with an analysis of more than 40 records, is as folllows. From a trace such as the low sensitivity Mark II on Plate 10, one reads off the times $T_n$ of the $n$-th maximum or minimum, and plots $T_n$ vs. $n$. Such typical plots are shown in Figures 20, 21 and 22. It will be seen that it is possible to draw a continuous curve unambiguously through the plotted points. One then reads off $T_n$ values for each $n$ from the continuous curve; and the period $P$ corresponding to any $T_n$ is computed from

$$P(T_n) = \tfrac{1}{2}(T_{n+1} - T_{n-1}). \tag{3}$$

This procedure involves, of course, a numerical differentiation of an observed curve, but it is seen from Figures 20, 21 and 22, which are typical, that the continuous curve is well defined by the experimental points.

After the $P(T_n)$ values are determined, they are plotted as Δ points in Figure 9. The abscissa in this figure is not the frequency $f$ but the nondimensional quantity

$$\gamma = \frac{H}{\lambda} = \frac{fH}{c_1} \tag{4}$$

where $H$ denotes the depth of water and $\lambda$ the wave length in water. $\gamma$, then, denotes the depth of water in units of the wave length of sound in water. On Figure 9 are plotted dispersion data from two other stations, giving a total range of $T_0$ of from 4.2 to 7.1 sec., and it will be noted that the three sets of plotted points cluster around a well-defined mean curve. Figure 8 shows a similar analysis of dispersion in three additional shots taken at the same locality. The six shots from Jacksonville Shoal have been plotted on two separate figures only for clarity. The mean curves through the plotted points are about the same in the two figures. The arrival times $T_0$ vary from 4.3 to 14.1 sec., while the range varies from 4 to 13 miles, the latter being more than 1000 times the depth of water.

An inspection of the remaining dispersion data plotted in Figures 6–19 reveals that:

1) Shots taken at different ranges in a given locality yield similar dispersion curves.
2) Though the general trend of the dispersion curves is similar in the various localities (for which there is a theoretical reason), distinct differences between localities exist.
3) The dispersion in the waves from the main explosion agrees closely with the dispersion in the waves generated by the first bubble expansion (Fig. 17).

An analysis of the dispersion phenomenon by wave theory produced a rational interpretation, which makes it possible to correlate the observed dispersion curve with the depth of water and the nature of the bottom. It is thus possible to gain information on the characteristics of the bottom from a study of the dispersion data. However, as the theory developed, it became clear that the records should exhibit additional easily recognizable features which are also characteristic of the bottom. These features were subsequently discovered in the water wave, in the phase immediately preceding it, and in the ground wave, and were studied on all records. A discussion of these new phenomena, which were suggested by the theory, will be postponed until after the presentation of some of the elements of the theory of propagation of explosive sound in shallow water. (The reader who wishes to acquaint himself immediately with these new phenomena may refer to page 24.)

## 2. QUALITATIVE DISCUSSION OF THE THEORY OF PROPAGATION OF EXPLOSIVE SOUND IN SHALLOW WATER

The principal observed features of the records of sound from an explosion in shallow water can be explained on the basis of a simple model in which the bottom is assumed to be a liquid of density $\rho_2$ and sound velocity $c_2$, which differ from the density $\rho_1$ and sound velocity $c_1$ in the water, as shown in Figure A. (Later we shall also discuss the modification introduced by a layered bottom.) Our problem is to determine the pressure field due to an explosion in the water. For the large ranges considered the disturbance can be assumed to be produced by a point source, which in the absence of the surface and the bottom would generate a spherically symmetrical wave whose amplitude would decrease as the inverse power of the range. Actually, of course, the initially spherical wave suffers multiple reflections both at the surface and the bottom, and at the extremely long ranges in which we are interested (up to a thousand times the depth of water) the number of such reflections which need be considered is very large.

A useful elementary notion in the analysis of the situation is the reflection of a *plane* wave at a plane surface of discontinuity in $\rho$ and $c$. According to Rayleigh (1896, p. 78) the reflection coefficient $K$ for the amplitude when the angle of incidence is $\theta$ is given by

$$K = \frac{\dfrac{\rho_2 c_2}{\rho_1 c_1}\cos\theta - \sqrt{1 - \dfrac{c_2^2}{c_1^2}\sin^2\theta}}{\dfrac{\rho_2 c_2}{\rho_1 c_1}\cos\theta + \sqrt{1 - \dfrac{c_2^2}{c_1^2}\sin^2\theta}}. \tag{5}$$

In our application we can limit the discussion to the case of a fast bottom ($c_2 > c_1$), since in all records the wave which traveled through the ground arrived earlier than the wave which traveled directly through the water (in one case by as many as 20 seconds). In the case of a fast bottom, the reflection coefficient starts with a value $(\rho_2 c_2 - \rho_1 c_1)/(\rho_2 c_2 + \rho_1 c_1)$ at normal incidence ($\theta = 0$) and increases to unity at the critical angle for *total reflection* $\theta_1$ given by

$$\theta_1 = \sin^{-1}(c_1/c_2). \tag{6}$$

For larger angles of incidence the reflection coefficient becomes complex of modulus one, so that no power is transmitted into the bottom, but the wave suffers a *change of phase upon reflection*, depending on $\theta$.

Another useful elementary notion is the system of *images* by which the action of the surface and bottom can be approximated, as shown in Figure B. This system consists of dipoles, due to the point source and its image in the surface, strung along a vertical through the source at a spacing of $2H$, the polarity of each dipole being opposed to that of its neighbors. At great distances from the source and under certain other conditions which are discussed in Part II, one can assign a definite *strength* to the images, which in the case of an image due to $m$ reflections from the surface and $n$ reflections from the bottom is $(-)^m K^n$. The reflection coefficient $K$, as given in Eq. (5), is a function of $\theta$, so that the images are directional.

For angles of incidence greater than the angle of total reflection $\theta_1$, the strength of all the sources becomes unity, and the system of images then bears a similarity to a self-luminous diffraction grating (Slater, 1942, p. 284). There are then certain discrete directions $\theta_n$ in which waves from neighboring dipoles interfere constructively, corresponding to the spectra of various orders in a diffraction grating. As illustrated in Figure B, the waves emanating in a direction $\theta(>\theta_1)$ from images $A$ and $B$ have a path difference $Aa = 2H\cos\theta$ as well as a phase difference $(-\pi - \psi)$, where

$$-K = e^{-i(\pi+\psi)}. \tag{7}$$

Hence, constructive interference will take place between the pair of images if

$$\frac{2\pi Aa}{\lambda} - \pi - \psi = \frac{4\pi H\cos\theta}{\lambda} - \pi - \psi = \pi(2n-2), \qquad n = 1, 2, 3 \cdots. \tag{8}$$

For angles $\theta_n$ for which this condition is satisfied, there will be constructive interference also between the pairs of images $C$ and $D$, $E$ and $F$, as well as the other such pairs of images situated in the bottom. Similarly, the source and the images situated above the surface give rise, at the same angle of incidence $\theta_n$, to a system of constructively interfering pairs of images producing a down-going train of waves. The combination of the two systems of up-going and down-going waves gives rise to the so-called *normal modes.* The normal mode of the $n$-th order can thus be conceived as arising from a superposition of two systems of up-going and down-going waves traveling at an angle $\theta_n$ with the vertical, where $\theta_n$, a function of the wave length, is determined from Eq. (8).

The physical picture just given for the origin of the normal modes shows that the alternative analysis of the pressure field by the so-called "ray theory" cannot avoid taking cognizance of the preferred directions $\theta_n$ for which constructive interference is possible. By writing down the expressions for all the rays, which are of course approximate, one will inevitably find that a pair of poles such as $A$, $B$ will show an interference pattern of the Lloyd Mirror type.

The corrugations of the surface and the bottom will, to be sure, impair the precise phasing required for constructive interference, but the experience with the interpretation of the data from transmission of explosive sound by the normal mode theory suggests that, at the grazing angles considered, the effect of corrugations is of the same order as the blurring of x-ray lines due to temperature agitation of the atoms in a crystal.

One consequence of Eq. (8) is the *existence of a cut-off frequency for each mode* below which constructive interference is impossible. When, namely, the distance $Aa$ in Figure B plus the corresponding contribution from $\psi$ in Eq. (7) is less than $\lambda/2$ for a given $\theta$, then constructive interference cannot occur. Now the smallest value of $\theta$ for which no energy is transmitted into the ground is the $\theta_1$ of total reflection, for which $\psi = 0$. Substituting $\cos \theta_1 = \sqrt{1 - (c_1^2/c_2^2)}$ into Eq. (8), we find that the limiting wave length $\lambda_n$, above which transmission by the $n$-th and all the lower order modes cannot take place, is given[2] by

$$\lambda_n = \frac{4H\sqrt{1 - (c_1^2/c_2^2)}}{(2n - 1)}, \qquad n = 1, 2, 3. \tag{9}$$

## 3. SUMMARY OF THE SOLUTION OF THE WAVE EQUATION FOR THE PROBLEM OF PROPAGATION OF SOUND PRODUCED BY A POINT-SOURCE EXPLOSION IN SHALLOW WATER

The elementary discussion given in the previous section was of a qualitative nature and was furthermore based on the assumption that the reflection coefficient for a *plane* wave is applicable to the reflection of a *spherical* wave. It is shown in Part II that this assumption is valid only in special cases; that it is not valid, for example, when the angle of incidence is equal to the angle of total reflection, or for the treatment of the "tail" of a pressure pulse. Since our purpose is to produce a theory

[2] The explanation of the physical origin of the cut-off frequency occurred to several investigators independently; among the latest is Dr. C. Herring.

which, for a given type and weight of explosive detonated at a given depth where the nature of the bottom is known, enables one to compute the pressure variation at large ranges, an exact solution of the wave equation is required. This is given in some detail in Part II, so that it will suffice here merely to present a summary of the results.

The mathematical problem is to solve the wave equation for the sound potential $\varphi$

$$\nabla^2 \varphi_1 = \frac{1}{c_1^2} \frac{\partial^2 \varphi_1}{\partial t^2}, \qquad 0 < z < H \quad \text{(water)}, \tag{10}$$

$$\nabla^2 \varphi_1 = \frac{1}{c_2^2} \frac{\partial^2 \varphi_2}{\partial t^2}, \qquad z > H \quad \text{(bottom)}, \tag{11}$$

where the subscripts 1 and 2 refer to the water and the bottom. The acoustic pressure $p$ and the horizontal and vertical components of velocity $u$ and $w$ are derived from the potential $\varphi$ through

$$p = \rho \frac{\partial \varphi}{\partial t}, \qquad u = -\frac{\partial \varphi}{\partial r}, \qquad w = -\frac{\partial \varphi}{\partial z}. \tag{12}$$

Eqs. (10) and (11) are to be solved subject to the conditions that

a) the pressure should vanish at the surface;

b) near the source, $\varphi_1$ should approach $f(t - R/c_1)/R$, where $R$ denotes distance from the source and $f(t)$ the time variation of the pressure pulse at the source;

c) the vertical component of the velocity $w$ and the pressure should be continuous across the bottom interface. Conditions (a) and (c) require that

$$\varphi_1 = 0, \qquad z = 0, \tag{13}$$

$$\frac{\partial \varphi_1}{\partial z} = \frac{\partial \varphi_2}{\partial z}, \qquad \rho_1 \varphi_1 = \rho_2 \varphi_2, \qquad z = H. \tag{14}$$

The solution of this problem is obtained in two steps by solving first for the case when the point source is periodic of circular frequency $\omega$:

$$\varphi = e^{i\omega t} \Psi(r, z, \omega), \tag{15}$$

and then generalizing the solution for an arbitrary pressure pulse $f(t)$ through a Fourier synthesis:

$$\varphi(r, z, t) = \frac{1}{2\pi} \int_{-\infty}^{\infty} e^{i\omega t} \Psi(r, z, \omega) g(\omega)\, d\omega, \tag{16}$$

where

$$g(\omega) = \int_{-\infty}^{\infty} e^{-i\omega t} f(t)\, dt. \tag{17}$$

The solution for $\Psi$ is derived in Part II as an integral in the complex plane. If $d$ denote the depth of the source, then

$$\Psi = 2 \int_0^{\infty} J_0(kr) k\, dk \frac{\sin(\beta_1 z)}{\beta_1} \left[ \frac{\beta_1 \cos \beta_1 (H - d) + ib\beta_2 \sin \beta_1 (H - d)}{\beta_1 \cos \beta_1 H + ib\beta_2 \sin \beta_1 H} \right], \qquad 0 < z < d, \tag{18}$$

$$\Psi = 2\int_0^\infty J_0(kr)k\,dk\,\frac{\sin(\beta_1 d)}{\beta_1}\left[\frac{\beta_1\cos\beta_1(H-z)+ib\beta_2\sin\beta_1(H-z)}{\beta_1\cos\beta_1 H+ib\beta_2\sin\beta_1 H}\right],\qquad d<z<H, \tag{19}$$

$$\Psi = 2b\int_0^\infty J_0(kr)k\,dk\,\frac{\sin(\beta_1 d)e^{-i\beta_2(z-H)}}{(\beta_1\cos\beta_1 H+ib\beta_2\sin\beta_1 H)},\qquad z>H, \tag{20}$$

where $b = \rho_1/\rho_2$, and

$$\beta_n = \sqrt{(\omega^2/c_n^2)-k^2},\qquad k<(\omega/c_n),$$
$$= -i\sqrt{k^2-(\omega^2/c_n^2)},\qquad k>(\omega/c_n),\qquad n=1,2. \tag{21}$$

The integrals in Eqs. (18), (19), and (20) can be evaluated by direct numerical integration only when the wave length is greater than a moderate fraction of the depth of water, and the range is not large in terms of the depth. This was done for a few cases, and the results are shown by the continuous curves in Figure 23.

For smaller wave lengths or larger ranges, the integrands oscillate extremely rapidly, and the numerical integration becomes well nigh impossible. An alternative expression for the potential, valid under these conditions, can be obtained by transforming the path of integration in the complex $k$-plane. The potential $\varphi$ is then expressed in terms of the residues of the integrands $\varphi'$, and an integral along a *branch-line* $\varphi''$. The residues thus obtained are the *normal modes*, while the integral along a branch line can be shown to decrease in relative importance as the range increases. The result is as follows:

$$\varphi = \varphi' + \varphi'', \tag{22}$$

$$\varphi' = \left(\frac{-2\pi i}{H}\right)e^{i\omega t}\sum_{n=1}^{\infty} H_0^{(2)}(k_n r)F(x_n)\sin(x_n d/H)\sin(x_n z/H),\qquad 0<z<H, \tag{23}$$

$$= \left(\frac{-2\pi ib}{H}\right)e^{i\omega t}\sum_{n=1}^{\infty} H_0^{(2)}(k_n r)F(x_n)\sin(x_n d/H)\sin x_n\,e^{-i\beta_2^{(n)}(z-H)},\qquad z>H, \tag{24}$$

where

$$F(x_n) \equiv \frac{x_n}{(x_n - \sin x_n\cos x_n - b^2\sin^2 x_n\tan x_n)}, \tag{25}$$

$$x_n \equiv \beta_1^{(n)}H = H\sqrt{\frac{\omega^2}{c_1^2}-k_n^2},\qquad \beta_2^{(n)} = \sqrt{\frac{\omega^2}{c_2^2}-k_n^2} = -i\sqrt{k_n^2-\frac{\omega^2}{c_2^2}}, \tag{26}$$

and the $x_n$ are the roots of the equation

$$\frac{\tan x}{x} = \frac{i}{bH\beta_2} = -\frac{1}{bH\sqrt{k_n^2-\dfrac{\omega^2}{c_2^2}}} = -\frac{1}{bH\sqrt{\dfrac{\omega^2}{c_1^2}-\dfrac{\omega^2}{c_2^2}-\dfrac{x^2}{H^2}}}, \tag{27}$$

$$\varphi'' = -2ib\int_{-i\infty}^{k_2} H_0^{(2)}(kr)k\,dk\,\frac{\beta_2\sin(\beta_1 d)\sin(\beta_1 z)}{[\beta_1^2\cos^2(\beta_1 H)+b^2\beta_2^2\sin^2(\beta_1 H)]}. \tag{28}$$

For large ranges one may use the asymptotic expression for the Hankel function

$$H_0^{(2)}(k_n r) \to \sqrt{\frac{2}{\pi k_n r}}\,e^{i\left(\frac{\pi}{4}-k_n r\right)}, \tag{29}$$

whereby expressions (23) and (24) are transformed into

$$\varphi' = \left(\frac{2\pi}{H}\right)\sqrt{\frac{2}{\pi r}}\sum_{n=1}^{\infty}\frac{1}{\sqrt{k_n}}e^{i\left(\omega t - k_n r - \frac{\pi}{4}\right)}F(x_n)\sin(x_n d/H)\sin(x_n z/H), \quad 0 < z < H, \tag{30}$$

$$\varphi' = \left(\frac{2\pi b}{H}\right)\sqrt{\frac{2}{\pi r}}\sum_{n=1}^{\infty}\frac{1}{\sqrt{k_n}}e^{i\left(\omega t - k_n r - \frac{\pi}{4}\right)}F(x_n)\sin(x_n d/H)\sin x_n e^{-i\beta_2^{(n)}(z-H)}, \quad z > H. \tag{31}$$

Similarly one finds that for large ranges and under certain other conditions specified on page 56.

$$\varphi'' \to \frac{(2ibk_2)e^{i(\omega t - k_2 r)}}{(k_1 r)^2}\frac{\sin(k_1 d\mu)\sin(k_1 z\mu)}{\mu^2\cos^2(k_1 H\mu)}, \qquad c_1 < c_2, \; z < H, \tag{32}$$

$$\varphi'' \to \frac{(2ibk_2)e^{i(\omega t - k_2 r)}}{(k_1 r)^2}\frac{\mathrm{sh}(k_1 d\nu)\,\mathrm{sh}(k_1 z\nu)}{\nu^2\,\mathrm{ch}^2(k_1 H\nu)}, \qquad c_1 > c_2, \; z < H, \tag{33}$$

where

$$\nu \equiv \sqrt{(c_1^2/c_2^2) - 1}, \qquad \mu \equiv \sqrt{1 - (c_1^2/c_2^2)}, \qquad k_n = \frac{\omega}{c_n}. \tag{34}$$

## 4. DISCUSSION OF THE SOLUTION FOR A PERIODIC POINT-SOURCE

### I. EVIDENCE FOR THE REALITY OF THE BRANCH-LINE INTEGRAL IN THE SOLUTION FOR THE POTENTIAL, AND ITS PHYSICAL MEANING

The appearance of the branch-line integral term $\varphi''$ in the solution (22) for the potential seems contrary to standard theories on the solution of the wave equation for a point-source in terms of normal modes. Some evidence for the reality of the branch-line integral is furnished by the asymptotic behavior of the solutions computed by numerical integration of (19), which are shown in Figure 23. The dashed lines in this figure, which show a variation of pressure amplitude as the inverse square power of the range, were computed from Eqs. (32) and (33). It will be seen that in all cases the exact solutions show an approach to an inverse-square variation of amplitude with range, and that the numerical agreement with the asymptotic curves is very good.[3] This is most remarkable since the cases treated include both slow and fast bottoms, and the coefficient $N$ defined in Figure 23 ranges from 0.05 to 8.2.

As to the physical nature of the component of the solution represented by the branch-line integral, one sees first from the appearance of $k_2$ in the exponents of (32) and (33) that it represents a wave which propagates with the speed of sound in the *bottom*. Secondly, for very long wave lengths ($k_1$ small) or when $\nu$ and $\mu$ are small (small contrast in velocity), (32) and (33) reduce to the asymptotic form for a point source and its image in the surface situated in a uniform medium possessing the properties of the bottom. It would seem, therefore, that the branch-line integral represents the Lloyd Mirror effect as modified by the discontinuity at the bottom.

[3] Curves $F$ and $G$ have not been plotted solely in order to avoid overcrowding in the figure.

Another point to notice is that for short wave lengths ($\lambda \ll H$) and $c_1 < c_2$,

$$\frac{sh(k_1 d\nu)sh(k_1 z\nu)}{\nu^2 ch^2(k_1 H\nu)} \rightarrow \frac{e^{-k_1\nu(2H-z-d)}}{\nu^2}, \tag{35}$$

as compared with a corresponding term of $k_1^2 \cdot d \cdot z$ in the ordinary Lloyd Mirror theory. The ratio of (35) to the latter $e^{-k_1\nu(2H-z-d)}/\nu^2 k_1^2 dz$ is very small unless both the source and receiver are very close to the bottom.

## II. VARIATION OF THE AMPLITUDE OF THE NORMAL MODES WITH DEPTH

Expressions (30) and (31) for the normal-mode component of the solution can be rewritten in the form

$$\varphi' = \left(\frac{2\pi}{H}\right)\sqrt{\frac{2}{\pi r}}\sum_{n=1}^{\infty}\frac{1}{\sqrt{k_n}}\,e^{i[\omega t-k_n r-(\pi/4)]}\,F(x_n)\varphi_n(d)\varphi_n(z), \qquad 0 < z < H, \tag{36}$$

$$\varphi' = \left(\frac{2\pi b}{H}\right)\sqrt{\frac{2}{\pi r}}\sum_{n=1}^{\infty}\frac{1}{\sqrt{k_n}}\,e^{i[\omega t-k_n r-(\pi/4)]}\,F(x_n)\varphi_n(d)\varphi_n(z), \qquad z > H, \tag{37}$$

where $\varphi_n(z)$ *represents the amplitude of the n-th normal mode*, and is given by

$$\begin{aligned} \varphi_n(z) &= \sin(x_n z/H), & 0 < z < H, \\ &= \sin(x_n)e^{-\sqrt{k_n^2-\omega^2/c_2^2}\,(z-H)}, & z > H. \end{aligned} \tag{38}$$

Here the $x_n$ and the $k_n$ are roots of Eq. (27):

$$\frac{\tan x}{x} = -\frac{1}{bH\sqrt{k_n^2 - \dfrac{\omega^2}{c_2^2}}} = -\frac{1}{bH\sqrt{\dfrac{\omega^2}{c_1^2} - \dfrac{\omega^2}{c_2^2} - \dfrac{x^2}{H^2}}}, \qquad x = H\sqrt{\frac{\omega^2}{c_1^2} - k_n^2}. \tag{27}$$

When $c_2 > c_1$, which is the case in which we are interested, Eq. (27) possesses *real* roots for $k_n$ and $x_n$, the latter varying in the range $\pi(n - \frac{1}{2}) < x_n < n\pi$. On the other hand, when $c_2 < c_1$, the roots $k_n$ are complex numbers with negative imaginary parts. In the latter case, therefore, the factor $e^{-ik_n r}$ in (31) and (37) implies horizontal attenuation, *whereas, in the case of a fast bottom, there exist solutions which suffer no horizontal damping.* This condition stems, of course, from the fact that, for angles of incidence greater than the critical angle, no power is transmitted into the bottom.

The variation of the amplitude of the first mode with depth is shown for several cases in Figures 45–48 (computed in Fall of 1941). The quantity $c$ is the so-called *phase velocity* of the first mode, which will be discussed in the next section. In Figures 45 and 46, the amplitude decreases exponentially with depth below the bottom. The decrement starts from zero at the cut-off frequency of 93.3 cps and increases with increasing frequency. At frequencies greater than about 1000 cps, very little energy of the first mode is left in the bottom, and the amplitude distribution approachs half a sine wave. In the triple-layered medium (Fig. 46) the limiting form of the amplitude distribution for very high frequencies is half a sine wave confined between the two internal surfaces of discontinuity. On the other hand, in the continuous cases shown in Figures 47 and 48, the amplitude of the first mode is compressed, with increasing frequency, to an *increasingly narrow range of depth near the minimum of sound velocity.* The trapping of the energy near the minimum of the sound velocity, as well as the difference between the limiting form of the amplitude distribution in the continuous and discontinuous cases, can be explained by well-known principles of quantum mechanics, which we shall however not discuss here.

The amplitude of the second mode has, in addition to the common node of the surface, another nodal surface within the water. Similarly, the $n$-th mode possesses $n$ nodal surfaces in the water.

One consequence of weak penetration of the energy of the first mode into the bottom with increasing frequency is that observations (of dispersion) on high frequencies can yield little information on the nature of the bottom, whereas the lower frequencies do make an appreciable "sounding" of the bottom.

The factors $F(x_n)/\sqrt{k_n}$ determine the *strength of excitation of the n-th mode.* The function $F(x_n)$ is plotted for several two-layered media in Figures 28 and 49. It will be noticed that it vanishes at the cut-off frequency and that it approaches unity at high frequencies.

### III. THE PHASE VELOCITY OF THE NORMAL MODES, AND THE ANGLES OF INCIDENCE OF THE COMPONENT PLANE WAVES OF THE NORMAL MODES

The factors $e^{i(\omega t-k_n r)}$ in Eqs. (36) and (37) allow of an obvious interpretation of $k_n$, namely $k_n = \omega/c_n$, where $c_n$ denotes the *phase velocity of the n-th normal mode.* The meaning of phase velocity is that, in case of an arbitrary disturbance, the amplitude of the Fourier spectrum of the disturbance at $\omega$ is propagated with the speed of the phase velocity. The phase velocity of the normal modes starts at the cut-off frequency with the value of the speed of sound in the bottom, and decreases continuously with increasing frequency toward the value of sound velocity in water. The variation of phase velocity with frequency is shown for several double-layered media in Figure 28 and for several modes in Figure 49. This would suggest that, in case of an arbitrary disturbance, the low-frequency components in the spectrum of a pressure pulse would get ahead of the high-frequency components, so that at large ranges the received pulse would appear in the form of a train of nearly sinusoidal waves in which the period decreases toward the rear. The actual situation is more complicated, however, because the component waves are not merely separated out by their different rates of advance but are also *superimposed*, thus producing complicated interference patterns. We shall return to this question later.

The factors

$$e^{i[\omega t-k_n r-(\pi/4)]}\sin(x_n z/H) = \tfrac{1}{2}\{e^{i[\omega t-k_n r+(x_n z/H)-(3\pi/4)]} - e^{-i[\omega t-k_n r-(x_n z/H)-(3\pi/4)]}\} \quad (39)$$

in Eqs. (36) and (37) show that the normal modes can be analyzed into two plane waves traveling obliquely upward and downward, respectively, as indicated in Figure B. The angle which these waves make with the vertical $\theta_n$ is given by

$$\theta_n = \sin^{-1}(k_n c_1/\omega) = \sin^{-1}(c_1/c_n) = \cos^{-1}(x_n c_1/H\omega). \quad (40)$$

An inspection of Figure 49, in which curves of $c_n/c_1$ are plotted against frequency for $n = 1, 2, 3$, shows that:

(a) $\theta_n$ is always greater than the angle of total reflection of $\sin^{-1}(c_1/c_2)$, as was anticipated in the Qualitative Discussion of the Theory of Propagation.

(b) In any given mode, $\theta_n$ starts with the value of the critical angle at the cut-off frequency and approaches grazing incidence in the limit of very high frequencies.

(c) For a given frequency the angle of incidence is smaller, the higher the order of the mode.

Since reflection by a *corrugated surface* approaches specular reflection at grazing incidence, it would follow from item (c) that under practical conditions the first mode would tend to persist to greater ranges than the higher-order modes. A similar conclusion with regard to the relative persistence of various frequencies in a given mode cannot be inferred from item (b) because the higher the frequency the higher is the angle of incidence required for the condition of specular reflection to be approached.

#### IV. THE QUESTION OF THE ORTHOGONALITY AND NORMALIZATION FACTORS OF THE NORMAL MODES

This question is dealt with in detail in Part II. Suffice it to mention here that the expressions for the normal modes given in Eq. (38) are *not orthogonal when there is a discontinuity of density at the bottom.* The reason for this is that in the presence of a discontinuity in density, the normal modes (as well as the horizontal components of velocity) are discontinuous at the bottom, because the acoustic pressure, which *is* continuous, is equal not to the potential but to the density times the potential. Again it is found that unless the densities of the water and bottom are equal, the normalization factors as obtained from the residues are *not* such that the integral of the square of the normal mode function from $z = 0$ to $z = \infty$ is unity.

## 5. PROPAGATION OF A PRESSURE PULSE IN SHALLOW WATER

#### I. FORMAL GENERALIZATION OF THE SOLUTION FOR AN EXPONENTIAL PULSE

In previous sections it was shown that the solution for a *periodic* point source can be expressed in terms of normal modes, as given by Eqs. (36) and (37), and by a branch-line integral which was shown in Eqs. (32) and (33) to vary like $r^{-2}$, as compared with the normal-modes variation of $r^{-\frac{1}{2}}$. Except near the beginning of the ground wave when the amplitude of the normal modes vanishes ($F = 0$ in Figs. 28 and 49), the contribution from the branch-line integral can be neglected for the large ranges which we are considering.

We shall now examine how the normal-mode solution

$$\varphi = \sum_{n=1}^{\infty} e^{i[\omega t - k_n r - (\pi/4)]} Q_n(r, z, d, \omega),$$

$$Q_n = \left(\frac{2\pi}{H}\right)\sqrt{\frac{2}{\pi k_n r}}\left[\frac{x_n \sin(x_n d/H)\sin(x_n z/H)}{(x_n - \sin x_n \cos x_n - b^2 \sin^2 x_n \tan x_n)}\right], \qquad 0 < z < H, \tag{41}$$

for a periodic point source can be formally generalized to the case of an arbitrary pressure pulse $f(t)$ at the source. For reasons to be explained later we shall assume that

$$f(t) = e^{-\lambda t}, \quad t > 0,$$
$$= 0 \;, \quad t < 0. \tag{42}$$

The pressure jumps from zero to unity at $t = 0$ and thereafter decays exponentially with time. We have

$$f(t) = \frac{1}{2\pi}\int_{-\infty}^{\infty} \frac{e^{i\omega t}}{(\lambda + i\omega)}, \tag{43}$$

$$P = \sum_{n=1}^{\infty} P_n(r, z, t), \tag{44}$$

$$P_n(r, z, t) = \frac{1}{2\pi}\int_{-\infty}^{\infty} \frac{e^{i[\omega t - k_n(\omega)r - (\pi/4)]}}{(\lambda + i\omega)} Q_n(r, z, \omega)\, d\omega$$
$$= \frac{1}{\pi}\int_0^{\infty} \frac{Q_n(r, z, \omega)}{\sqrt{\lambda^2 + \omega^2}} \cos\left[\omega t - k_n(\omega)r - \frac{\pi}{4} - \tan^{-1}\left(\frac{\omega}{\lambda}\right)\right] d\omega, \tag{45}$$

where $P_n(r, z, t)$ represents the contribution to the pressure from the $n$-th mode.

## II. THE GROUP VELOCITY OF THE NORMAL MODES

The integral in Eq. (45) represents a superposition of sinusoidal waves traveling with different phase velocities $c_n = \omega/k_n(\omega)$, the amplitude of the waves of the circular frequency $\omega$ being about $Q_n(r, z, \omega)/\sqrt{\lambda^2 + \omega^2}$. Denoting

$$f(\omega, r, t) = \omega t - k(\omega)r - \pi/4$$ [4]

as the *phase*, we see that, for such values of $\omega$, $r$, and $t$ for which the phase varies with $\omega$, the cosine factor in the integral in (45) will tend to be cancellatory. Cancellation of the integrand will be minimized however at such points $\omega$ (called points of stationary phase) where $\dot{f}(\omega) = 0$. It is to be noted that, whereas in considering the *phase velocity* we seek the increments $\Delta r$ and $\Delta t$ which are required in order to keep the phase *at a given frequency* $\omega$ unchanged, in looking for points of stationary phase we seek such values of $\omega$ where, for given values of $r$ and $t$, the phase is unchanged by a slight increment $\Delta\omega$. A point of stationary phase is therefore not one for which two neighboring frequencies travel with the same phase velocity. Such points do not exist in fact.

At frequencies $\omega$ for which the phase is stationary, mutual interference will be at a minimum, and these frequencies will therefore be dominant at the prescribed values of $t$ and $r$. The values of $t$ and $r$, for which the phase is stationary for a given frequency, therefore determine the rate of propagation of this frequency in the mutually interfering train of sinusoidal waves, or the so-called *group velocity* $U$:

$$\frac{df}{d\omega} = t - r\frac{dk(\omega)}{d\omega} = 0,$$
$$U = \frac{r}{t} = \frac{d\omega}{dk}. \tag{46}$$

[4] The term $\tan^{-1}(\omega/\lambda)$ in the phase can be considered as a slowly varying quantity such as $Q_n(\omega)/\sqrt{\lambda^2 + \omega^2}$.

*We have therefore defined the group velocity as the velocity with which a given frequency (or period) is propagated in a train of waves which results from interference of component sinusoidal waves traveling with different phase velocities.*

That the group velocity as defined above is different from the phase velocity can be seen from the following considerations. In Figure C we have sketched the pulse shape at time $t_1$ when the phase $A_1$ (point of zero pressure) has reached $r_1$, and at a later time $t_2$ when it has reached $r_2$. It is assumed that the phase velocity increases with wave length so that the pulse becomes *drawn out* as it progresses. If $\Delta r = r_2 - r_1$ is small, then the phase velocity is $\Delta r/\Delta t$. This is, however, not equal to the group velocity because at $t_2$ the dominant wave length near $A_2$ has increased, and the original wave length is now somewhere to the rear of $A_2$. The distance covered by the wave length is therefore less than the distance $\Delta r$ covered by the phase, and the group velocity is less than the phase velocity.

It can be shown that the group velocity $U$ is always less than the phase velocity when the phase velocity decreases with increasing frequency, as in our case. We have

$$\omega = ck, \qquad U = \frac{d\omega}{dk} = \frac{d(ck)}{dk} = c + k\frac{dc}{dk}, \tag{47}$$

and, since $\dfrac{dc}{dk} < 0$, it follows that $U$ is always less than phase velocity $c$.

Figure 28 shows the variation of group velocity of the first mode with frequency for a series of two-layered liquid half-spaces. It will be noted that in all cases the group velocity passes through a minimum, and that for values of $U < c_1$ *two* frequencies correspond to a given value of $U$. It will be shown later that both these features of the group-velocity curve have important consequences for the interpretation of propagation of explosive sound in shallow water. Group-velocity curves for three-layered media are shown in Figures 29, 30, 31, and 32. The significance of some of the characteristics of these curves in the study of records from explosive sound will also be taken up later.

## III. THE GROUND WAVE, WATER WAVE AND AIRY PHASE IN A TWO-LAYERED LIQUID HALF-SPACE

If a pressure pulse from a point source is initiated in shallow water, and if the pulse is not a single frequency ping but covers a moderately broad spectrum, then the pressure wave at large ranges due to the first mode would be expected, on the basis of the group velocity curve in Figure D, to show the following sequence of events. The first arrivals would be nearly sinusoidal waves of frequency $f_L$, where $f_L$ denotes the limiting frequency for the first mode

$$f_L^1 = \frac{c_2}{4H\sqrt{1 - (c_1^2/c_2^2)}}. \tag{48}$$

These waves would arrive at $t = r/c_2$.[5] As time progresses, the frequency in this so-called *ground wave* would decrease, and the amplitude would increase (for reasons

[5] This is not strictly true, but we shall not enter upon a discussion of this point here. (*See* Pekeris, 1946.)

to be given later). This is because at later epochs the group velocity is less, and therefore one proceeds down the left branch of the group velocity curve in Figure D in the direction indicated by the arrow. At the time $r/c_1$, a new train of high-frequency waves due to the right-hand branch of the group-velocity curve would suddenly be superimposed on the ground wave. This new high-frequency wave, which would arrive with an apparent velocity equal to the velocity of sound in water, we shall designate as the *water wave.* The frequency in the water wave would decrease as time progresses, while in the ground wave the frequency would continue to increase. At a time $t = r/U_1$, for example, the first mode would consist of a superposition of two frequencies, one $f_g$ due to the ground wave and another $f_w$ due to the water wave. Still later, $f_g$ and $f_w$ would approach each other until at $t = r/U_0$, where $U_0$ denotes the minimum group velocity, they would coincide. The pressure then would consist of a single frequency, $f_A$, and we shall designate this portion of the pressure record as the *Airy phase*, because Airy was the first to treat a mathematically related problem of diffraction of light near a caustic.

The sequence of these events is illustrated in the theoretical curves drawn in Figures 24A, 24, and 25. Figure 24 shows the ground wave up to the time of arrival of the water wave. The upper portion of this figure is rather complex, because we have here superimposed the contributions from the first *three* modes. Perhaps a clearer illustration of the events described above for the first mode can be obtained from the lower portion of the figure, in which the higher modes have been relatively suppressed by low-pass filtering. The ground wave is seen to consist of a nearly periodic wave which is gradually modulated both in amplitude and frequency. The change in frequency from the first arrival up to the time (=5.542 sec.) of arrival of the water wave is small, corresponding to the small difference between $f_L$ and $f_R$ in Figure D. $f_R$, the so-called *rider frequency*, is the frequency of the ground wave at $t = 5.542$ sec., which is seen to be around 50 cps.

The details of the water wave and of the accompanying ground wave, as well as of the Airy phase, are shown in Figure 25, which is a continuation of Figure 24 on a different scale. The amplitudes of both the water wave and the ground wave continue to increase while their periods tend toward equality. The maximum amplitude is reached shortly before $t = 5.668$ sec., which is the arrival time of the Airy frequency $f_A(= 75$ cps) corresponding to the minimum group velocity $U_0$. Thereafter we have the *Airy phase* in which the frequency remains constant at the value $f_A$, and the amplitude decreases continuously, ultimately approaching an exponential rate.

## IV. EXPRESSIONS FOR THE GROUND WAVE, WATER WAVE, AND AIRY PHASE

The contribution $P_n(r, z, t)$ from the $n$-th mode to the potential is given in Eq. (45):

$$P_n(r, z, t) = \frac{1}{\pi} \int_0^\infty \frac{Q_n(r, z, \omega)}{\sqrt{\lambda^2 + \omega^2}} \cos\left[\omega t - k_n(\omega) r - \frac{\pi}{4} - \tan^{-1}\left(\frac{\omega}{\lambda}\right)\right] d\omega,$$

$$Q_n = \left(\frac{2\pi}{H}\right) \sqrt{\frac{2}{\pi k_n r}}\, 0_n. \tag{45}$$

$$0_n = \frac{x_n \sin(x_n d/H) \sin(x_n z/H)}{(x_n - \sin x_n \cos x_n - b^2 \sin^2 x_n \tan x_n)} \equiv F(x_n) \sin(x_n d/H) \sin(x_n z/H). \tag{49}$$

As previously explained, the integral in (45) is evaluated by the method of *stationary phase*, the details of the calculation are given in Part II. It will therefore suffice to give the final results here.

To compute $P_n$ at a given point $(r, z)$ and a given time $t$, in case of an exponential pulse $e^{-\lambda t}$, one first computes the group velocity $U = r/t$, and then determines from the abscissa of a group-velocity curve (Fig. 28), the dominant frequency $f$ at that time $(\gamma = fH/c_1)$. One also determines from the dispersion curves the corresponding quantities

$$k = 2\pi f/c = \omega/c, \qquad \ddot{k} = \frac{d^2k}{d\omega^2}, \qquad \text{etc.} \tag{50}$$

$P_n$ is then computed from

$$P_n = P_n^g, \qquad t < r/c_1,$$
$$P_n = P_n^g + P_n^w, \qquad t > r/c_1,$$

where $P_n^g$ denotes the ground wave, and $P_n^w$ the water wave.

We have

$$P_n^g = \frac{4\cos\left[\omega t - rk - \tan^{-1}\left(\dfrac{\omega}{\lambda}\right) - \dfrac{\pi}{2}\right]0_n}{Hr\sqrt{k\cdot\ddot{k}(\lambda^2+\omega^2)}}, \tag{51}$$

$$P_n^w = \frac{4\cos\left[\omega t - rk - \tan^{-1}\left(\dfrac{\omega}{\lambda}\right)\right]0_n}{Hr\sqrt{k\,|\,\ddot{k}\,|\,(\lambda^2+\omega^2)}}. \tag{52}$$

In these expressions the factors other than the arguments of the cosine are slowly varying functions of time; Eqs. (51) and (52) therefore represent waves which are modulated both in frequency and amplitude. It will be noted that

$$\frac{d^2k}{d\omega^2} = -\left(\frac{H}{2\pi c_1}\right)\frac{1}{U^2}\frac{dU}{d\gamma}, \tag{53}$$

so that the *amplitudes of the ground wave and the water wave vary inversely as the square root of the slope of the group-velocity curves in Figure 28.*

Expressions (51) and (52) are approximate and may be used only for large ranges and at times removed from the epoch of the minimum group velocity, when $\ddot{k} = 0$. The precise condition to be observed in using (51) and (52) is

$$\frac{1}{24r}\left[-\frac{5(\dddot{k})^2}{(\ddot{k})^3} + \frac{3\ddddot{k}}{(\ddot{k})^2}\right] = \frac{1}{96\pi^2}\left(\frac{H}{r}\right)\left[-\frac{5\dot{Z}^2}{Z^3} + \frac{3\ddot{Z}}{Z^2}\right] \ll 1, \tag{54}$$

where the $Z$'s are the nondimensional quantities:

$$Z = \frac{c_1^2}{H}\frac{d^2k}{d\omega^2}, \qquad \frac{dZ}{d\gamma} = \dot{Z} = \frac{2\pi c_1^3}{H^2}\frac{d^3k}{d\omega^3}, \qquad \ddot{Z} = \frac{4\pi^3 c_1^4}{H^3}\frac{d^4k}{d\omega^4}. \tag{55}$$

When condition (54) is not met because of the proximity to the point of the minimum group velocity—that is for some time prior to the Airy epoch and for all times thereafter—one can use, instead of the *sum* of expressions (51) and (52), the single expression

$$P_n = \frac{4\cos\left[\omega_0 t - k_0 r - \tan^{-1}\left(\frac{\omega_0}{\lambda}\right) - \frac{\pi}{4}\right] 0_n(\omega_0)E(v)}{3^{\frac{2}{3}} H r^{\frac{5}{6}} (-\ddot{k}_0)^{\frac{1}{3}} \sqrt{(\lambda^2 + \omega_0^2)k_0/2\pi}} \tag{56}$$

where the subscript $_0$ refers to the point of the minimum group velocity, and

$$v = \frac{4\sqrt{\pi}}{3\sqrt{-\dot{z}}}\left(\frac{r}{H}\right)|\tau - \tau_m|^{\frac{3}{2}}, \qquad \tau = \frac{tc_1}{r} - 1, \qquad \tau_m = \frac{c_1}{U_0} - 1,$$

$$E(v) = v^{\frac{1}{3}}[J_{-\frac{1}{3}}(v) + J_{\frac{1}{3}}(v)], \qquad t < \frac{r}{U_0},$$

$$= v^{\frac{1}{3}}[I_{-\frac{1}{3}}(v) - I_{\frac{1}{3}}(v)], \qquad t > \frac{r}{U_0}. \tag{57}$$

Again, Eq. (56) is to be used only when

$$\frac{1}{(2\pi)^{\frac{1}{3}}}\left(\frac{H}{r}\right)^{\frac{1}{3}} \frac{\ddot{z}_0}{(-\dot{z}_0)^{\frac{4}{3}}} \frac{G(v)}{E(v)} \ll 1, \tag{58}$$

the function $G(v)$ being defined in Eqs. (A114) and (A115) in Part II.

The *Airy phase* as represented by Eq. (56) is an amplitude-modulated train of waves. Some theoretical curves of the Airy phase alone are shown in Figure 26. The curves in Figs. 24A, 24 and 25 were computed from Eqs. (51), (52), and (56).

## V. RELATIVE EXCITATION OF THE VARIOUS MODES BY AN EXPLOSION IN SHALLOW WATER

Our discussion thus far has been concerned with the contribution to the pressure variations from individual modes, and we have also intimated that the first mode would impress its characteristics on the pressure record to a greater extent than the higher-order modes. This is an assumption which is usually made in discussions of the subject, but in trying to check it qualitatively the writer found that it is not of general validity.

The theory of normal modes developed in previous sections makes definite predictions as to what the relative amplitudes of the various modes should be. If we define

$$G_1^n = \frac{x_n \sin^2(x_n)}{(x_n - \sin x_n \cos x_n - b^2 \sin^2 x_n \tan x_n)c_1\sqrt{k\dot{k}}}, \tag{59}$$

$$G_2^n = \frac{x_n \sin^2(x_n)}{(x_n - \sin x_n \cos x_n - b^2 \sin^2 x_n \tan x_n)c_1\sqrt{k|\ddot{k}|}}, \tag{60}$$

then it follows from Eqs. (51) and (52) that, when both the charge and the hydrophone are beached on the bottom ($d = z = H$), we have

$$|P_n^g| = \frac{4c_1}{Hr\sqrt{\lambda^2 + \omega^2}} G_1^{(n)}, \tag{61}$$

$$|P_n^w| = \frac{4c_1}{Hr\sqrt{\lambda^2 + \omega^2}} G_2^{(n)}, \tag{62}$$

for the amplitude of the ground wave and the water wave, respectively. With the exception of the factor $(\lambda^2 + \omega^2)^{-\frac{1}{4}}$, which depends on the particular size of charge used ($\lambda$) and is slowly varying in any case, the relative amplitudes of the various modes are given by $G_1^{(n)}$ and $G_2^{(n)}$.

Figures 33, 34, 35, and 36 show curves of $G_1$ and $G_2$ for the first three modes in the case of a two-layered liquid half-space. The abscissae are reduced time scales $(T - T_0)/T_0$, where $T$ denotes the time after the explosion, and $T_0$ the arrival time of the water wave ($= r/c_1$). It will be noted that the various modes are distinguished not only by different excitation amplitudes but also by *different frequencies* arriving at a given time, as shown by the $\gamma$-curves. The higher the order of the mode, the larger are the frequencies arriving at a given time.

In the ground wave ($G_1$), the amplitude of the first mode is about three times the amplitude of the second mode and about five times the amplitude of the third mode (Fig. 24, top). On the other hand, *in the water wave the theoretical contrast in the amplitudes of the various modes is seen to be very much less.* One would therefore expect that a receiver which is characterized by a flat spectral response would record a water wave composed of several trains of waves of about the same amplitude but of different frequencies. Such a record is likely to have a rather complicated appearance. However, in the case of a low-pass receiver system, the higher-order modes would be relatively suppressed on account of their higher frequencies, and the record would exhibit the expected dispersion characteristic of a single (the first) mode.

This I consider to be one reason for the complicated appearance of the Mark II high-frequency traces shown on Plates 1–11, in contrast to the simple dispersion pattern shown by the Mark II low-frequency system. The Mark II high-frequency system has a flat response up to about 1000 cps, whereas the Mark II low-frequency system is a low-pass filter with a cut-off frequency around 150 cps. (*See* Figures 43, 44, and 41, 42.) The effect of the Mark II low-frequency system in enhancing the first mode in the ground wave and the water wave is illustrated in Figures 24 (bottom) and 25 (bottom). A similar effect on the Airy phase is shown in Figure 26.

Another factor which needs to be considered when comparing the relative strengths of excitation of the various modes is *the effect of the roughness of boundaries.* It is known that for a given frequency a condition of nearly specular reflection is approached, even for a rough surface, as grazing incidence is approached. This condition is approached earlier, the longer the wavelength. Since the normal modes can be analyzed into two plane waves traveling upward and downward at definite angles of incidence $\theta_n$, it is of interest to inquire how $\theta_n$ varies with the order $n$ of the mode. If one makes the comparison on the *basis of a given frequency*, then since $\theta_n = \sin^{-1}(c_1/c^{(n)})$ where $c^{(n)}$ is the phase velocity of the $n$-th mode, and since (Fig. 49) $c^{(n)}/c_1$ increases with the order $n$, it follows that the first mode travels with the highest angle of incidence and should therefore suffer least attenuation by scattering from rough boundaries. However, this conclusion must be tempered by the fact that the comparison should be made not for a given frequency but for *equal times of arrival—i.e.*, we wish to compare the relative amplitudes of the various modes as they are superimposed at a given time. Figures 33, 34, 35, and 36 show that the higher modes arriving at a given time are of higher frequency and, since the angle of incidence increases with increasing frequency, it is necessary to make a quantitative study of the variation of the angles of incidence with the order of the mode for a given arrival time. This is done in Figure 50. It will be seen that in the ground wave the difference in $\theta$ is rather small and this difference is in any case not of practical importance for the low angles of incidence involved. In the water wave the difference in angles of incidence between the modes is somewhat larger, and this difference is of greater physical consequence because of the rapid change of reflectivity near grazing incidences. Whatever difference exists in the water wave favors the higher modes. No conclusions can, however, be drawn from this result with regard to relative effects of rough boundaries on the various modes, because the higher angles of incidence of the higher-order modes are counterbalanced by the closer approach to grazing incidence required to achieve the condition of nearly specular reflection at their higher frequencies.

## 6. FEATURES OF THE PRESSURE WAVE FROM AN EXPLOSION IN SHALLOW WATER WHICH CAN BE IDENTIFIED AND MEASURED ON THE RECORDS AND FROM WHICH THEORETICAL DEDUCTIONS CAN BE MADE ABOUT THE STRUCTURE OF THE BOTTOM

### I. ARRIVAL TIMES OF THE GROUND WAVES AND OF THE WATER WAVES AND THEIR USE IN DETERMINING THE STRUCTURE OF THE BOTTOM BY STANDARD REFRACTION METHODS

One of the simple features to identify on the records is the time of arrival of the wave. For the ranges we are considering this is a wave which has traveled in the bottom for most of its course, and which therefore arrives ahead of the wave which reaches the receiver directly through the water. In Plate 1, for example, the arrival time in shot 47 is 1.372 sec.[6] after detonation of the charge, and this phase is marked by the arrow on the geophone trace. The placing of the arrival time at the position of the arrow is based on the judged time of first slanting of the geophone trace. The beginning of shot 48 on Plate 1 is placed at 1.685 sec., that of shots 58 and 59 (Pl. 2) at .791 sec., and .768 sec., respectively, and so on. With a receiver system consisting of seven independent channels which are recorded simultaneously on the oscillogram, the identification of the beginning of the wave presents little difficulty in most cases.

In reading the beginning of the wave, one picks the *earliest* definite indication of a disturbance on any of the traces in the record. The position of the judged beginning of the wave is marked in Plates 1–9 either by a number giving the arrival time or by an arrow on the particular trace which shows the earliest disturbance from quiescence. An inspection of the identification of the first arrivals on the records in Plates 1–9 will reveal that without exception they appear either on the lower (sensitive) Mark II low-frequency trace or on the geophone trace, both of which are insensitive to frequencies greater than about 150 cps. On the other hand, the high-pass systems such as the Mark II high-frequency and the Mark II rectified (*see* Figs. 41, 42, and 43) respond very weakly and belatedly to the first arrivals. The difference between the responses of the high- and low-pass systems to the beginning of the ground wave cannot be explained on the supposition that the amplification of the low-pass systems

[6] The time marks on the traces include a correction to the beginning of the time scale appearing on top of the records.

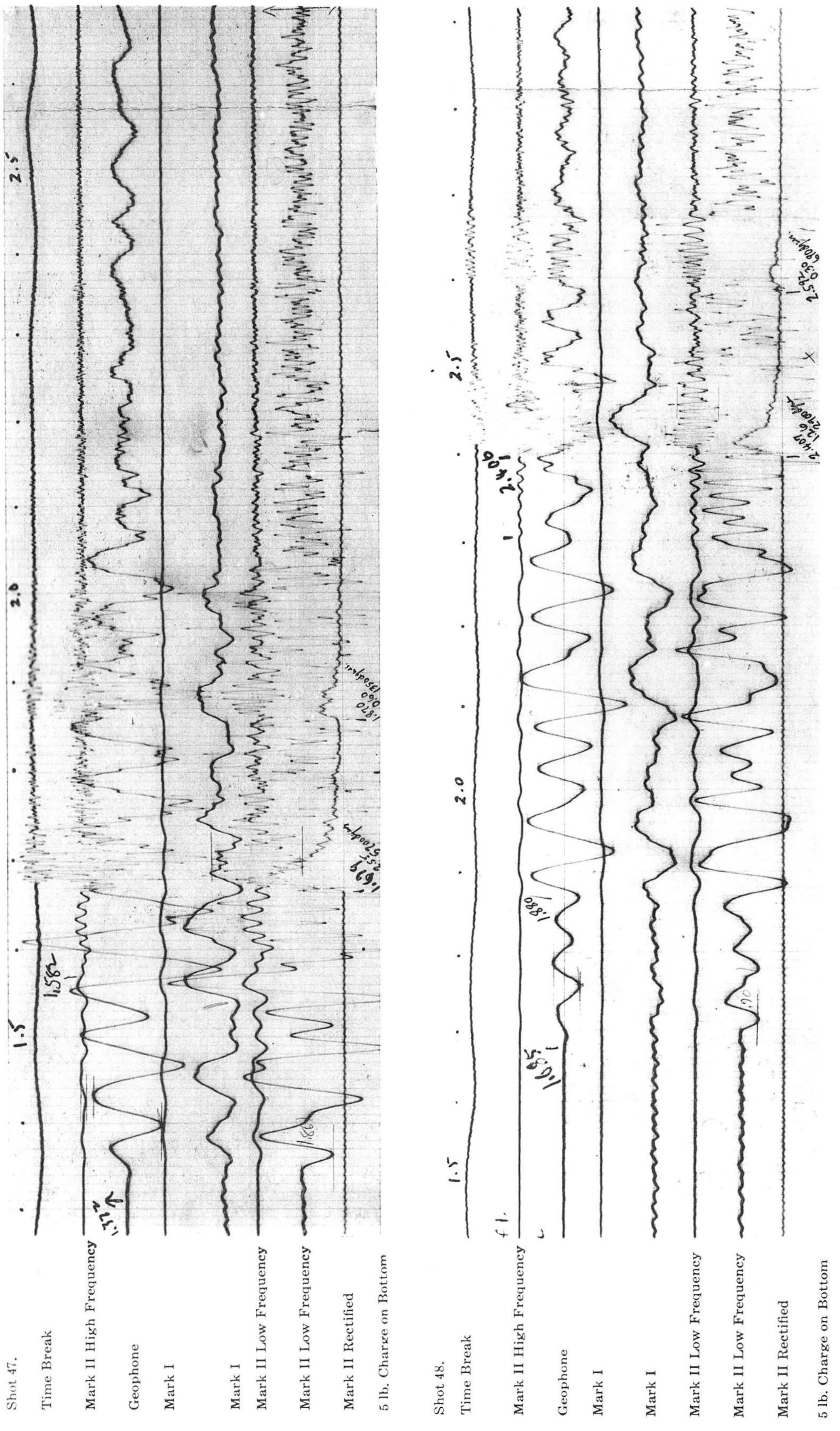


RECORDS AT SOLOMONS SHOAL

Shot 58.
Time Break
Mark II High Frequency
Geophone
Mark I
Mark I
Mark II Low Frequency
Mark II Low Frequency
Mark II Rectified
½ lb. Charge Mid-depth

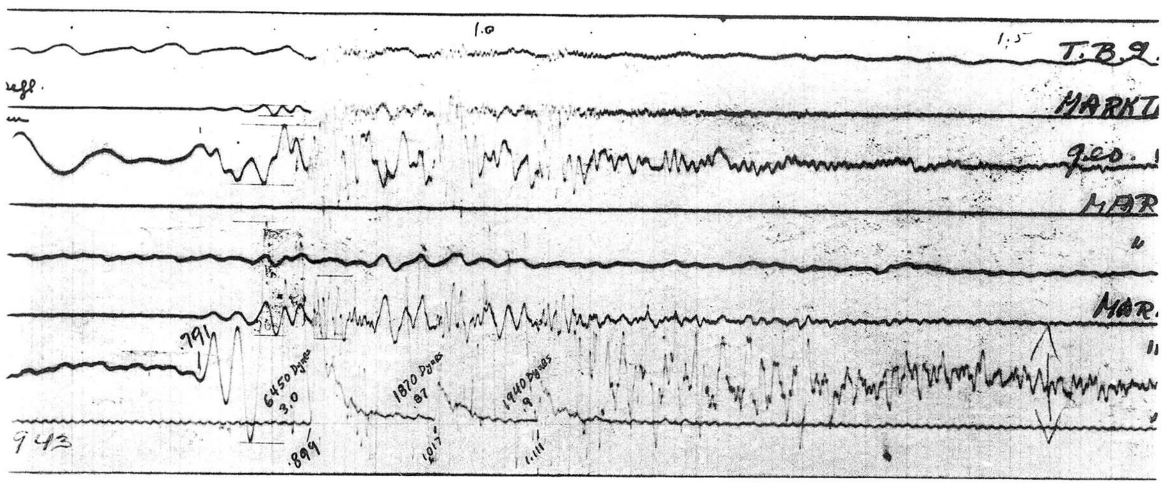


Shot 59.
Time Break
Mark II High Frequency
Geophone
Mark I
Mark I
Mark II Low Frequency
Mark II Low Frequency
Mark II Rectified
5 lb. Charge Mid-depth

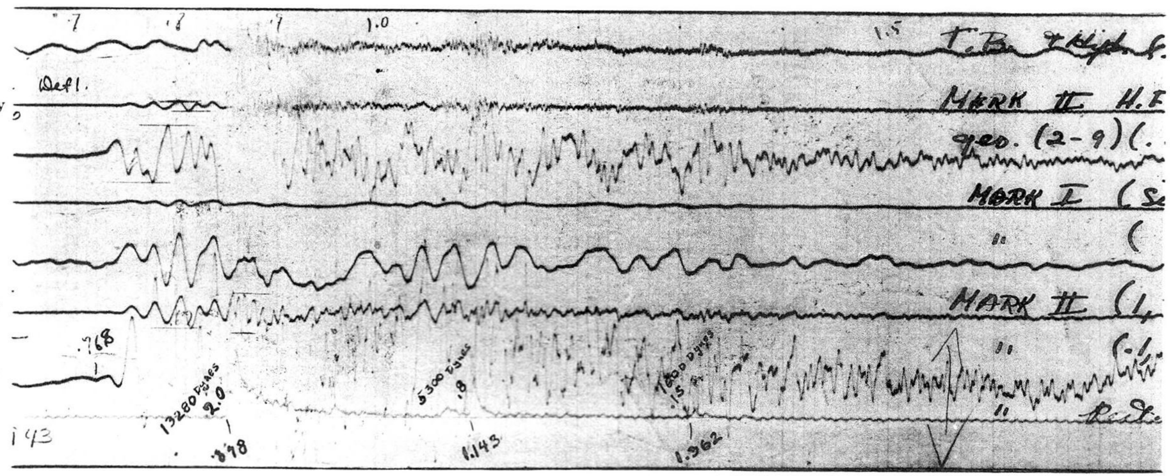


RECORDS AT SOLOMONS SHOAL

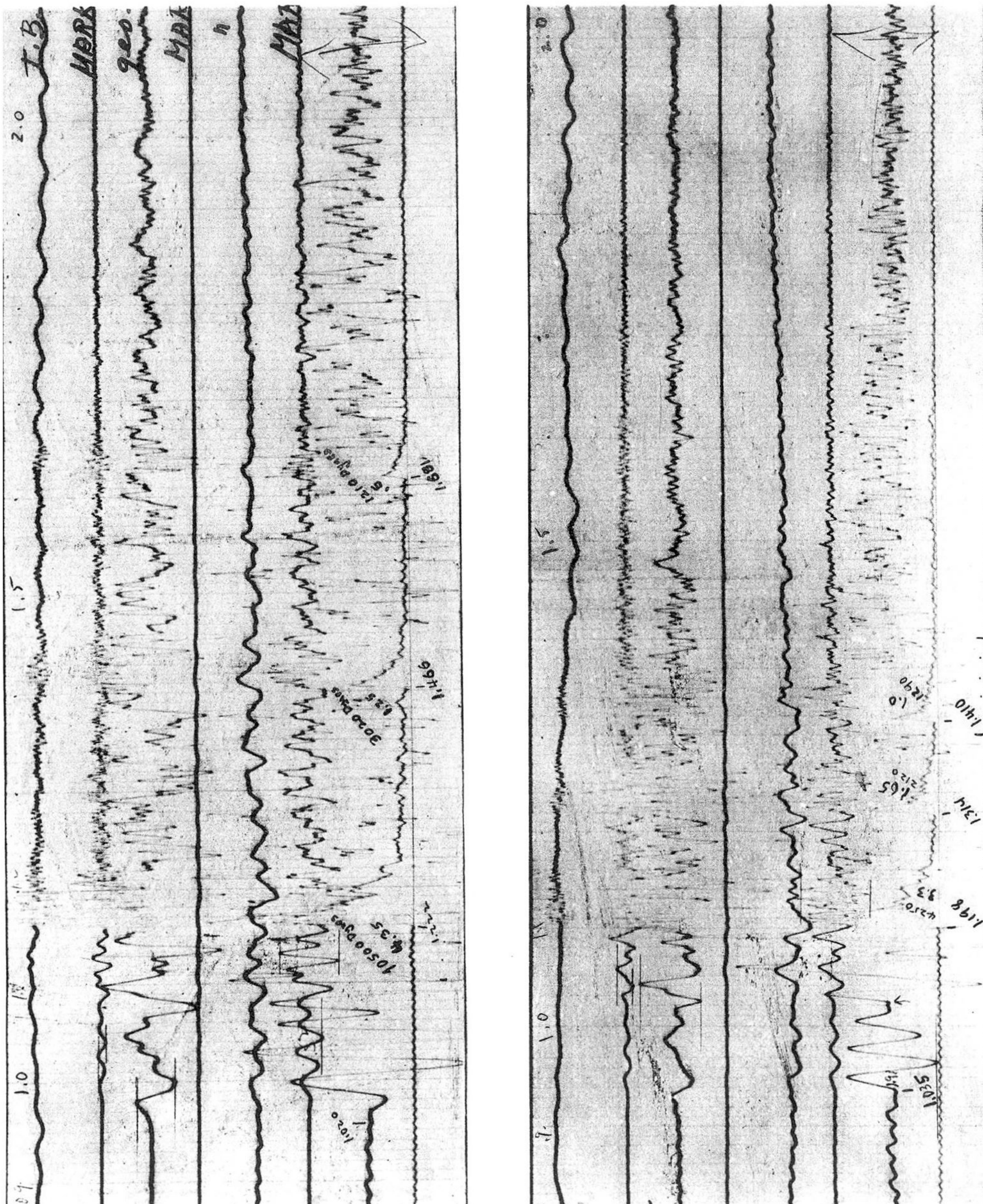


Shot 60.
Time Break
Mark II High Frequency
Geophone
Mark I
Mark I
Mark II Low Frequency
Mark II Low Frequency
Mark II Rectified
5 lb. Charge Mid-depth

Shot 61.
Time Break
Mark II High Frequency
Geophone
Mark I
Mark I
Mark II Low Frequency
Mark II Low Frequency
Mark II Rectified
½ lb. Charge Mid-depth

RECORDS AT SOLOMONS SHOAL

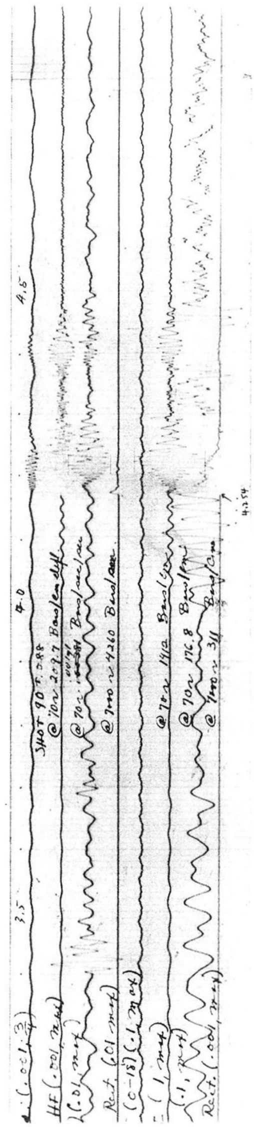

Shot 90.
Time Break
Mark II High Frequency
Geophone
Mark II Rectified
Mark I
Mark II
Mark II
Mark II Rectified
5 lb.

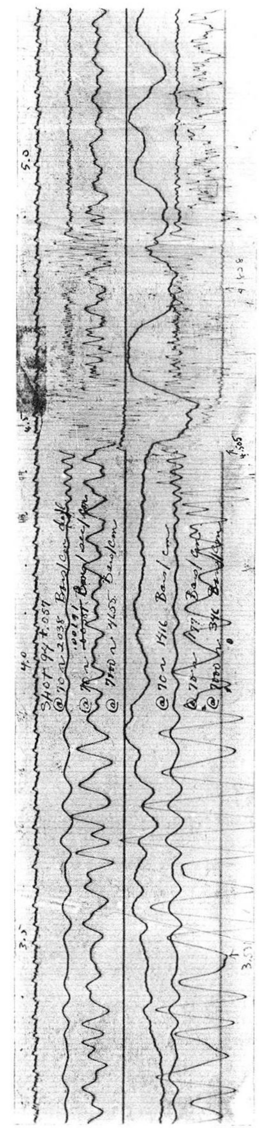

Shot 94.
Time Break
Mark II High Frequency
Geophone
Mark II Rectified
Mark I
Mark II
Mark II
Mark II Rectified
25 lb.

RECORDS AT JACKSONVILLE SHOAL

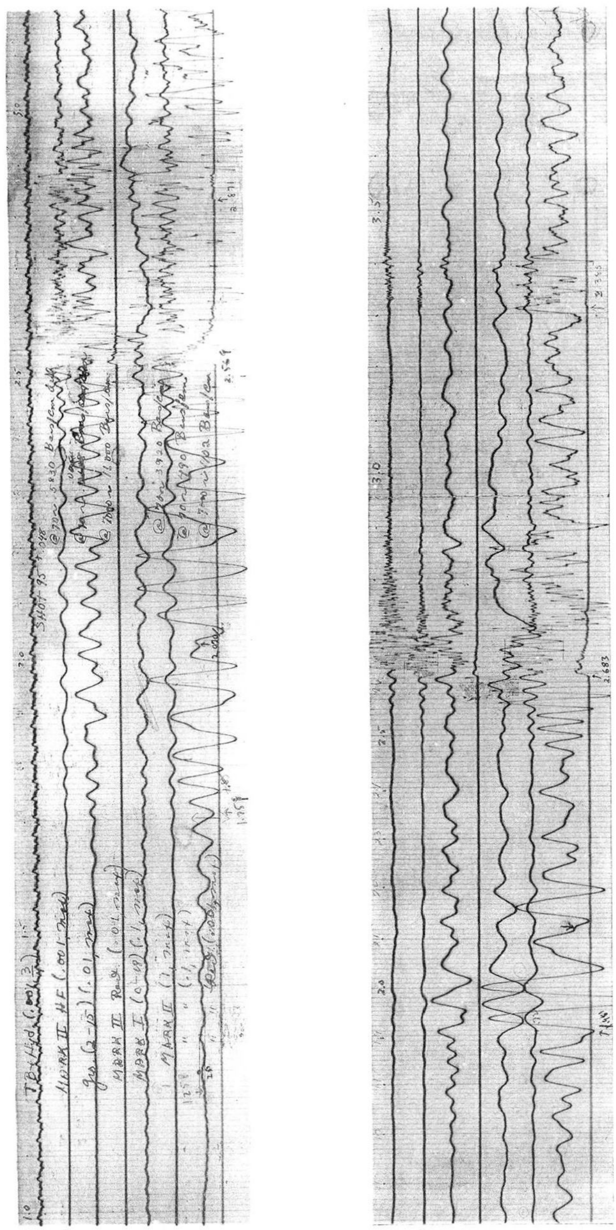


RECORDS AT JACKSONVILLE SHOAL

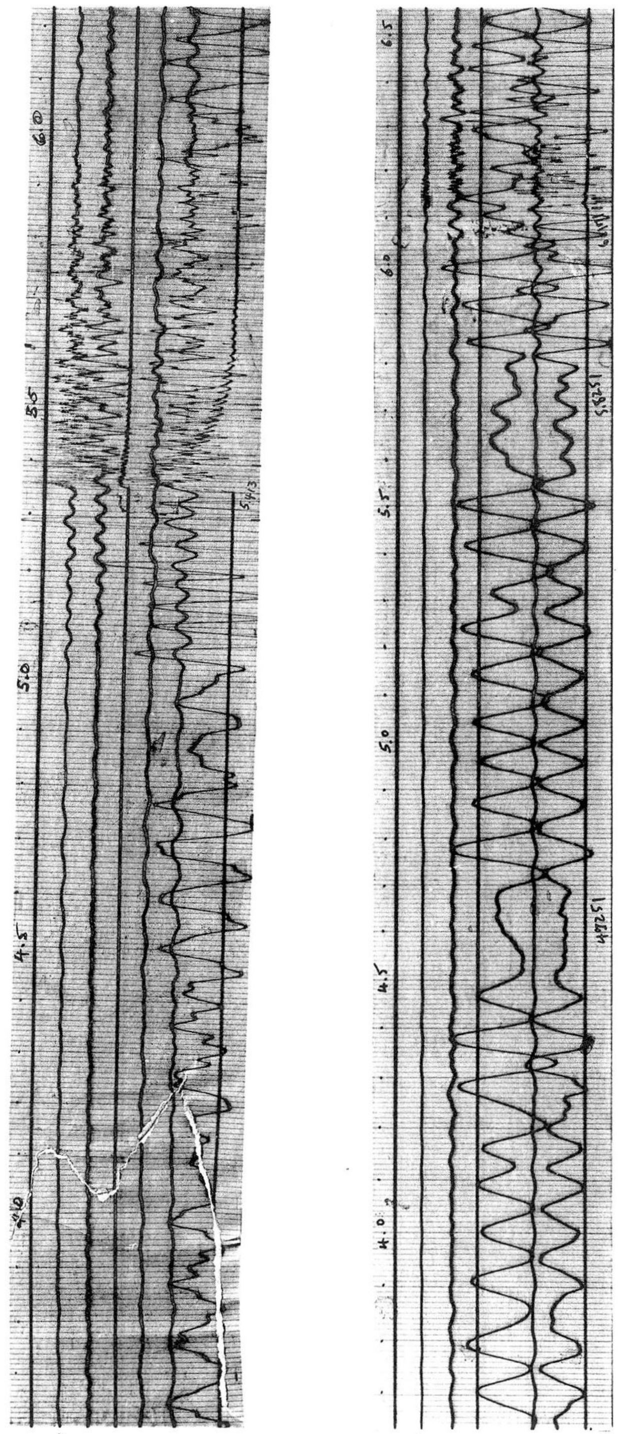

Shot 135.
Time Break
Mark II High Frequency
Geophone
Mark II Rectified
Mark I
Mark II
Mark II
Mark II Rectified
4½ lb.

Shot 156.
Time Break
Mark II High Frequency
Geophone
Mark II Rectified
Mark I
Mark II
Mark II
Mark II Rectified
300 lb. Charge on Bottom

RECORDS AT JACKSONVILLE DEEP

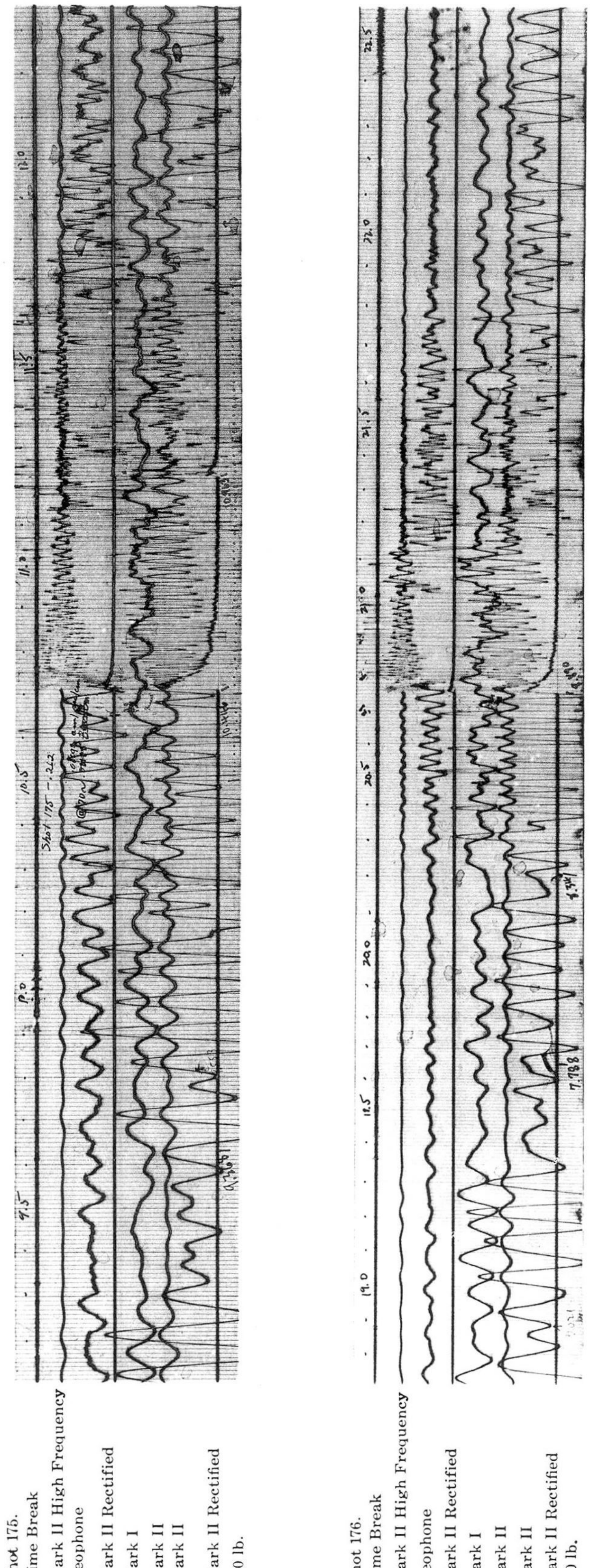


RECORDS AT JACKSONVILLE DEEP

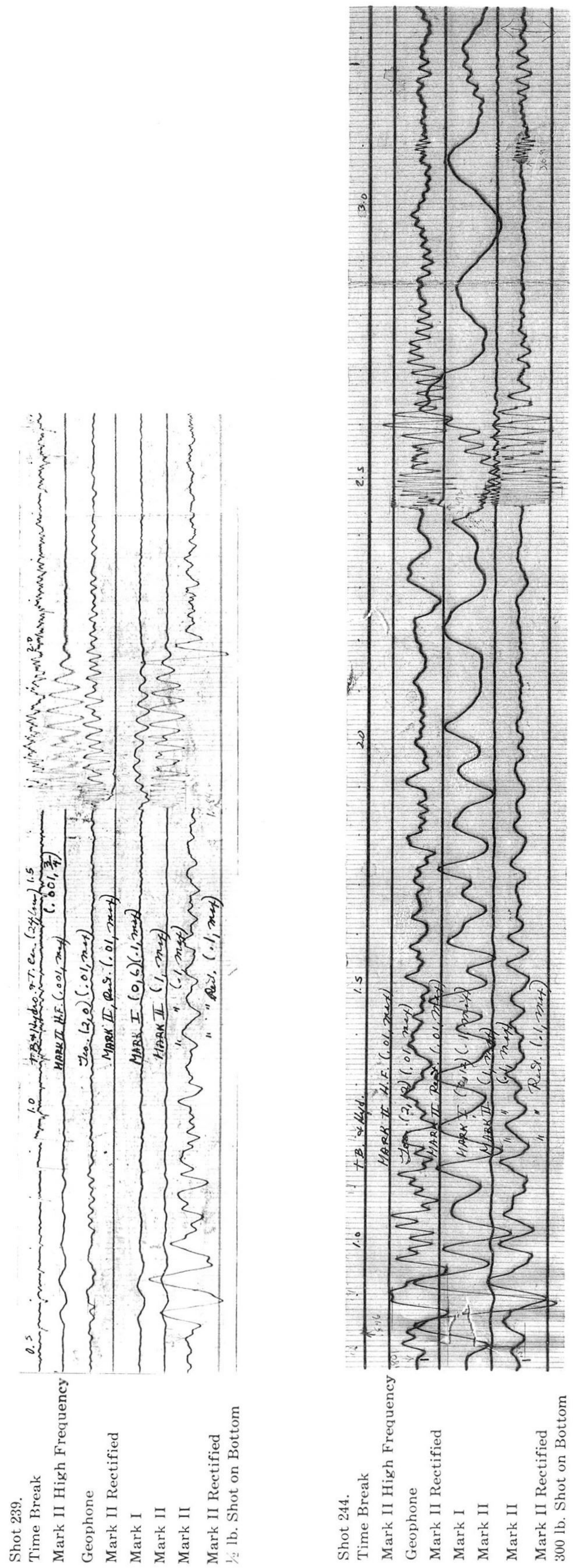


RECORDS AT VIRGIN ISLANDS SHOAL

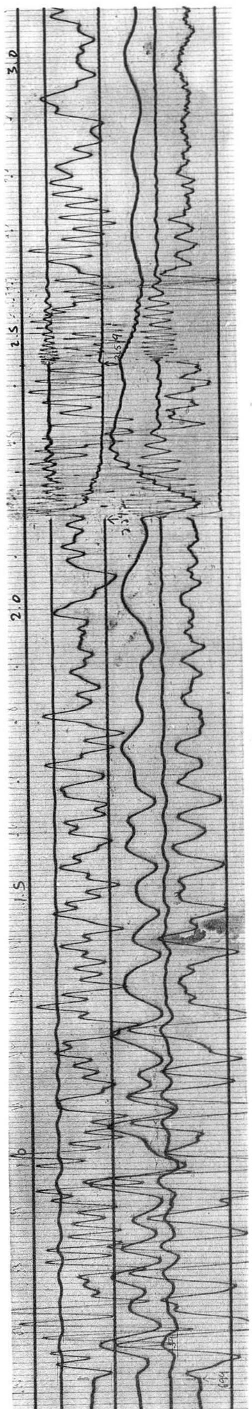

Shot 253.
Time Break
Mark II High Frequency
Geophone
Mark II Rectified
Mark I
Mark II
Mark II
Mark II Rectified
25 lb.

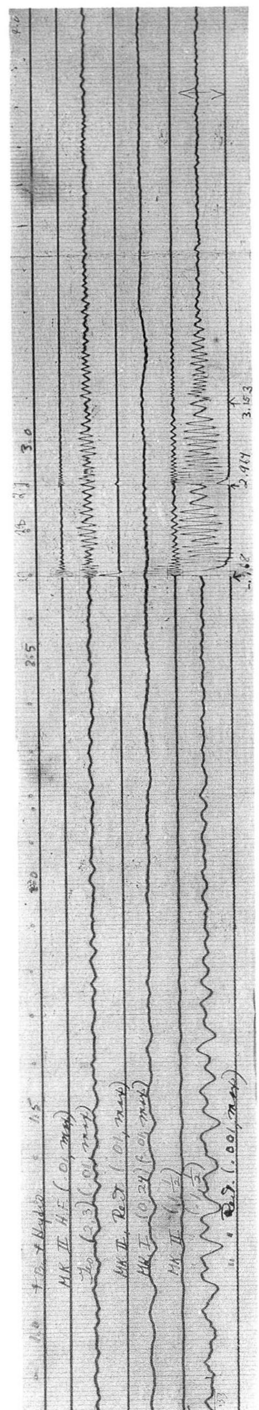

Shot 275.
Time Break
Mark II High Frequency
Geophone
Mark II Rectified
Mark I
Mark II
Mark II
Mark II Rectified
3½ lb. Shot Mid-depth

RECORDS AT VIRGIN ISLANDS SHOAL

is higher than in the high-pass systems, because in the case of the arrival of the *water wave* which is visibly rich in high frequencies it is the high-pass systems which respond earliest and most strongly. One is therefore driven to the conclusion that the ground wave is a low-frequency disturbance which starts gently with a weak amplitude, while the water wave is a high-frequency disturbance which builds up quickly to a considerable amplitude. *This is precisely what the normal-mode theory predicts, and is illustrated in Figs. 24A, 24, 25, 33, 34, 35, and 36.*

Another easily identifiable feature is the arrival time of the *water wave*. As mentioned above, this phase appears first and strongest on the Mark II rectified and the Mark II high-frequency traces. In Plate 1 the water wave arrives in shot 47 at $t = 1.679$ sec., in shot 48 at $t = 2.407$ sec., etc. It is clear from this and the other records that the arrival time of the water wave can be read with high precision off the Mark II rectified trace as well as off the Mark II high-frequency trace.

The data of the arrival times of the ground wave and the water wave can be utilized, by an application of standard-refraction methods used in geophysical prospecting, to gain information on the variation of sound velocity with depth in the bottom. Consider the case shown in Figure E in which the charge and receiver are beached on the bottom at $A$ and $D$, respectively, and where the bottom consists of a layer of thickness $h$ and sound velocity $c_2$ which is underlain by an infinite half-space of sound velocity $c_3$. Beyond ranges greater than $2h/\sqrt{(c_3/c_2)^2 - 1}$, the receiver will register

(a) the water wave which travels in the water along $AD$,

(b) a ground wave traveling along $AD$ in the bottom with speed $c_2$, and

(c) a ground wave traveling along the path $ABCD$, where the leg $BC$ is covered with the speed $c_3$ of the lower medium. At great ranges the first arrival is the ground wave ($c$), while at intermediate ranges the ground wave ($b$) is the first to arrive. The travel time of the ground wave ($b$) is simply $r/c_2$, while the travel time of ground wave ($c$) is the time required to cover the legs $AB$ and $CD$ with speed $c_2$ and the leg $BC$ with speed $c_3$:

$$t_{ABCD} = \frac{r}{c_3} + \frac{2h}{c_3}\sqrt{(c_3/c_2)^2 - 1} = t_w(c_1/c_3) + \tau, \tag{63}$$

$$\tau = \frac{2h}{c_3}\sqrt{(c_3/c_2)^2 - 1}, \tag{64}$$

where $t_w = r/c_1$ denotes the travel time of the water wave. If one now plots the arrival times of the ground waves versus the arrival times of the water waves, the points line up on two straight lines in the manner shown in Figure 1 for the shots made at Solomons Shoal. The first line, which passes close to the origin, shows that $c_2 = 1.15c_1$. The second line has a slope indicating that $c_3 = 1.79c_1$. From this plot one can also determine the thickness of the intermediate layer. According to Eq. (64) the intercept $\tau$ of the second line with the axis of ordinates is equal to $(2h/c_3)\sqrt{(c_3/c_2)^2 - 1}$. In Figure 1, $\tau = .345$ sec., $(c_3/c_2) = 1.79/1.15$, from which *one arrives at a value of 1280 feet for the thickness of the intermediate layer h.*

It will be noted (Fig. 1) that for $t_w > 2.6$ sec., the arrival times of the ground wave indicate the presence of a faster layer than the third at some greater depth.

From our conclusion that the layer of speed $1.15c_1$ is 1280 feet deep, which is more than 25 times the depth of water of 52 feet, it follows, in the light of the theory of normal modes in a three-layered liquid half-space, that the dispersion in the water wave at Solomons Shoal should be very nearly the same as if the intermediate layer extended to infinity. This is illustrated in Figures 29 and 31; when the thickness of the intermediate layer is 10 times the depth of water (cases 3.8 and 3.9), the dispersion due to the water-bottom discontinuity is very nearly the same as when the intermediate layer is of infinite thickness (cases VI and V). The above theoretical deduction is closely confirmed by the observed dispersion characteristics at Solomons Shoal. In fact, it will be shown in the next section that the records taken at Solomons Shoal offer a text-book experimental illustration of the normal-mode theory in a two-layered liquid half-space.

Another consequence of the theory of normal modes in a three-layered liquid half-space is that the dominant wave length in the ground wave which travels in the intermeidate layer along $AD$ should be less than the dominant wave length in the ground wave which takes the path $ABCD$ of Figure E. Referring to Figure 31, for example, the value of $\gamma(= H/\lambda)$ in the former is about 0.6, while in the latter $\gamma = .028$. This theoretical result is very well confirmed in Figure 1, in which the periods of the points marked by $\triangle$ are more than twice the periods of the points marked by $\odot$. The same characteristics are shown by the data in Figure 2, and to a lesser extent in Figure 3.

A refraction curve which is entirely different from the one obtained at Solomons Shoal is shown in Figure 4 for Virgin Islands Shoal. In both Figures 1 and 4, the closest refraction points begin at about 0.3 sec. travel time, but in Figure 4 all the points seem to line up along a straight line *which does not pass through the origin.* This last feature implies that between the water and the medium in which $c = 3.02c_1$ there is an intermediate layer of, probably, an intermediate sound velocity. The dispersion characteristics at Virgin Islands Shoal, shown in Figures 12, 13, 14, and 15, suggest, as will be explained later, that the speed of sound in the layer contiguous to the water is $1.05c_1$ to $1.1c_1$. With a value of the intercept on the axis of ordinates $(= \tau)$ in Figure 4 of about .029 sec., one derives from Eq. (64) a value for the thickness of the intermediate layer of about 80 feet in either case. On the basis of the refraction data and aided by the indications from the dispersion data in the water wave, we thus deduce that the bottom at Virgin Islands Shoal is made up of

(a) a top layer of a thickness of the order of the depth of water (= 70 feet) in which the velocity of sound is about $1.05c_1$ to $1.1c_1$, and

(b) an underlying medium in which the velocity of sound is $3.02c_1$. The structure of the bottom at Virgin Islands Shoal (as well as in Virgin Islands Deep) therefore differs from the structure of the bottom in Solomons Shoal, which is characterized by a thickness of the intermediate layer of speed $1.15c_1$ of more than 25 times the depth of water. The difference in structure of the bottoms in the two stations carries with it a very important theoretical consequence which is strikingly confirmed by the observations, namely, that the *ground wave at Virgin Islands Shoal* (*as well as*

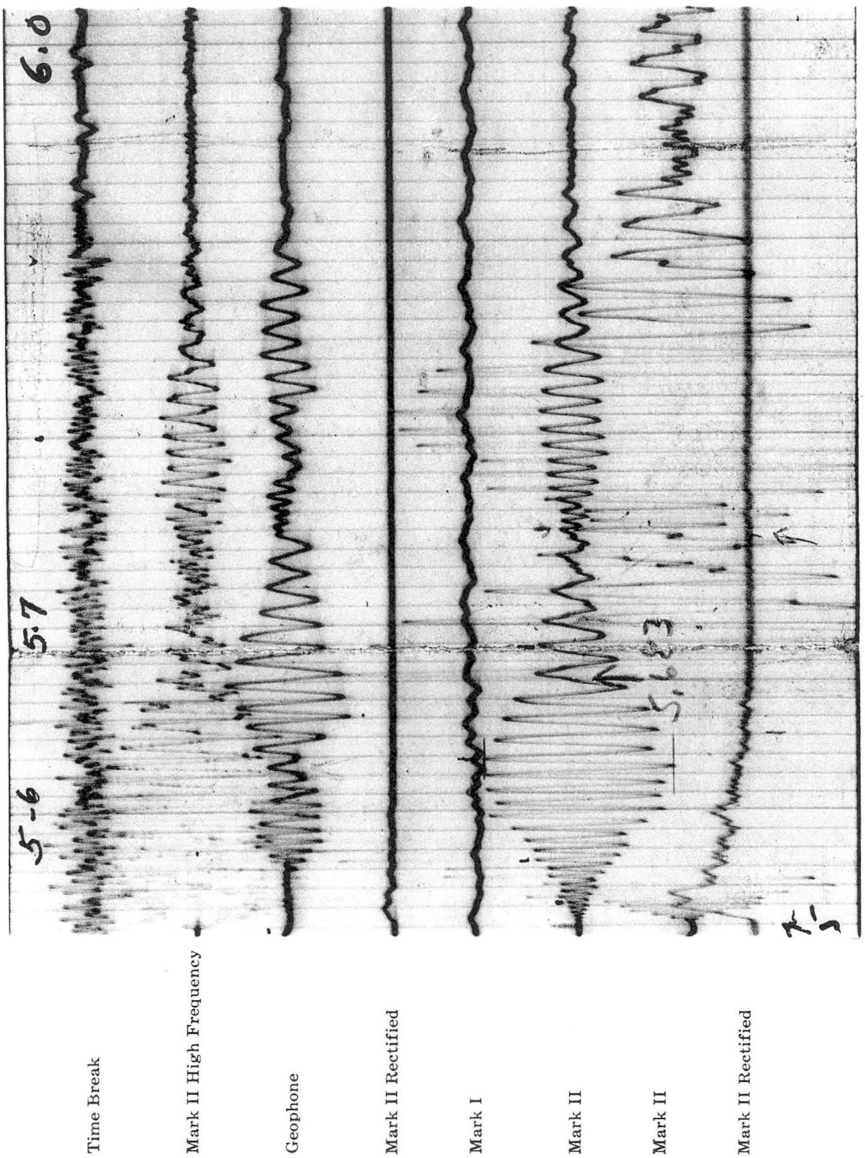


DISPERSION IN WATER WAVE

Shot No. 91, Jacksonville Shoal. Depth of water, 60 feet; charge weight, 5 lbs. Charge and hydrophone beached on bottom.

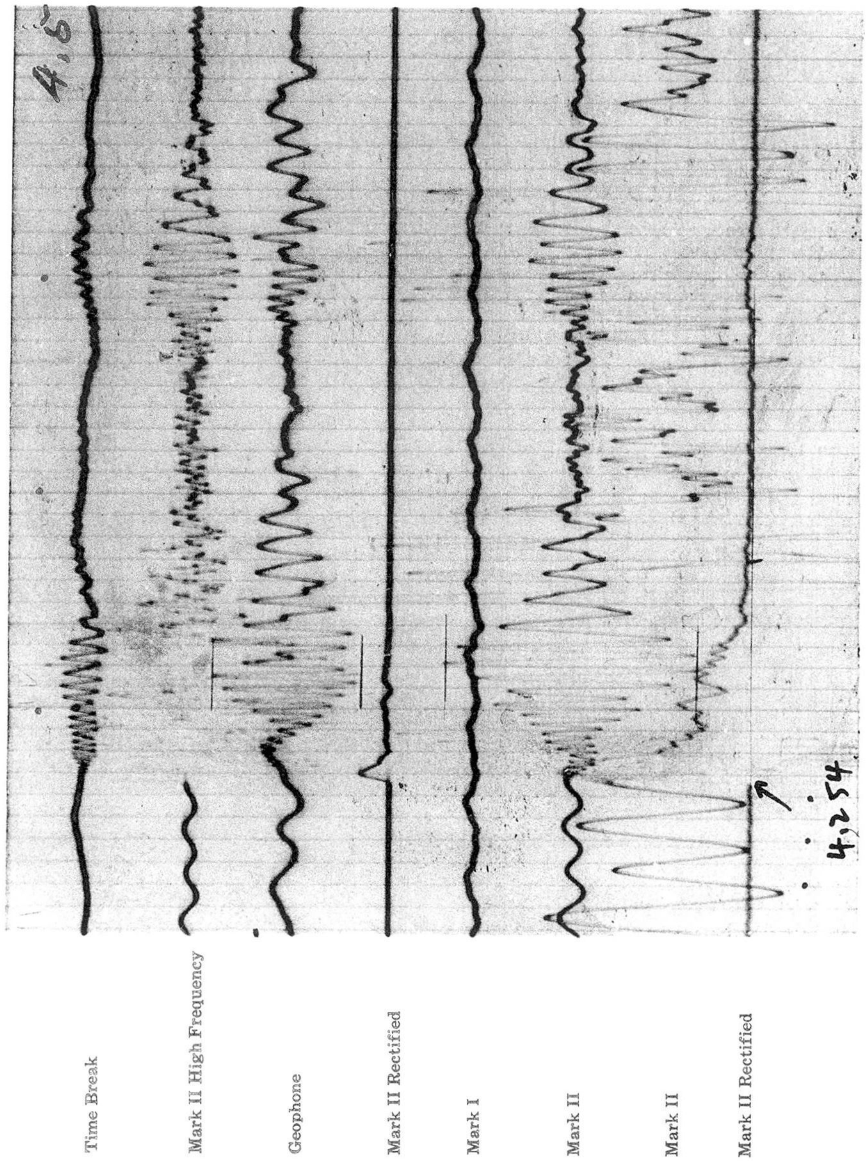


DISPERSION IN WATER WAVE AND RIDER WAVE

Shot No. 90, Jacksonville Shoal. Depth of water, 60 feet; charge weight, 5 lbs. Charge and hydrophone beached on bottom.

*at Virgin Islands Deep) should be relatively weak in secondary arrivals and in the so-called "rider" wave.* This will be discussed in a later section.

To complete the discussion of the refraction data, we find that the observed points at Jacksonville Shoal (Fig. 2) are too few during the first second of arrival time to allow any conclusions to be drawn about the structure of the top layer in the bottom. The refraction data for Jacksonville Deep shown in Figure 3 display a complicated array of *secondary arrivals*, some of which may not be real. However, concentrating our attention on the first arrivals only, we may assume that the points during the first second of arrival time line up along the $(c/c_1) = 1.14$ line which passes through the origin, and that from 1 to 3.5 secs. arrival time the points fall on the $(c/c_1) = 2.13$ line. The intercept of the latter line with the axis of ordinates is 0.36 sec. $(= \tau)$, and from Eq. (64) one infers that *at Jacksonville Deep the thickness of the intermediate layer in which* $(c/c_1) = 1.15$ *is about 1200 feet.*

The refraction data for Virgin Islands Deep (Fig. 5) are too meager for any definite conclusions. The indicated structure of the bottom is very much like that of Virgin Islands Shoal. Taking the value of $\tau$ as 0.05 sec., one finds that the thickness of an intermediate layer in which $(c/c_1) = 1.05$ or 1.1 is from 140 to 150 feet.

## II. THE EWING EFFECT

The phenomenon of dispersion in the water wave which was discovered by Ewing and which is illustrated on Plates 10 and 11 has already been discussed. It was explained how from a record such as the third trace from the bottom on Plate 10 one can determine the times of arrival $T$ of the various frequencies, and it was also pointed out that when $(T - T_0)/T_0$ is plotted against $\gamma(= H/\lambda)$, where $T_0$ denotes the arrival time of the water wave, the observed points align themselves along a single curve, *independently of the range* (Figs. 6–19). We shall now take up the question of the possible interpretation, in terms of the structure of the bottom, which one can give to the mean dispersion curve obtained at a given station.

Figures 6–19 contain a background of theoretical dispersion curves for various assumed uniform bottoms in which the sound velocity ranges from $1.05c_1$ to $3c_1$, and also for three cases in which the bottom is composed of two layers. The maximum ordinate on the curves corresponds to the epoch of the Airy phase; the branch of the curve to the right of the maximum represents dispersion in the water wave, while the branch of the curve to the left of the maximum represents the slight dispersion in the ground wave (Fig. 24). It will be noted that the vertical separation of the curves in the water-wave branch is greatest between the cases $(c_2/c_1) = 1.05$ and $(c_2/c_1) = 1.1$, and that for high values of $(c_2/c_1)$ the dispersion curves becomes insensitive to changes in $(c_2/c_1)$. In case of a bottom consisting of a layer of thickness $h$ in which $c = 1.1c_1$ and an underlying infinite layer of $c = 3.0c_1$, the curve —— · —— · ——, in which $h = H$, is seen to coincide with the $(c_2/c_1) = 1.1$ curve for all $\gamma > 1.3$, showing that, as far as dispersion in the water wave at these frequencies is concerned, this composite bottom is indistinguishable from one in which the intermediate layer extends to infinity. On the other hand, the curve —— ·· —— ·· —— shows that in case of the thinner intermediate layer $(h = 0.1H)$, the dispersion in the water wave deviates significantly both from the $(c_2/c_1) = 1.1$ and the $(c_2/c_1) =$

3.0 curves in the practically relevant range of $\gamma = 1$ to $\gamma = 6$. The variation of group velocity with frequency ($\gamma$) in the above-mentioned three-layered media is shown in Figure 32 by curves 3.7 and 3.3, respectively.

If the observed dispersion points line up along one of the theoretical curves for a two-layered medium, then that furnishes evidence that the layer contiguous to the water is of the corresponding sound velocity. From the previous discussion it is however clear that this value of sound velocity need not obtain at great depth, that the dispersion for high frequencies is controlled by the properties of the bottom in a rather thin layer next to the water. The physical reason for this can be seen in Figs. 45–48 which show that at high frequencies very little of the energy of the first mode is contained inside the bottom. We therefore cannot expect to obtain information on the structure of the deep layers from an analysis of dispersion data of a wave which hardly penetrates to those layers. As a measure of the *depth of penetration* of the first mode into the bottom, we can take a layer at the top of the bottom in which is contained 99 per cent of the total energy in the bottom. The significance of the depth of penetration is that *no information on the structure of the bottom at greater depths* can be obtained from dispersion data. Curves of depth of penetration are plotted vs. $\gamma$ in Figures 6–19. To illustrate the use of these curves, let us assume that the observed points fall on the $(c_2/c_1) = 1.05$ curve for all values of $\gamma > 4.0$. The corresponding depth of penetration is $0.32H$, implying that the evidence that the velocity in the bottom is $1.05c_1$ pertains only to a top layer of about one third of the depth of water at the most. Curve —— —— —— shows that, when $h = \frac{1}{2}H$, the dispersion for $\gamma > 4$ is practically indistinguishable from the $(c_2/c_1) = 1.05$ curve, in agreement with the above deduction.

As a further illustration of the application of the depth-of-penetration curves to the interpretation of dispersion data which *cross* the theoretical curves for uniform bottoms, consider the —— —— —— curve. As was pointed out above, the fact that this curve hugs the 1.05 curve for $\gamma > 4$ can be interpreted to mean that in a top layer of the bottom extending to a depth of not more than about one third of the depth of water the sound velocity is $1.05c_1$. Again, from the fact that the —— —— —— curve lies below the 1.1 curve for all $\gamma > 1.4$, we may infer that in a top layer of the bottom extending to a depth of not more than $0.72H$ the mean sound velocity is about $1.1c_1$. This is actually true of the mean velocity down to that depth. Similarly the —— · —— · —— curve indicates that in a top layer of the bottom of about nine tenths the depth of water $c = 1.1c_1$, which is exactly true. On the other hand, the crossing of the —— ·· —— ·· —— and the 1.3 curves at $\gamma = 2.5$ would imply, according to the above rule, that the mean velocity in a top layer of the bottom of about one quarter the depth of water is less than 1.3, whereas the actual mean velocity in such a layer is close to 2. The discrepancy in this case arises from the large contrast in sound velocity (1.1 vs. 3) between the intermediate layer and the bottom layer plus the fact that the "depth of penetration" is heavily biased by the properties of the topmost section of the layer on account of the exponential decrease of amplitude with depth in the bottom.

It appears from the preceding discussion that in the case when the observed dispersion curve crosses the theoretical dispersion curves for uniform bottoms, one can infer with fair accuracy from the points of intersection the mean velocity through a top layer of a thickness equal to the "depth of penetration", except in cases when the velocity varies extremely rapidly with depth.

In Table 1 are set out the conclusions about the structure of the bottom at the various stations, which can be drawn on the basis of the mean dispersion curves alone.

TABLE 1.—*Evidence on the structure of the bottom deduced from dispersion data*

H = depth of water; D.o.P. = Depth of Penetration (*see* Figure 6); $c_2$ = inferred mean sound velocity in a top layer of the bottom of thickness D.o.P. A slanting dispersion curve means one which crosses the theoretical dispersion curves for uniform bottoms.

| Place | Fig. | $c_2/c_1$ | D.o.P. | $c_2/c_1$ | D.o.P. | $c_2/c_1$ | D.o.P. | H in feet | Nature of mean dispersion curve |
|---|---|---|---|---|---|---|---|---|---|
| Solomons Shoal | 6 | 1.2 | .53H | | | | | 52 | not slanting |
| | 7 | 1.2 | .53H | | | | | | not slanting |
| Jacksonville Shoal | 8 | 1.05 | .42H | 1.1 | 1.2H | | | 60 | slanting strongly |
| | 9 | 1.05 | .56H | 1.1 | 1.4H | | | | slanting strongly |
| Jacksonville Deep | 10 | 1.1 | .18H | 1.2 | .3H | 1.4 | .5H | 115 | slanting slightly |
| | 11 | | | 1.2 | .25H | 1.3 | .7H | | slanting slightly |
| Virgin Islands Shoal | 12 | 1.05 | .45H | 1.1 | .50H | 1.2 | .63H | 70 | slanting strongly |
| | 13 | 1.05 | .45H | 1.1 | .63H | 1.2 | .80H | | slanting strongly |
| | 14 | 1.075 | .45H | 1.1 | .48H | 1.2 | .52H | | slanting strongly |
| | 15 | 1.075 | .36H | | | | | | |
| Virgin Islands Deep | 16 | 1.05 | .37H | 1.1 | .45H | 1.3 | .45H | 140 | slanting strongly |
| | 17 | 1.05 | .45H | 1.1 | .46H | 1.3 | .46H | | slanting strongly |
| | 18 | 1.05 | .37H | 1.1 | .38H | | | | slanting strongly |

The observed dispersion points for Solomons Shoal shown in Figures 6 and 7 are confined between the 1.1 and 1.3 theoretical curves, and they show no systematic tendency to cross these curves. One can therefore infer from the dispersion data that the mean sound velocity in the top 25 feet of the bottom at this station is about $1.2c_1$. The fact that the mean dispersion curve shows no tendency toward "crossing" would suggest also that the bottom is uniform down to a greater depth, although strictly speaking any inference about the structure of the bottom below the depth of penetration is risky. These conclusions agree with the evidence from the refraction data for this station (Fig. 1)—namely, that in the top 1280 feet of the bottom the sound velocity is uniform and equal to $1.15c_1$.

The dispersion data for Jacksonville Shoal (Figs. 8, 9) are quite different from the data for Solomons Shoal. In the former station there is definite evidence that the mean sound velocity in the top 30 feet of the bottom is about $1.05c_1$ and that the mean sound velocity in the first 80 feet is about $1.1c_1$. The indicated increase of velocity with depth is also evidenced by the "slanting" of the mean dispersion curve.

The refraction data for Jacksonville Shoal (Fig. 2) (during the first second of travel time) are too meager to allow any conclusions to be drawn about the structure of the first 100 feet of the bottom.

The evidence from the dispersion data for Jacksonville Deep (Figs. 10, 11) is that the mean velocity in the first 30 feet is about $1.2c_1$ and that the mean velocity in the first 70 feet is about $1.35c_1$. The slanting tendency is rather slight, suggesting a uniform velocity down to considerable depth. These conclusions are in conformity with the evidence from refraction data shown in Figure 3—namely, that an intermediate layer in which $c/c_1$ is about 1.14 extends down to 1200 feet. The value of 1.14 for $c/c_1$ is not so well determined as in Figure 1 for Solomons Shoal; there is indeed an indication of curvature in the observed points, and a mean value of $(c/c_1) = 1.35$ in the first 70 feet is not only not excluded but is even suggested by the data.

The dispersion data for Virgin Islands Shoal and Virgin Islands Deep are of a similar nature. There is a strong slanting tendency, indicating rapid variation of sound velocity with depth. This is also indicated by the slow variation of the D.o.P. values (Table 1). As was explained, the inference that an intermediate layer of the order of the depth of water in which $(c/c_1) \simeq 1.1$ intervenes between the water and the high speed base of $(c/c_1) = 3.02$ agrees with the refraction data as well as with the general character of the ground wave at these stations.

## III. THE RIDER WAVE, AIRY WAVE, AND LIMITING WAVE LENGTHS

While the interpretation of the first arrivals by the refraction method and the interpretation of the dispersion in the water wave by the theory of group velocity of normal modes are known procedures in practical and theoretical Geophysics, the discovery of the features of the pressure records to be discussed presently is entirely new and was made by the writer during a systematic analysis of *all* the predictions of the theory.

One consequence of the theory of normal modes is illustrated in Figure D—namely, that the high-frequency water wave should be superimposed not on a quiescent base line but on the low-frequency ground wave. The water wave should therefore appear "riding" on a low-frequency wave in the manner illustrated in Figures 25 and 24A. While this "rider wave" may be masked by the striking features of the water wave, it should be distinct and measurable just prior to the arrival of the water wave. Furthermore, it follows from the theory that the *frequency $f_R$ of the rider wave* at the instant of arrival of the water wave is determined by the depth of water and the structure of the bottom. In Figure 37 the curve $\gamma_R$ gives the variation of $(H/\lambda_R)$ with the sound velocity in the bottom in case of a uniform bottom.

Another consequence of the theory which is also illustrated in Figure D is that for a given structure of the bottom the ground wave should begin with a characteristic "*limiting frequency*" $f_L$. The dependence of $\gamma_L = H/\lambda_L$ on the structure of the bottom in case the latter is uniform is shown in Figure 37. Still a third identifiable feature which is predicted by theory is that with time the frequency in the water wave should decrease while the frequency in the ground wave should increase until the two coincide at the so-called *Airy frequency* $f_A$ which again is characteristic of the structure of the bottom. The amplitude of the water wave reaches a maximum near the time of arrival of the Airy frequency and decreases thereafter while the frequency remains constant (Figs. 25, 26).

The pressure records of all the shots were searched by the writer for the three features mentioned above, and satisfactory results were obtained. The *rider wave* can be seen on most of the records in Plates 1–7. In Plate 1 shot No. 47, for example, the rider wave of a period of 0.014 sec. is seen clearly on the Mark II low-frequency traces between $t$ = 1.6 sec. (on the time scale appearing at the top of the record)

TABLE 2.—*Characteristics of ground waves and water waves in Solomons Shoal*

The charge was placed on the bottom in shots 40 to 49 and in shot 63; it was suspended at a depth of 25 feet in shots 56 to 62. The hydrophone was located on the bottom in all shots. The Airy Period could not be determined in most records due to insufficient dispersion at the relatively small ranges. In shot No. 48 the Airy Period was 0.012 sec., and $\bar{H}/\lambda$ was 0.89. The Limiting Period waves are believed to be those of longest period associated with the discontinuity between the water and the bottom.

| Shot No. | Water depth near charge | Water depth near hydrophone | "Mean" water depth $\bar{H}$ | Ground Waves | | | | | | Rider Wave | | Water wave arrival time | Charge Weight |
|---|---|---|---|---|---|---|---|---|---|---|---|---|---|
| | | | | Longest Period | $\bar{H}/\lambda$ | Period | $\bar{H}/\lambda$ | Limiting period | $\bar{H}/\lambda$ | Period | $\bar{H}/\lambda$ | | |
| | *ft.* | *ft.* | *ft.* | *Sec.* | | *Sec.* | | *Sec.* | | *Sec.* | | *Sec.* | *lbs.* |
| 40 | 51 | 52 | 51.5 | | | .073 | .14 | | | .015 | .70 | .672 | 0.5 |
| 41 | 51 | 52 | 51.5 | | | | | .021 | .50 | .0155 | .67 | .954 | 0.5 |
| 42 | 49 | 52 | 50.5 | | | .080 | .13 | | | .014 | .73 | 1.286 | 0.5 |
| 43 | 49 | 52 | 50.5 | | | .075 | .14 | | | | | 2.580 | 0.5 |
| 45 | 48 | 52 | 50 | | | | | .025 | .41 | .0145 | .70 | .616 | 5 |
| 46 | 51 | 52 | 51.5 | | | .063 | .17 | .029 | .36 | | | 1.203 | 5 |
| 47 | 50 | 52 | 51.5 | | | .067 | .16 | | | .014 | .74 | 1.679 | 5 |
| 48 | 53 | 52 | 52.5 | .087 | .12 | .067 | .16 | | | .015 | .71 | 2.407 | 5 |
| 49 | 49 | 52 | 50.5 | .088 | .12 | | | | | | | 2.874 | 5 |
| 56 | 53 | 55 | 54 | | | | | .035 | .31 | | | .605 | 5 |
| 58 | 53 | 55 | 54 | | | | | .024 | .46 | .016 | .69 | .899 | 0.5 |
| 59 | 53 | 55 | 54 | | | | | .024 | .46 | .015 | .73 | .878 | 5 |
| 60 | 53 | 55 | 54 | | | | | .031 | .35 | .015 | .73 | 1.222 | 5 |
| 61 | 53 | 55 | 54 | | | | | .029 | .38 | .015 | .73 | 1.198 | 0.5 |
| 62 | 53 | 55 | 54 | | | | | .030 | .37 | .013 | .84 | .595 | 25.5 |
| 63 | 53 | 55 | 54 | | | | | .036 | .30 | .016 | .69 | .664 | 25.5 |
| Average | 51 | 53 | 52 | .0875 | .12 | .071 | .15 | .028 | .39 | .015 | .72 | | |

and the arrival of the water wave. In shot No. 48 (Pl. 1) the rider wave appears clearly after $t$ = 2.35 sec. on the lower (sensitive) Mark II low-frequency trace. On Plate 4, shot No. 94, the same traces register the rider wave just prior to the arrival of the water wave: and similarly in shot No. 97 and so on. In the last two shots one can see that the frequency in the rider wave increases with time, $f_R$ being determined by the value of the frequency just prior to the arrival of the water wave. The rider waves in these shots are preceded by trains of long waves which are characteristic of the deep structure in the bottom. In shots 58, 59, 60, and 61 (Pls. 2, 3) however, the rider waves appear to continue all the way back to the beginning of the ground wave. Leaving out the first swing or so in the ground wave, one can read off these records the frequency in the *beginning* of the rider wave and identify it with the *limiting frequency* $f_L$. This was done on all the records taken at Solomons Shoal, and the results are shown in Table 2.

It is seen that the mean value of .72 for $\gamma_R (= H/\lambda_R)$ is determined with little scatter. Referring to Figure 37, we find that on the assumption of a uniform bottom, the corresponding value of the sound velocity in the bottom is $1.09c_1$. This compares well with the values of $1.15c_1$ and $1.2c_1$ deduced from the refraction data and the dispersion data, respectively.

The mean value of 0.39 for $\gamma_L$ is subject to greater uncertainty. By Figure 37 this value corresponds to a sound velocity in the bottom equal to $1.29c_1$. Since the limiting frequency is more sensitive to the structure in deep layers than is the rider frequency (*see* Figures 38, 29, and 31), we may consider this value satisfactory.

On account of the small ranges used at this station, the Airy period could not be determined with sufficient accuracy in most of the records. In the one shot (No. 48) in which the Airy period was measurable, a value of $\gamma_A = 0.89$ was obtained, and this corresponds to a sound velocity of $1.1c_1$ in the bottom (Fig. 37).

(It is perhaps appropriate to relate here an incident which occurred during the analysis of the records taken at Solomons Shoal and which helped to increase the writer's confidence in the theoretical interpretation. Plots of dispersion data from shots Nos. 58–62 gave unreasonable dispersion curves, which were out of line with the dispersion curves from the other shots. The same discrepancy was shown in the values of $\gamma_L$ and $\gamma_R$. Since the records exhibited qualitatively all the expected features, the anomaly proved disturbing. The only possible explanation appeared to be an error in the quoted value of 25 feet for the depth of water. A check with Ewing revealed that this value for the depth appearing in the report by him and Worzel is wrong; the correct value is 53 feet.)

Some records taken at Jacksonville Shoal are reproduced on Plates 4 and 5 and the results of the analysis of all the records at this station are given in Table 3. On account of the larger ranges involved, the ground wave and the other phases are more fully developed than at Solomons Shoal. At this station it was possible to measure the Airy period as well as the rider period. The mean values $\gamma_R = .53$ and $\gamma_A = .90$ correspond to sound velocities in a uniform bottom of $1.17c_1$ and $1.10c_1$. Though the refraction data at Jacksonville Shoal are insufficient for a determination of the sound velocity in the top layers of the bottom, we may assume that the value of $(c/c_1) = 1.15$ obtained for the adjacent station of Jacksonville Deep is applicable also for the Shoal. The dispersion data for Jacksonville Shoal indicate that the mean velocity in the top 30 feet of the bottom is about $1.05c_1$ and that the mean velocity in the top 80 feet is about $1.1c_1$. The evidence from the various sources about the structure of the top layers of the bottom is therefore in good agreement. We shall not take up here the interpretation of the various phases of the *ground waves* because these depend on the detailed structure of the deep layers in the bottom, and, as will appear later, their theory is much more involved.

Some records for Jacksonville Deep are shown on Plates 6 and 7, and the results of the analysis of all the records obtained at this station are given in Table 4. The depth of water at this station is 115 feet as compared with 60 feet at Jacksonville Shoal, and the mean value of the period of the rider wave is found to be .038 sec. as compared with the value of .023 at Jacksonville Shoal. *Since the dispersion data* (see Table 1) *indicate that the bottoms at the two stations are similar in structure* (the

TABLE 3.—*Characteristics of ground waves and water waves in Jacksonville Shoal*

The charge was placed on the bottom in shots 76 to 101, and was suspended at a depth of 25 feet in shots 103 to 117. The hydrophone was located on the bottom in all the shots.

| Shot No. | Water depth near charge | Water depth near hydrophone | "Mean" water depth $\bar{H}$ | Ground Waves | | | | Rider Wave | | Airy Wave | | Water-wave arrival time | Charge weight |
|---|---|---|---|---|---|---|---|---|---|---|---|---|---|
| | | | | Period | $\bar{H}/\lambda$ | Period | $\bar{H}/\lambda$ | Period | $\bar{H}/\lambda$ | Period | $\bar{H}/\lambda$ | | |
| | *ft.* | *ft.* | *ft.* | *Sec.* | | *Sec.* | | *Sec.* | | *Sec.* | | *Sec.* | *lbs.* |
| 76 | 54 | 62 | 58 | .070 | .17 | | | .025 | .47 | | | .857 | 0.5 |
| 79 | 61 | 62 | 61.5 | .078 | .16 | | | .0234 | .53 | .019 | 65 | 2.472 | 0.5 |
| 80 | ? | 62 | ? | | | .0570 | ? | .0230 | ? | .020 | ? | 2.700 | 0.5 |
| 81 | 52 | 62 | 57 | | | .057 | .20 | .0223 | .51 | .011 | 1.0 | 3.247 | 0.5 |
| 82 | 59 | 62 | 60.5 | | | | | .0230 | .53 | .012 | 1.0 | 1.991 | 0.5 |
| 83 | 59 | 62 | 60.5 | .070 | .17 | | | .022 | .55 | | | 1.376 | 0.5 |
| 84 | 51 | 62 | 56.5 | | | | | .0225 | .51 | | | 1.060 | 0.5 |
| 85 | 59 | 62 | 60.5 | | | .0556 | .218 | .022 | .55 | | | 1.095 | 5 |
| 86 | 59 | 62 | 60.5 | | | .0570 | .213 | .023 | .53 | | | 1.758 | 5 |
| 87 | 55 | 62 | 58.5 | | | .051 | .23 | .0235 | .50 | | | 2.331 | 5 |
| 88 | 55 | 62 | 58.5 | | | | | .022 | .54 | .013 | .91 | 2.829 | 5 |
| 89 | 53 | 62 | 57.5 | | | .057 | .20 | .0224 | .52 | .012 | .96 | 3.404 | 5 |
| 90 | 53 | 62 | 57.5 | | | .055 | .210 | .0210 | .55 | .0123 | .94 | 4.254 | 5 |
| 91 | 61 | 60 | 60.5 | | | .0554 | .220 | .024 | .51 | .014 | .87 | 5.555 | 5 |
| 92 | 59 | 60 | 59.5 | .077 | .16 | .0580 | .206 | | | .013 | .92 | 7.144 | 25 |
| 93 | 59 | 60 | 59.5 | | | | | .0235 | .51 | .015 | .80 | 5.875 | 25 |
| 94 | 59 | 60 | 59.5 | .068 | .18 | .061 | .196 | .0233 | .51 | .015 | .80 | 4.505 | 25 |
| 95 | 59 | 60 | 59.5 | | | .056 | .214 | .0250 | .48 | | | 2.569 | 25 |
| 96 | 55 | 60 | 57.5 | .082 | .14 | | | .024 | .48 | | | 1.407 | 25 |
| 97 | 62 | 60 | 61 | .068 | .18 | | | .0245 | .50 | .017 | .72 | 2.683 | 300 |
| 98 | 60 | 60 | 60 | .0686 | .18 | .0554 | .218 | | | .0135 | .89 | 5.525 | 300 |
| 101 | 59 | 60 | 59.5 | .073 | .16 | | | | | .0125 | .96 | — | 300 |
| 103 | 53 | 63 | 58 | | | | | .020 | .59 | | | .565 | 0.5 |
| 105 | 54 | 63 | 58.5 | | | | | .024 | .49 | .011 | 1.1 | 1.903 | 0.5 |
| 106 | 54 | 63 | 58.5 | | | .061 | .193 | .023 | .51 | .013 | .91 | 1.716 | 0.5 |
| 107 | 65 | 63 | 64 | | | .0530 | .243 | | | .012 | 1.1 | 3.003 | 0.5 |
| 109 | 65 | 63 | 64 | | | .0516 | .249 | .020 | .64 | | | 4.849 | 0.5 |
| 110 | 61 | 63 | 62 | | | .052 | .239 | | | | | 6.253 | 0.5 |
| 111 | 61 | 63 | 62 | | | .055 | .226 | | | | | 6.493 | 25 |
| 112 | 64 | 63 | 63.5 | | | .0552 | .231 | .0238 | .54 | .016 | .80 | 5.017 | 5 |
| 113 | 64 | 63 | 63.5 | .0658 | .19 | .0566 | .225 | .0218 | .58 | .015 | .85 | 3.602 | 25 |
| 114 | 67 | 63 | 65 | | | | | .022 | .59 | .015 | .87 | 2.512 | 5 |
| 115 | 67 | 63 | 65 | | | .058 | .225 | .022 | .59 | | | 1.135 | 5 |
| 117 | 67 | 63 | 60 | | | .057 | .213 | | | .013 | .94 | 5.429 | 5 |
| Average | 59 | 62 | 60 | .072 | .17 | .056 | .22 | .023 | .53 | .014 | .90 | | |

one in the Deep is only slightly faster), *the observed approximate agreement between the ratio of the rider wave periods (1.7) and of the depths of water at the two stations (1.9) is a striking confirmation of the theory.* From the mean value of 0.62 for $\gamma_A$, which

TABLE 4.—*Characteristics of ground waves and water waves in Jacksonville Deep*

The charge was placed on the bottom in shots 123 to 159 and was suspended at a depth of 50 feet in shots 160 to 174. The hydrophone was located on bottom in all shots. The Airy Period could not be determined precisely in most records due to insufficient dispersion at the large depth. In shots 175 and 176 the Airy Periods were .023 and .025 sec., giving values of $\bar{H}/\lambda$ of 1.0 and .93, respectively. The ground waves were arbitrarily segregated into two groups of about 0.1 sec. and .08 sec., respectively.

| Shot No. | Water depth near charge | Water depth near hydro-phone | "Mean" water depth $\bar{H}$ | Ground Waves | | | | Rider Wave | | Water-wave arrival time | Charge weight |
|---|---|---|---|---|---|---|---|---|---|---|---|
| | | | | Period | $\bar{H}/\lambda$ | Period | $\bar{H}/\lambda$ | Period | $\bar{H}/\lambda$ | | |
| | *ft.* | *ft.* | *ft.* | *Sec.* | | *Sec.* | | *Sec.* | | *Sec.* | *lbs.* |
| 123 | 116 | 119 | 117.5 | | | | | .042 | .56 | 1.195 | 0.5 |
| 124 | 115 | 119 | 117 | | | .082 | .29 | | | 1.752 | 0.5 |
| 125 | 114 | 119 | 116.5 | | | .080 | .29 | .042 | .562 | 2.334 | 0.5 |
| 126 | 114 | 119 | 116.5 | | | .082 | .29 | .044 | .53 | 3.074 | 0.5 |
| 127 | 112 | 119 | 115.5 | .088 | .26 | .076 | .32 | .036 | .65 | 3.802 | 0.5 |
| 130 | 114 | 119 | 116.5 | .09 | .26 | | | .035 | .67 | 7.488 | 0.5 |
| 131 | 115 | 119 | 117 | .095 | .25 | .079 | .30 | .041 | .57 | 7.640 | 4.5 |
| 134 | 113 | 119 | 116 | .115 | .20 | | | .037 | .63 | 5.974 | 4.5 |
| 135 | 115 | 119 | 117 | .112 | .21 | | | .038 | .63 | 5.413 | 4.5 |
| 143 | 113 | 119 | 116 | .092 | .25 | | | .037 | .63 | 1.829 | 4.5 |
| 144 | 112 | 119 | 115.5 | .09 | .26 | | | .037 | .63 | 2.553 | 4.5 |
| 146 | 106 | 119 | 112.5 | .113 | .20 | .087 | .26 | .038 | .59 | 2.624 | 4.5 |
| 147 | 106 | 119 | 112.5 | .093 | .24 | | | .041 | .55 | 2.042 | 4.5 |
| 149 | 106 | 119 | 112.5 | .094 | .24 | | | | | 5.283 | 25 |
| 150 | 113 | 119 | 116 | .114 | .20 | | | .036 | .64 | 4.269 | 25 |
| 151 | 115 | 119 | 117 | .098 | .24 | | | .038 | .62 | 3.096 | 25 |
| 155 | 115 | 119 | 117 | | | .082 | .29 | .034 | .69 | 3.164 | 300 |
| 156 | 112 | 119 | 110.5 | .108 | .21 | | | .037 | .61 | 6.171 | 300 |
| 157 | 115 | 119 | 117 | .102 | .23 | | | .038 | .63 | 9.632 | 300 |
| 158 | 107 | 119 | 113 | .093 | .25 | .086 | .27 | .038 | .61 | 12.409 | 300 |
| 159 | 115 | 119 | 117 | .093 | .25 | .086 | .27 | .036 | .65 | 15.675 | 300 |
| 160 | 111 | 119 | 115 | .092 | .25 | .086 | .27 | .039 | .60 | 7.638 | 0.5 |
| 161 | 111 | 119 | 110 | .091 | .24 | | | .038 | .59 | 6.294 | 0.5 |
| 162 | 112 | 119 | 110.5 | .096 | .23 | .086 | .26 | .037 | .61 | 6.313 | 0.5 |
| 171 | 111 | 119 | 115 | .10 | .23 | | | .035 | .66 | 4.296 | 25 |
| 173 | 107 | 119 | 113 | | | .079 | .29 | .036 | .63 | 5.470 | 4.5 |
| 174 | 113 | 119 | 116 | .093 | .25 | | | .037 | .62 | 6.704 | 25 |
| 175* | 113 | 119 | 116 | .10 | .23 | .089 | .26 | .034 | .69 | 10.446 | 300 |
| 176* | 113 | 119 | 116 | .10 | .23 | .086 | .27 | .0365 | .64 | 8.890 | 300 |
| Average | 112 | 119 | 115 | .098 | .235 | .083 | .28 | .038 | .62 | | |

* Charge depth = 75 feet.

is seen to show little scatter, one deduces a value of $1.12c_1$ for the sound velocity in a uniform bottom. This is in agreement with the value of $1.14c_1$ deduced from the refraction data and with the value of $1.2c_1$ for the first 30 feet indicated by the dispersion data.

To sum up the results of this section, we may state that *the features of the Rider wave, the Airy wave, and the Limiting wave lengths which were predicted by theory were* *identified and measured on most of the records, and the resulting average values for* $\gamma_R$, $\gamma_A$, *and* $\gamma_L$ *yield values for the velocity in the top layer of the bottom which agree with the entirely independent evidence obtained from refraction data and dispersion data.*

## IV. EFFECT OF THE STRUCTURE OF DEEP LAYERS IN THE BOTTOM ON THE CHARACTER OF THE GROUND WAVE AND THE RIDER WAVE

When we come to discuss the results of the analysis of the records obtained at Virgin Islands Shoal and at Virgin Islands Deep (Tables 5, 6) we again find agreement with our previous deductions about the structure of the bottoms at these stations made on the basis of dispersion data and refraction data. Thus, the average values of $\gamma_A = .84$ and $\gamma_A = 1.4$ correspond to $(c_2/c_1) = 1.12$ and 1.05 for Virgin Islands Shoal and Deep, respectively, and these conform with the evidence from dispersion data given in Table 1. However, the values of $\gamma_A$ for the Deep are too few, while those for the Shoal show considerable scatter.

The distinctive feature of these stations, which puts them in a class by themselves, is shown in Plates 8 and 9 where it is seen that *the records are devoid of rider waves and of secondary arrivals after the first arrivals in the ground wave.* Geologically the bottom at Virgin Islands is known to be coral, as against the sandy and muddy bottoms at Jacksonville and Solomons. We have also found previously that whereas in the last two stations the bottoms are uniform and of $(c_2/c_1) \simeq 1.15$ down to a depth of more than 10 times the depth of water, in the Virgin Islands stations an intermediate layer of $(c_2/c_1) \simeq 1.15$ which is only about as thick as the depth of water intervenes between the water and a bottom layer in which $(c_2/c_1)$ has the high value of 3. The theory of group velocity of the normal modes in a three-layered liquid half-space shows that when the thickness of the intermediate layer is about 10 times, or more, greater than the depth of water, the dispersion arising from each of the two interfaces is very nearly independent of the other interface. This is illustrated in Figure 31 where the group-velocity curve for case 3.9 exhibits *two minima* corresponding to the two interfaces. A comparison of curves V and 3.9 shows that the phase velocities $(c/c_1)$ are indistinguishable between the two cases, and that even the group velocities agree up to very nearly the limiting frequency for case V. Similarly, a comparison of curves 3.9 and VIII shows that the dispersion due to the lower interface is approximately unaffected by the presence of the upper discontinuity. Similar conclusions can be drawn from the dispersion curves shown in Figure 29. Referring now to Figure 32 where the dispersion curve for medium 3.9 is replotted, the following features of the ground wave for this medium may be predicted. The ground wave will commence rather weakly with a characteristic limiting wave length corresponding to $\gamma_L = .028$. The amplitude of the ground wave will increase gradually until the time $t = r/1.09c_1$, when an *Airy-phase-in-reverse* will commence due to the *maximum* in the group velocity. Between $t = r/1.09c_1$ and $t = r/c_1$, the ground wave will consist of a superposition of *three* frequencies corresponding, for example, to the points $A$, $B$, and $C$. At $t = r/c_1$, the water wave due to the upper interface will be superimposed, giving a total of four component frequencies. This water wave will culminate in the Airy phase due to the upper discontinuity at about $t = r/.98c_1$. Thereafter, there will remain only the phases due to the water wave

TABLE 5.—*Characteristics of ground waves and water waves in Virgin Islands Shoal*

**The charge was placed on the bottom in shots 235 to 273 and was suspended at a depth of 25 feet in shots 274 to 280. The hydrophone was placed on the bottom in all shots. The records are characterized by ground waves *lacking any secondary arrivals* after the first arrivals, by an absence or extreme feebleness of "rider" waves, and by excellent dispersion in the water waves. The bottom is sloping.**

| Shot No. | Water depth near charge | Water depth near hydrophone | "Mean" water depth $\bar{H}$ | Ground Waves | | | | Airy Wave | | Water-wave arrival time | Charge weight |
|---|---|---|---|---|---|---|---|---|---|---|---|
| | | | | Longest Period | $\bar{H}/\lambda$ | Period | $\bar{H}/\lambda$ | Period | $\bar{H}/\lambda$ | | |
| | *ft.* | *ft.* | *ft.* | *Sec.* | | *Sec.* | | *Sec.* | | *Sec.* | *lbs.* |
| 235 | 70 | 62 | 66 | | | | | .010 | 1.3 | 4.168 | 0.5 |
| 237 | 70 | 62 | 66 | | | .056 | .24 | .011 | 1.2 | 3.102 | 0.5 |
| 238 | 74 | 62 | 68 | | | .065 | .21 | | | 2.080 | 0.5 |
| 239 | 70 | 62 | 66 | | | .068 | .19 | .033* | .40 | 1.684 | 0.5 |
| 240 | 81 | 62 | 71.5 | .102 | .14 | .077 | .19 | | | 1.007 | 0.5 |
| 241 | 83 | 62 | 72.5 | .099 | .15 | .061 | .24 | | | .847 | 0.5 |
| 242 | 85 | 62 | 73.5 | .088 | .17 | .071 | .21 | | | .560 | 0.5 |
| 244 | 77 | 62 | 69.5 | .083 | .17 | .057 | .24 | .0285* | .49 | 2.472 | 300 |
| 245 | 82 | 62 | 72 | .090 | .16 | .060 | .24 | | | 5.203 | 300 |
| 246 | 83 | 62 | 72.5 | .11 | .13 | .060 | .24 | | | 6.469 | 300 |
| 247 | 83 | 62 | 72.5 | | | .074 | .20 | | | 8.520 | 300 |
| 251 | 76 | 62 | 69 | .087 | .16 | .060 | .22 | .012 | 1.1 | 4.790 | 25 |
| 252 | 72 | 62 | 67 | | | .056 | .24 | .0246 | .55 | 3.405 | 25 |
| 253 | 77 | 62 | 69.5 | .10 | .14 | .056 | .25 | .033* | .42 | 2.242 | 25 |
| 254 | 73 | 62 | 67.5 | | | .058 | .23 | .022 | .61 | 1.053 | 25 |
| 266 | 80 | 65 | 72.5 | .12 | .12 | .069 | .21 | .023 | .63 | .811 | 3.5 |
| 267 | 70 | 65 | 67.5 | .12 | .12 | .050 | .27 | .026 | .52 | 1.446 | 3.5 |
| 268 | 74 | 65 | 69.5 | | | .046 | .31 | .017 | .82 | 2.068 | 3.5 |
| 269 | 66 | 65 | 65.5 | .088 | .15 | | | .011 | 1.2 | 2.971 | 3.5 |
| 270 | 65 | 65 | 65 | .083 | .16 | .045 | .29 | .010 | 1.3 | 3.707 | 3.5 |
| 271 | 70 | 65 | 67.5 | | | | | .010 | 1.4 | 4.616 | 3.5 |
| 272 | 74 | 65 | 69.5 | .083 | .17 | | | .010 | 1.4 | 5.112 | 3.5 |
| 273 | 83 | 65 | 74 | .092 | .16 | .06 | .25 | | | 5.786 | 3.5 |
| 274 | 82 | 65 | 73.5 | .095 | .16 | | | | | 5.802 | 3.5 |
| 275 | 74 | 65 | 69.5 | .0955 | .15 | | | .021* | .66 | 2.768 | 3.5 |
| 276 | 77 | 65 | 71 | .103 | .14 | | | .022 | .65 | 1.102 | 3.5 |
| 277 | 81 | 65 | 73 | .093 | .16 | | | | | .522 | 0.5 |
| 278 | 79 | 65 | 72 | .10 | .14 | | | .022 | .65 | 1.003 | 0.5 |
| 279 | 69 | 65 | 67 | .10 | .13 | .051 | .26 | .018 | .74 | 1.638 | 0.5 |
| 280 | 71 | 65 | 68 | .096 | .14 | | | .020 | .69 | 2.209 | 0.5 |
| Average | 76 | 64 | 70 | .0965 | .15 | .060 | .24 | .019 | .84 | | |

* Well developed Airy period.

and ground wave arising from the lower discontinuity, which will culminate in another Airy phase of $t = r/.92c_1$. Examples of such lively ground waves are shown in Plates 4 and 5 by the lower Mark II traces in shots Nos. 94, 95, and 97, and in Plates 6 and 7. Also, the records at Jacksonville Deep, and to a lesser extent those at Jacksonville Shoal, are rich in *trains of waves which arrive after the water wave.*

On the other hand, the three-layered media such as 3.3 and 3.7 shown in Figure 32, in which the thickness of the intermediate layer is only of the order of the depth of water, will exhibit a ground-wave and water-wave system whose main features are similar to those characteristic of uniform bottoms. The presence of the lower interface will no longer be revealed by a secondary arrival such as the Airy phase-in-

TABLE 6.—*Characteristics of ground waes and water waves in Virgin Islands Deep*

The hydrophone was placed on the bottom in all shots. The records are characterized by generally weak ground waves (in 25 out of 42 shots the ground wave appears to be completely absent) lacking any secondary arrivals after the first arrivals, by an absence or extreme feebleness of rider waves, and by excellent dispersion in the water waves. The bottom is sloping.

| Shot No. | Charge depth | Water depth near charge | Water depth near hydrophone | "Mean" water depth $\bar{H}$ | Ground Waves | | | | Airy Wave | | Water-wave arrival time | Charge weight |
|---|---|---|---|---|---|---|---|---|---|---|---|---|
| | | | | | Period | $\bar{H}/\lambda$ | Period | $\bar{H}/\lambda$ | Period | $\bar{H}/\lambda$ | | |
| | *ft.* | *ft.* | *ft.* | *ft.* | *sec.* | | *sec.* | | *sec.* | | *sec.* | *lbs.* |
| 186 | 169 | 169 | 120 | 145 | 112 | .22 | | | | | 5.408 | 300 |
| 188 | 173 | 173 | 120 | 147 | | | | | .023 | 1.3 | 7.890 | 300 |
| 191 | 154 | 154 | 120 | 137 | .16 | .17 | .107 | .26 | | | 1.348 | 25 |
| 192 | 165 | 165 | 120 | 143 | .18 | .16 | | | | | 2.323 | 25 |
| 201 | 166 | 166 | 120 | 143 | .12 | .25 | | | | | 1.491 | 4.5 |
| 202 | 160 | 160 | 120 | 140 | | | .11 | .25 | | | 1.100 | 4.5 |
| 203 | (150) | (150) | 120 | (135) | | | .090 | (.30) | | | .523 | 4.5 |
| 213 | 75 | 170 | 120 | 145 | | | | | .0183 | 1.6 | 5.951 | 4.5 |
| 215 | 75 | 152 | 120 | 136 | .13 | .21 | .10 | .27 | | | 1.100 | 4.5 |
| 216 | 147 | 147 | 120 | 133 | | | .080 | .33 | | | .593 | 0.5 |
| 217 | 100 | (160) | 120 | (140) | | | .09 | (.31) | | | 2.453 | 300 |
| 219 | 100 | (160) | 120 | (140) | | | | | .024 | (1.2) | 7.385 | 300 |
| 220 | 100 | (160) | 120 | (140) | | | | | .017 | (1.6) | 10.069 | 300 |
| Average | 133 | 160 | 120 | 140 | .14 | .21 | .096 | .29 | .021 | 1.4 | | |

reverse in medium 3.9 which propagates with a speed nearly equal to the sound velocity in the intermediate layer.

Not only will there be no secondary arrival which propagates with the speed of the intermediate layer, but theory also predicts that the rider wave in media 3.3 and 3.7 should be relatively weaker than in a medium such as V or 3.9, while the water wave should be of about the same intensity. The amplitude of the ground wave is given by Eq. (51) where the factor $0_n$ is defined in Eq. (49). This expression was derived for the case of an exponential pressure pulse $e^{-\lambda t}$, but its form is of more general validity. In comparing the amplitudes of the rider waves for different media, we need to examine the values of the factor $O_n/\sqrt{k\ddot{k}}$ at the points where $U = c_1$. Now

$$k\ddot{k} = -\frac{\alpha}{2\pi U^2}\frac{d}{d\gamma}\left(\frac{U}{c_1}\right), \tag{65}$$

where $\alpha = kH$ is, like $O_n$, a function of $x_n$ defined in Eq. (A76). The relative amplitudes of the rider waves in different media are therefore proportional to the nondimensional quantity

$$S_n^R = \frac{O_n}{\sqrt{\alpha}} \frac{1}{\sqrt{-\frac{d}{d\gamma}\left(\frac{U}{c_1}\right)}}. \tag{66}$$

It turns out that for the rider waves the factor $0_n/\sqrt{\alpha}$ does not vary rapidly with changes in the structure of the bottom. The principal difference in the amplitude of the rider waves for various media arises therefore from the factor $1\Big/\sqrt{-\frac{d}{d\gamma}(U/c_1)}$, where $\frac{d}{d\gamma}(U/c_1)$ is simply the slope of the curves in Figure 32 evaluated along the line $(U/c_1) = 1$. The slope of the 3.9 curve at the point $F$ is much less than the slopes of either the 3.3 curve at $E$ or of the 3.7 curve at $D$. Numerical values of the quantities involved in expression (66) are as follows:

| Medium | $O_n/\sqrt{\alpha}$ | $\frac{d}{d\gamma}\left(\frac{U}{c_1}\right)$ | $S_1^R$ |
|---|---|---|---|
| 3.9 | 0.24 | −0.37 | 0.4 |
| 3.7 | 0.20 | −18 | 0.05 |
| 3.3 | 0.31 | −25 | 0.06 |

It follows that *the amplitudes of the rider waves in media 3.7 and 3.3 should be from 7 to 8 times smaller than in medium 3.9.*

On the other hand, the dispersion in the water wave is determined by the shape of the group velocity curve for $\gamma > 1$ (Figs. 12–19), and Figure 32 shows that beyond $\gamma = 2$ the three curves coalesce. One would therefore expect water waves of comparable amplitudes in the three media considered. Both of these theoretical predictions are verified on all the records taken at Virgin Islands Shoal and Virgin Islands Deep, some of which are reproduced in Plate 8 and 9.

The physical basis of the phenomenon discussed in this section is analogous to the process of making "invisible glass" and to similar problems in impedance matching. (*See* Slater, 1942, p. 62.)

## 7. SOME REMARKS ON THE HISTORY OF THE DEVELOPMENT OF THE THEORY OF NORMAL MODES IN ELASTIC HALF-SPACES AND OF ITS APPLICATIONS TO PROBLEMS OF PROPAGATION OF SHOCKS

The first discovery of a *free* elastic wave which can be propagated over the surface of an isotropic elastic half-space was made by Lord Rayleigh (1887, p. 441). These waves have subsequently been identified in earthquake records and are known as Rayleigh waves. In 1911 Love showed that the Rayleigh waves are the limiting form assumed by the normal modes of a homogeneous elastic sphere as the radius of the sphere increases indefinitely. In the same memoir Love shows that a free shear wave can be transmitted in a *layered* elastic half-space when the velocity of distortional waves in the surface layer is less than in the medium below. These so-called Love waves closely resemble the normal modes of a layered liquid half-space discussed in this report.

In 1924 Gutenberg made the first study of dispersion of Love waves in earthquake records with a view to determining the thickness of the crust of the earth. In this first attempt he wrongly identified the observed speed of propagation of each frequency with the phase velocity instead of the group velocity, but later (1926) he rectified the error. The importance of group velocity in the study of dispersion of Love waves was first stressed by Stoneley (1925). The subject has since been investigated extensively by Stoneley, Jeffreys, Gutenberg, and others.

The possibility that a layered liquid half-space might propagate free *compressional* waves analogous to Love waves occurred to the writer in November 1941. The results were first announced at a conference with L. B. Slichter and J. T. Tate, and were later communicated to V. O. Knudsen in the preliminary report reproduced on pages 40 through 42. The Figures 1–4 referred to there have been included in this paper as Figures 45–48, respectively. This study was then interrupted on account of other pressing duties, and it was not until the Spring of 1943 that the writer could return to the subject. At that time the steady state solution for a periodic point source in a layered medium was thoroughly investigated. The technique of deriving the normal mode solution from the residues of the integral in the complex $k$-plane, which was used by the writer on this and other occasions, is due originally to H. Lamb who in a classical paper (1904) gave the first exact solution of the problem of radiation from a point source in a homogeneous elastic half-space. Unfortunately this paper seems to have escaped the attention of recent writers on the subject, who have independently rediscovered some of Lamb's results but have, in some cases, omitted certain terms of the solution such as branch-line integrals, which Lamb was careful to retain.

The solution for the propagation of sound in a layered liquid half-space derived by the writer was communicated in various preliminary memoranda to interested members of Division 6 of NDRC. Final publication of a complete report was withheld pending an opportunity to test the theory against experimental data. This opportunity arose in July, 1944 when Dr. Ewing communicated to the writer his discovery of dispersion in the water wave and his finding that each frequency is propagated with a characteristic velocity[7]. The idea of applying the Gutenberg-Stoneley technique, used in the study of Love waves, which is based on group velocity of normal modes, immediately occurred to the author, since it soon became clear that, if the dispersion were governed by the phase velocity, the long periods should have arrived ahead of the short periods—in complete contradiction to the observations.

While the principal features of the mean dispersion curves observed at the various stations could be explained on the basis of the shape of the group velocity curve for the *first* mode, there remained three outstanding problems. One was the existence of the low-frequency branch of the group-velocity curve (to the left of the minimum group velocity), which it was thought at first could be relegated to a footnote. Upon closer examination it was discovered that this low-frequency branch of the group-

[7] Ewing noted dispersion in the water wave, with high-frequency components arriving ahead of lower ones, in seismic prospecting of water-covered areas of Louisiana in 1927, but had not been able to get systematic data on the phenomenon before his 1943–1944 work.

velocity curve furnishes, for the first time, a theory of the ground wave and that in addition it demands the existence on the records of the rider wave and the Airy wave. This led to the discovery of the above-mentioned features on the records.

The second outstanding problem was to produce a justification for basing the theory essentially on the *first mode alone*. Numerical investigation of the expected relative amplitudes of the higher modes showed that, whereas in the ground wave they should be smaller, in the water wave they should be comparable to the first mode (Figs. 33–36). The final resolution of this difficulty was made principally on the basis of the suppression of the high-frequency higher modes by the low-pass receivers. In support of this hypothesis we have the fact that the receivers with a flat response show a very complicated pressure variation.

The third unsolved problem was to explain the lack of both secondary arrivals and rider waves in all the records taken at the stations of Virgin Islands Shoal and Deep. This necessitated a study of the theory of propagation in a three-layered liquid half-space which finally led to the complete clearing up of this question along the lines discussed on pages 35–38.

The *steady state* theory of normal modes in a liquid half-space has recently been studied independently by other investigators.

## 8. PRELIMINARY REPORT ON FREE ACOUSTIC WAVES

(Prepared in November 1941)

A half-space in which the sound velocity either increases with depth, or first decreases and then increases with depth, is capable of propagating *free* waves. When excited by a point source or a vertical line source these free waves have vertical wave fronts of cylindrical form, with axis passing through the source. Once established, the waves have a two-dimensional attenuation, i.e. the amplitude of the pressure decreases with distance $r$ from the source like $r^{-\frac{1}{2}}$ instead of $r^{-1}$, as in the case of body waves. At great distances these waves are found (in seismology) therefore to predominate over the body waves. The amplitude of the waves varies with depth in the manner shown for the first mode in Figures 1 to 4.* The velocity of propagation varies with frequency, the lowest frequencies traveling with the maximum speed of the medium and the high frequencies with the minimum speed found in the medium. For conditions that are met in surface sea waters the dispersion is, however, slight and the group velocity is essentially the same as the phase velocity.

In order to bring out the analogy with other free acoustic waves, let us consider the free waves in a room bounded by rigid walls. There, a pulse started inside the room sends out waves which are reflected from the walls, and whenever the reflected wave reinforces the incident wave we have a free mode of vibration of the room. In an ideal case no energy is required to maintain these free modes of vibration and once excited they can last indefinitely. The original energy of the pulse remains confined in the room in the form of standing waves. The origin of these free modes is bound up with the existence of reflecting walls.

* Figures 1–4 have been reproduced in this report as Figures 45–48.

Under the conditions postulated above for the half-space there is reflection, abrupt or continuous, from horizontal planes, and the situation is similar to that in a room without vertical walls, but with an infinitely long ceiling and floor. There being no reflection from vertical planes, the energy of a pulse is radiated away, but in a two-dimensional rather than a three-dimensional manner. Whereas in an enclosed room the free modes trap the energy of an originally outgoing wave and convert it into standing waves, the free modes in the half-space merely convert an outgoing *spherical* wave into an outgoing *cylindrical* wave.

The periods of the low order free modes of an enclosed room are of the order of magnitude of the time required for a wave to travel a distance of the dimensions of the room. There is no *period* of the free waves in a half-space, since these waves are *progressive* and not standing ones. (There are no reflecting walls at great distances to return them). Starting with a minimum frequency, which is characteristic of the given medium, all higher frequencies can be propagated as *free* waves, there being only a slight variation of velocity of propagation with frequency. To round out the argument, we might add that if we consider the ocean as enveloping the earth, then it will have a *free period* of the order of magnitude of the time required for the wave to travel around the world. In the case of gravitational waves, this is the so-called *free-period* of the oceans. The free acoustic waves are indeed similar in nature to gravitational waves visible at the surface. The origin of the latter is, however, due entirely to the possibility of storing potential energy at the air-water interface, there being no gravitational body waves (in non-relationistic mechanics).

In the applications in view we are interested in the amplitudes of the various modes which are excited by a subsurface pulse. This question is being investigated now, but some qualitative remarks can be made in advance. The magnitude of the amplitude of a given mode which is excited by a given pulse depends on the frequency distribution and the location as well as the directional properties of the pulse. As to the dependence on the location (depth) of the pulse, one can say that the amplitude of any mode will be highest if the source is located at a depth where this mode has the maximum amplitude, and that it will be zero if the source is located at a level at which the mode has a node (in the fundamental modes shown in Figures 1 to 4 the only nodes are at the surface and at great depth, but the modes of higher order have additional nodes.) In this respect, the higher frequencies are favored for a shallow source in medium 3, while the lower frequencies are favored in the other media. In general, the amplitude of the fundamental mode is a maximum near the level of minimum velocity, and the relative concentration there is highest for the high frequencies. (In the case of certain *free* waves in the atmosphere which were excited by the Krakatau eruption of 1883 the fundamental mode predominated, essentially because in this mode the amplitude is a maximum at the surface. See a paper by the author in Proc. Roy. Soc. 171A pp. 434–449, 1939). More information on this question will be available when computations now in progress will have been completed.

As to the dependence of the existence of free modes on the medium, the following can be said. The low frequencies depend in their amplitude distribution on the properties of the medium extending from the surface to great depths. The high frequencies depend essentially only on the structure of the medium near the level of minimum velocity. The modes of these high frequencies will not be appreciably altered by deviations from the assumed velocity distribution at levels removed from the level of minimum velocity.

We will now add some comments on the free waves in the media shown in Figures 1 to 4. In a medium of type 1, free waves are possible only if the velocity $c_2$ in the lower layer is greater than the velocity $c_1$ in the surface layer. The minimum frequency $f$ for the fundamental mode is given by

$$f = \frac{c_1 c_2}{4H\sqrt{c_2^2 - c_1^2}}.$$

This frequency propagates with a velocity $c_2$ while the velocity of the high frequencies approaches $c_1$.

In medium 2 let the velocity in the top layer be denoted by $c_1$, in the middle layer by $c_2$ and in the bottom layer by $c_3$. Free waves are possible if $c_2$ is less than $c_1$ and $c_3$. $c_3$ may be less than $c_1$, but must be greater than $c_2$.

The minimum frequency $f$ is given by the roots $x_1$ and $x_2$ of the equation

$$\tan x_1 \cdot \tan x_2 = \frac{x_1}{x_2},$$

where

$$x_1 = \frac{2\pi f H\sqrt{c_3^2 - c_1^2}}{c_3 c_1}, \qquad x_2 = \frac{2\pi f H\sqrt{c_3^2 - c_2^2}}{c_3 c_2}.$$

The velocity of propagation of this frequency is $c_3$, that of very high frequencies being $c_2$.

In medium 3, the lowest frequency is given by

$$f = \frac{3uc_2 c_1}{4\pi H\sqrt{c_2^2 - c_1^2}},$$

where $u$ is the root of $J_{-\frac{1}{3}}(u) = 0$ and is equal to 1.865. The lowest frequency in medium 4 is given by

$$f = \frac{3uc_1 c_2}{4\pi H\sqrt{c_2^2 - c_1^2}}$$

where $u$ is the root of the equation $J_{\frac{1}{3}}(u)J_{\frac{2}{3}}(u) = J_{-\frac{1}{3}}(u)J_{-\frac{2}{3}}(u)$ and is equal to 0.73082.

# PART II: THEORY

## INTRODUCTION

In this section we give a brief account of the theory of propagation of explosive sound in shallow water. No detailed exposition of the theory will be attempted, however, since that would carry us beyond the scope of this paper which aims primarily at a wave theoretical interpretation of a particular set of experimental data. A more comprehensive treatment is reserved for a future occasion when an attempt will be made to develop systematically the theory of wave propagation in layered media as well as in media with continuously varying properties. This will include a treatment of the so-called "ray-theory" and the wave theory, and the relationship between the two.

## A. THEORY OF PROPAGATION OF SOUND IN WATER UNDERLAIN BY A UNIFORM BOTTOM OF DIFFERENT DENSITY AND SOUND VELOCITY

### 1. FORMAL SOLUTION.

The simplest model which exhibits the essential features of the observed dispersion in the water wave is one in which the bottom is assumed to be a liquid of density $\rho_2$ and sound velocity $c_2$, which differ from the density $\rho_1$ and sound velocity $c_1$ in water, as shown in Figure F. A point source is situated at a depth $d$ below the surface, and the depth of water is $H$. The boundaries of the water are assumed to be parallel and flat. For purposes of analysis, it is convenient to divide the water into regions (1) and (2) above and below the source, respectively, and to denote the bottom by (3).

Our problem is to determine, at any point in the water, the pressure field due to an explosion at the source. To a first approximation the explosion at the source can be assumed to be represented by a sudden rise of pressure which decays exponentially with time. As is customary, the analysis is made first for a periodic pressure variation at the source of circular frequency $\omega$, and subsequently the solution is Fourier-synthesized to represent an arbitrary time variation of the pressure pulse.

The pressure field is determined from the potential $\varphi$ through

$$p = \rho \frac{\partial \varphi}{\partial t}, \qquad w = -\frac{\partial \varphi}{\partial z}, \qquad u = -\frac{\partial \varphi}{\partial r}, \tag{A1}$$

where $p$ denotes the acoustic pressure, $w$ the vertical velocity, and $u$ the velocity in the horizontal direction $r$. The potential $\varphi$ satisfies the wave equation

$$\nabla^2 \varphi = \frac{1}{c_1^2} \frac{\partial^2 \varphi}{\partial t^2} \tag{A2}$$

in the water, and

$$\nabla^2 \varphi = \frac{1}{c_2^2} \frac{\partial^2 \varphi}{\partial t^2} \tag{A3}$$

in the bottom. To satisfy the boundary conditions at $z = 0$ and $z = H$, we seek in the first instance solutions of the form

$$\varphi = e^{i\omega t} J_0(kr) F(z) G(k), \tag{A4}$$

where $k$ is an arbitrary variable of integration with respect to which one eventually integrates along a certain path in the complex $k$ plane. If one thinks of a spherical wave as made up of a superposition of plane waves, then, as long as $k$ is numerically less than the wave number, one can attach to it the physical meaning of $k = 2\pi \sin(\theta/\lambda)$, where $\theta$ denotes the angle of incidence of the elementary waves.[8] Substituting expression (A4) into Eqs. (A2) and (A3), we get

$$\frac{d^2F}{dz^2} + \beta_1^2 F = 0, \tag{A5}$$

in the water and

$$\frac{d^2F}{dz^2} + \beta_2^2 F = 0 \tag{A6}$$

in the bottom, where

$$\begin{aligned}
\beta_1 &= \sqrt{\frac{\omega^2}{c_1^2} - k^2}, & k &< \frac{\omega}{c_1}, \\
&= -i\sqrt{k^2 - \frac{\omega^2}{c_1^2}}, & k &> \frac{\omega}{c_1}, \\
\beta_2 &= \sqrt{\frac{\omega^2}{c_2^2} - k^2}, & k &< \frac{\omega}{c_2}, \\
&= -i\sqrt{k^2 - \frac{\omega^2}{c_2^2}}, & k &> \frac{\omega}{c_2}.
\end{aligned} \tag{A7}$$

Let $F_1$, $F_2$ and $F_3$ represent $F(z)$ in the regions (1), (2) and (3) of Figure F. Then

$$F_1 = A \sin \beta_1 z, \tag{A8}$$

$$F_2 = B \sin \beta_1 z + C \cos \beta_1 z, \tag{A9}$$

$$F_3 = De^{-i\beta_2 z}. \tag{A10}$$

The choice of the sine function for $F_1$ is made in order to satisfy the condition of $F = 0$ at $z = 0$; the expression (A10) for $F_3$ is adopted in order to make $F_3$ vanish exponentially with depth for large $k$, or rather in order to avoid an exponential increase with depth as $k$ becomes large. The arbitrary constants $A$, $B$, $C$, and $D$ are determined by the boundary conditions at $z = H$ and $z = d$, and by the strength of the point source.

At $z = H$ we must have continuity of pressure and of the vertical component of velocity $w$:

$$\rho_1 F_2 = \rho_2 F_2, \quad \frac{dF_2}{dz} = \frac{dF_3}{dz} \quad \text{at} \quad z = H. \tag{A11}$$

[8] For a detailed discussion of this point *see* Pekeris (1946).

At $z = d$, the depth of the point source, we again must have

$$F_1 = F_2 \quad \text{at} \quad z = d, \tag{A12}$$

because of the required continuity of pressure. The boundary condition for the vertical velocity $w$ is, however, more complicated; $w$ is continuous everywhere in the plane $z = d$ except at the point source, where the fluid above and below the source moves in *opposite* directions. This condition is met by putting

$$\frac{dF_1}{dz} - \frac{dF_2}{dz} = 2k \quad \text{at} \quad z = d, \tag{A13}$$

for when expression (A4) is integrated with respect to $k$ from 0 to $\infty$, the discontinuity in $w$ at $z = d$ becomes proportional to $\int_0^\infty J_0(kr)k\,dk$, which function vanishes everywhere except at $r = 0$, where it becomes infinite in such a manner that its integral over the plane $z = d$ is finite.

It follows from Eqs. (A11), (A12), and (A13) that

$$A = \frac{2k}{\beta_1}\left[\frac{\beta_1 \cos \beta_1(H-d) + ib\beta_2 \sin \beta_1(H-d)}{\beta_1 \cos \beta_1 H + ib\beta_2 \sin \beta_1 H}\right], \qquad b \equiv \rho_1/\rho_2, \tag{A14}$$

$$B = \frac{2k \sin \beta_1 d}{\beta_1}\left[\frac{\beta_1 \sin \beta_1 H - ib\beta_2 \cos \beta_1 H}{(\beta_1 \cos \beta_1 H + ib\beta_2 \sin \beta_1 H)}\right], \tag{A15}$$

$$C = \frac{2k \sin \beta_1 d}{\beta_1}, \qquad D = \frac{2bke^{ik\beta_2 H} \sin \beta_1 d}{(\beta_1 \cos \beta_1 H + ib\beta_2 \sin \beta_1 H)}. \tag{A16}$$

Hence the formal solution for the sound potential due to a periodic point source is

$$\varphi = e^{i\omega t}\,\Psi(r,z,\omega),$$

$$\Psi_1 = 2\int_0^\infty J_0(kr)k\,dk\,\frac{\sin \beta_1 z}{\beta_1}\left[\frac{\beta_1 \cos \beta_1(H-d) + ib\beta_2 \sin \beta_1(H-d)}{\beta_1 \cos \beta_1 H + ib\beta_2 \sin \beta_1 H}\right], \qquad 0 \le z \le d, \tag{A17}$$

$$\Psi_2 = 2\int_0^\infty J_0(kr)k\,dk\,\frac{\sin \beta_1 d}{\beta_1}\left[\frac{\beta_1 \cos \beta_1(H-z) + ib\beta_2 \sin \beta_1(H-z)}{\beta_1 \cos \beta_1 H + ib\beta_2 \sin \beta_1 H}\right], \qquad d \le z \le H, \tag{A18}$$

$$\Psi_3 = 2b\int_0^\infty J_0(kr)k\,dk\,\frac{\sin(\beta_1 d)e^{-i\beta_2(z-H)}}{(\beta \cos \beta_1 H + ib\beta_2 \sin \beta_1 H)}, \qquad z \ge H. \tag{A19}$$

It will be noted that $\psi_1$ and $\psi_2$ are transformed into each other by interchanging $z$ and $d$, and that the integrands are *even* functions of $\beta_1$, but mixed functions of $\beta_2$. The integrands are of course functions of the frequency $\omega$ through $\beta_1$ and $\beta_2$.

When the discontinuity in density and sound velocity at $z = H$ is removed,

$$b \to 1, \qquad \beta_2 \to \beta_1,$$

and

$$\varphi_1 \to 2e^{i\omega t}\int_0^\infty J_0(kr)k\,dk\,\frac{\sin \beta_1 z}{\beta_1}\,e^{-i\beta_1 d}$$

$$= e^{i\omega t}\int_0^\infty J_0(kr)\frac{k\,dk}{i\beta_1}\left[e^{-i\beta_1(d-z)} - e^{-i\beta_1(d+z)}\right] = e^{i\omega t}\left[\frac{e^{-i(\omega/c_1)R_1}}{R_1} - \frac{e^{-i(\omega/c_1)R_2}}{R_2}\right],$$

$$R_1 = \sqrt{r^2 + (d-z)^2}, \qquad R_2 = \sqrt{r^2 + (d+z)^2}. \tag{A20}$$

Similarly, it is found that $\varphi_2$ and $\varphi_3$ also reduce to the correct solution consisting of a point source and its image in the surface.

Expressions (A17), (A18), and (A19) give the steady-state solution for a periodic point source. The solution for the case of a pressure pulse at the source of the form $f(t)$ is obtained by first computing the Fourier transform

$$g(\omega) = \int_{-\infty}^{\infty} e^{-i\omega t} f(t)\, dt, \tag{A21}$$

so that

$$f(t) = \frac{1}{2\pi} \int_{-\infty}^{\infty} e^{i\omega t} g(\omega)\, d\omega, \tag{A22}$$

and then evaluating

$$\varphi(r, z, t) = \frac{1}{2\pi} \int_{-\infty}^{\infty} e^{i\omega t} \Psi(r, z, \omega) g(\omega)\, d\omega. \tag{A23}$$

This completes the formal solution of our problem, but for most practical applications the theory at its present stage is useless because neither the integrals for $\Psi(r, z, \omega)$ nor the integral in (A23) can be carried out without immense labor and with sufficient accuracy to yield useful results. The integrals for $\Psi$ can be evaluated by numerical integration only when the wave length is a fraction of the depth of water and the range $r$ is a small multiple of the depth, as was done in computing the solid curves of Figure 23. For smaller wave lengths and greater ranges the integrands are rapidly oscillatory functions of $k$, and it soon becomes impracticable to evaluate $\Psi$ by straightforward numerical integration. Even if $\Psi$ were known, the computation of $\varphi(r, z, t)$ from (A23) would be practically impossible for such important applications as the first-arrival time, as has been shown by the writer (1940). For this reason it is necessary first to transform the integrals for $\Psi$, the transformation used depending on the particular application in view. Thus, for the purpose of determining the beginning of the record at a distant point or for determining the steady-state solution up to moderate ranges (in terms of the depth of water), a transformation of the integrals which yields the so-called "ray-theory" is useful. On the other hand, if one is interested in the steady-state solution at large ranges, where many rays need to be considered, or in the later phases of the received pressure pulse at large ranges, another transformation is useful which yields the *normal mode solution.*

## 2. THE RAY THEORY.

a) *Expansion of the potential into a series of integrals each of which represents a "ray"*—In this section we shall indicate how the ray theory can be derived from our formal solution given in Equations (A17), (A18), and (A19). The account will be limited mostly to a statement of results because the ray theory is not used in the applications of this paper. Rayleigh (1896) showed that, when a *plane* sound wave is reflected at a discontinuity in density $\rho$ and sound velocity $c$, the reflection coefficient $K$ is given by

$$K = \frac{\dfrac{\rho_2 c_2}{\rho_1 c_1}\cos\theta - \sqrt{1 - \dfrac{c_2^2}{c_1^2}\sin^2\theta}}{\dfrac{\rho_2 c_2}{\rho_1 c_1}\cos\theta + \sqrt{1 - \dfrac{c_2^2}{c_1^2}\sin^2\theta}}, \tag{A24}$$

where $\theta$ denotes the angle of incidence. If we recall that $k$ in (A7) is given by

$$k = 2\pi \sin\theta/\lambda = \left(\frac{\omega}{c_1}\right)\sin\theta, \tag{A25}$$

it follows that

$$\beta_1 = \left(\frac{\omega}{c_1}\right)\cos\theta; \qquad \beta_2 = \left(\frac{\omega}{c_2}\right)\sqrt{1 - \frac{c_2^2}{c_1^2}\sin^2\theta}, \tag{A26}$$

$$K = \frac{\beta_1 - b\beta_2}{\beta_1 + b\beta_2}. \tag{A27}$$

The solution in terms of rays for a *point source* is obtained by expanding the expression in brackets in (A18) as follows

$$\begin{aligned}\left[\frac{\beta_1 \cos\beta_1(H - z) + ib\beta_2 \sin\beta_1(H - z)}{\beta_1 \cos\beta_1 H + ib\beta_2 \sin\beta_1 H}\right] &= e^{-i\beta_1 z}\left[\frac{1 + Ke^{-i2\beta_1(H-z)}}{1 + Ke^{-i2\beta_1 H}}\right] \\ &= e^{-i\beta_1 z}[1 + Ke^{-i2\beta_1(H-z)}][1 - Ke^{-i2\beta_1 H} + K^2 e^{-i4\beta_1 H} + \cdots],\end{aligned} \tag{A28}$$

$$\begin{aligned}\Psi_2 = \int_0^\infty J_0(kr)\,\frac{k\,dk}{i\beta_1}\,\{&[e^{-i\beta_1(z-d)} - e^{-i\beta_1(z+d)}] \\ &+ K[e^{-i\beta_1(z-d+2H-2z)} - e^{-i\beta_1(z+d+2H-2z)} - e^{-i\beta_1(z-d+2H)} \\ &+ e^{-i\beta_1(z+d+2H)}] + K^2[\quad] + \cdots\}.\end{aligned} \tag{A29}$$

The two terms in the first bracket give the direct ray and the ray reflected from the surface, as was shown explicitly in Eq. (A20). The four terms in the second bracket which are multiplied by $K$ represent the four rays which suffer only a single reflection from the bottom. The next four terms which are multiplied by $K^2$ represent the four rays which suffer two reflections from the bottom, and so on. The reason for identifying the integrals having a factor $K^n$ in the integrand with rays which suffer $n$ reflections from the bottom is suggested by the formal analogy with the theory of reflection of *plane* waves, but actually goes deeper than that. In the first place, when one solves the problem of the reflection of a spherical-sound wave from a single-plane boundary, one obtains precisely an integral of type $K$, where the factor multiplying $\beta_1$ in the exponent is the sum of the elevations of the source and receiver above the reflecting surface. The principal reason for the identification of the integrals with the rays is, however, that, in case of a pressure pulse which begins at a definite time, the integrals representing the rays vanish until the corresponding arrival-time of the rays. However, while the beginning of the received pulse will conform in shape to the pulse at the source, the later phases will be different, due to the modifications introduced by the fact that the initial wave is not plane but spherical. The pressure recorded at a distance, as given by the integral, will therefore, strictly speaking, not be the original pulse weakened by a $1/R$ factor; indeed, in the case of a pressure pulse which starts at $t = 0$ and ends at $t = \tau$, the integral representing a ray (other than the direct and first surface-reflected) will begin after an appropriate travel time $t_0$ and will continue beyond $t = t_0 + \tau$ to $t = \infty$. This phenomenon is the well-known "tail" characteristic of two-dimensional wave propagation which is imposed on the initially spherical wave by the plane boundaries.

In the sequel we shall understand by a "ray" not the customary meaning of the term but the integral corresponding to it in the expansion (A29).

b) *Some results on the reflection of spherical waves from plane boundaries.*

I. General Considerations. The propagation of a shear pulse in a layered medium

The first *complete* analysis of the reflection of spherical waves from plane boundaries—*i.e.*, the evaluation of integrals of the type

$$\Psi_n(r, z, \omega) \equiv \int_0^\infty J_0(kr)\,\frac{k\,dk}{i\beta_1}\left(\frac{\beta_1 - b\beta_2}{\beta_1 + b\beta_2}\right)^n e^{-i\beta_1 z_n}, \tag{A30}$$

where $\beta_1$ and $\beta_2$ are defined in (A7) and $z_n$ represents the vertical distance of the receiver from the n-th image, has been given by the writer (1941). The crux of the problem in the case of a pulse which begins at a definite time is to transform the integral in (A30) into the form

$$\Psi_n = \int F(r, z, x)e^{-i\omega M(r,z,x)}\,dx, \tag{A31}$$

where neither $F$ nor $M$ depends on $\omega$, in order to allow for an easy Fourier synthesis. When this is accomplished, the solution for the potential of the n-th reflected wave $\varphi_n$ is

$$e^{i\omega t}\int F(r, z, x)e^{-i\omega M(r,z,x)}\,dx$$

in case of a periodic pulse at the source, and this allows one to write down immediately the solution for a pulse of a general shape $f(t)$, namely

$$\Psi_n = \int F(r, z, x)f[t - M(r, z, x)]\,dx. \tag{A32}$$

The transformation in (A31) is equivalent to seeking an equivalent system of continuously distributed sources. We shall not give here the explicit expressions for $F$ and $M$ in case of reflection from a $(\rho, c)$ discontinuity but shall merely state that in this case $F$ and $M$ are obtained as functions of $r$, $z$, and of *two* variables of integration $x$ and $y$, and the integration is double. In this way it has been possible to give a wave-theoretical proof for the existence of the so-called "refracted wave" and to compute and exhibit graphically the actual shape of this type of wave from its first arrival out to $t = \infty$.

II. Asymptotic expression for the potential of a singly reflected spherical wave at high frequencies, and the conditions for the validity of the plane wave approximation

It is possible to treat the integral (A30) by the method of stationary phase and to obtain asymptotic expressions valid for high frequencies. One finds, for example, for a wave reflected once from the bottom

$$\Psi_1 = \int_0^\infty J_0(kr)\,\frac{k\,dk}{i\beta_1}\left(\frac{\beta_1 - b\beta_2}{\beta_1 + b\beta_2}\right)e^{-i\beta_1 z_1} = \frac{e^{-i(\omega/c_1)R}}{R}\{\ \},$$

$$\{\ \} = \left\{\frac{\cos\theta - b\delta}{\cos\theta + b\delta} - \frac{ic_1\,b\nu^2}{\omega R\delta^3(\cos\theta + b\delta)^3}[\sin^2\theta\cos^2\theta + 2\delta^2(1 + b\delta\cos\theta) + 3b\delta\sin^2\theta\cos\theta] + O(c_1^2/\omega^2R^2) + \cdots\right\}, \quad \text{(A33)}$$

where

$$R = \sqrt{r^2 + z_1^2}, \qquad \delta = \sqrt{\frac{c_1^2}{c_2^2} - \sin^2\theta}, \qquad \nu = \sqrt{\frac{c_1^2}{c_2^2} - 1}, \qquad \cos\theta = \frac{z_1}{R}.$$

The first term in the braces is the reflection coefficient $K$ for *plane* waves incident at an angle $\theta$, which was given in (A24); the second term gives the conditions under which the plane-wave approximation is valid, namely when $\dfrac{c_1}{\omega R\delta^3} = \dfrac{\lambda}{2\pi R\delta^3}$ is small.

It follows that in the case of a very low-speed bottom $\left(\dfrac{c_1^2}{c_2^2} \geq 2\right)$, the plane-wave approximation for a singly reflected wave is valid at distances from the source greater than about one wave length. This is not true when $c_1 \simeq c_2$ and for grazing angles of incidence $\theta$. In case of a high-speed bottom ($c_1 < c_2$), the plane-wave approximation breaks down completely as $\theta$ approaches the angle $\theta_1$ of total reflection given by $\theta_1 = \sin^{-1}(c_1/c_2)$, because $\delta$ vanishes at $\theta = \theta_1$.

Even under conditions when the expression $\Psi_1$ for the steady-state potential can be approximated by the leading term in (A33), this is not true for a pressure pulse of arbitrary time variation $f(t)$. Whereas the leading term in (A33) yields $\dfrac{K}{R}f\left(t - \dfrac{R}{c_1}\right)$, the second term is proportional to $\dfrac{1}{R^2}\displaystyle\int_{R/c_1}^{t} f\left(x - \dfrac{R}{c_1}\right)dx$ on account of the $(1/\omega)$ factor. In the case of a pressure pulse of finite duration $\tau$, $f\left(t - \dfrac{R}{c_1}\right)$ vanishes after $t = \dfrac{R}{c_1} + \tau$, while $\displaystyle\int_{R/c_1}^{t} f\left(x - \dfrac{R}{c_1}\right)dx$ approaches a constant limit. During the "tail" phase of the record, the leading term may therefore become small in comparison with the second term.

III. Reflection of a spherical sound wave from a plane boundary in case the receiver is situated on the same vertical with the source

An interesting case, which is also of some practical importance, is when the receiver is situated on the same vertical with the source ($r = 0$). The reflection coefficient varies with the height of the source above the boundary when the height is less than about a wave length (the result applies of course also for any position of the receiver as long as the distance of the image from the receiver is less than the wave length). The reason for this is that within a distance of only a fraction of a wave length from the source the energy in the field is predominantly kinetic, and the flow proceeds as if the medium were incompressible. In the limit of very long wave lengths the reflectivity of the bottom becomes independent of its compressibility and the compressibility of the water, and approaches a value of $\left(\frac{\rho_2 - \rho_1}{\rho_2 + \rho_1}\right)$ for normal incidence, instead of the acoustic value of $(\rho_2 c_2 - \rho_1 c_1)/(\rho_2 c_2 + \rho_1 c_1)$. We shall designate the field in the immediate vicinity of the source as *potential flow*, in contrast to the *acoustic flow* which prevails at distances greater than about a wave length from the source. The transition from acoustic flow to potential flow takes place for a point below the projector in the range $0 < z/\lambda < 0.5$, where $z$ denotes the height of the projector above the bottom, and $\lambda$ the wave length.

We have for the wave reflected $n$ times from the bottom

$$\Psi_n = \int_0^\infty \frac{k\,dk}{i\beta}\left(\frac{\beta_1 - b\beta_2}{\beta_1 + b\beta_2}\right)^n e^{-i\beta_1 z_n} \tag{A34}$$

$$= \frac{1}{z_n}\left\{\left(\frac{\rho_2 - \rho_1}{\rho_2 + \rho_1}\right)^n + i\left(\frac{\omega z_n}{c_1}\right) e^{i(\omega z_n/c_1)} \int_1^\infty e^{-i(\omega z_n/c_1)x}\left[\left(\frac{x - b\sqrt{x^2 + \nu^2}}{x + b\sqrt{x^2 + \nu^2}}\right)^n - \left(\frac{1-b}{1+b}\right)^n\right]dx\right\}$$

$$\backsimeq \frac{1}{z_n}\left(\frac{\rho_2 - \rho_1}{\rho_2 + \rho_1}\right)^n \left\{1 + \frac{nb\nu^2}{(b^2 - 1)}\, i\left(\frac{\omega z_n}{c_1}\right) e^{i(\omega z_n/c_1)} \int_1^\infty e^{-i(\omega z_n/c_1)x}\frac{dx}{x^2} + 0\left(\frac{\omega^2 z_n^2}{c_1^2}\right)\right\}, \tag{A35}$$

$$\backsimeq \frac{1}{z_n}\left(\frac{\rho_2 c_2 - \rho_1 c_1}{\rho_2 c_2 + \rho_1 c_1}\right)^n \left\{1 + \frac{2\,\text{in}\,\nu^2 c_2^3 \rho_1 \rho_2}{\omega z_n(\rho_2 c_2 + \rho_1 c_1)(\rho_2 c_2 - \rho_1 c_1)} + 0\left(\frac{c_1^2}{\omega^2 z_n^2}\right)\right\}. \tag{A36}$$

Here Eq. (A34) is exact, Eq. (A35) is an approximation useful for small values of $\omega z_n/c_1$ (potential flow), while Eq. (A36) gives an asymptotic expansion valid for large values of $\omega z_n/c_1$ (acoustic flow). Figure 51 shows how the reflection coefficient for a singly reflected wave varies at normal incidence from the value $(\rho_2 - \rho_1)/(\rho_2 + \rho_1)$ for very long wave lengths to the value $(\rho_2 c_2 - \rho_1 c_1)/(\rho_2 c_2 + \rho_1 c_1)$ valid in the limit of short wave lengths.

## IV. Reflection of a spherical pulse of square shape from a bottom characterized by a discontinuity in density and sound velocity when the receiver is situated on the same vertical with the source

Let the shape of the pulse be a square wave $\_|\leftarrow\tau\rightarrow|\_$ of duration $\tau$ seconds and of unit strength. Let $t$ = time reckoned from the beginning of the pulse at source,

$P_n^m$ = pressure amplitude of the wave which has suffered $m$ reflections from the surface and $n$ reflections from the bottom,

$z = z_n^m$ total vertical component of path traversed by wave from source to receiver,

$$\nu^2 = \frac{c_1^2}{c_2^2} - 1, \qquad b = \rho_1/\rho_2, \qquad f(t) \equiv \left[\frac{c_1 t - b\sqrt{c_1^2 t^2 + \nu^2 z^2}}{c_1 t + b\sqrt{c_1^2 t^2 + \nu^2 z^2}}\right], \tag{A37}$$

then

$$P_n^m = 0, \qquad t < \frac{z}{c_1}$$

$$P_n^m = (-)^m \frac{1}{z} [f(t)]^n, \qquad \frac{z}{c_1} < t < \frac{z}{c_1} + \tau \tag{A38}$$

$$P_n^m = (-)^m \frac{1}{z} \{[f(t)]^n - [f(t - \tau)]^n\}, \qquad t > \frac{z}{c_1} + \tau. \tag{A39}$$

When the pulse is zero for negative $t$ and unity for positive $t$, $P_n^m$ is given by (A38) for all $t > \frac{z}{c_1}$. From this expression one can, of course, compute $P_n^m$ for any form of the pulse. A simple and useful pulse shape which has been analyzed in this way is the exponential one, but we shall not give the results here.

Eq. (A37) gives a simple illustration of the transition from acoustic flow to potential flow. (*See* III.) The beginning of the pulse is controlled by the high-frequency components and, at $t = \frac{z}{c}, f(t) = (\rho_2 c_2 - \rho_1 c_1)/(\rho_2 c_2 + \rho_1 c_1)$: at late epochs the pulse is controlled by the low-frequency components, and $f(t) \to (\rho_2 - \rho_1)/(\rho_2 + \rho_1)$. We have here also an explicit illustration of the "tail" which is characteristic of two-dimensional wave propagation.

All the results of the "ray theory" given above can be generalized to apply to the case of a bottom which is characterized by a normal impedance $Z = \rho_1 c_1 \zeta$ by the simple expedient of letting in each expression $b \to 0$, $c_1/c_2 \to \infty$, $b\delta = b\nu \to 1/\zeta$.

### 3. THE NORMAL MODE SOLUTION.

a) *Evaluation of the integral for the potential in terms of residues and of an integral along a branch line.*—The normal-mode solution represents another transformation of the original expression for the potential, say,

$$\Psi_2 = 2 \int_0^\infty J_0(kr) k\, dk \frac{\sin \beta_1 d}{\beta_1} \left[ \frac{\beta_1 \cos \beta_1 (H - z) + ib\beta_2 \sin \beta_1 (H - z)}{\beta_1 \cos \beta_1 H + ib\beta_2 \sin \beta_1 H} \right] d \leq z \leq H, \tag{A18}$$

which is useful at large ranges and for wave lengths which are of the order of a fraction of the depth of water or greater. When the range is great for a large number of images to be required, the radiation from the images is mutually reinforced in certain particular directions as in the case of a diffraction grating (Slater, 1942, p. 284). The waves traveling in these directions, together with their reflections at the surface and the bottom, constitute the normal modes. The analogy with the diffraction grating is not complete because the strength of the n-th image is not unity but $K^n$, where $K$ denotes the reflection coefficient. One also needs to take into account the fact that the waves emanating from the point images are not plane but spherical.

Both these factors of divergence are automatically taken into account by our method of derivation of the normal-mode solution from the exact integral (A18). By this method the normal-mode solution is obtained from the residues of the integrand in the $k$-plane (Lamb, 1904). In doing so, one must observe the circumstance that, by (A7), $\beta_1$ and $\beta_2$ are multiple-valued functions of $k$ with branch points at

$$k = k_1 = \omega/c_1 \quad \text{and} \quad k = k_2 = \omega/c_2$$

respectively. We therefore cut up the $k$-plane as is shown in Figure G.

The poles of the integrand in (A18) lie either on the real axis between $k_2$ and $k_1$ ($c_1 < c_2$) or in the fourth quadrant. Let

$$F(\beta_1, \beta_2) \equiv \frac{\sin \beta_1 d}{\beta_1} \left[ \frac{\beta_1 \cos \beta_1(H - z) + ib\beta_2 \sin \beta_1(H - z)}{\beta_1 \cos \beta_1 H + ib\beta_2 \sin \beta_1 H} \right], \tag{A40}$$

this being a function which is *even* in $\beta_1$ but mixed in $\beta_2$. Then

$$\Psi_2 = 2 \int_0^\infty J_0(kr)k\, dkF(\beta_1, \beta_2) = \int_0^\infty [H_0^{(1)}(kr) + H_0^{(2)}(kr)]F(\beta_1, \beta_2)k\, dk. \tag{A41}$$

$$\int_0^\infty H_0^{(1)}(kr)F(\beta_1, \beta_2)k\, dk = \int_0^{i\infty} H_0^{(1)}(kr)F(\beta_1, \beta_2)k\, dk = -\int_0^\infty H_0^{(1)}(iur)F(\beta_1, \beta_2)u\, du$$

$$= \frac{2i}{\pi} \int_0^\infty K_0(ur)F(\beta_1, \beta_2)u\, du, \tag{A42}$$

because the integral along the real axis can be transformed into an integral along the positive imaginary axis, and

$$H_0^{(1)}(iu) = -\frac{2i}{\pi} K_0(u) = -H_0^{(2)}(-iu). \tag{A43}$$

The integral with the $H_0^{(2)}(kr)$ function can be transformed into one along the paths $B+(C+D)+(E+F)+$ the contribution from the residues in the fourth quadrant:

$$\int_0^\infty H_0^{(2)}(kr)F(\beta_1, \beta_2)k\, dk = \left[ \int_0^{-i\infty} + \overset{\uparrow}{C} \int \underset{\downarrow}{D} + \overset{\uparrow}{E} \int \underset{\downarrow}{F} \right] H_0^{(2)}(kr)F(\beta_1, \beta_2)k\, dk + \text{Residues}. \tag{A44}$$

Now

$$\int_0^{-i\infty} H_0^{(2)}(kr)F(\beta_1, \beta_2)k\, dk = -\int_0^\infty H_0^{(2)}(-iur)F(\beta_1, \beta_2)u\, du$$

$$= -\frac{2i}{\pi} \int_0^\infty K_0(ur)F(\beta_1, \beta_2)u\, du = -\int_0^\infty H_0^{(1)}(kr)F(\beta_1, \beta_2)k\, dk, \tag{A45}$$

so that this term just cancels the integral with the $H_0^{(1)}(kr)$ function. Also, in the term $\overset{\uparrow}{E} \int \underset{\downarrow}{F}$, $F(\beta_1, \beta_2)$ has the same value on either side of the $k$-cut because it is one-valued there with respect to the argument $\beta_2$, and $\beta_1$ merely changes sign, which leaves $F(\beta_1, \beta_2)$ unaffected. Hence the integral along $F$ exactly cancels the integral along $E$ *and* $\overset{\uparrow}{E} \int \underset{\downarrow}{F}$ *vanishes.*

The remaining integral does not vanish:

$$\overset{\uparrow}{C} \int \underset{\downarrow}{D} H_0^{(2)}(kr)F(\beta_1, \beta_2)k\, dk = \overset{\uparrow}{C} \int H_0^{(2)}(kr)[F(\beta_1, \beta_2) - F(\beta_1, -\beta_2)]k\, dk$$

$$= \int_{-i\infty}^{k_2} H_0^{(2)}(kr)[F(\beta_1, \beta_2) - F(\beta_1, -\beta_2)]k\, dk. \tag{A46}$$

We have thus accomplished a transformation of the integral (A18) into an integral along a branch line and a sum of residues

$$\Psi_2 = \int_{-i\infty}^{k_2} H_0^{(2)}(kr)[F(\beta_1, \beta_2) - F(\beta_1, -\beta_2)]k\,dk + \Sigma \text{ Residues.} \tag{A47}$$

b) *The residues or "normal modes".*—The last term in (A47) can be written as

$$\Psi_2' \equiv \Sigma \text{ Res} = \Sigma \text{ Res} \int_0^{\infty} H_0^{(2)}(kr)F(\beta_1, \beta_2)k\,dk$$

$$= -2\pi i \sum_n H_0^{(2)}(k_n r)k_n \frac{\sin \beta_1 d[\beta_1 \cos \beta_1(H - z) + ib\beta_2 \sin \beta_1(H - z)]}{\beta_1 \dfrac{\partial}{\partial k}[\beta_1 \cos \beta_1 H + ib\beta_2 \sin \beta_1 H]},$$

$$\Psi_2' = -\frac{2\pi i}{H} \sum_n \frac{H_0^{(2)}(k_n r)(\beta_1 H) \sin (\beta_1 d) \sin (\beta_1 z)}{[\beta_1 H - \sin (\beta_1 H) \cos (\beta_1 H) - b^2 \sin^2 (\beta_1 H) \tan (\beta_1 H)]}, \qquad 0 < z < H. \tag{A48}$$

In deriving (A48), use was made of the fact that the terms appearing there are to be evaluated at the roots $k = k_n$ of the equation

$$\beta_2 = \frac{i\beta_1}{b \tan (\beta_1 H)}. \tag{A49}$$

If instead of (A18) we had used (A17), we would have obtained precisely the identical expression for the residues. This expression therefore holds for the whole range of $0 < z \leq H$. For $z > H$ we find similarly by operating on (A19) that the residues are given by

$$\Psi_3' = -\frac{2\pi i b}{H} \sum_n \frac{H_0^{(2)}(k_n r)(\beta_1 H) \sin (\beta_1 d) \sin (\beta_1 H) e^{-i\beta_2 (z-H)}}{[(\beta_1 H) - \sin (\beta_1 H) \cos (\beta_1 H) - b^2 \sin^2 (\beta_1 H) \tan (\beta_1 H)]}, \qquad z > H. \tag{A50}$$

c) *The question of the orthogonality and the normalization factors of the normal modes.*—The appearance of the branch-line integral in the solution for a point source given in (A47) would seem to be in contradiction to standard theory of normal modes. According to this theory, if $F_n(z)$ are a set of solutions of the equation

$$\frac{d^2 F_n}{dz^2} + \left[\frac{\omega^2}{c(z)^2} - k_n^2\right] F_n = 0, \tag{A51}$$

which satisfy the boundary conditions, then the solution for a point source situated at depth $d$ is

$$\Psi_2 = -i\pi \sum_n H_0^{(2)}(k_n r) F_n(z) F_n(d)/C_n^2, \tag{A52}$$

$$C_n^2 = \int_0^h F_n^2(z)\,dz, \tag{A53}$$

where $h$ denotes the lower boundary of the medium. In deriving this result one makes use of the orthogonality of $F_n$, which can be proved by multiplying (A51) by

$F_m$, and the differential equation for $F_m$ by $F_n$, and subtracting, which yields

$$\frac{d}{dz}(\dot{F}_n F_m - F_n \dot{F}_m) = (k_n^2 - k_m^2) F_n F_m, \tag{A54}$$

$$(\dot{F}_n F_m - F_n \dot{F}_m)_{z=0}^{z=h} = (k_n^2 - k_m^2) \int_0^h F_n F_m \, dz. \tag{A55}$$

Here the left-hand side vanishes because of the boundary conditions, showing that the integral on the right vanishes when $n \neq m$.

In our case $h = \infty$, and we may take

$$\begin{aligned} F_n(z) &= \sin \beta_1^{(n)} z \qquad z < H \\ &= \sin (\beta_1^{(n)} H) e^{-i\beta_2^{(n)}(z-H)} \qquad z > H, \end{aligned} \tag{A56}$$

which ensures continuity at $z = H$.

Now, first with regard to the question of orthogonality we find, on using (A49), that

$$\int_0^H \sin (\beta_1^{(n)} z) \sin (\beta_1^{(m)} z) \, dz = \frac{ib \sin (\beta_1^{(n)} H) \sin (\beta_1^{(m)} H)}{(\beta_2^{(n)} + \beta_2^{(m)})}, \tag{A57}$$

$$\sin (\beta_1^{(n)} H) \sin (\beta_1^{(m)} H) \int_H^\infty e^{-i(z-H)(\beta_2^{(n)} + \beta_2^{(m)})} \, dz = \frac{-i \sin (\beta_1^{(n)} H) \sin (\beta_1^{(m)} H)}{(\beta_2^{(n)} + \beta_2^{(m)})}, \tag{A58}$$

$$\int_0^\infty F_n(z) F_m(z) \, dz = \frac{i(b-1) \sin (\beta_1^{(n)} H) \sin (\beta_1^{(m)} H)}{(\beta_2^{(n)} + \beta_2^{(m)})}. \tag{A59}$$

Eq. (A57) shows that when the integral is extended only over the depth of water, as it should not be, the $F$'s are not orthogonal. Even when the integration includes the bottom, Eq. (A59) shows that *the $F$'s are not orthogonal except in case $b = 1$*, when the densities in the water and the bottom are equal.

As for the normalization factors $C_n^2$ defined in (A53), we get

$$\begin{aligned} C_n^2 &= \int_0^H \sin^2 \beta_1(z) \, dz + \sin^2 \beta_1 H \int_H^\infty e^{-2i\beta_2(z-H)} \, dz \\ &= \left(\frac{1}{2\beta_1}\right) [\beta_1 H - \sin \beta_1 H \cos \beta_1 H - b \sin^2 \beta_1 H \tan \beta_1 H]. \end{aligned} \tag{A60}$$

When this is substituted into (A52), we get an expression which is identical with (A48) except for the $b$ in (A60) which appears in place of $b^2$ in the bracket of (A48). Hence, we find again that *the expansion (A52) holds only in the case $b = 1$.*

The reason for the disagreement between our results and the standard theory of normal modes is that the latter is based on certain assumed continuity conditions which do not obtain in our case, due to the discontinuity at the bottom. These assumed conditions are those which are implicit in going from Eq. (A54) to (A55), namely that the function $(\dot{F}_n F_m - F_n \dot{F}_m)$ should be continuous throughout the region of integration. In the case of a sound problem, this condition is violated at a surface of discontinuity of density because the boundary conditions of equality of vertical velocity and *pressure* require that $\dot{F}$ and $\rho F$, not $F$, should be continuous. The vertical component of velocity and the pressure are continuous, but the horizontal component of velocity is discontinuous. In case of a discontinuity in density at the boundary between medium 1 and medium 2, Eq. (A55) becomes

$$(k_n^2 - k_m^2)\int_0^h F_nF_m\,dz = (\dot{F}_nF_m - F_n\dot{F}_m)_{z=0}^{z=h} + (\dot{F}_nF_m - F_n\dot{F}_m)_1 - (\dot{F}_nF_m - F_n\dot{F}_m)_2$$

$$= -(b-1)(\dot{F}_nF_m - F_n\dot{F}_m)_1; \qquad (b \equiv \rho_1/\rho_2). \tag{A61}$$

*Hence, even in the case of a continuous sound velocity $c(z)$, the peculiar boundary conditions imposed by the sound problem make the normal functions nonorthogonal in the presence of a density discontinuity.*

When the densities in the bottom and the water are equal, but not the sound velocities, the normal functions are orthogonal, and the normalization factors agree with (A53). *Still, even in this case, the branch-line integral in (A47) does not vanish.*

Possibly the theorem upon which expansion (A52) is based does not apply to our case where, although the $F$'s and their first derivatives are continuous, the second and all higher derivatives are discontinuous on account of the velocity discontinuity. It is also possible that in the section of the $k$-plane cut out in Figure G are not included all the poles of the integrand (the set of normal functions in (A47) is not complete) and that the branch-line integral is equivalent to the contribution from the omitted normal modes. We reserve the elucidation of this point for another occasion but merely point out here that the integral for the potential of a point source in a *uniform* medium given in (A20) does not possess any poles, and therefore possesses no associated normal modes. It can be transformed into a branch-line integral which coincides with the limit approached by the branch-line integral in (A47) as $\rho_2 \to \rho_1$ and $c_2 \to c_1$.

It will be shown in the next section that the branch-line integral in (A47) behaves asymptotically for large horizontal ranges $r$ like a dipole, modified by the presence of the bottom (or rather of the water), due to the interference between the source and its image.

d) *Asymptotic behavior of the branch line integral for large horizontal ranges.*— The integral under discussion is

$$\Psi_2'' \equiv \int_{-i\infty}^{k_2} H_0^{(2)}(kr)[F(\beta_1, \beta_2) - F(\beta_1, -\beta_2)]\,k\,dk$$

$$= -2ib\int_{-i\infty}^{k_2} H_0^{(2)}(kr)k\,dk\,\frac{\beta_2\sin(\beta_1 d)\sin(\beta_1 z)}{[\beta_1^2\cos^2(\beta_1 H) + b^2\beta_2^2\sin^2(\beta_1 H)]}, \tag{A62}$$

with

$$F(\beta_1, \beta_2) \equiv \frac{\sin(\beta_1 d)}{\beta_1}\left[\frac{\beta_1\cos\beta_1(H-z) + ib\beta_2\sin\beta_1(H-z)}{\beta_1\cos(\beta_1 H) + ib\beta_2\sin(\beta_1 H)}\right], \tag{A40}$$

$$\beta_1 = \sqrt{k_1^2 - k^2}, \qquad \beta_2 = \sqrt{k_2^2 - k^2}, \qquad k_1 = \omega/c_1, \qquad k_2 = \omega/c_2.$$

We shall state here without proof that under certain conditions $\Psi_2''$ has the following asymptotic behavior for large $r$

$$\Psi_2'' \longrightarrow \frac{(2ibk_2)}{(k_1r)^2} \frac{\sin(k_1 d\mu)\sin(k_1 z\mu)e^{-ik_2r}}{\mu^2\cos^2(k_1H\mu)}; \qquad \begin{matrix} c_1 < c_2 \\ z < H \end{matrix}, \tag{A63}$$

$$\Psi_2'' \longrightarrow \frac{(2ibk_2)}{(k_1r)^2} \frac{sh(k_1 d\nu)sh(k_1z\nu)e^{-ik_2r}}{\nu^2ch^2(k_1H\nu)}; \qquad \begin{matrix} c_1 > c_2 \\ z < H \end{matrix}, \tag{A64}$$

$$\Psi_2'' \longrightarrow \frac{(2ibk_2)}{(k_1r)^2} \frac{\sin(k_1 d\mu)[k_1(z-H)\mu\cos(k_1H\mu) + b\sin(k_1H\mu)]}{\mu^2\cos^2(k_1H\mu)}; \qquad \begin{matrix} c_1 < c_2 \\ z > H \end{matrix}, \tag{A65}$$

$$\Psi_2'' \longrightarrow \frac{(2ibk_2)}{(k_1r)^2} \frac{sh(k_1 d\nu)[k_1(z-H)\nu ch(k_1H\nu) + bsh(k_1H\nu)]}{\nu^2ch^2(k_1H\nu)}; \qquad \begin{matrix} c_1 > c_2 \\ z > H \end{matrix}, \tag{A66}$$

where

$$\nu \equiv \sqrt{\frac{c_1^2}{c_2^2} - 1}, \qquad \mu \equiv \sqrt{1 - \frac{c_1^2}{c_2^2}}. \tag{A67}$$

The conditions for the validity of these asymptotic forms are that $(k_1H\mu)$ should be removed from a zero of the cosine in the denominators of (A63) and (A65), and that $k_1\nu(z-H)$ or $k_1\mu(z-H)$ should not be large.

The above expressions bear an analogy to the asymptotic form assumed for large $r$ by the solution for a point source in a uniform medium:

$$\Psi = \left(\frac{e^{-ikR_1}}{R_1} - \frac{e^{-ikR_2}}{R_2}\right) \longrightarrow \frac{2i}{R}\sin\left(\frac{kzd}{R}\right)e^{-ikR} \longrightarrow \frac{2ikzd}{r^2}e^{-ikr}. \tag{A68}$$

The last limit is the one approached by Eqs. (A63) to (A66) as $c_2 \to c_1$ and $\rho_2 \to \rho_1$.

e) *Phase velocity and group velocity of the normal modes in a two-layered liquid half-space.*—Let

$$x_n \equiv \beta_1^{(n)}H = H\sqrt{\frac{\omega^2}{c_1^2} - k_n^2}, \qquad \left(\beta_2^{(n)} = \sqrt{\frac{\omega^2}{c_2^2} - k_n^2} = -i\sqrt{k_n^2 - \frac{\omega^2}{c_2^2}}\right), \tag{A69}$$

then the normal-mode component of the solution for the potential can be written as

$$\Psi_2' = \left(\frac{-2\pi i}{H}\right)\sum_{n=1}^{\infty}\frac{H_0^{(2)}(k_nr)x_n\sin(x_nd/H\sin(x_nz/H)}{(x_n - \sin x_n\cos x_n - b^2\sin^2 x_n\tan x_n)}, \qquad 0 < z < H, \tag{A48}$$

$$\Psi_2' = \left(\frac{-2\pi ib}{H}\right)\sum_{n=1}^{\infty}\frac{H_0^{(2)}(k_nr)x_n\sin(x_nd/H)\sin x_n e^{-i\beta_2^{(n)}(z-H)}}{(x_n - \sin x_n\cos x_n - b^2\sin^2 x_n\tan x_n)}, \qquad z > H, \tag{A50}$$

where the $x_n$ are roots of the equation

$$\frac{\tan x}{x} = \frac{i}{bH\beta_2} = -\frac{1}{bH\sqrt{k_n^2 - \frac{\omega^2}{c_2^2}}} = -\frac{1}{bH\sqrt{\frac{\omega^2}{c_1^2} - \frac{\omega^2}{c_2^2} - \frac{x^2}{H^2}}}. \tag{A49}$$

For large $r$ the Hankel function may be approximated by its asymptotic form

$$H_0^{(2)}(k_nr) \to \sqrt{\frac{2}{\pi k_nr}}\, e^{i[(\pi/4) - k_nr]}, \tag{A70}$$

and the normal-mode component of the sound potential $\varphi_2' = e^{i\omega t}\Psi_2'$ becomes

$$\varphi_2' = \left(\frac{2\pi}{H}\right)\sqrt{\frac{2}{\pi r}}\sum_{n=1}^{\infty}\frac{1}{\sqrt{k_n}}e^{i(\omega t-k_n r-\pi/4)}F(x_n)\sin(x_n d/H)\sin(x_n z/H), \qquad 0 < z < H, \quad \text{(A71)}$$

$$\varphi_2' = \left(\frac{2\pi b}{H}\right)\sqrt{\frac{2}{\pi r}}\sum_{n=1}^{\infty}\frac{1}{\sqrt{k_n}}e^{i(\omega t-k_n r-\pi/4)}F(x_n)\sin(x_n d/H)\sin x_n e^{-i\beta_2^{(n)}(z-H)},$$

$$z > H, \quad \text{(A72)}$$

$$F(x_n) \equiv \frac{x_n}{(x_n - \sin x_n \cos x_n - b^2 \sin^2 x_n \tan x_n)}. \quad \text{(A73)}$$

The physical meaning of $k_n$ is now apparent from the term

$$e^{i(\omega t-k_n r-\pi/4)}, \quad \text{namely,} \quad k_n = \frac{\omega}{c_n},$$

where $c_n$ is the *phase velocity* of the n-th mode. The factor $F(x_n)/\sqrt{k_n}$ gives the relative strength of each mode, while the factor $\sin(x_n d/H)\sin(x_n z/H)$ gives the variation of the amplitude of the mode with depth of source and depth of receiver. Let

$$\alpha_n = k_n H, \qquad \delta = (\rho_2 c_2/\rho_1 c_1), \qquad \epsilon^2 = \frac{c_2^2}{c_1^2} - 1. \quad \text{(A74)}$$

Then, upon omitting the subscript $n$ in the sequel, Eq. (A49) can be written as

$$\frac{\tan x}{x} = -\frac{\delta}{\sqrt{(\alpha^2 - x^2 + \alpha^2\epsilon^2}}, \quad \text{or} \quad \text{(A75)}$$

$$\alpha = \frac{x}{\epsilon}\sqrt{1 + \delta^2 \cot^2 x}, \quad \text{(A76)}$$

$$c = c_1\sqrt{1 + x^2/\alpha^2} = c_1\sqrt{1 + \frac{\epsilon^2}{(1 + \delta^2\cot^2 x)}}. \quad \text{(A77)}$$

We shall be interested primarily in the case of a high-speed bottom ($c_2 > c_1$), where Eq. (A49) or (A75) possesses an infinite set of *real* roots $x_n$ in the range $\pi(n - \frac{1}{2}) < x_n < n\pi$ for the $n$-th mode. In that case $k_n$ and the phase velocity are real, and the propagation of the modes proceeds without damping. The physical reason for the undamped propagation, which is discussed elsewhere in this paper, is briefly that the normal modes are made up of mutually reinforcing elementary waves (emanating from the various images) which are *totally* reflected by the bottom.

It is seen from Eq. (A49) that $x_n$ is a function of the circular frequency $\omega$, and therefore, from Eq. (A77), that the phase velocity $c$ is a function of frequency. The frequency corresponding to any given value of $x_n$ can be obtained from

$$\gamma \equiv \frac{\omega H}{2\pi c_1} = \frac{H}{\lambda} = \frac{\alpha c}{2\pi c_1} = \frac{x}{2\pi\epsilon}\sqrt{1 + \epsilon^2 + \delta^2\cot^2 x}\cdot \quad \text{(A78)}$$

$\gamma$ denotes the ratio of the depth of water $H$ to the wave length of sound in water $\lambda$. When $x_n$ is near its upper limit of $n\pi$, $\gamma$ is very large by (A78), and by (A77) $c \to c_1$. Hence, *in the limit of very high frequencies the phase velocity of all the modes approaches* *the sound velocity $c_1$ in the water.* On the other hand, when $x_n$ is near its lower limit of $(n - \frac{1}{2})\pi$, $\gamma$ does not become zero but approaches the limit.

$$\gamma_n = \frac{H}{\lambda_n} \rightarrow \bar{\gamma}_n = \frac{(n - 1/2)\pi\sqrt{1+\epsilon^2}}{2\pi\epsilon} = \frac{(n - 1/2)}{2\sqrt{1 - \frac{c_1^2}{c_2^2}}}, \qquad \gamma_n = (2n - 1)\gamma_1. \tag{A79}$$

*This means that for each mode there is a limiting frequency below which undamped propagation is impossible.* The physical reason for the limiting frequency, which is bound up with the inception of total reflection at the critical angle of incidence, is discussed elsewhere in the report. From (A77) it follows that at the critical frequency $(x = n\pi - \pi/2)$, $c \rightarrow c_1\sqrt{1 + \epsilon^2} = c_2$. The phase velocity therefore varies from the value $c_2$ at the critical frequency down to $c_1$ in the limit of very high frequencies. The variation is monotone and is shown for several media in Figure 28.

In a medium in which the phase velocity varies with frequency, the energy in an arbitrary disturbance embracing a band of frequencies is known to propagate with the so-called *group-velocity* (Lamb, 1932, p. 380–398; Jeffreys, 1931, p. 84–94). This is an important consideration in our study of propagation of explosive sound in shallow water. In the next section we shall show how the notion of group velocity appears in the analysis of the mutual interference of a band of frequencies advancing with different phase velocities. Here we shall merely define the group velocity $U$ as

$$U \equiv \frac{d\omega}{dk} = \frac{d}{dk}(kc) = c + k\frac{dc}{dk} = c + \alpha\frac{dc}{d\alpha}, \tag{A80}$$

$c$ denoting the phase velocity, and derive an expression for it in the case of the normal modes in a two-layered liquid half-space. We have from (A77)

$$\alpha\frac{dc}{d\alpha} = \frac{c_1 x\left(\frac{dx}{d\alpha} - \frac{x}{\alpha}\right)}{\sqrt{\alpha^2 + x^2}} \tag{A81}$$

and from (A76)

$$\frac{dx}{d\alpha} = 1\Big/\frac{d\alpha}{dx} = \frac{\epsilon\sqrt{1 + \delta^2 \cot^2 x}}{(1 + \delta^2 \cot^2 x - \delta^2 x \cos x/\sin^3 x)}. \tag{A82}$$

Substituting (A82) into (A81) and using the latter in (A80), we get

$$\frac{U}{c_1} = \left(\frac{c_1}{c}\right)\left[1 + \frac{\epsilon^2}{\varphi(x)}\right] = \left[1 + \frac{\epsilon^2}{(1 + \delta^2 \cot^2 x)}\right]^{-\frac{1}{2}} \cdot \left[1 + \frac{\epsilon^2}{\varphi(x)}\right]. \tag{A83}$$

$$\varphi(x) \equiv [1 + \delta^2(\cot^2 x - x \cos x/\sin^3 x)]. \tag{A84}$$

For the purpose of computing the *amplitude of a wave packet* we shall need in the next section the function $\frac{d^2k}{d\omega^2}$. This we now proceed to derive:

$$\frac{dk}{d\omega} = \frac{1}{U}, \qquad \frac{d^2k}{d\omega^2} = -\frac{1}{U^2}\frac{dU}{d\omega} = -\frac{1}{U^3}\frac{dU}{dk} = -\frac{H}{U^3}\frac{dU}{d\alpha} = -\frac{H}{U^3}\frac{dU}{dx}\cdot\frac{dx}{d\alpha}. \tag{A85}$$

One finds that

$$\frac{d\varphi}{dx} = -\frac{3\delta^2 \cos x}{\sin^3 x} + \frac{x\delta^2}{\sin^4 x}(1 + 2\cos^2 x).$$

$$\frac{d}{dx}\left(\frac{c_1}{c}\right) = -\frac{\delta^2 x^4 \cos x}{\alpha\epsilon^2 \sin^3 x(\alpha^2 + x^2)^{3/2}}.$$

$$\frac{d^2k}{d\omega^2} = \frac{Hc_1\delta^2}{U^3}\left\{\frac{x^3 \cos x[\epsilon^2 + \varphi(x)]}{\sin^3 x\varphi(x)^2(\alpha^2 + x^2)^{3/2}} + \frac{\alpha^2\epsilon^4(x + 2x\cos^2 x - 3\sin x\cos x)}{x\varphi(x)^3 \sin^4 x\sqrt{\alpha^2 + x^2}}\right\}. \quad \text{(A86)}$$

Eqs. (A77), (A78), (A83), and (A86) now provide a convenient scheme for determining corresponding values of the phase velocity, frequency, group velocity, and $\frac{d^2k}{d\omega^2}$ respectively, by computing the functions in the whole range of $\pi(n - \frac{1}{2}) < x_n < n\pi$ for the $n$-th mode. Otherwise one has to resort to time-wasting trial and error calculations.

f) *The propagation of explosive sound in a two-layered liquid half-space.*

I. The ground-wave and water-wave phases

In previous sections we discussed the solution for the potential (which is proportional to the acoustic pressure) due to a periodic point source of circular frequency $\omega$. It was shown that at large ranges $r$ the potential $\varphi_2$ in the water is given by a series of normal modes,

$$\varphi_2' = \sum_{n=1}^{\infty} e^{i(\omega t - k_n r - \pi/4)} Q_n(\omega),$$

$$Q_n(\omega) = \left(\frac{2\pi}{H}\right)\sqrt{\frac{2}{\pi k_n r}}\left[\frac{x_n \sin(x_n d/H)\sin(x_n z/H)}{(x_n - \sin x_n \cos x_n - b^2 \sin^2 x_n \tan x_n)}\right], \quad 0 < z < H, \quad \text{(A71)}$$

and by a branch-line integral $\varphi_2'' = e^{i\omega t}\Psi_2''$ which, as was shown in Eq. (A63), decreases with range like $r^{-2}$. Since we shall be interested primarily in propagation to large ranges, we shall disregard the contribution from the branch-line integral. This term is relatively important at the very onset of the ground wave, because the amplitude of the normal modes is zero at that instant, but during the major span of the received record it fades into insignificance on account of its $r^{-2}$ variation, as compared with the $r^{-\frac{1}{2}}$ (or $r^{-1}$ for a wave packet) of the normal modes.

If the time variation of the pressure pulse at the source is not periodic but an arbitrary function $f(t)$ represented by its Fourier transform

$$f(t) = \frac{1}{2\pi}\int_{-\infty}^{\infty} e^{i\omega t} g(\omega)\, d\omega, \quad \text{(A22)}$$

then the pressure is given by

$$P(r, z, t) = \frac{1}{2\pi}\int_{-\infty}^{\infty} g(\omega)\varphi_2'(\omega)\, d\omega = \sum_{n=1}^{\infty} P_n(r, z, t), \quad \text{(A87)}$$

$$P_n(r, z, t) = \frac{1}{2\pi}\int_{-\infty}^{\infty} e^{i[\omega t - k_n(\omega)r - \pi/4]} g(\omega) Q_n(\omega, r, z)\, d\omega \quad \text{(A88)}$$

The term $P_n(r, z, t)$ represents the contribution to the pressure from the $n$-th mode.

We shall be interested in the case when

$$f(t) = e^{-\lambda t} \qquad t > 0 \qquad \text{(A89)}$$
$$= 0 \qquad t < 0,$$

where

$$f(t) = \frac{1}{2\pi}\int_{-\infty}^{\infty} \frac{e^{i\omega t}}{(\lambda + i\omega)}, \qquad g(\omega) = \frac{1}{(\lambda + i\omega)}, \qquad \text{(A90)}$$

$$P_n(r, z, t) = \frac{1}{2\pi}\int_{-\infty}^{\infty} \frac{Q_n(\omega, r, z)}{(\lambda + i\omega)} e^{i[\omega t - k_n(\omega)r - \pi/4]}\, d\omega. \qquad \text{(A91)}$$

In treating the integral (A91), we take cognizance of the fact that the term $Q_n(\omega)/(\lambda + i\omega)$ is a slowly varying function of $\omega$, whereas the exponential factor is rapidly oscillatory. The principal contribution to the integral arises from small ranges of $\omega$ in the vicinity of the points of *stationary phase—i.e.*, at the points at which $\dot{f}(\omega) = 0$, where

$$f(\omega) \equiv \omega t - k_n(\omega)r - \pi/4, \qquad \dot{f}(\omega) = t - r \cdot \frac{dk}{d\omega} = 0. \qquad \text{(A92)}$$

In the vicinity of a point of stationary phase $\omega_0$ we write

$$\omega = \omega_0 + u, \qquad f(\omega) = f(\omega_0) - \frac{r\ddot{k}(\omega_0)}{2}u^2 - \frac{r\dddot{k}(\omega_0)}{6}u^3 - \cdots. \qquad \text{(A93)}$$

$$\frac{1}{2\pi}\int_{-\infty}^{\infty} \frac{Q_n(\omega)}{(\lambda + i\omega)} e^{if(\omega)}\, d\omega = \frac{1}{2\pi}\frac{Q_n(\omega_0)\, e^{if(\omega_0)}}{(\lambda + i\omega_0)}\int_{-\infty}^{\infty} e^{-i[(r/2)\ddot{k}(\omega_0)u^2 + (r/6)\dddot{k}(\omega_0)u^3 + \cdots]}\, du,$$

$$\int_{-\infty}^{\infty} e^{-i[(r/2)\ddot{k}u^2 + (r/6)\dddot{k}u^3 + \cdots]}\, du \simeq \sqrt{\frac{2\pi}{r|\ddot{k}|}}\, e^{\pm i\pi/4}\left\{1 + \frac{i}{r}\left[-\frac{5(\dddot{k})^2}{24(\ddot{k})^3} + \frac{\ddddot{k}}{8(\ddot{k})^2}\right] + 0\left(\frac{1}{r^2}\right)\right\}, \qquad \text{(A94)}$$

where the + sign in $e^{+i\pi/4}$ is to be taken if $\ddot{k} < 0$, and the − sign when $\ddot{k} > 0$. Hence

$$P_n = \frac{1}{2\pi}\int_{-\infty}^{\infty} \frac{Q_n(\omega)}{(\lambda + i\omega)} e^{if(\omega)}\, d\omega = \frac{Q_n(\omega_0)}{2\pi(\lambda + i\omega_0)} e^{i[\omega_0 t - rk(\omega_0)]}\sqrt{\frac{2\pi}{r|\ddot{k}(\omega_0)|}}\,\{\,\}, \quad \ddot{k} < 0 \qquad \text{(A95)}$$

$$= \frac{1}{2\pi}\frac{Q_n(\omega_0)}{(\lambda + i\omega_0)} e^{i[\omega_0 t - rk(\omega_0) - \pi/2]}\sqrt{\frac{2\pi}{r\ddot{k}(\omega_0)}}\,\{\,\}, \qquad \ddot{k} > 0, \qquad \text{(A96)}$$

$$\{\,\} = \left\{1 + \frac{i}{r}\left[-\frac{5(\dddot{k})^2}{24(\ddot{k})^3} + \frac{\ddddot{k}}{8(\ddot{k})^2}\right] + 0\left(\frac{1}{r^2}\right)\right\}. \qquad \text{(A97)}$$

At this stage we must consider the location of the points of stationary phase $\omega_0$ in the complex $\omega$-plane. The phase $f(\omega) = [\omega t - k_n(\omega)r - \pi/4]$ was arrived at by assuming a factor $e^{+i\omega t}$ for the steady-state potential and then adding the phase of the $-iH_0^{(2)}(k_n r)$ given in (A70). Had we assumed instead a time factor $e^{-i\omega t}$, the term $-iH_0^{(2)}(k_n r)$ would have been replaced by its conjugate $+iH_0^{(1)}(k_n r)$, and the phase would have changed sign. It follows that, whereas $Q_n(\omega)$ is an even function of $\omega$, (because $x$ defined in (A69) is even in $\omega$), $f(\omega)$ is an odd function of $\omega$; and for every positive value of $\omega_0$ where $\dot{f}(\omega_0)$ vanishes there is another stationary point at $\omega = -\omega_0$. We have therefore to add to the expressions (A95) and (A96) their complex conjugates:

$$P_n(r, z, t) = \frac{2Q_n(\omega_0) \cos [\omega_0 t - rk(\omega_0) - \tan^{-1}(\omega_0/\lambda)]}{[2\pi r \,|\, \ddot{k}(\omega_0) \,|\, (\lambda^2 + \omega_0^2)]^{\frac{1}{2}}} \left\{ \quad \right\}, \qquad \ddot{k} < 0, \tag{A98}$$

$$= \frac{2Q_n(\omega_0) \cos [\omega_0 t - rk(\omega_0) - \tan^{-1}(\omega_0/\lambda) - \pi/2]}{[2\pi r \ddot{k}(\omega_0) (\lambda^2 + \omega_0^2)]^{\frac{1}{2}}} \left\{ \quad \right\}, \qquad \ddot{k} > 0, \tag{A99}$$

$$\left\{ \quad \right\} = \left\{ 1 - \frac{\tan [\quad]}{r} \left[ \frac{-5(\dddot{k})^2}{24(\ddot{k})^3} + \frac{\ddddot{k}}{8(\ddot{k})^2} \right] + 0\left( \frac{1}{r^2} \right) \right\}, \tag{A100}$$

where tan [ ] denotes the tangent of the respective arguments of the cosines in (A98) and (A99).

The factor { } is used only for purposes of estimating the range of validity of the approximation made in applying the method of stationary phase. Expressions (A98) and (A99) are to be used only when

$$\frac{1}{r} \left[ -\frac{5(\dddot{k})^2}{24(\ddot{k})^3} + \frac{\ddddot{k}}{8(\ddot{k})^2} \right] \ll 1. \tag{A101}$$

This condition is violated for small ranges and near the point of the minimum group velocity, where $\ddot{k} = 0$. In the vicinity of that point the integral (A91) requires special treatment which was devised by Airy.

It is convenient to express the correction term given in (A101) in terms of the nondimensional quantities

$$\gamma = \frac{H}{\lambda} = \frac{\omega H}{2\pi c_1}, \qquad Z = \frac{c_1^2}{H} \frac{d^2 k}{d\omega^2}, \qquad \frac{dZ}{d\gamma} = \frac{2\pi c_1^3}{H^2} \frac{d^3 k}{d\omega^3}, \qquad \frac{d^2 Z}{d\gamma^2} = \frac{4\pi^2 c_1^4}{H^3} \frac{d^4 k}{d\omega^4},$$

of which $Z(\gamma)$ can be computed directly from Eq. (86), and $\dot{Z}$ and $\ddot{Z}$ can then be computed by numerical differentiation from the tabulated values of $Z$ as a function of $\gamma$. Substituting into (A101), we find that

$$\frac{1}{24r} \left[ -\frac{5(\dddot{k})^2}{(\ddot{k})^3} + \frac{3\ddddot{k}}{(\ddot{k})^2} \right] = \frac{1}{96\pi^2} \left( \frac{H}{r} \right) \left[ -\frac{5\dot{Z}^2}{Z^3} + \frac{3\ddot{Z}}{Z^2} \right] \ll 1 \tag{A102}$$

is the condition to be observed when applying (A98) and (A99).

We now summarize the results of this section. In order to compute the contribution from the $n$-th mode $P_n$ at a given time $t$ and point $(r, z)$ in case of an exponential pulse, one first finds the points $\omega_0$ on the dispersion curve $k_n(\omega)$, characteristic of the medium, such that

$$t - \frac{r}{U} = 0, \qquad \frac{1}{U} = \frac{dk}{d\omega}. \tag{A103}$$

$P_n$ is then computed from

$$P_n = \frac{4\cos[\omega_0 t - rk - \tan^{-1}(\omega_0/\lambda)]}{Hr\sqrt{k_n|\ddot{k}_n|(\lambda^2+\omega_0^2)}}\left[\frac{x_n \sin(x_n d/H)\sin(x_n z/H)}{(x_n - \sin x_n \cos x_n - b^2\sin^2 x_n \tan x_n)}\right]; \quad \ddot{k} < 0, \quad \text{(A104)}$$

$$P_n = \frac{4\cos\left[\omega_0 t - rk - \tan^{-1}(\omega_0/\lambda) - \frac{\pi}{2}\right]}{Hr\sqrt{k_n \cdot \ddot{k}_n(\lambda^2+\omega_0^2)}}\left[\frac{x_n \sin(x_n d/H)\sin(x_n z/H)}{(x_n - \sin x_n \cos x_n - b^2\sin^2 x_n \tan x_n)}\right],$$

$$\ddot{k} > 0, \quad \text{(A105)}$$

provided that the range is large enough and the time is sufficiently removed from the value $t_m = r/U_0$, where $U_0$ denotes the minimum group velocity at which $\ddot{k} = 0$, so that condition (A102) is satisfied. For reasons explained elsewhere in the paper, (A104) represents the so-called *water wave*, and (A105) the *ground wave.*

The cosine factors in the above expressions represent periodic functions of circular frequency $\omega_0$, but $\omega_0$ itself as well as the other factors are slowly varying functions of time on account of (A103). Expressions (A104) and (A105) therefore represent *trains of waves which are modulated both in frequency and amplitude.*

## II. The Airy phase

Near the point of the minimum group velocity, where $\ddot{k}(\omega_0) = 0$, we set in the integral

$$P_n(r, z, t) = \frac{1}{2\pi}\int_{-\infty}^{\infty}\frac{Q_n(\omega)e^{if(\omega)}}{(\lambda + i\omega)}\,d\omega, \quad \text{(A91)}$$

$$\omega = \omega_0 + u, \qquad f(\omega) = \omega t - k(\omega)r - \frac{\pi}{4} = f(\omega_0) + au + bu^3 + cu^4 + \cdots, \quad \text{(A106)}$$

$$a = t - r\dot{k}_0 = t - r/U_0, \qquad b = \frac{-r}{6}\dddot{k}_0 > 0, \qquad c = -\frac{r}{24}\ddddot{k}_0. \quad \text{(A107)}$$

The subscript $_0$ in the derivatives of $k$ signifies that they are to be evaluated at the *fixed point* $\omega_0$ where $\ddot{k}(\omega)$ vanishes. In contrast to the situation in the preceding section, these derivatives are therefore constants *independent of t and r.* We shall retain in the expansion (A106) powers of $u$ up to the fourth and shall use the last power only as a correction term.

In view of the fact that $f(\omega)$ is an odd function of $\omega$ and $Q_n(\omega)$ is even in $\omega$, we have from (A91)

$$P_n = \frac{1}{\pi}\int_0^{\infty}\frac{Q_n(\omega)}{\sqrt{\lambda^2+\omega^2}}\cos[f(\omega) - \tan^{-1}(\omega/\lambda)]\,d\omega$$

$$\simeq \frac{1}{\pi}\frac{Q_n(\omega_0)}{\sqrt{\lambda^2+\omega_0^2}}\int_{-\infty}^{\infty}\cos[A + au + bu^3 + cu^4]\,du, \quad \text{(A108)}$$

$$A = [\omega_0 t - k(\omega_0)r - \tan^{-1}(\omega_0/\lambda)].$$

$$\int_{-\infty}^{\infty} \cos [A + au + bu^3 + cu^4]\, du$$

$$= 2 \cos A \int_0^{\infty} \cos (au + bu^3) \cos (cu^4)\, du - 2 \sin A \int_0^{\infty} \cos (au + bu^3) \sin (cu^4)\, du$$

$$\simeq 2 \cos A\, T(a, b) + 2 \sin A\, c \frac{\partial^2 T}{\partial a\, \partial b}, \tag{A109}$$

where

$$T(a, b) \equiv \int_0^{\infty} \cos (au + bu^3)\, du = \frac{\pi}{3(2b)^{\frac{1}{3}}} E(v),$$

$$E(v) = v^{\frac{1}{2}}[J_{-\frac{1}{3}}(v) + J_{\frac{1}{3}}(v)], \qquad t < \frac{r}{U_0}, \tag{A110}$$

$$= v^{\frac{1}{2}}[I_{-\frac{1}{3}}(v) - I_{\frac{1}{3}}(v)], \qquad t > \frac{r}{U_0}, \tag{A111}$$

and

$$v = \frac{2}{3\sqrt{3}} \frac{|a|^{\frac{3}{2}}}{|b|^{\frac{1}{2}}} = \frac{4\sqrt{\pi}}{3\sqrt{-\dot{Z}}} \left(\frac{r}{H}\right) |\tau - \tau_m|^{\frac{3}{2}}, \tag{A112}$$

$$\tau = \frac{tc_1}{r} - 1, \qquad \tau_m = \frac{c_1}{U_0} - 1.$$

One finds that

$$\frac{\partial^2 T}{\partial a \partial b} = \frac{\pi}{b^{\frac{5}{3}}} \left(\tfrac{2}{3}\right)^{\frac{4}{3}} G(v), \tag{A113}$$

$$G(v) = \frac{3^{\frac{1}{3}}}{4} \{-\tfrac{2}{3}v^{\frac{3}{2}} [J_{-\frac{2}{3}}(v) - J_{\frac{2}{3}}(v)] + \tfrac{1}{2}v^{\frac{5}{3}} [J_{-\frac{1}{3}}(v) + J_{\frac{1}{3}}(v)]\}, \qquad t < \frac{r}{U_0}, \tag{A114}$$

$$G(v) = \frac{3^{\frac{1}{3}}}{4} \{-\tfrac{2}{3}v^{\frac{3}{2}} [I_{-\frac{2}{3}}(v) - I_{\frac{2}{3}}(v)] + \tfrac{1}{2}v^{\frac{5}{3}} [I_{-\frac{1}{3}}(v) - I_{\frac{1}{3}}(v)]\}, \qquad t > \frac{r}{U_0}. \tag{A115}$$

Hence

$$\int_{-\infty}^{\infty} \cos [f(\omega_0) + au + bu^3 + cu^4]\, du \simeq \frac{2\pi \cos A}{3(2b)^{\frac{1}{3}}} E(v) + \frac{2\pi \sin A \cdot c}{b^{\frac{5}{3}}(3/2)^{\frac{4}{3}}} G(v), \tag{A116}$$

of which the second term is to be considered a correction term. The use of the leading term only in (A116) is justified when

$$\frac{2^{\frac{5}{3}} cG(v)}{3^{\frac{1}{3}} b^{\frac{4}{3}} E(v)} = -\frac{(\ddddot{k})G(v)}{r^{\frac{1}{3}}(-\dddot{k})^{\frac{4}{3}} F(v)} = -\frac{1}{(2\pi)^{\frac{1}{3}}} \left(\frac{H}{r}\right)^{\frac{1}{3}} \frac{\ddot{Z}G(v)}{(-\dot{Z})^{\frac{4}{3}} E(v)} \ll 1. \tag{A117}$$

Summarizing our results for the Airy phase, we have as the contribution $P_n$ from the $n$-th mode, in case of an exponential pulse, near the time $t_m$ corresponding to the minimum group velocity

$$P_n(r, s, t) = \frac{4 \cos \left[ \omega_0 t - k(\omega_0) r - \tan^{-1}(\omega_0/\lambda) - \frac{\pi}{4} \right] E(v)}{H 3^{\frac{2}{3}} \sqrt{(\lambda^2 + \omega_0^2) k_0 / 2\pi} (-\dddot{k}_0)^{\frac{1}{3}} r^{\frac{5}{6}}} \cdot \left[ \frac{x_n \sin (x_n d/H) \sin (x_n z/H)}{x_n - \sin x_n \cos x_n - b^2 \sin^2 x_n \tan x_n} \right]_0, \tag{A118}$$

with $v$ defined in (A112), provided the range is large enough and the time not far removed from $t_m$ for condition (A117) to be satisfied. In contrast to expressions (A104) and (A105) which represent waves which are *both frequency-modulated and amplitude-modulated*, expression (A118) represents an amplitude-modulated wave of constant circular frequency $\omega_0$. The amplitude modulation is contained in the factor $E(v)$, $v$ depending on time in the manner described in (A112).

Expression (A118) allows the computation of $P_n$ for all $t > t_m$ as well as for a certain period prior to $t_m$. For still earlier epochs (A118) cannot be used because condition (A117) is violated ($v$ is too large); but then it is usually found that condition (A102) is met, so that $P_n$ can be computed from (A104) and (A105).

## B. THEORY OF PROPAGATION OF SOUND IN A THREE-LAYERED LIQUID HALF-SPACE

### 1. FORMAL SOLUTION

The medium considered consists of three liquids characterized by densities $\rho_1$, $\rho_2$, $\rho_3$ and sound velocities $c_1$, $c_2$, $c_3$, (Fig. H). A point source, which in the first instance will be assumed to be periodic of circular frequency $\omega$, is situated in the first layer at a depth $d$. (The solution for any other location of the point source can be readily obtained by the method used in this section.) The problem is to determine the pressure field at any point in the half-space. Later the steady-state solution for the frequency $\omega$ is generalized to yield a solution for the case of a pressure pulse at the source of arbitrary time variation.

The pressure field is determined by the sound potential $\varphi$ through

$$p = \rho \frac{\partial \varphi}{\partial t}, \qquad w = -\frac{\partial \varphi}{\partial z}, \qquad u = -\frac{\partial \varphi}{\partial r}, \tag{A1}$$

where $p$ denotes the acoustic pressure, $w$ the vertical component of velocity, and $u$ the horizontal component of velocity. The potential $\varphi$ satisfies the wave equation

$$\nabla^2 \varphi = \frac{1}{c^2} \frac{\partial^2 \varphi}{\partial t^2}, \tag{A2}$$

where $c$ takes on the three values $c_1$, $c_2$ and $c_3$ in the three media respectively. In order to satisfy the boundary conditions at $z = 0$, $z = H$ and $z = H + h$, we seek, in the first instance, solutions for $\varphi$ of the form

$$\varphi = e^{i\omega t} J_0(kr) F(z) G(k), \tag{A4}$$

where $k$ is an arbitrary parameter with respect to which one eventually integrates along a certain path in the complex $k$-plane. (For a more detailed discussion of this point *see* Pekeris, 1946.) It is convenient to label quantities referring to the middle and lower layers by the subscripts $_2$ and $_3$ respectively, while quantities referring to the section of the upper layer above the source are labelled $_1{}'$, and those referring to the section of the upper layer below the source are labelled by the subscript $_1$.

Substituting (A4) in (A2), we get

$$\frac{d^2F_n}{dz^2} + \beta_n^2 F_n(z) = 0, \qquad n = 1, 2, 3, \tag{A119}$$

$$\begin{aligned} \beta_n &= \sqrt{\frac{\omega^2}{c_n^2} - k^2}, \qquad k < \frac{\omega}{c_n}, \\ &= -i\sqrt{k^2 - \frac{\omega^2}{c_n^2}}, \qquad k > \frac{\omega}{c_n}. \end{aligned} \tag{A120}$$

Solutions of (A119) have to be chosen which vanish at $z = 0$, have continuous vertical components of velocity and pressure at $z = H$ and $z = H + h$, and which do not become infinite at great depths as $k$ becomes large. These conditions are met by putting

$$F_1' = A \sin \beta_1 z, \tag{A121}$$

$$F_1 = B \sin \beta_1 z + C \cos \beta_1 z, \tag{A122}$$

$$F_2 = D \sin \beta_2 z + E \cos \beta_2 z, \tag{A123}$$

$$F_3 = Ee^{-i\beta_3 z}, \tag{A124}$$

where the arbitrary constants $A$, $B$, $C$, and $D$ (functions of $k$ and $\omega$) are determined by the boundary conditions and the strength of the source. The boundary conditions require that

$$\dot{F}_3 = \dot{F}_2, \qquad \rho_3 F_3 = \rho_2 F_2, \qquad z = H + h, \tag{A125}$$

$$\dot{F}_2 = \dot{F}_1, \qquad \rho_2 F_2 = \rho_1 F_1, \qquad z = H, \tag{A126}$$

$$\frac{dF_1'}{dz} - \frac{dF_1}{dz} = 2k, \qquad F_1' = F_1, \qquad z = d, \tag{A127}$$

with the understanding that the elementary solution (A4) is to be integrated with respect to $k$ from 0 to $\infty$. When this is done, the difference of the vertical component of velocity $w$ at the two sides of the plane $z = d$ becomes proportional to $\int_0^\infty J_0(kr)kdk$, a function which is zero everywhere except $r = 0$, where it becomes infinite in such a way that its integral over the plane $z = d$ is finite.

Let

$$x = \beta_1 H, \qquad b = \rho_1/\rho_2, \qquad g = \rho_2/\rho_3, \tag{A128}$$

$$S = \left[\frac{g\beta_3 \tan(\beta_2 h) - i\beta_2}{g\beta_3 + i\beta_2 \tan(\beta_2 h)}\right], \qquad V = (\beta_1 S \cos x + b\beta_2 \sin x), \tag{A129}$$

then on solving Eqs. (A125) to (A127) for $A$, $B$, $C$, and $D$, substituting the results into Eqs. (A121) to (A124) and performing the integration with respect to $k$, we get

$$\varphi_1' = 2e^{i\omega t}\int_0^\infty J_0(kr)kdk\,\frac{\sin\beta_1 z}{\beta_1 V}\left[S\beta_1\cos\beta_1(H-d)+b\beta_2\sin\beta_1(H-d)\right],\quad 0<z<d, \tag{A130}$$

$$\varphi_1 = 2e^{i\omega t}\int_0^\infty J_0(kr)kdk\,\frac{\sin\beta_1 d}{\beta_1 V}\left[S\beta_1\cos\beta_1(H-z)+b\beta_2\sin\beta_1(H-z)\right],\quad d<z<H, \tag{A131}$$

$$\varphi_2 = 2be^{i\omega t}\int_0^\infty J_0(kr)kdk\,\frac{\sin\beta_1 d}{V}\left[S\cos\beta_2(z-H)-\sin\beta_2(z-H)\right],\quad H<z<H+h, \tag{A132}$$

$$\varphi_3 = 2bge^{i\omega t}\int_0^\infty J_0(kr)kdk\,\frac{\sin\beta_1 d}{V}\left[S\cos\beta_2 h-\sin\beta_2 h\right]e^{-i\beta_3(z-H-h)},\quad z>H+h. \tag{A133}$$

As in the case of a two-layered medium, $\varphi_1'$ goes over into $\varphi_1$ by interchanging $z$ and $d$ and vice versa. It will be noted also that the integrands in Eqs. (A130) to (A133) are even functions of $\beta_1$ and $\beta_2$, but mixed functions of $\beta_3$.

## 2. THE NORMAL-MODE SOLUTION

(a) *Evaluation of the integral for the potential in terms of residues and an integral along a branch line.*—We shall dispense here with a discussion of the "ray theory" for a three-layered medium, since it can be developed along the lines used in the two-layered medium. In seeking the normal-mode solution of, say,

$$\varphi_1 = 2e^{i\omega t}\int_0^\infty J_0(kr)kdkF(\beta_1,\beta_2,\beta_3),\qquad d<z<H, \tag{A131}$$

$$F(\beta_1,\beta_2,\beta_3) = \frac{\sin\beta_1 d}{\beta_1 V}\left[S\beta_1\cos\beta_1(H-z)+b\beta_2\sin\beta_1(H-z)\right], \tag{A134}$$

where the $\beta$'s and the other quantities are defined in Eqs. (A120), (A128), and (A129), we first cut up the $k$-plane in the manner shown in Figure G, adding a *third cut* which begins on the real axis of $k$ at $k = k_3 = \omega/c_3$ and extends to $k_3 - i\infty$ in a direction parallel to the negative imaginary axis. The integral (A131) is now treated like the integral (A18). It is found that on account of the fact that $F(\beta_1, \beta_2, \beta_3)$ is even in $\beta_1$ and in $\beta_2$, the branch-line integrals around the $k_1$ and $k_2$ cuts vanish. There remains the branch-line integral around the $k_3$ cut and the residues:

$$\varphi_1 = e^{i\omega t}\int_{-i\infty}^{k_3} H_0^{(2)}(kr)[F(\beta_1,\beta_2,\beta_3)-F(\beta_1,\beta_2,-\beta_3)]\,kdk+\varphi_1', \tag{A135}$$

$$\begin{aligned}\varphi_1' &= e^{i\omega t}\Sigma\text{ Residues} = e^{i\omega t}\Sigma\text{ Res}\int_0^\infty H_0^{(2)}(kr)F(\beta_1,\beta_2,\beta_3)\,kdk\\ &= -2\pi i e^{i\omega t}\Sigma_n H_0^{(2)}(k_n r)k_n\,\frac{\sin\beta_1 d}{\beta_1}\,\frac{[S\beta_1\cos\beta_1(H-z)+b\beta_2\sin\beta_1(H-z)]}{(\partial V/\partial k)_n}.\end{aligned} \tag{A136}$$

One finds that at the zeros of $V$

$$\frac{1}{k}\frac{\partial V}{\partial k} = \frac{\{\ \}}{\beta_1^2 \beta_2 \cos x}, \qquad x = \beta_1 H,$$

$$\{\ \} = \left\{ \begin{array}{l} b(\beta_2^2 - \beta_1^2) \sin x \cos x - b\beta_2^2 x - h\beta_1 \cos^2 x(\beta_1^2 + b^2 \beta_2^2 \tan^2 x) \\ \qquad + \dfrac{ig\beta_1(\beta_3^2 - \beta_2^2) \cos^2 x(\beta_1^2 + b^2 \beta_2^2 \tan^2 x)}{\beta_3(\beta_3^2 g^2 - \beta_2^2)} \end{array} \right\}, \tag{A137}$$

$$[S\beta_1 \cos \beta_1(H - z) + b\beta_2 \sin \beta_1(H - z)] = -\frac{b\beta_2 \sin \beta_1 z}{\cos x}. \tag{A138}$$

Hence

$$\varphi_1' = \left(\frac{2\pi i b}{H}\right) e^{i\omega t} \sum_n H_0^{(2)}(k_n r) \frac{x_n \beta_2^2 \sin (x_n d/H) \sin (x_n z/H)}{\{\ \}_n} \tag{A139}$$

$$\text{When } h \to 0, \qquad S \to -\frac{i\beta_2}{g\beta_3}, \qquad \tan x \to \frac{i\beta_1}{gb\beta_3},$$

$\{\ \} \to b\beta_2^2[-x + \sin x \cos x + b^2 g^2 \sin^2 x \tan x]$, and (A139) reduces to (A48).

(b) *Phase velocity and group velocity of the normal modes in a three-layered liquid half-space*

## I. The dispersion equation

We confine the discussion to the case when $c_3 > c_1$, which is of interest in our applications. In that case total reflection takes place for angles of incidence exceeding a certain critical value, and this implies the existence of unadmped normal modes for frequencies exceeding the critical frequency. The sound velocity $c_2$ in the intermediate layer will be assumed to be confined between $c_1$ and $c_3$, although the case $c_2 < c_1 < c_3$ is of some interest also. Under the above assumptions ($c_1 < c_2 < c_3$) the phase velocity $c$ of any mode starts with the value $c_3$ at the respective critical frequency and approaches $c_1$ in the limit of very high frequencies.

Let

$$s_1 = \sqrt{\frac{c^2}{c_1^2} - 1}; \qquad s_2 = \sqrt{\frac{c^2}{c_2^2} - 1} \ \text{ or } \ \sqrt{1 - \frac{c^2}{c_2^2}}; \qquad s_3 = \sqrt{1 - \frac{c^2}{c_3^2}}, \tag{A140}$$

then, with $k = \omega/c$,

$$\beta_1 = ks_1; \qquad \beta_3 = -iks_3; \qquad \beta_2 = ks_2 \text{ when } c > c_2, \qquad \beta_2 = -iks_2 \text{ when } c < c_2, \tag{A141}$$

$$S = \left[\frac{g\beta_3 \tan (\beta_2 h) - i\beta_2}{g\beta_3 + i\beta_2 \tan (\beta_2 h)}\right] = \left[\frac{gs_3 \tan \beta_2 h + (\beta_2/k)}{gs_3 - (\beta_2/k) \tan (\beta_2 h)}\right]. \tag{A142}$$

The dependence of the phase velocity $c$ on frequency $\omega$ is determined from

$$V = 0, \quad \text{or} \quad \tan x = -\frac{\beta_1 S}{b\beta_2}, \qquad x = \beta_1 H = ks_1 H, \tag{A143}$$

which becomes

$$\tan x = -\frac{s_1}{bs_2}\left[\frac{gs_3 \tanh(s_2 kh) + s_2}{gs_3 + s_2 \tanh(s_2 kh)}\right] = -\frac{s_1}{bs_2}\left[\frac{gs_3 \tanh\left(x\frac{s_2 h}{s_1 H}\right) + s_2}{gs_3 + s_2 \tanh\left(x\frac{s_2 kh}{s_1 H}\right)}\right], \tag{A144}$$

when $c < c_2$, and

$$\tan x = -\frac{s_1}{bs_2}\left[\frac{gs_3 \tan(s_2 kh) + s_2}{gs_3 - s_2 \tan(s_2 kh)}\right] \quad \text{when} \quad c > c_2. \tag{A145}$$

II. The cut-off frequencies

At the cut-off frequency $c = c_3$, $s_3 = 0$, and Eq. (A145) reduces to

$$\tan x \cdot \tan y = \frac{bs_1}{s_2}, \tag{A146}$$

$$k = \omega/c_3, \qquad x = ks_1 H = \frac{\omega H}{c_1}\sqrt{1 - \frac{c_1^2}{c_3^2}}, \qquad y = ks_2 h = \frac{\omega h}{c_2}\sqrt{1 - \frac{c_2^2}{c_3^2}}.$$

When $\frac{h}{H} \to 0$, Eq. (A146) becomes

$$\tan x = \left(\frac{bx}{Hs_2}\right)\operatorname{cotan}\left(x\frac{s_2}{s_1}\frac{h}{H}\right) \to \left(\frac{b}{Hs_2}\right)\left(\frac{s_1 H}{s_2 h}\right) \to \infty,$$

$$x_n = (n - \tfrac{1}{2})\pi = \frac{\omega_n H}{c_1}\sqrt{1 - \frac{c_1^2}{c_3^2}}, \qquad \gamma_n = \frac{\omega_n H}{2\pi c_1} = \frac{H}{\lambda_n} = \frac{(2n-1)}{4\sqrt{1 - \frac{c_1^2}{c_3^2}}}. \tag{A147}$$

Similarly when $\frac{h}{H} \to \infty$, Eq. (A146) yields

$$y_n = \frac{\omega_n h}{c_2}\sqrt{1 - \frac{c_2^2}{c_3^2}} = (n - \tfrac{1}{2})\pi, \qquad \gamma_n = \frac{(2n-1)\left(\frac{c_2}{c_1}\right)\left(\frac{H}{h}\right)}{4\sqrt{1 - \frac{c_2^2}{c_3^2}}}, \tag{A148}$$

showing that the cut-off frequencies become very small. However, it will be shown in the next section that even in this case the cut-off frequency given in (A147) is of importance.

III. Behavior of the dispersion equation when the thickness of the intermediate layer becomes very large in comparison with the thickness of the upper layer

*When* $(h/H) \gg 1$ *and* $c$ *is not very close to* $c_2$, the term $\tanh\left(x\frac{s_2 h}{s_1 H}\right)$ in (A144) approaches unity, and (A144) reduces to

$$\tan x = -\frac{s_1}{bs_2}, \qquad c_1 < c < c_2, \tag{A149}$$

which is the dispersion equation for a two-layered liquid consisting of the upper and intermediate layers. Under the same conditions we may write Eq. (A145) as

$$-\frac{s_1}{bs_2}\left[\frac{gs_3 \tan y + s_2}{gs_3 - s_2 \tan y}\right] = \tan\left(y\frac{s_1}{s_2}\frac{H}{h}\right) \to y\frac{s_1}{s_2}\frac{H}{h} \to 0, \qquad y \equiv ks_2 h, \tag{A150}$$

and therefore

$$gs_3 \cdot \tan y + s_2 = 0, \qquad c_2 < c < c_3, \tag{A151}$$

which is the dispersion equation for a two-layered medium consisting of the intermediate layer and the bottom layer. It follows that when the thickness $h$ of the intermediate layer is much greater than the thickness $H$ of the upper layer, the dispersion in the range $c_1 < c < c_2$ is almost unaffected by the bottom layer, while in the range $c_2 < c < c_3$ the dispersion is nearly independent of the top layer. The separation of the dispersion into two nearly independent regimes controlled by the two surfaces of discontinuity respectively reflects itself also in the variation of group velocity with frequency, with the result that the *group velocity has two minima in the manner illustrated in Figures 29, 30, 31, and 32.*

## IV. The group velocity

The group velocity of the normal modes for a three-layered medium can be computed in the following manner. Write the dispersion equation in the form

$$F(c, k) \equiv -bs_2[gs_3 + s_2\tanh(s_2kh)]\tan(s_1kH) - s_1[gs_3\tanh(s_2kh) + s_2] = 0, \qquad c < c_2, \tag{A152}$$

$$= -bs_2[gs_3 - s_2\tan(s_2kh)]\tan(s_1kH) - s_1[gs_3\tan(s_2kh) + s_2] = 0, \qquad c > c_2, \tag{A153}$$

then the group velocity $U$ is given by

$$U = c + k\frac{dc}{dk} = c - \frac{k\dfrac{\partial F(c, k)}{\partial k}}{\dfrac{\partial F(c, k)}{\partial c}}, \tag{A154}$$

or in the nondimensional form

$$\frac{U}{c_1} = \left(\frac{c_1}{c}\right)\left[\left(\frac{c}{c_1}\right)^2 - \frac{k\dfrac{\partial F}{\partial k}}{Q}\right], \qquad Q \equiv \frac{c_1^2}{c}\frac{\partial F(c, k)}{\partial c}. \tag{A155}$$

Let

$$\mu = \left(\frac{c_1}{c_2}\right)^2, \qquad \nu = \left(\frac{c_1}{c_3}\right)^2, \qquad x = s_1 kH, \qquad y = s_2 kh,$$

then for $c < c_2$ we have

$$k\frac{\partial F}{\partial k} = -\frac{bxs_2}{\cos^2 x}(s_2 \tanh y + gs_3) - \frac{b \tan x \cdot s_2^2 y}{\cosh^2 y} - \frac{gs_1 s_3 y}{\cosh^2 y}, \tag{A156}$$

$$Q = \left\{\begin{aligned} & b(s_2 \tanh y + gs_3)\left[\frac{\mu \tan x}{s_2} - \frac{s_2 x}{s_1^2 \cos^2 x}\right] + bs_2 \tan x\left[\frac{\mu \tanh y}{s_2} + \frac{\mu y}{s_2 \cosh^2 y} + \frac{g\nu}{s_3}\right] \\ & \qquad - g\left(\frac{s_3}{s_1}\right)\tanh y + \frac{gs_1\nu}{s_3}\tanh y + \frac{gs_1 s_3 y\mu}{s_2^2 \cosh^2 y} - \frac{s_2}{s_1} + \frac{s_1\mu}{s_2}\end{aligned}\right\}, \tag{A157}$$

and for $c > c_2$:

$$k \frac{\partial F}{\partial k} = \frac{bxs_2}{\cos^2 x}(s_2 \tan y - gs_3) + \frac{bs_2^2 y \tan x}{\cos^2 y} - \frac{gs_1 s_3 y}{\cos^2 y}, \tag{A158}$$

$$Q = \left\{ \begin{aligned} &(bs_2 \tan y - gs_3)\left[\frac{\mu \tan x}{s_2} + \frac{s_2 x}{s_1^2 \cos^2 x}\right] + bs_2 \tan x \left[\frac{\mu \tan y}{s_2} + \frac{\mu y}{s_2 \cos^2 y} + \frac{g\nu}{s_3}\right] \\ &\qquad - g\left(\frac{s_3}{s_1}\right)\tan y + \left(\frac{gs_1 \nu}{s_3}\right)\tan y - \frac{gs_1 s_3 \mu y}{s_2^2 \cos^2 y} - \frac{s_2}{s_1} - \frac{s_1 u}{s_2} \end{aligned} \right\} \tag{A159}$$

# REFERENCES CITED


Gutenberg, B. (1924) *Dispersion und Extinktion von seismischen Oberflächenwellen,* Phys. Zs. **25,** 377.

——— (1926) *Über Gruppengeschwindigkeit bei Erdoberflächenwellen,* Phys. Zs., **27, 111.**

Jeffreys, H. (1931) *Operational methods,* Cambridge Univ. Press.

Lamb, H. (1904) *On the Propagation of tremors over the surface of an elastic solid,* Phil. Tr. Roy. Soc. A, **203, 1.**

——— (1932) *Hydrodynamics,* Cambridge Univ. Press.

Love, A. E. H. (1911) *Some problems in geodynamics,* Cambridge Univ. Press.

Pekeris, C. L. (1940) *A pathological case in the numerical solution of integral equations,* Nat. Acad., Pr., vol. 26, p. 433.

——— (1941) *The propagation of an SH pulse in a layered medium,* Am. Geophys. Union, pt. I, p. 392. *See also* M. Muskat (1932) *The theory of refraction shooting,* Physics, vol. 4, p. 14.

——— (1946) *Theory of propagation of sound in a half-space of variable sound velocity,* Jr. Acous. Soc. Am., vol. 18, p. 295.

Rayleigh, Lord. (1896) *Theory of sound,* Vol. II, The Macmillan Co.

Slater, J. C. (1942) *Microwave transmission,* McGraw Hill Co.

Stoneley, R. (1925) Dispersion of Seismic Waves, M.N.R.A.S., Geoph. Supp. 1, 280.

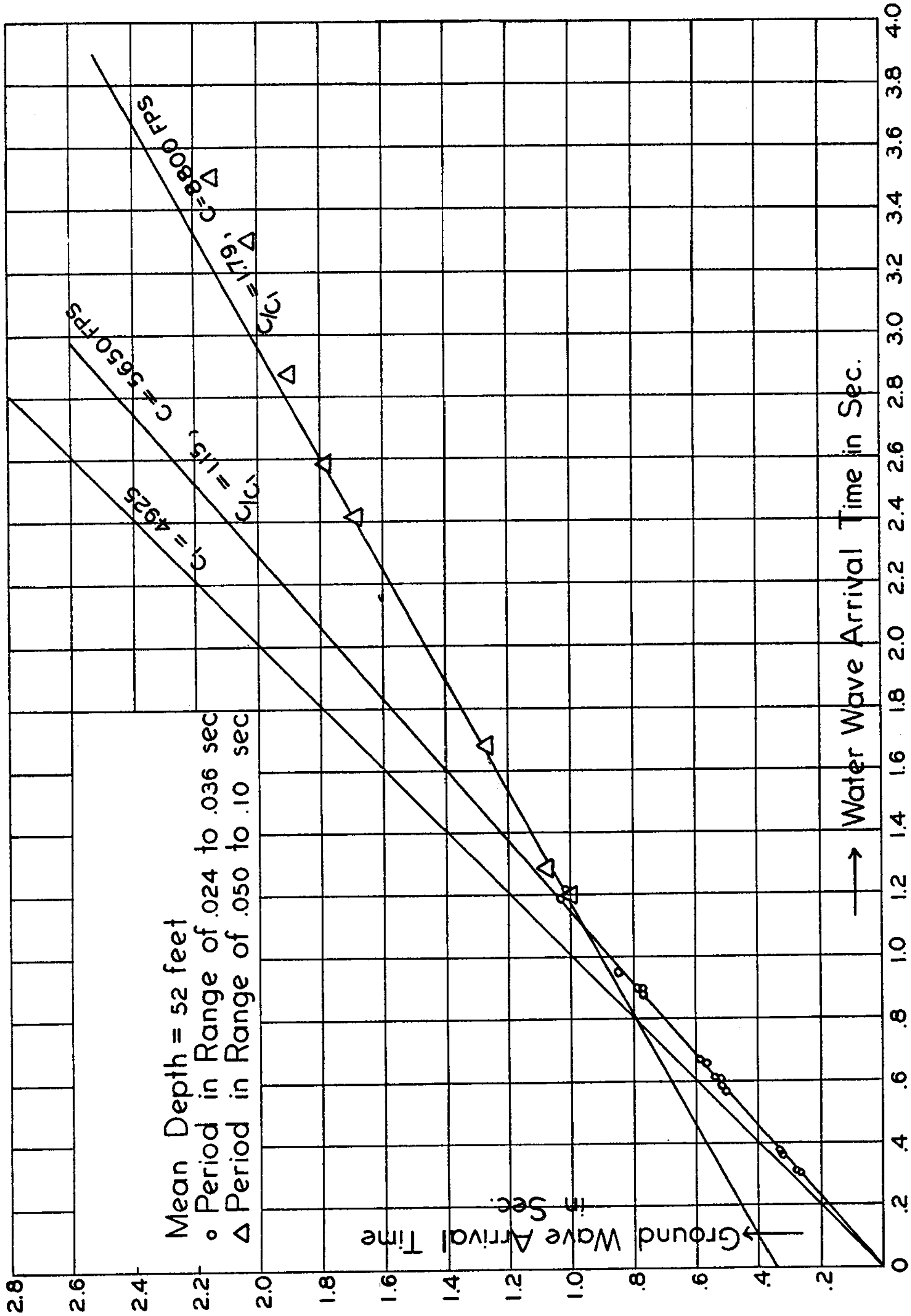


FIGURE 1.—*Refraction data for Solomons Shoal*

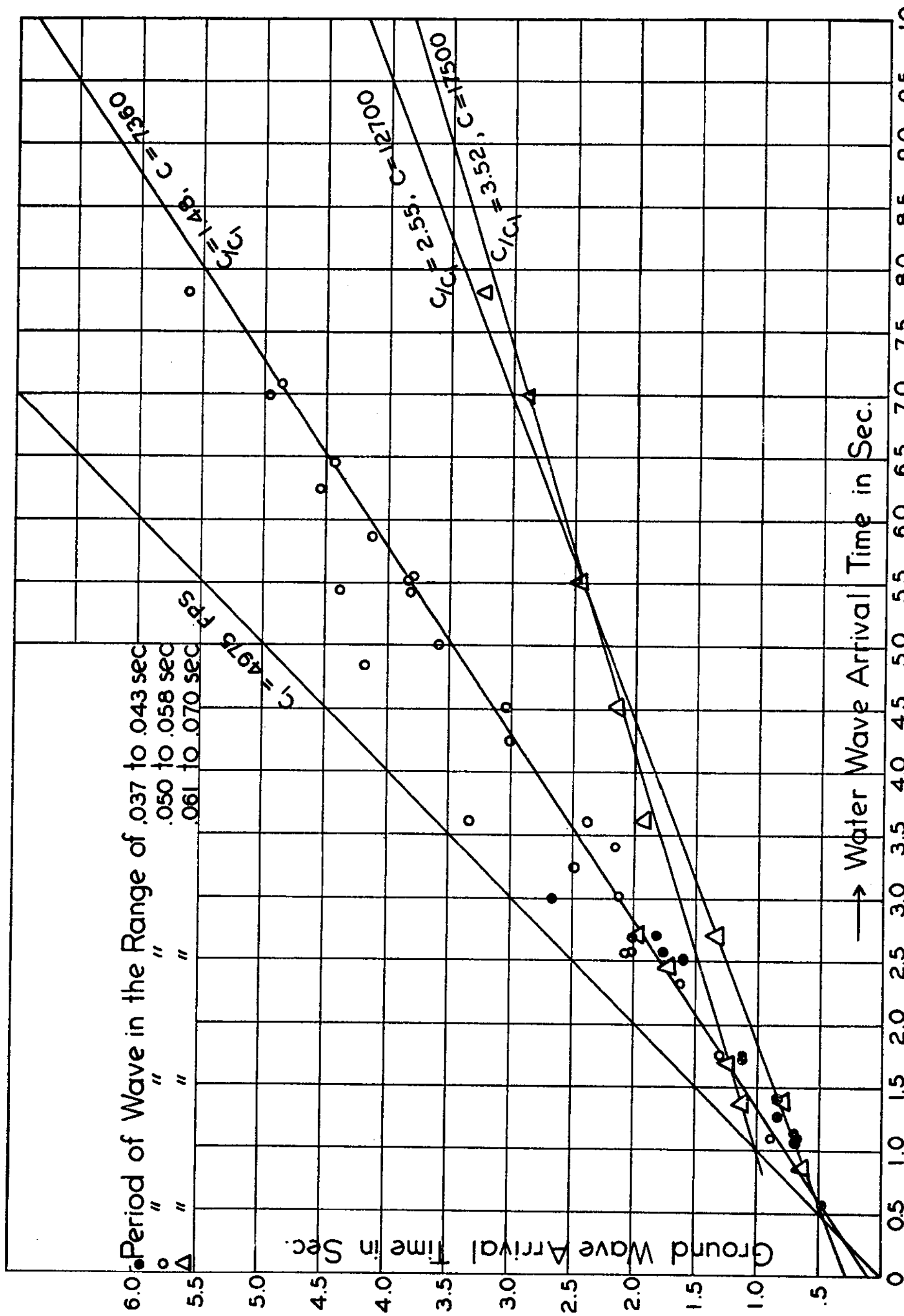


FIGURE 2.—*Refraction data for Jacksonville Shoal*

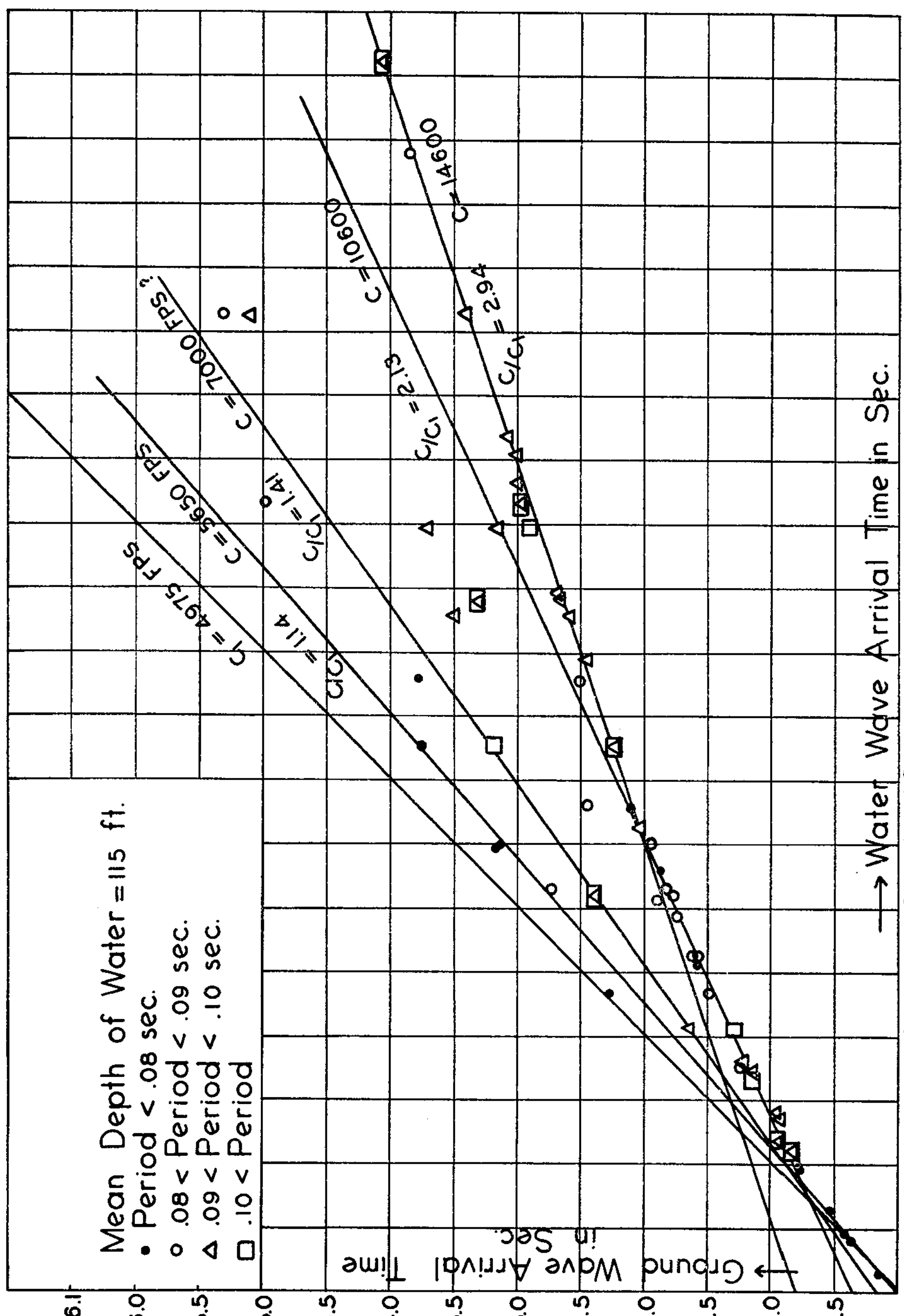


FIGURE 3.—*Refraction data in Jacksonville Deep*

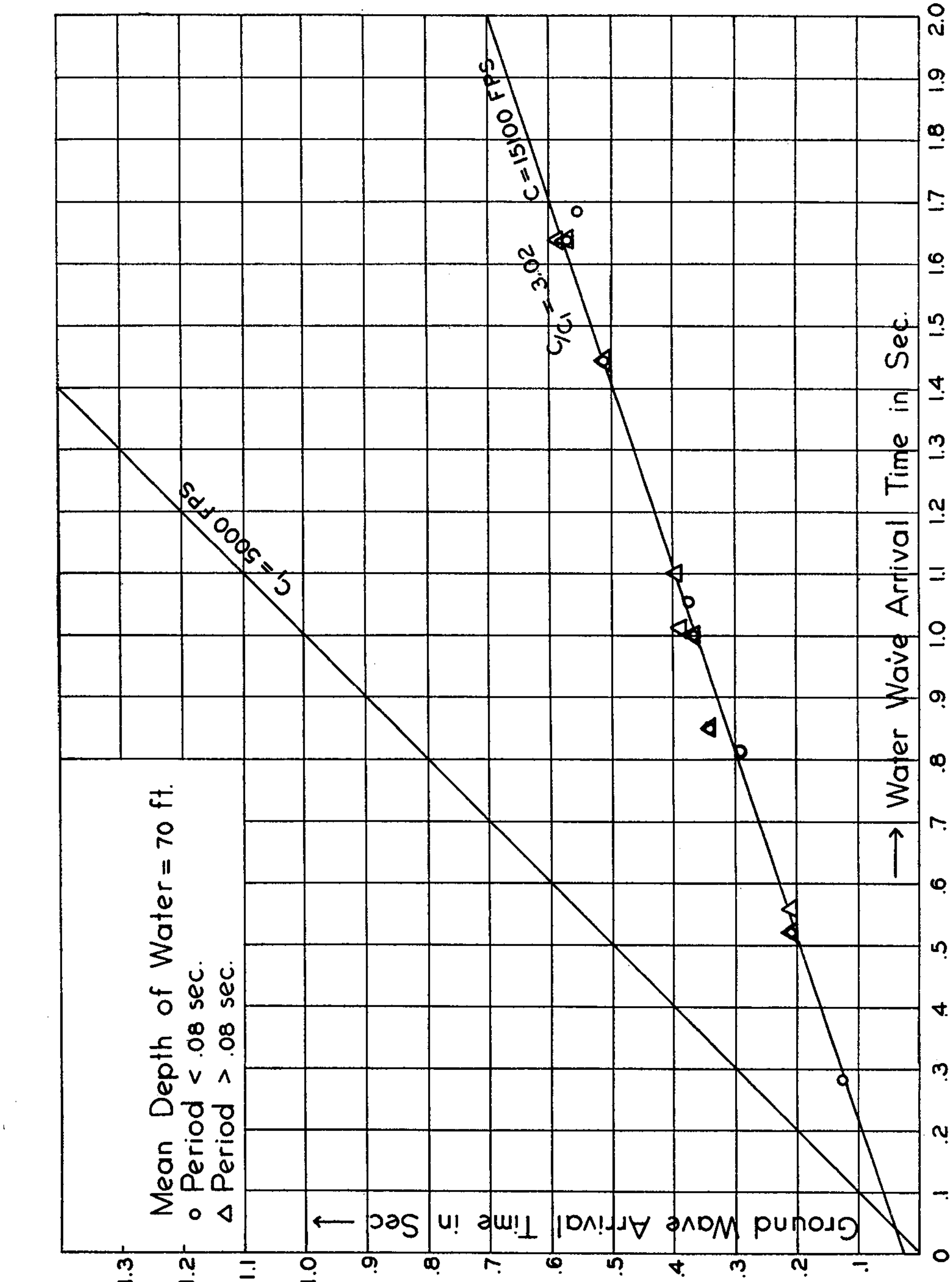


FIGURE 4.—*Refraction data in Virgin Islands Shoal*

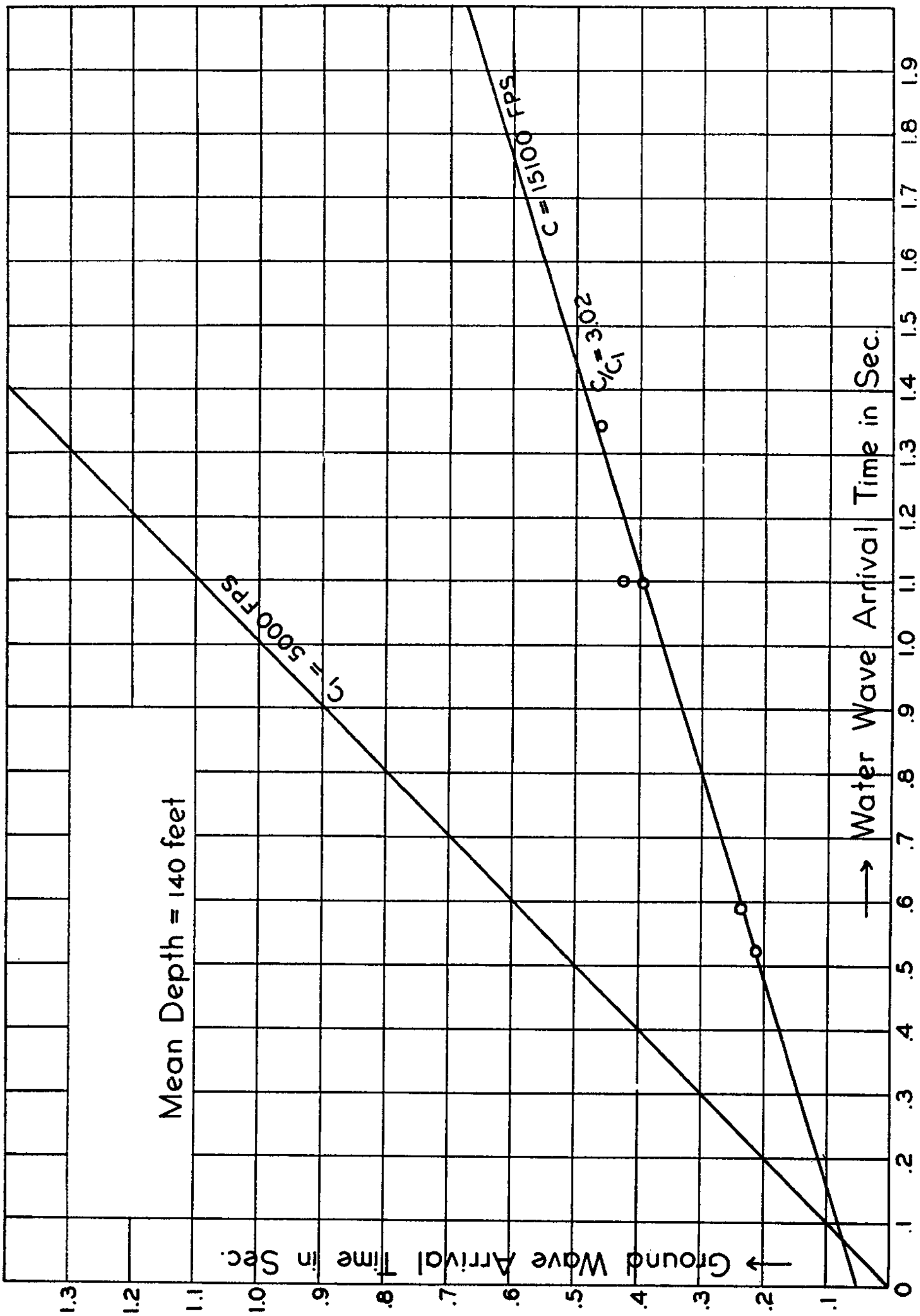


FIGURE 5.—*Refraction data in Virgin Island Deep*

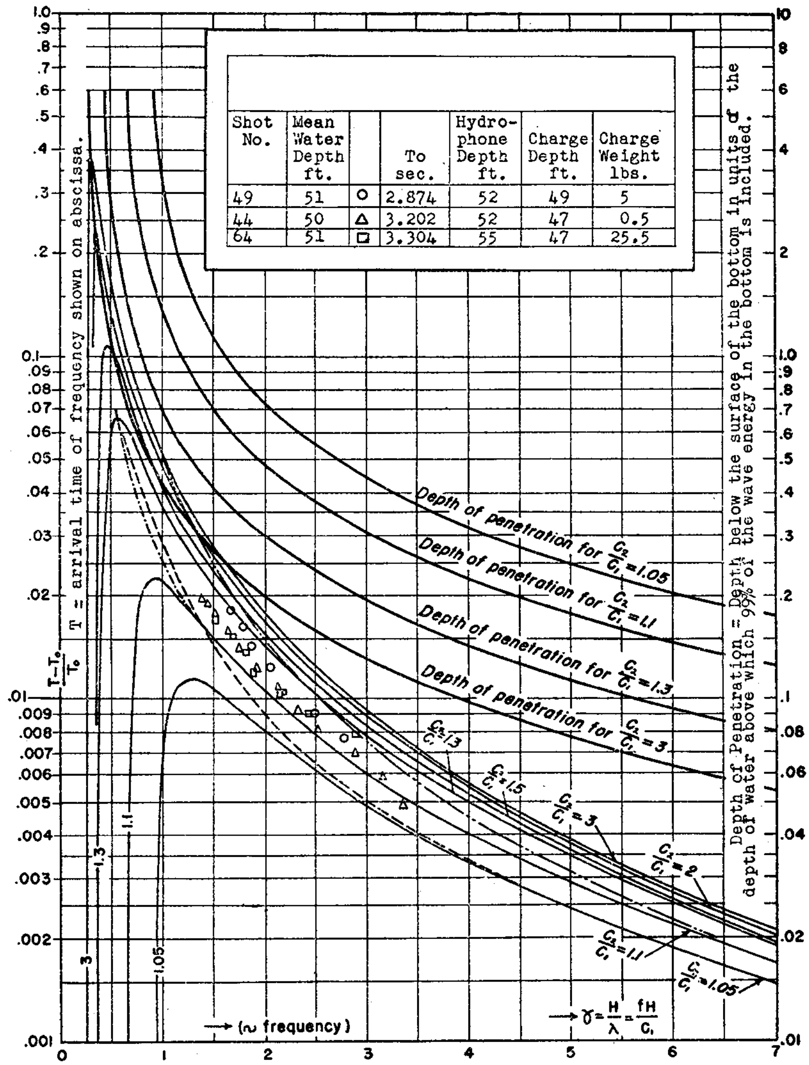


FIGURE 6.—*Dispersion in the water wave at Solomons Shoal*

$H$ = Depth of Water. $C_1$ = Sound Velocity in Water. $C_2$ = Sound Velocity in Bottom. Density of Bottom assumed = 2. — — — — — Layer of thickness $\frac{1}{2}H$ and $\frac{C_2}{C_1}$ = 1.05 underlain by infinite layer of $\frac{C_3}{C_1}$ = 1.3. — · — · — · — · — · — Layer of thickness $H$ and $\frac{C_2}{C_1}$ = 1.1 underlain by layer of $\frac{C_3}{C_1}$ = 3. — ·· — ·· — ·· — ·· — Layer of thickness 0.1$H$ and $\frac{C_2}{C_1}$ = 1.1 underlain by layer of $\frac{C_3}{C_1}$ = 3.

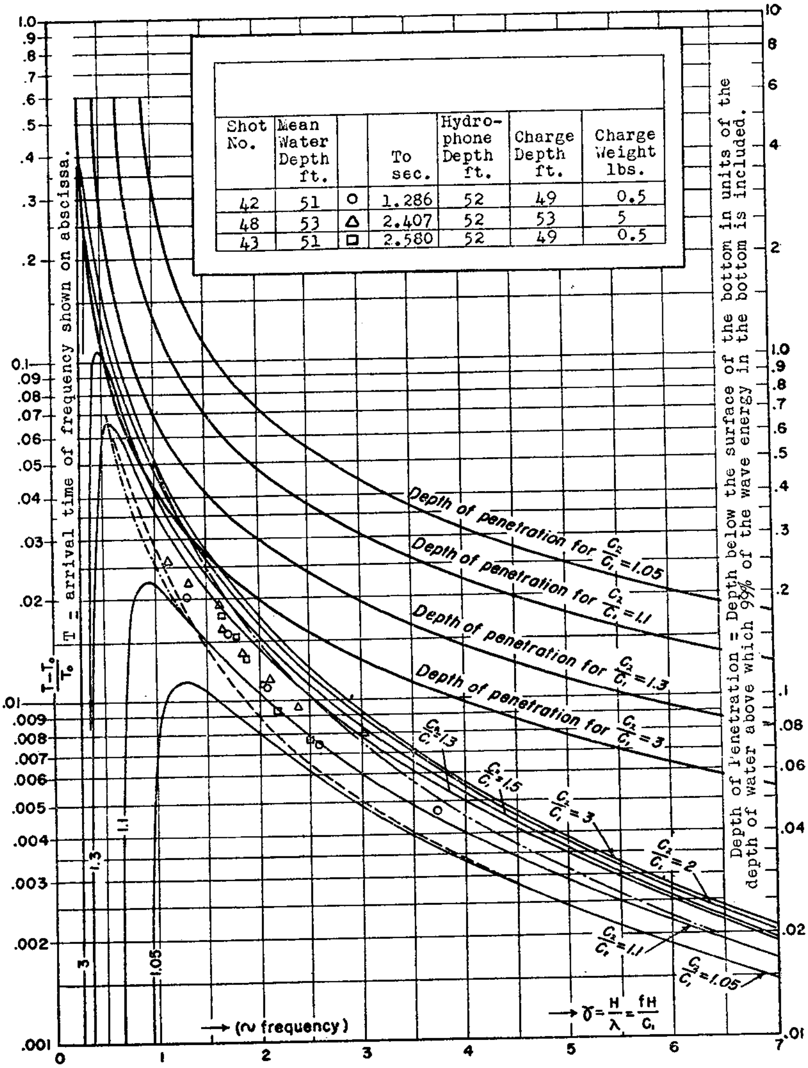


FIGURE 7.—*Dispersion in the water wave at Solomons Shoal*

$H$ = Depth of Water. $C_1$ = Sound Velocity in Water. $C_2$ = Sound Velocity in Bottom. Density of Bottom assumed = 2. — — — — Layer of thickness $\frac{1}{2}H$ and $\frac{C_2}{C_1}$ = 1.05 underlain by infinite layer of $\frac{C_3}{C_1}$ = 1.3. — · — · — · — Layer of thickness $H$ and $\frac{C_2}{C_1}$ = 1.1 underlain by layer of $\frac{C_3}{C_1}$ = 3. — ·· — ·· — ·· — Layer of thickness 0.1$H$ and $\frac{C_2}{C_1}$ = 1.1 underlain by layer of $\frac{C_3}{C_1}$ = 3.

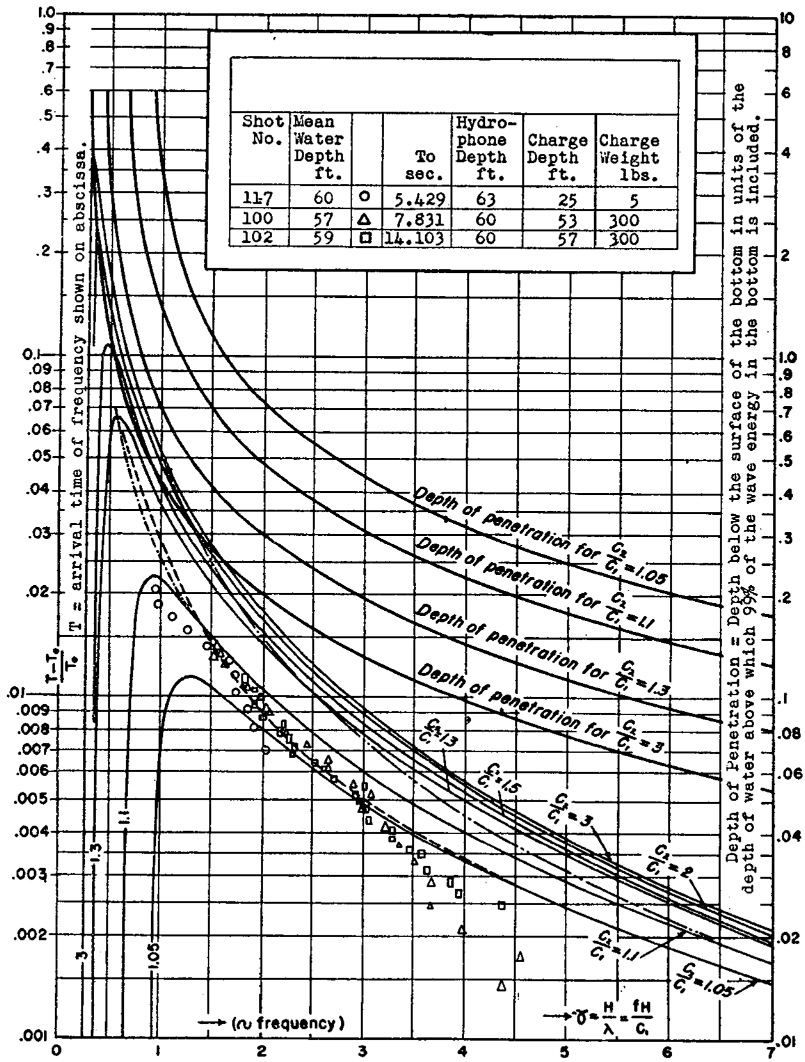


| Shot No. | Mean Water Depth ft. | | To sec. | Hydro-phone Depth ft. | Charge Depth ft. | Charge Weight lbs. |
|---|---|---|---|---|---|---|
| 117 | 60 | ○ | 5.429 | 63 | 25 | 5 |
| 100 | 57 | △ | 7.831 | 60 | 53 | 300 |
| 102 | 59 | □ | 14.103 | 60 | 57 | 300 |

FIGURE 8.—*Dispersion in the water wave at Jacksonville Shoal*

$H$ = Depth of Water. $C_1$ = Sound Velocity in Water. $C_1$ = Sound Velocity in Bottom. Density of Bottom assumed = 2. ———— Layer of thickness ½$H$ and $\frac{C_2}{C_1}$ = 1.05 underlain by infinite layer of $\frac{C_3}{C_1}$ = 1.3. —·—·—·— Layer of thickness $H$ and $\frac{C_2}{C_1}$ = 1.1 underlain by layer of $\frac{C_3}{C_1}$ = 3. —··—··—··— Layer of thickness 0.1$H$ and $\frac{C_2}{C_1}$ = 1.1 underlain by layer of $\frac{C_3}{C_1}$ = 3.

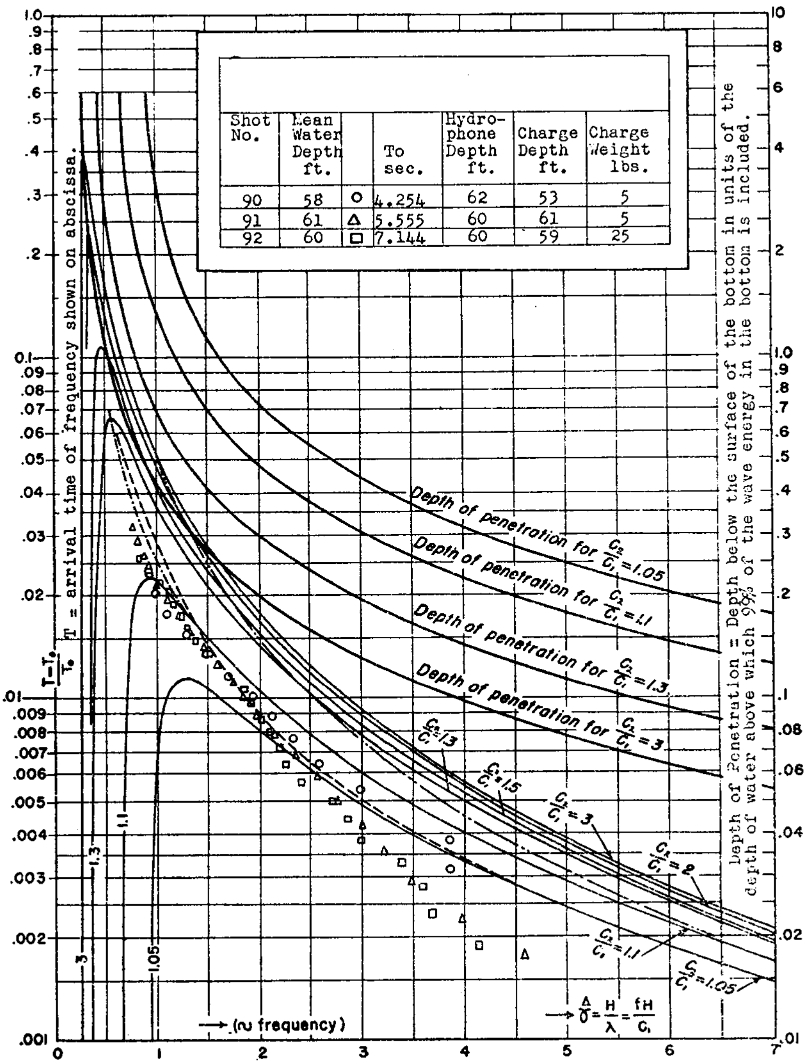


| Shot No. | Mean Water Depth ft. | | To sec. | Hydro-phone Depth ft. | Charge Depth ft. | Charge Weight lbs. |
|---|---|---|---|---|---|---|
| 90 | 58 | ○ | 4.254 | 62 | 53 | 5 |
| 91 | 61 | △ | 5.555 | 60 | 61 | 5 |
| 92 | 60 | □ | 7.144 | 60 | 59 | 25 |

FIGURE 9.—*Dispersion in the water wave at Jacksonville Shoal*

$H$ = Depth of Water. $C_1$ = Sound Velocity in Water. $C_2$ = Sound Velocity in Bottom. Density of Bottom assumed = 2.0. — — — — — — Layer of thickness ½ $H$ and $\frac{C_2}{C_1}$ = 1.05 underlain by infinite layer of $\frac{C_3}{C_1}$ = 1.3. — · — · — · — · —Layer of thickness $H$ and $\frac{C_2}{C_1}$ = 1.1 underlain by layer of $\frac{C_3}{C_1}$ = 3. — ·· — ·· — ·· — ·· — Layer of thickness 0.1$H$ and $\frac{C_2}{C_1}$ = 1.1 underlain by layer of $\frac{C_3}{C_1}$ = 3.

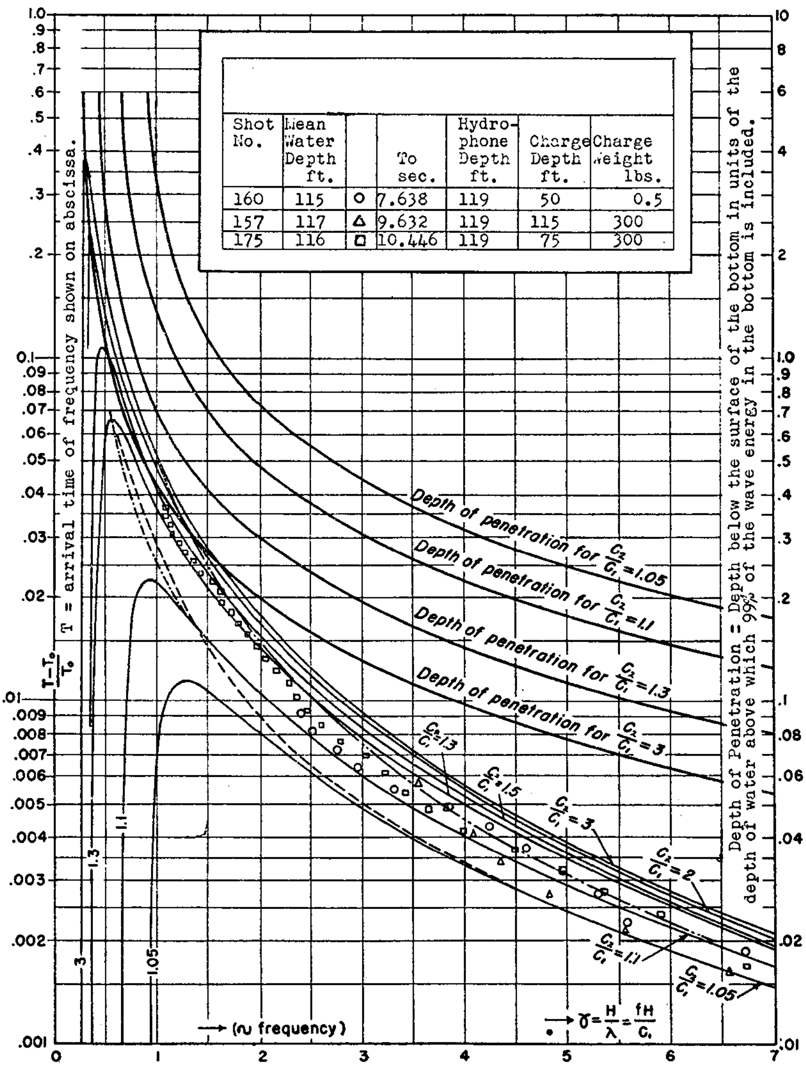


FIGURE 10.—*Dispersion in the water wave at Jacksonville Deep*

$H$ = Depth of Water. $C_1$ = Sound Velocity in Water. $C_2$ = Sound Velocity in Bottom. Density of Bottom assumed = 2. — — — — Layer of thickness $\frac{1}{2}H$ and $\frac{C_2}{C_1}$ = 1.05 underlain by infinite layer of $\frac{C_3}{C_1}$ = 1.3. — · — · — · — · — Layer of thickness $H$ and $\frac{C_2}{C_1}$ = 1.1 underlain by layer of $\frac{C_3}{C_1}$ = 3. — ·· — ·· — ·· — ·· — Layer of thickness 0.1$H$ and $\frac{C_2}{C_1}$ = 1.1 underlain by layer of $\frac{C_3}{C_1}$ = 3.

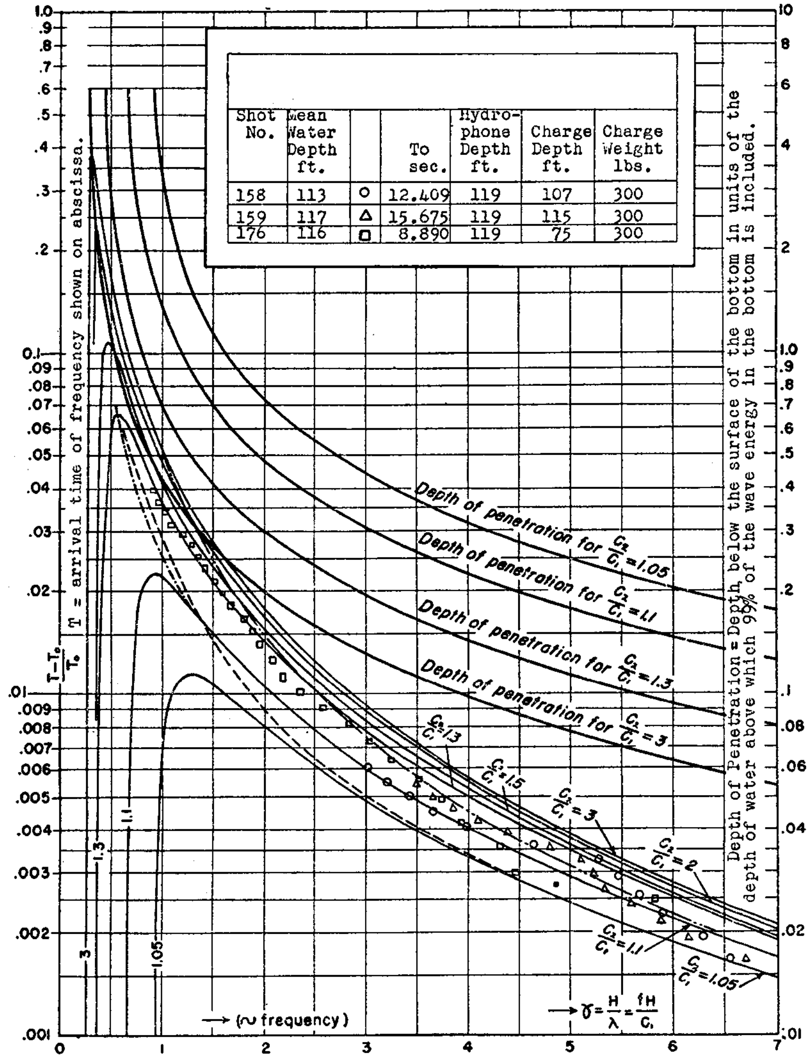


FIGURE 11.—*Dispersion in the water wave at Jacksonville Deep*

$H$ = Depth of Water. $C_1$ = Sound Velocity in Water. $C_2$ = Sound Velocity in Bottom. Density of Bottom assumed = 2. — — — — Layer of thickness $\frac{1}{2}H$ and $\frac{C_2}{C_1} = 1.05$ underlain by infinite layer of $\frac{C_3}{C_1} = 1.3$. — · — · — · — · — Layer of thickness $H$ and $\frac{C_2}{C_1} = 1.1$ underlain by layer of $\frac{C_3}{C_1} = 3$. — ·· — ·· — ·· — ·· — Layer of thickness $0.1H$ and $\frac{C_2}{C_1} = 1.1$ underlain by layer of $\frac{C_3}{C_1} = 3$.

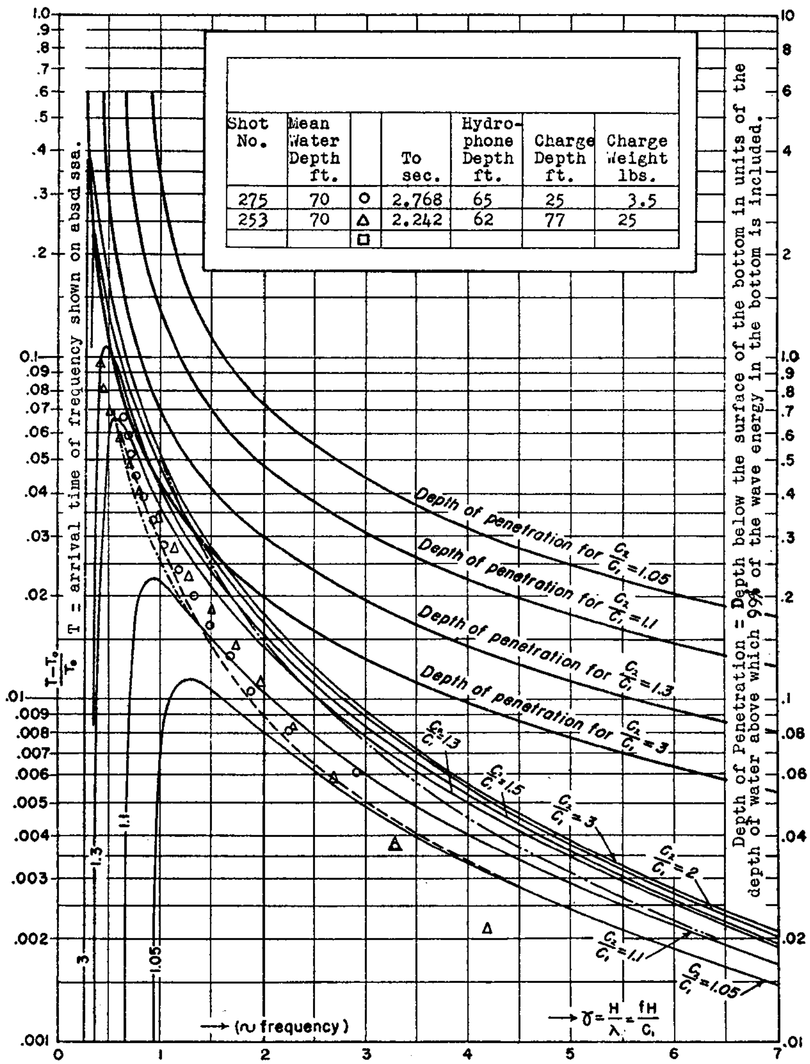


FIGURE 12.—*Dispersion in the water wave at Virgin Islands Shoal*

$H$ = Depth of Water. $C_1$ = Sound Velocity in Water. $C_2$ = Sound Velocity in Bottom. Density of Bottom assumed = 2. — — — —Layer of thickness $\frac{1}{2}H$ and $\frac{C_2}{C_1}$ = 1.05 underlain by infinite layer of $\frac{C_3}{C_1}$ = 1.3. — · — · — · — Layer of thickness $H$ and $\frac{C_2}{C_1}$ = 1.1 underlain by layer of $\frac{C_3}{C_1}$ = 3. — ·· — ·· — ·· — Layer of thickness 0.1$H$ and $\frac{C_2}{C_1}$ = 1.1 underlain by layer of $\frac{C_3}{C_1}$ = 3.

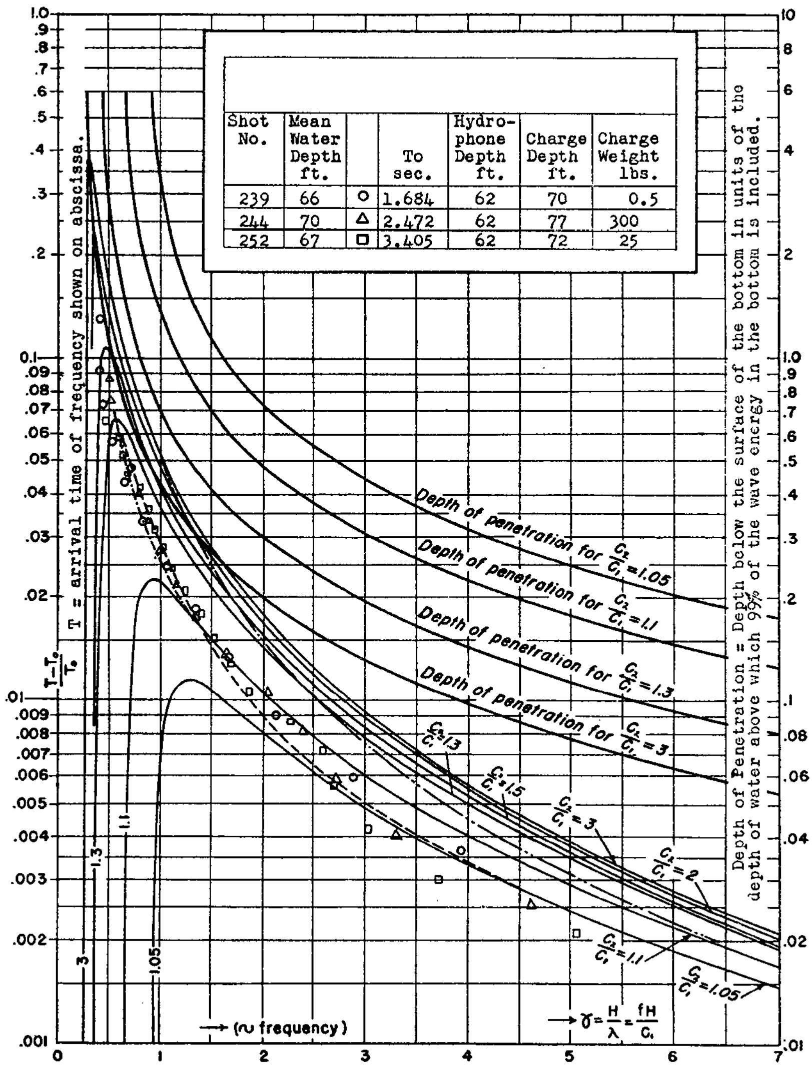


| Shot No. | Mean Water Depth ft. | | To sec. | Hydro-phone Depth ft. | Charge Depth ft. | Charge Weight lbs. |
|---|---|---|---|---|---|---|
| 239 | 66 | ○ | 1.684 | 62 | 70 | 0.5 |
| 244 | 70 | △ | 2.472 | 62 | 77 | 300 |
| 252 | 67 | □ | 3.405 | 62 | 72 | 25 |

FIGURE 13.—*Dispersion in the water wave at Virgin Islands Shoal*

$H$ = Depth of Water. $C_1$ = Sound Velocity in Water. $C_2$ = Sound Velocity in Bottom. Density of Bottom assumed = 2. — — — — Layer of thickness $\frac{1}{4}H$ and $\frac{C_2}{C_1}$ = 1.05 underlain by infinite layer of $\frac{C_2}{C_1}$ = 1.3. — · — · — · — Layer of thickness $H$ and $\frac{C_2}{C_1}$ = 1.1 underlain by layer of $\frac{C_2}{C_1}$ = 3. — ·· — ·· — ·· — Layer of thickness $0.1H$ and $\frac{C_2}{C_1}$ = 1.1 underlain by layer of $\frac{C_2}{C_1}$ = 3.

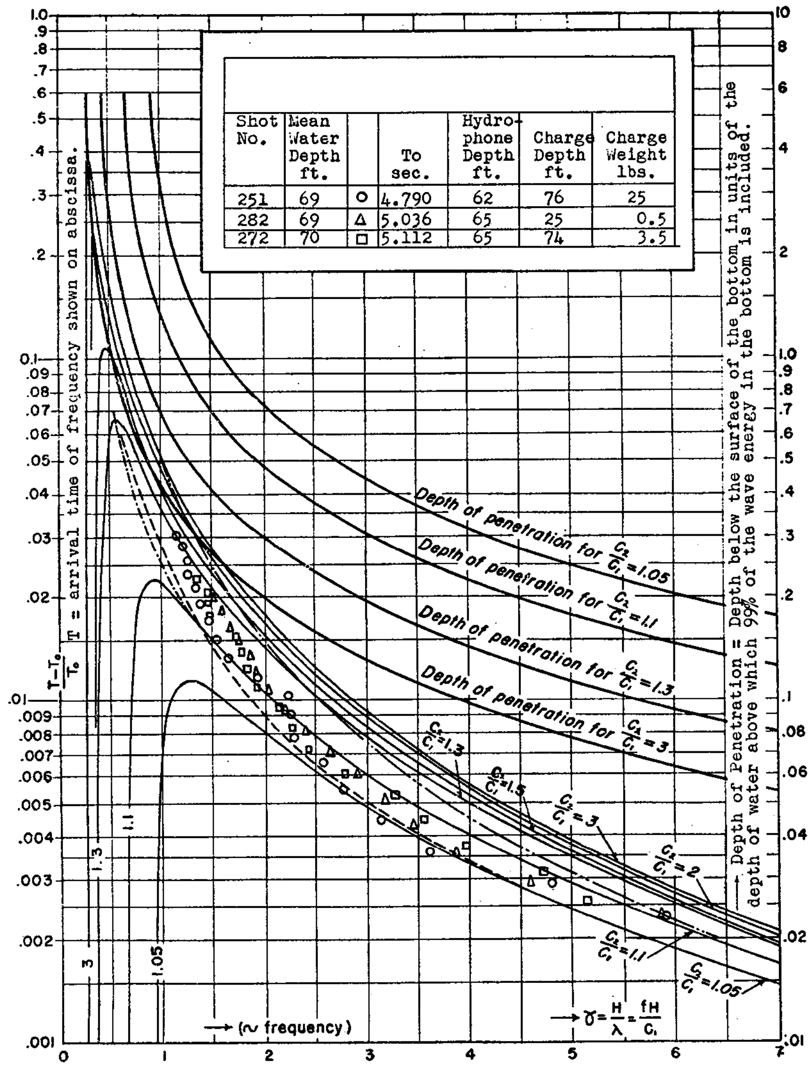


FIGURE 14.—*Dispersion in the water wave in Virgin Islands Shoal*

$H$ = Depth of Water. $C_1$ = Sound Velocity in Water. $C_2$ = Sound Velocity in Bottom. Density of Bottom assumed = 2. ————— Layer of thickness $\frac{1}{2}H$ and $\frac{C_2}{C_1}$ = 1.05 underlain by infinite layer of $\frac{C_3}{C_1}$ = 1.3. —·—·—·—·— Layer of thickness $H$ and $\frac{C_2}{C_1}$ = 1.1 underlain by layer of $\frac{C_3}{C_1}$ = 3. —··—··—··—··— Layer of thickness 0.1$H$ and $\frac{C_2}{C_1}$ = 1.1 underlain by layer of $\frac{C_3}{C_1}$ = 3.

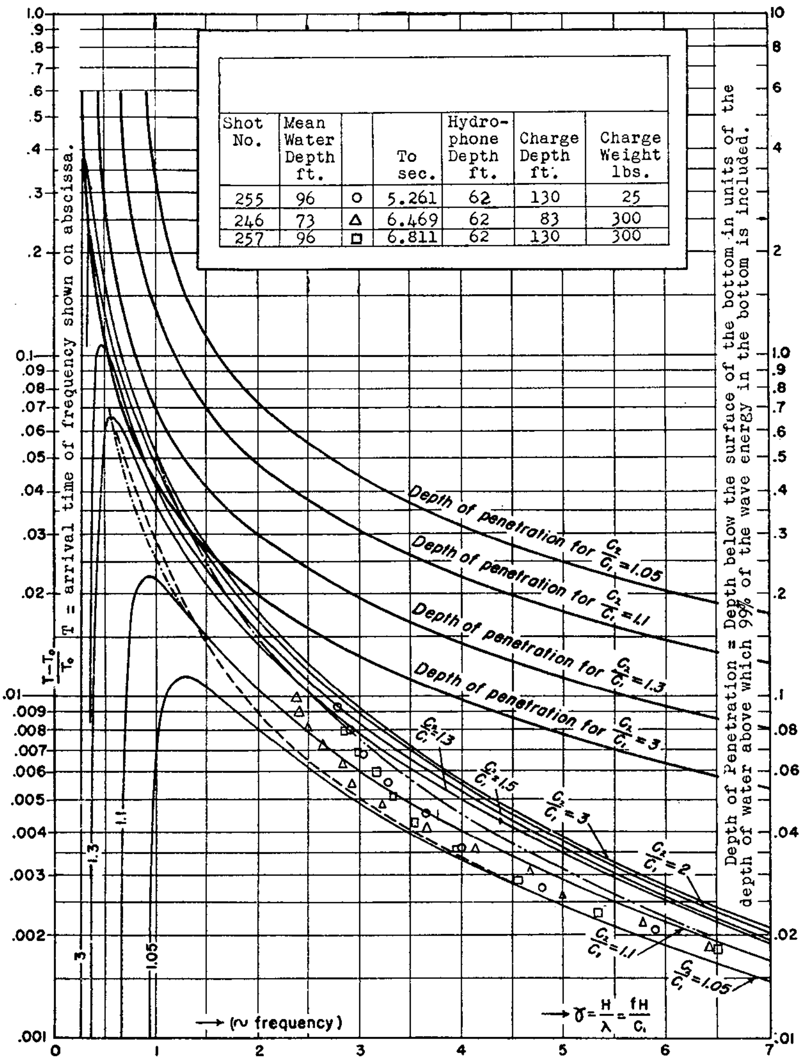


| Shot No. | Mean Water Depth ft. | | To sec. | Hydrophone Depth ft. | Charge Depth ft. | Charge Weight lbs. |
|---|---|---|---|---|---|---|
| 255 | 96 | ○ | 5.261 | 62 | 130 | 25 |
| 246 | 73 | △ | 6.469 | 62 | 83 | 300 |
| 257 | 96 | □ | 6.811 | 62 | 130 | 300 |

FIGURE 15.—*Dispersion in the water wave at Virgin Islands Shoal*

$H$ = Depth of Water. $C_1$ = Sound Velocity in Water. $C_2$ = Sound Velocity in Bottom. Density of Bottom assumed = 2. — — — — Layer of thickness $\frac{1}{2}H$ and $\frac{C_2}{C_1}$ = 1.05 underlain by infinite layer of $\frac{C_3}{C_1}$ = 1.3. — · — · — · — Layer of thickness $H$ and $\frac{C_2}{C_1}$ = 1.1 underlain by layer of $\frac{C_3}{C_1}$ = 3. — ·· — ·· — ·· — Layer of thickness 0.1$H$ and $\frac{C_2}{C_1}$=1.1 underlain by layer of $\frac{C_3}{C_1}$ = 3.

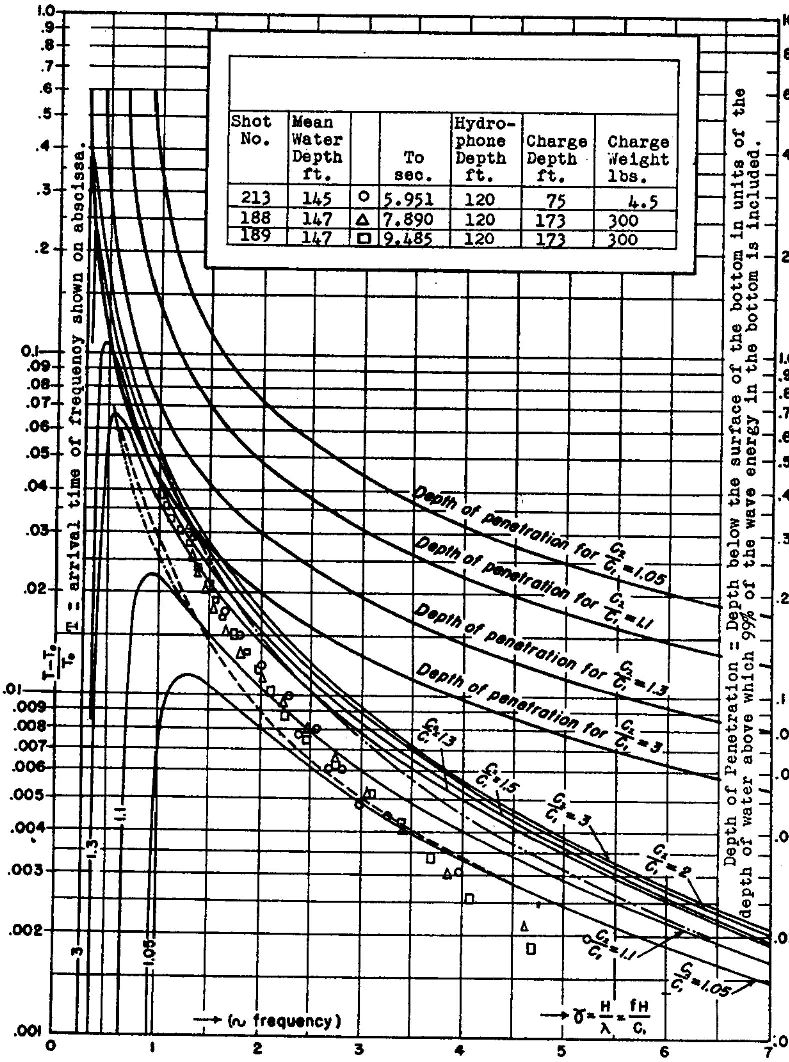


FIGURE 16.—*Dispersion in the water wave at Virgin Islands Deep*

$H$ = Depth of Water. $C_1$ = Sound Velocity in Water. $C_2$ = Sound Velocity in Bottom. Density of Bottom assumed = 2. ———— Layer of thickness $\frac{1}{2}H$ and $\frac{C_2}{C_1}$ = 1.05 underlain by infinite layer of $\frac{C_3}{C_1}$ = 1.3. —·—·—·— Layer of thickness $H$ and $\frac{C_2}{C_1}$ = 1.1 underlain by layer of $\frac{C_3}{C_1}$ = 3. —··—··—··— Layer of thickness 0.1$H$ and $\frac{C_2}{C_1}$ = 1.1 underlain by layer of $\frac{C_3}{C_1}$ = 3.

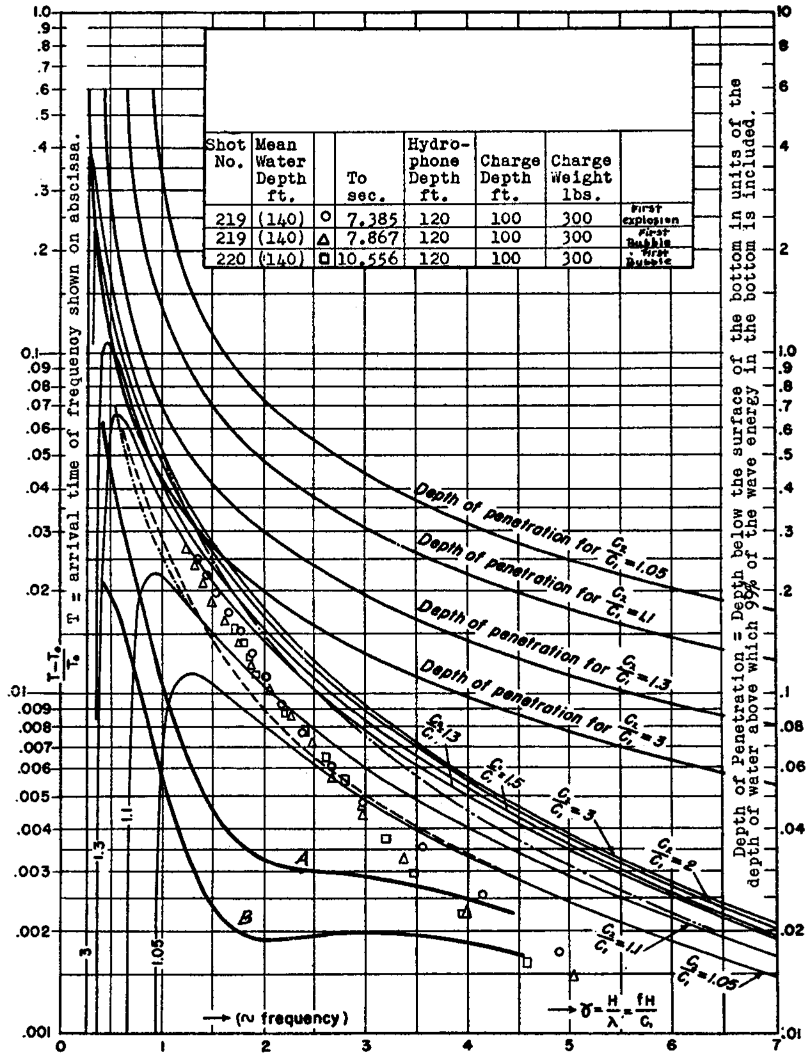


FIGURE 17.—*Dispersion in the water wave at Virgin Islands Deep and comparison of dispersion in the waves from the main explosion and from the first bubble expansion*

$H$ = Depth of Water. $C_1$ = Sound Velocity in Water. $C_2$ = Sound Velocity in Bottom. Density of Bottom assumed = 2. ———— Layer of thickness $\frac{1}{2}H$ and $\frac{C_2}{C_1}$ = 1.05 underlain by infinite layer of $\frac{C_3}{C_1}$ = 1.3. —·—·—·— Layer of thickness $H$ and $\frac{C_2}{C_1}$ = 1.1 underlain by layer of $\frac{C_3}{C_1}$ = 3. —··—··—··— Layer of thickness 0.1$H$ and $\frac{C_2}{C_1}$ = 1.1 underlain by layer of $\frac{C_3}{C_1}$ = 3. A—Layer of thickness $H$ and $\frac{C_2}{C_1}$ = 0.98 underlain by a layer of $\frac{C_3}{C_1}$ = 3.0. B—Layer of thickness $H$ and $\frac{C_2}{C_1}$ = 0.98 underlain by a layer of $\frac{C_3}{C_1}$ = 1.1.

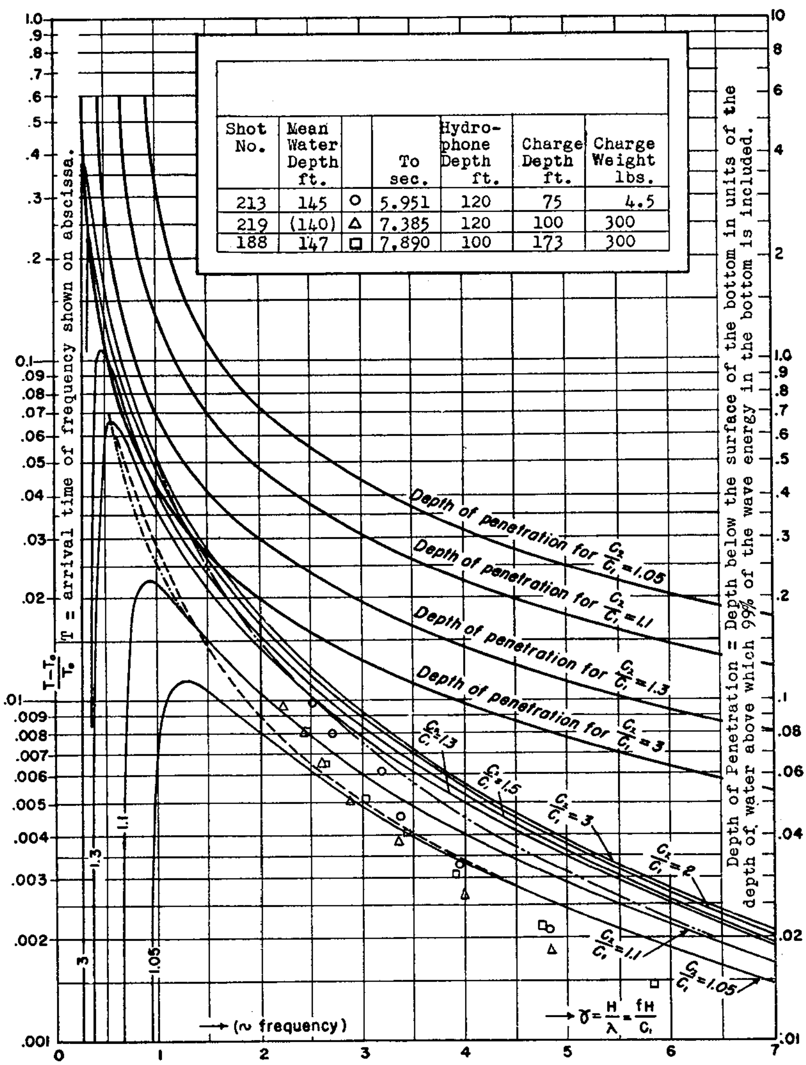


FIGURE 18.—*Dispersion in the water wave at Virgin Islands Deep*

$H$ = Depth of Water. $C_1$ = Sound Velocity in Water. $C_2$ = Sound Velocity in Bottom. Density of Bottom assumed = 2. ——————Layer of thickness ½$H$ and $\frac{C_2}{C_1}$ = 1.05 underlain by infinite layer of $\frac{C_3}{C_1}$ = 1.3. —·—·—·—·— Layer of thickness $H$ and $\frac{C_2}{C_1}$ = 1.1 underlain by layer of $\frac{C_3}{C_1}$ = 3. —··—··—··—··— Layer of thickness 0.1$H$ and $\frac{C_2}{C_1}$ = 1.1 underlain by layer of $\frac{C_3}{C_1}$ = 3.

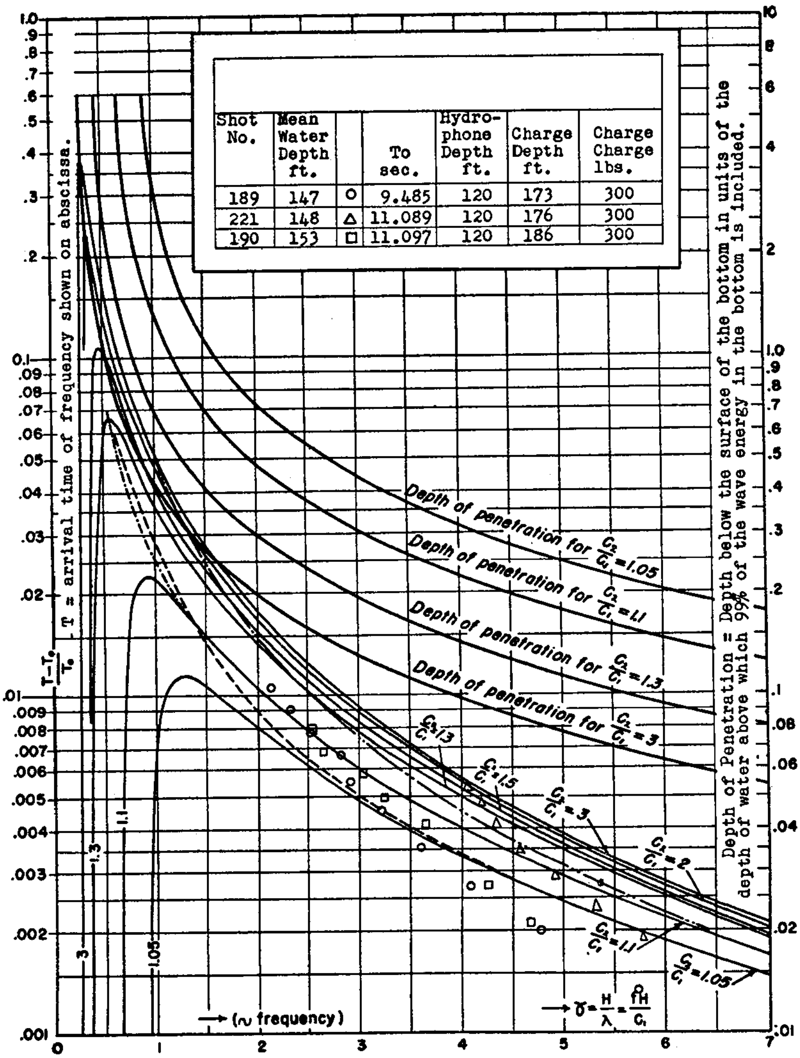


| Shot No. | Mean Water Depth ft. | | To sec. | Hydrophone Depth ft. | Charge Depth ft. | Charge Charge lbs. |
|---|---|---|---|---|---|---|
| 189 | 147 | ○ | 9.485 | 120 | 173 | 300 |
| 221 | 148 | △ | 11.089 | 120 | 176 | 300 |
| 190 | 153 | □ | 11.097 | 120 | 186 | 300 |

FIGURE 19.—*Dispersion in the water wave at Virgin Islands Deep*

$H$ = Depth of Water. $C_1$ = Sound Velocity in Water. $C_2$ = Sound Velocity in Bottom. Density of Bottom assumed = 2. ———— Layer of thickness $\frac{1}{2}H$ and $\frac{C_2}{C_1}$ = 1.05 underlain by infinite layer of $\frac{C_3}{C_1}$ = 1.3. —·—·—·—·— Layer of thickness $H$ and $\frac{C_2}{C_1}$ = 1.1 underlain by layer of $\frac{C_3}{C_1}$ = 3. —··—··—··—··— Layer of thickness 0.1$H$ and $\frac{C_2}{C_1}$ = 1.1 underlain by layer of $\frac{C_3}{C_1}$ = 3.

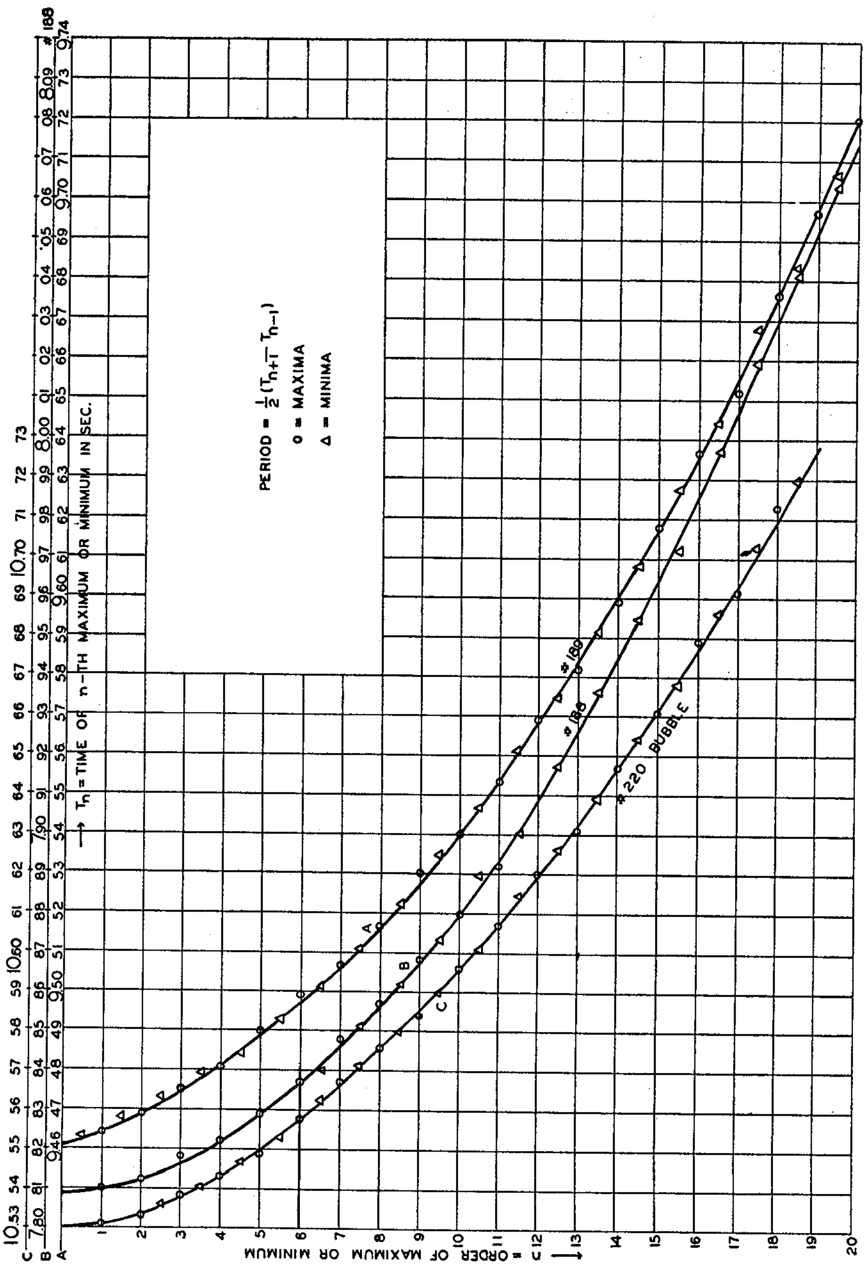


FIGURE 20.—*Analysis of dispersion data in Virgin Islands Deep*

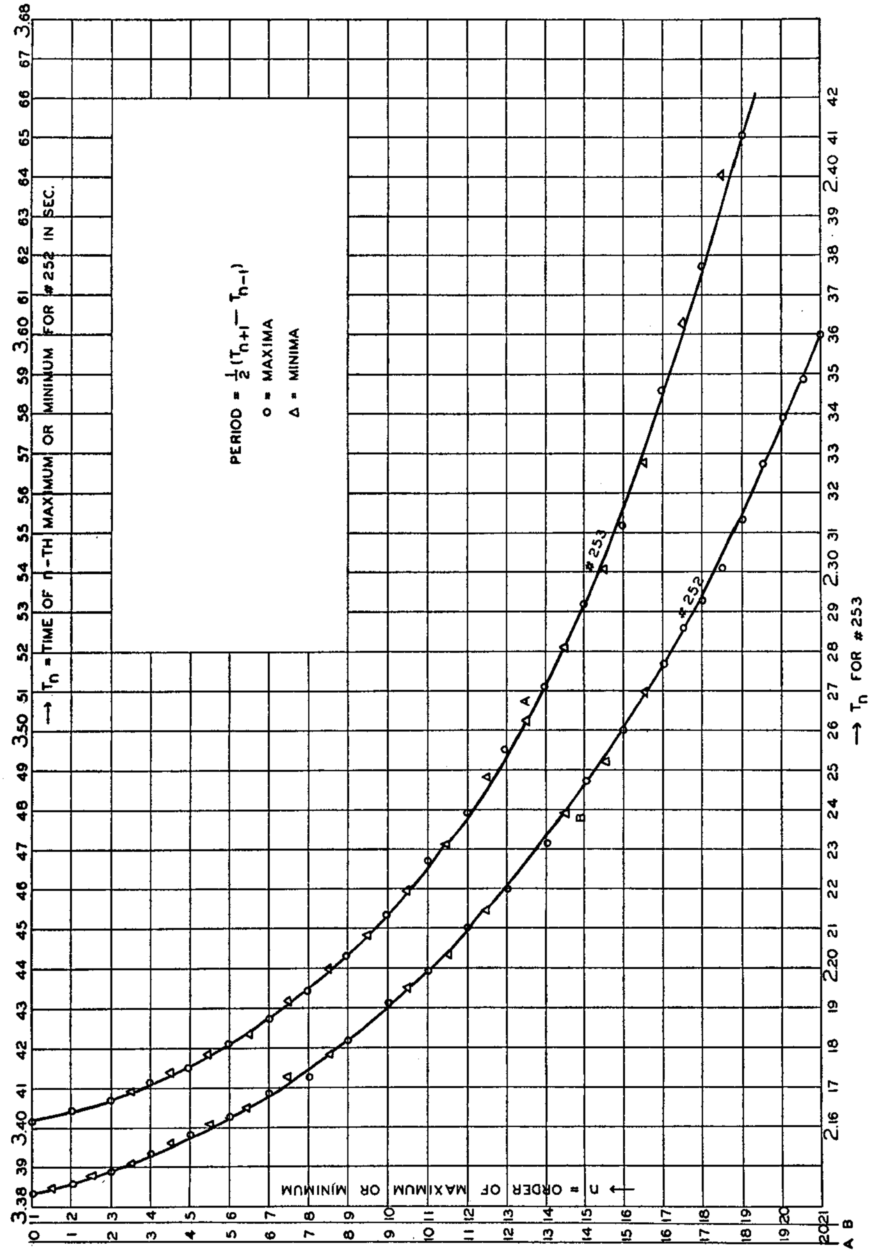


FIGURE 21.—*Analysis of dispersion data in Virgin Islands Shoal*

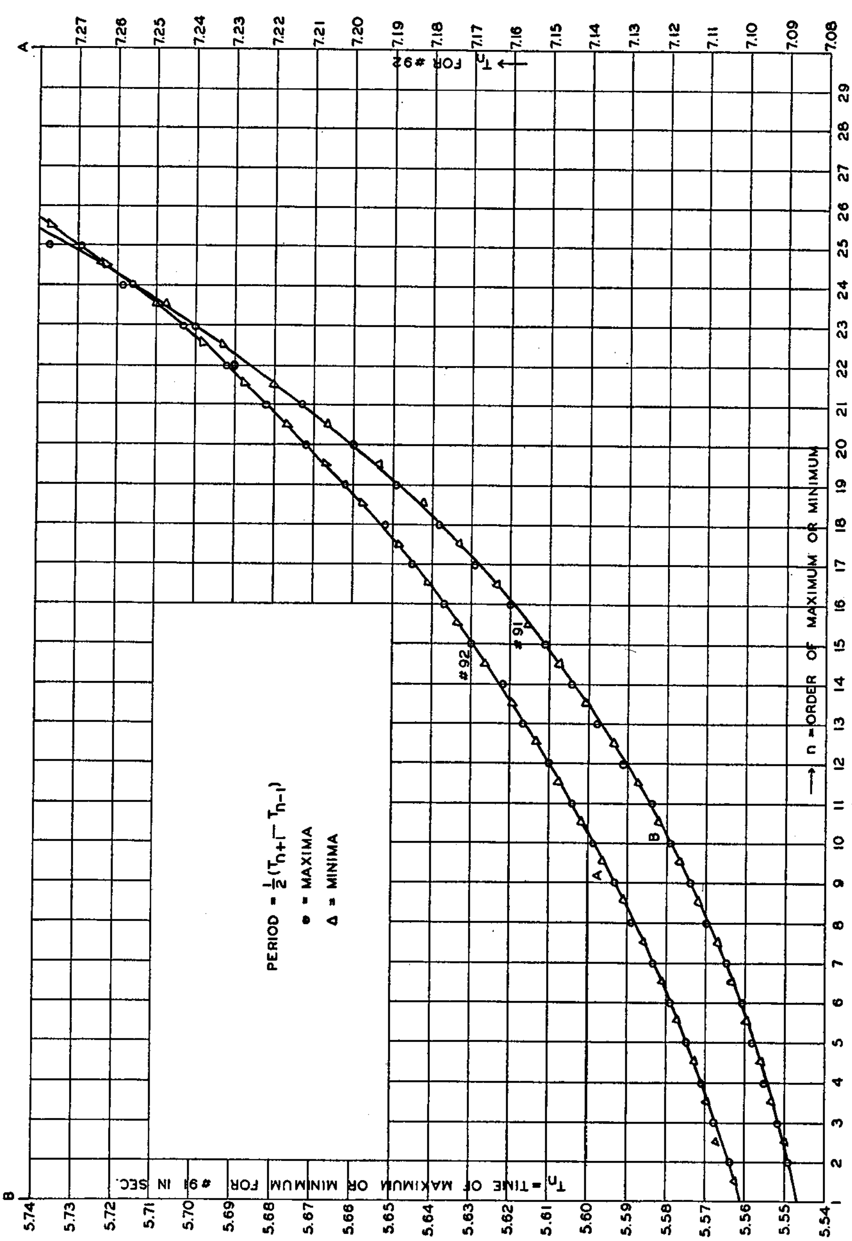


FIGURE 22.—*Analysis of dispersion data in Jacksonville Shoal*

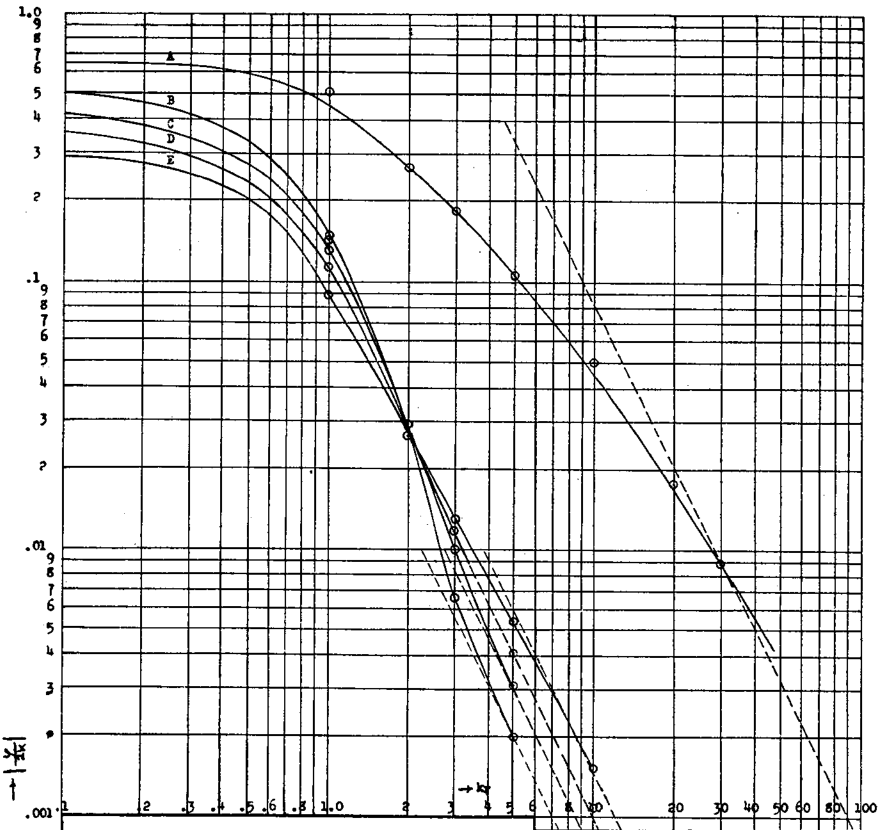


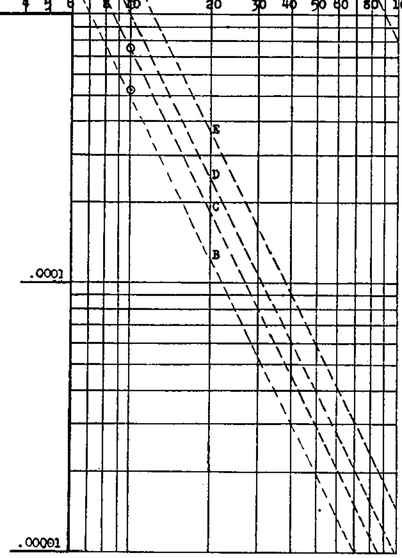

FIGURE 23.—*Variation of pressure with range due to a periodic point source in shallow water*

---- Asymptotic values given by equations (32) and (33) = $N/(kr)^2$

$\rho_1$ = Density of water
$\rho_2$ = Density of bottom
$c_1$ = Sound velocity in water
$c_2$ = Sound velocity in bottom
$d$ = Depth of point source
$z$ = Depth of receiver
$H$ = Depth of water
$k$ = $2\pi/\lambda$($\lambda$ = wavelength in water)
$\varphi$ = Sound potential (proportional to pressure amplitude)
$r$ = Horizontal distance from source
⊙ = Computed points from equation (19)

| Graph | $c_1/c_2$ | $\rho_1/\rho_2$ | $kH$ | $d/H$ | $z/H$ | $N$ | $100 \left\lvert\frac{\varphi(10)}{2k}\right\rvert$ | $900 \left\lvert\frac{\varphi(30)}{2k}\right\rvert$ |
|---|---|---|---|---|---|---|---|---|
| A | 0.6 | 0.50 | 1.7952 | .30 | 0.6 | 8.2500 | 5.000 | 8.0 |
| B | 2.0 | 0.50 | .84 | .25 | 1.0 | 0.0492 | 0.053 | |
| C | 2.0 | 0.75 | .84 | .25 | 1.0 | 0.0738 | 0.075 | |
| D | 2.0 | 1.00 | .84 | .25 | 1.0 | 0.0984 | 0.109 | |
| E | 2.0 | 1.50 | .84 | .25 | 1.0 | 0.1476 | 0.151 | |
| F | 1.2 | 0.50 | .84 | .25 | 1.0 | 0.0832 | 0.086 | not plotted |
| G | 0.6 | 0.50 | .84 | .25 | 1.0 | 0.0797 | 0.086 | not plotted |

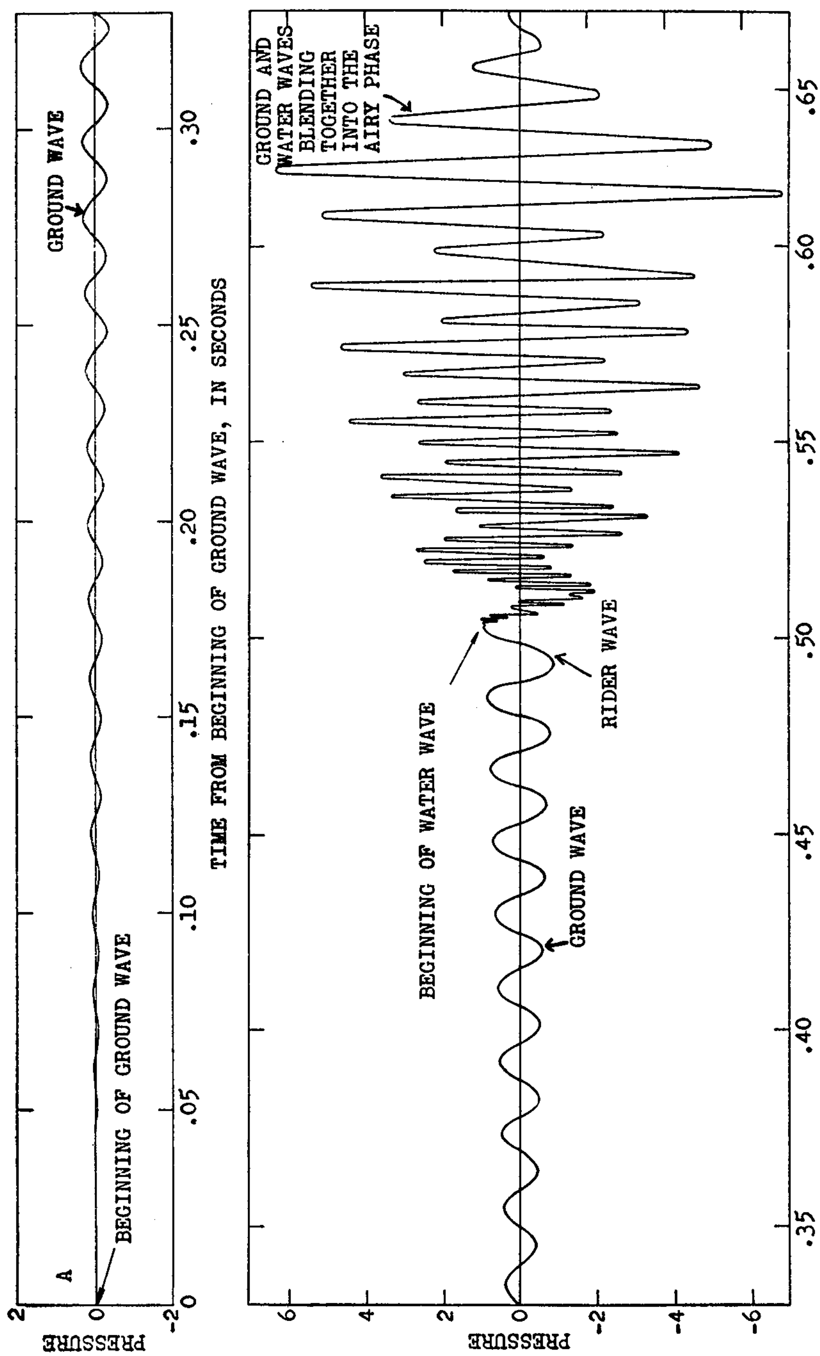


FIGURE 24A.—*Theoretical contribution of the first mode to the disturbance at a distance from an explosion in shallow water*

Source and receiver both assumed to be on the bottom
Range: 460 × depth of water
Depth of water: 60 feet

Velocity of sound in bottom = 1.1 × velocity in water
Density of bottom = 2 × density of water
Charge weight = 5 pounds

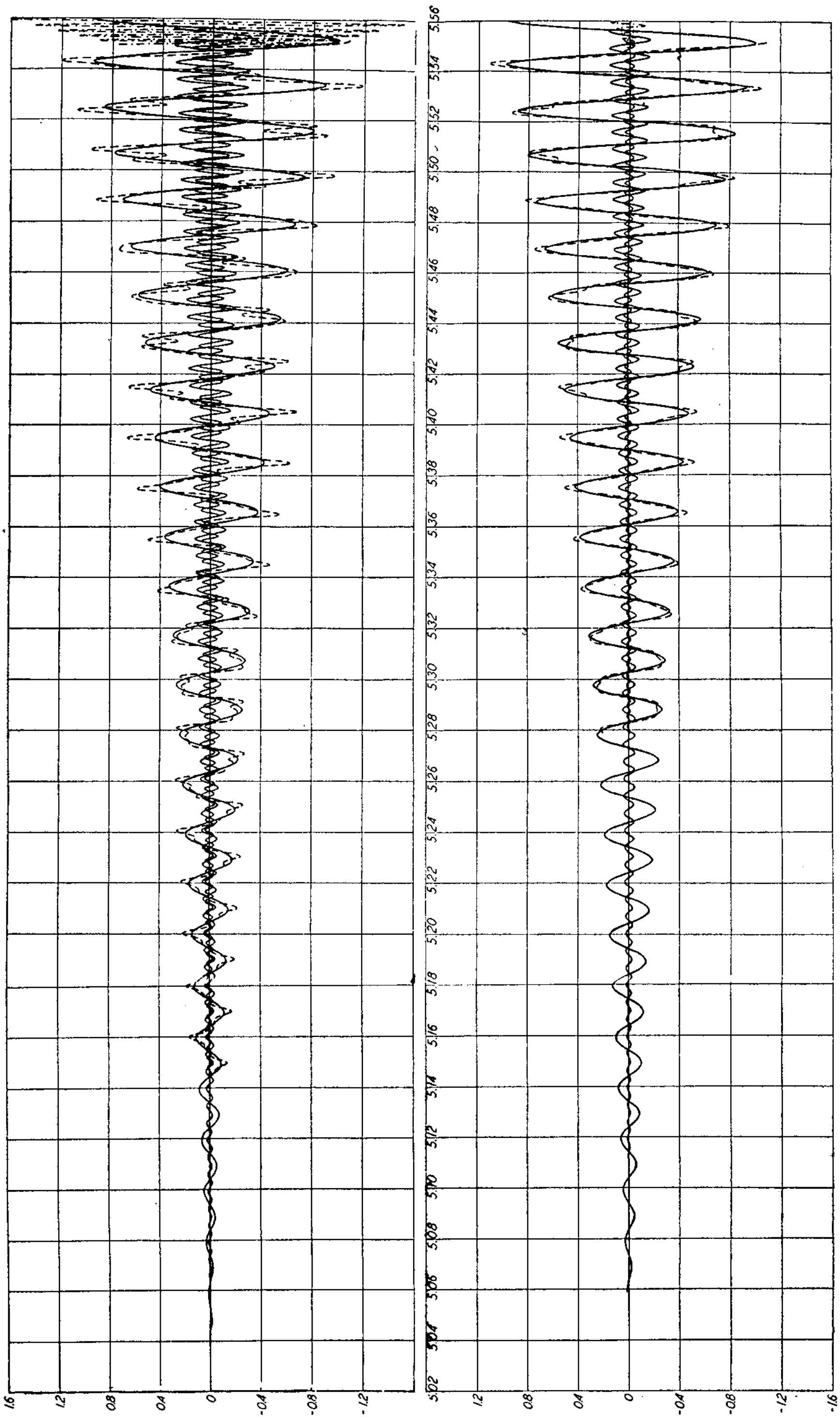


FIGURE 24.—*Theoretical pressure variation in ground wave due to the first three modes*

Dashed curve is the sum of the contributions from all three modes. Lower part gives modification of pressure record by Mk II low frequency system. The set-up is the same as in Figure 24A.

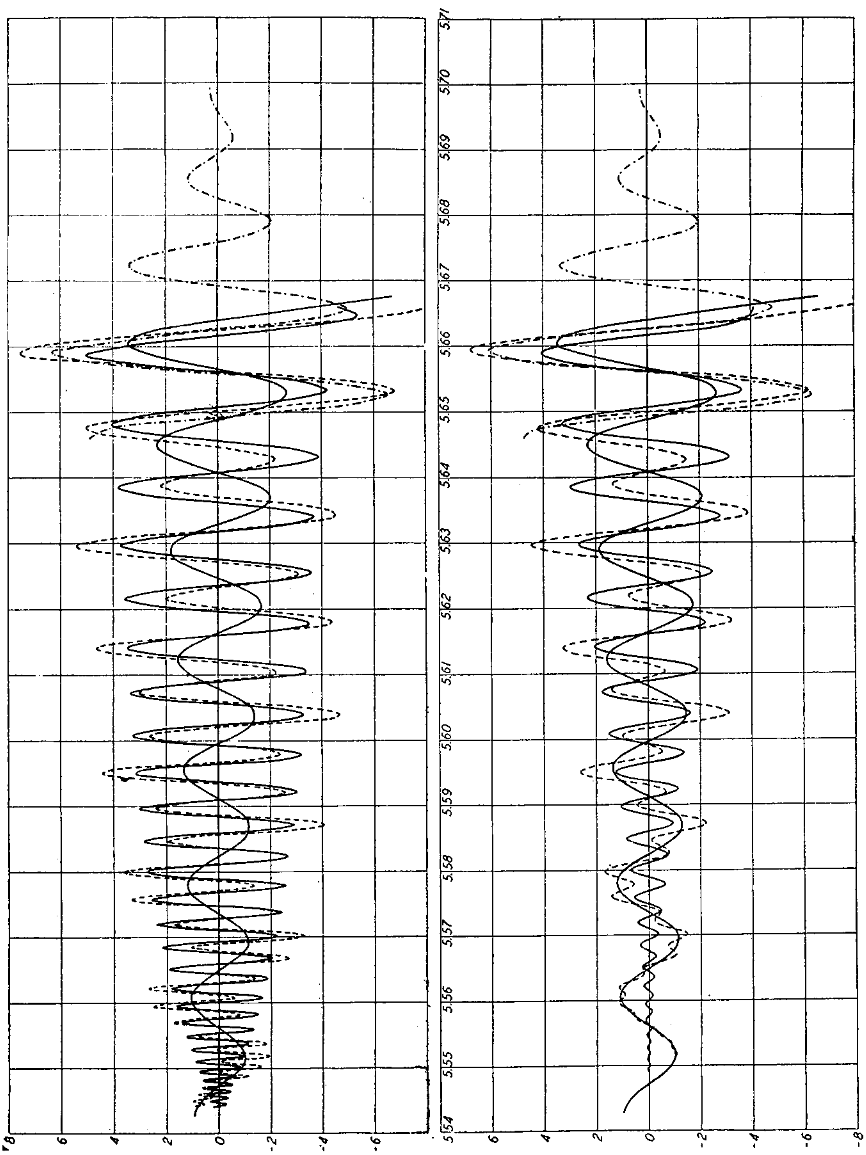


FIGURE 25.—*Continuation of the record shown in Figure 24 into the water wave phase*
Only the first mode was plotted.

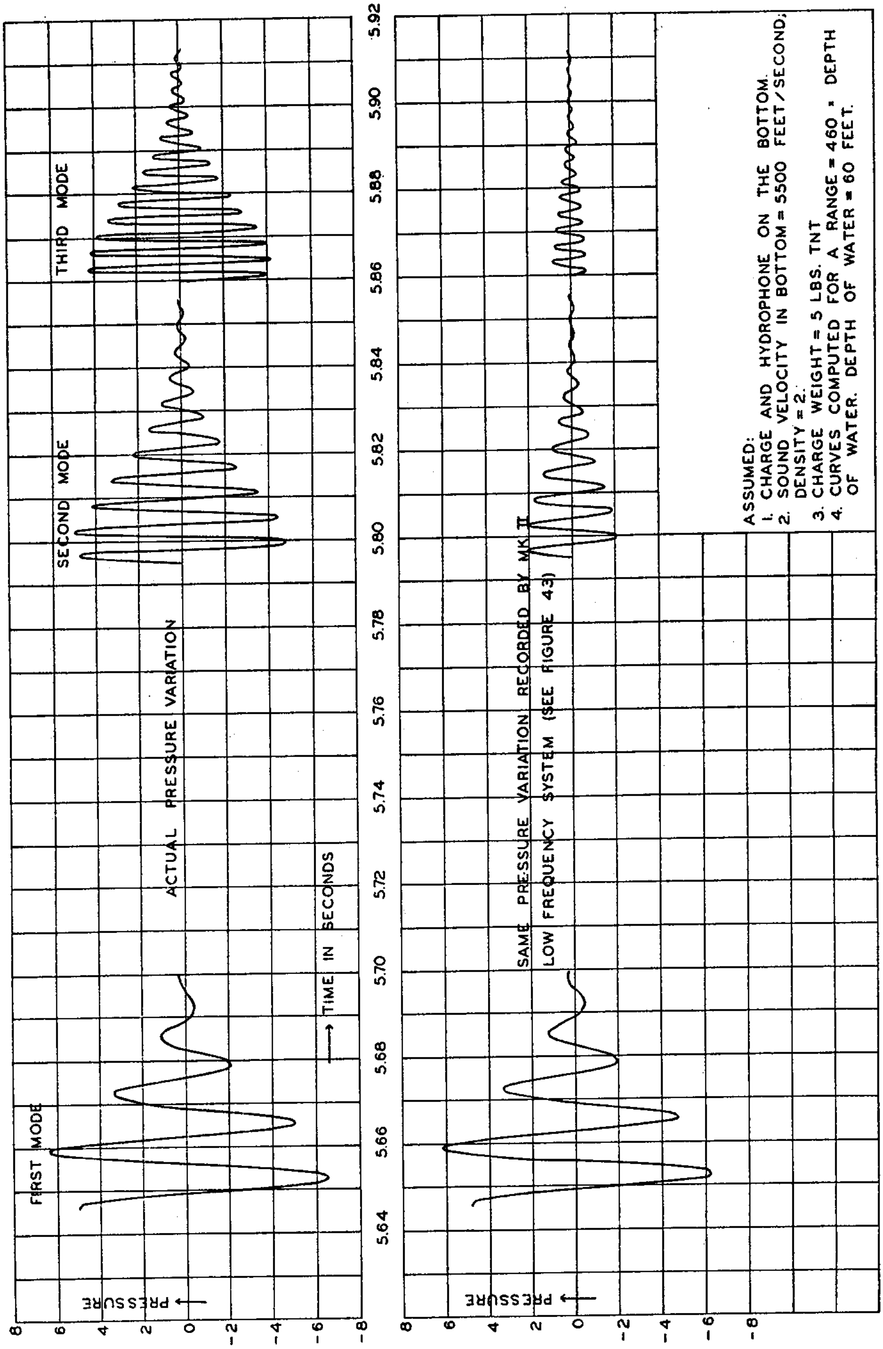


FIGURE 26.—*Theoretical pressure variation in the "Airy" phases of the first three modes, and the effect of a low-pass filtering system in suppressing the higher modes*

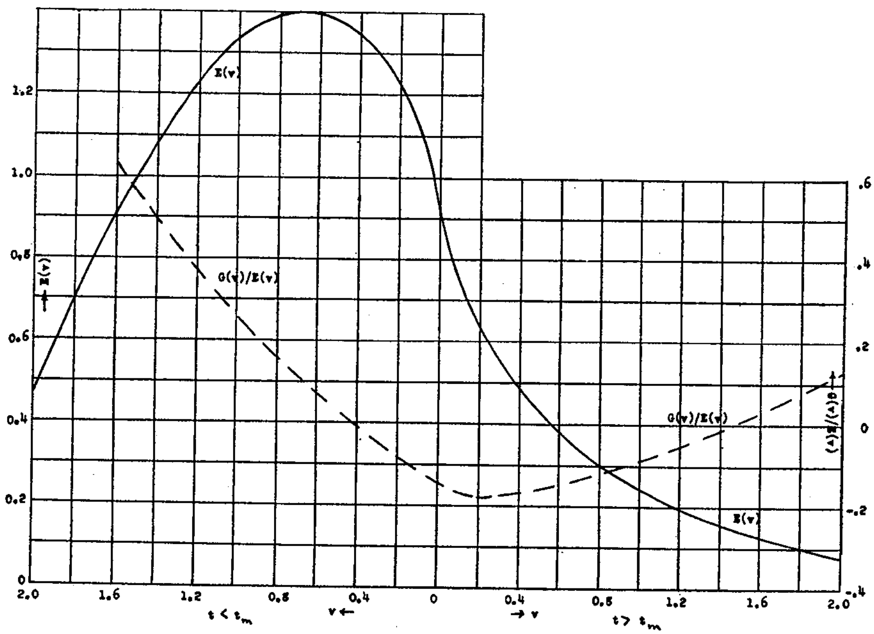


FIGURE 27.—*Envelope of the Airy phase*

For definition of $v$, $E(v)$ and $G(v)$ *see* Eqs. (A112, A110, A111, A114 and A115)

$t_m = r/U_0$, $U_0$ = minimum group velocity

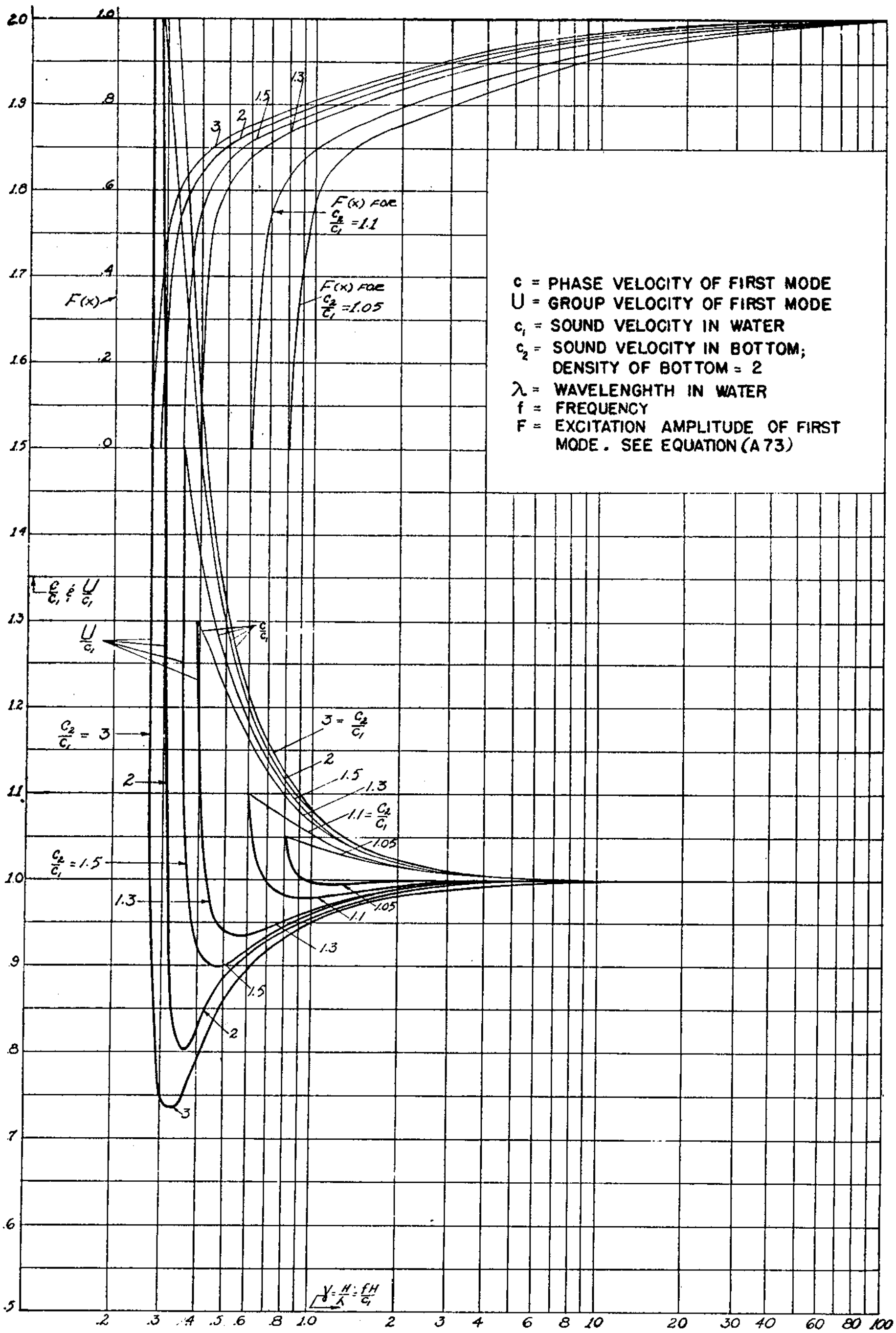


FIGURE 28.—*Phase velocity and group velocity of the first mode in at wo-layered liquid half-space*

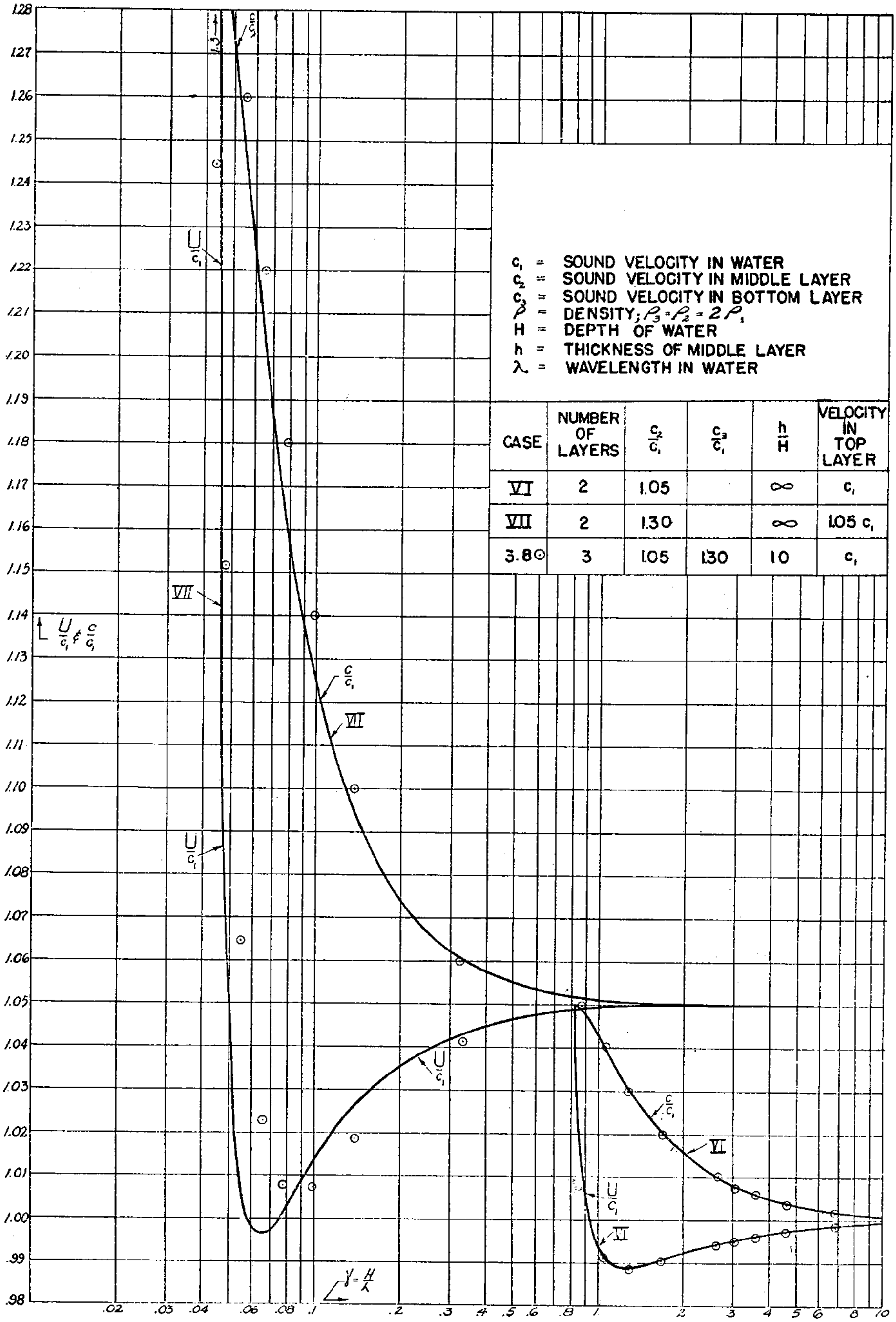


FIGURE 29.—*Phase velocity c and group velocity U for the first mode in a three-layered liquid half-space*

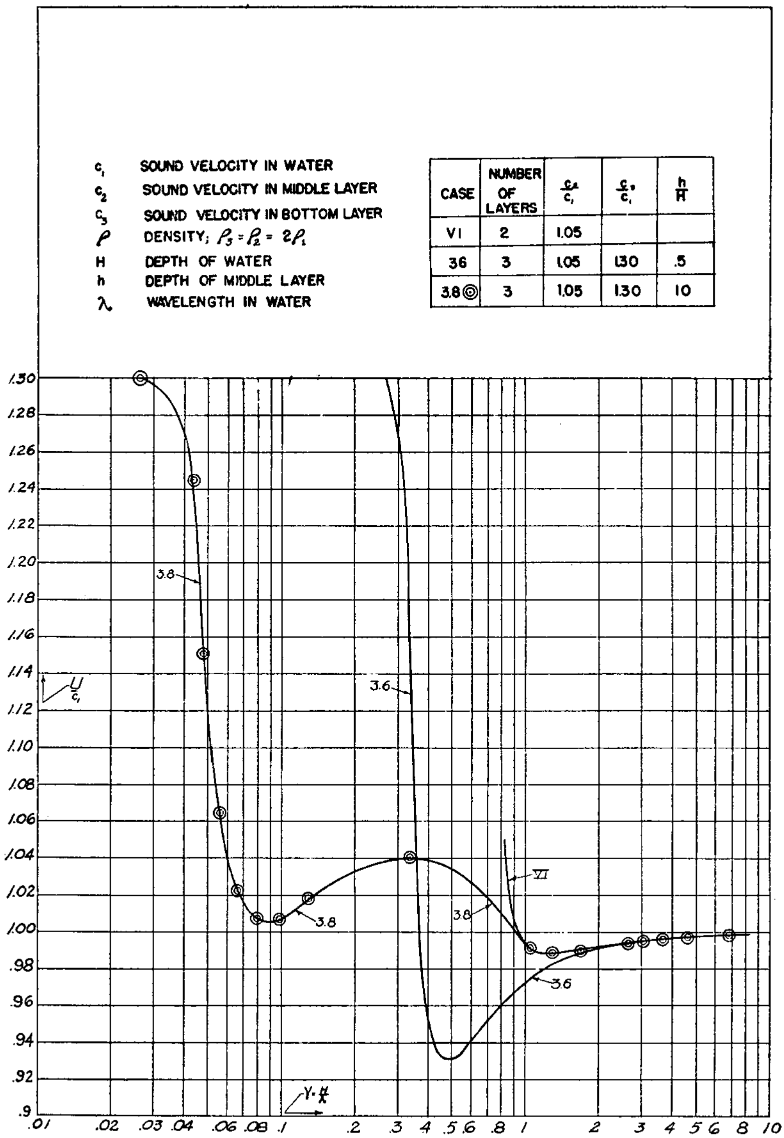


FIGURE 30.—*Group velocity U for the first mode in a three-layered liquid half-space*

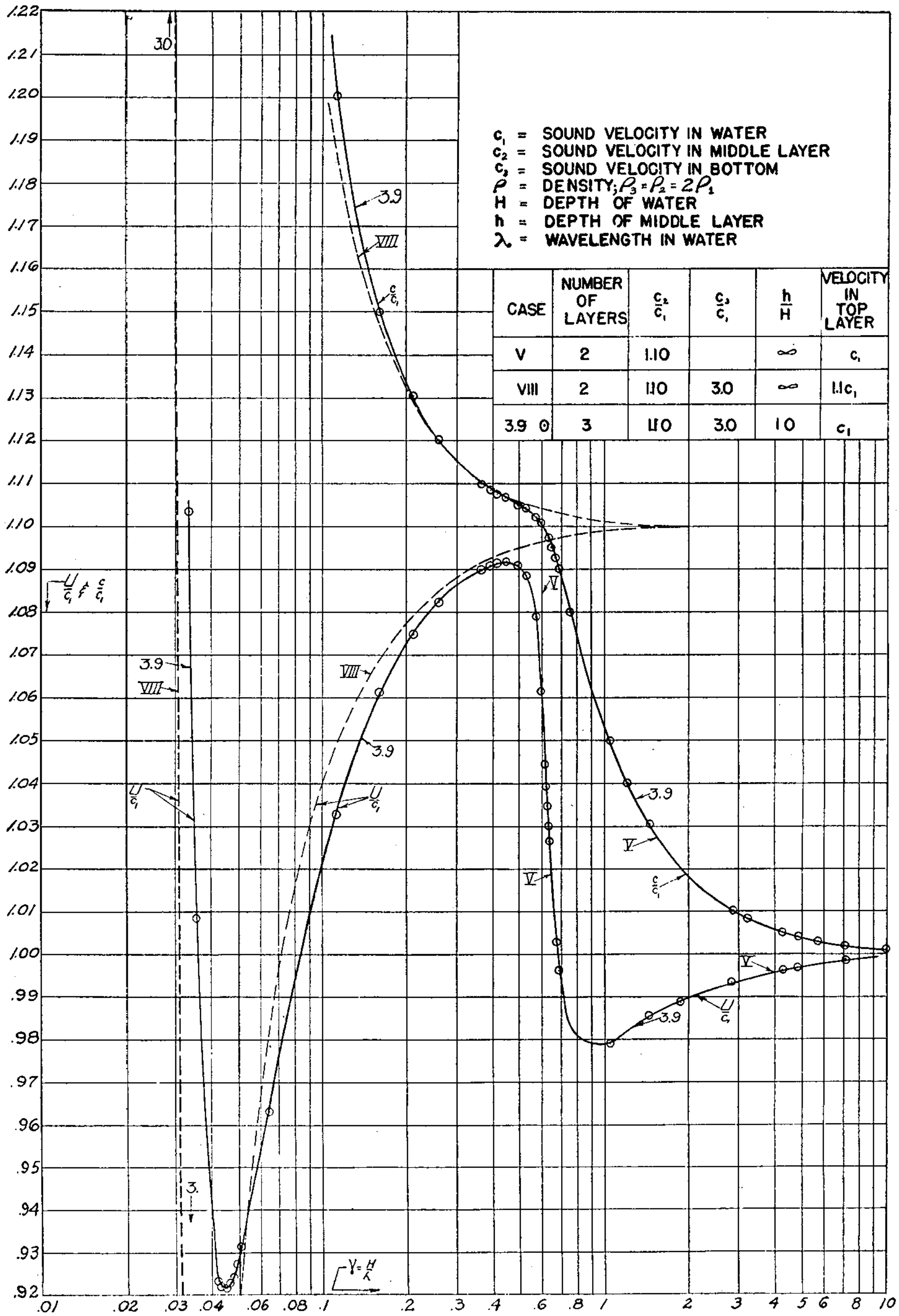


FIGURE 31.—*Phase velocity c and group velocity U for the first mode in a three-layered liquid half-space*

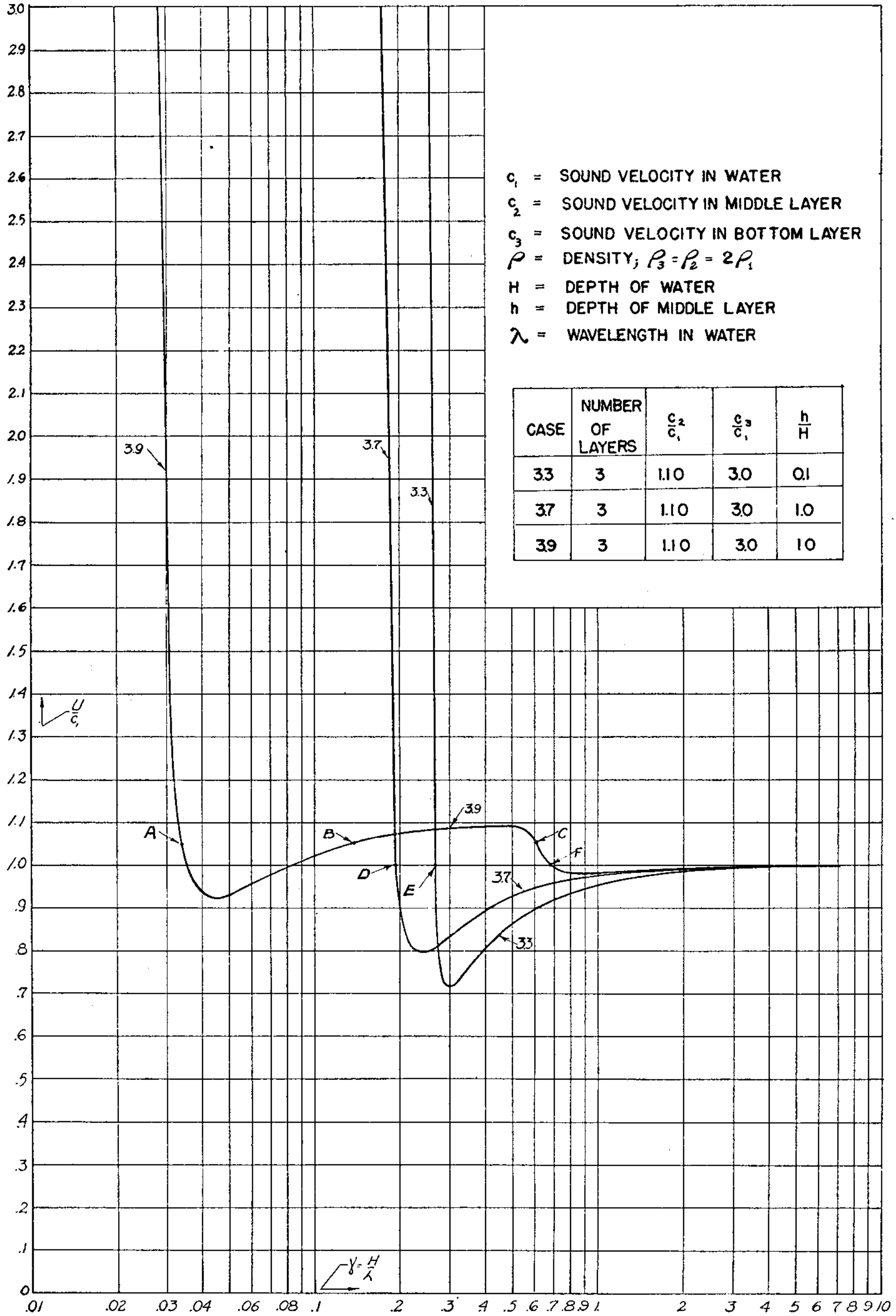


FIGURE 32.—*Group velocity U for the first mode in a three-layered liquid half-space*

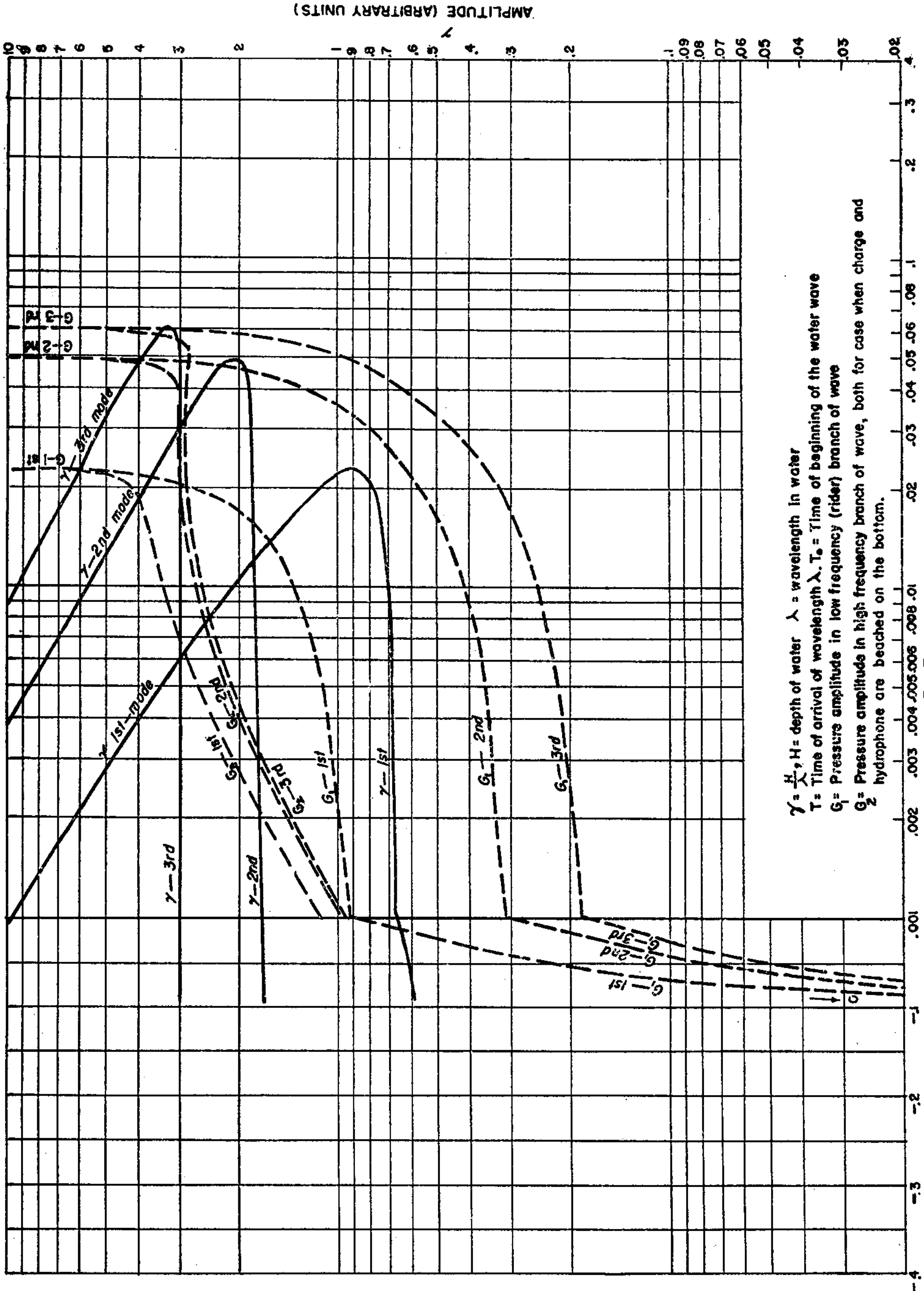


FIGURE 33.—*Theoretical time of arrival and amplitude of the various frequencies in the water wave for the case (A) of a bottom of uniform sound velocity (=5500 fps) and density (=2)*

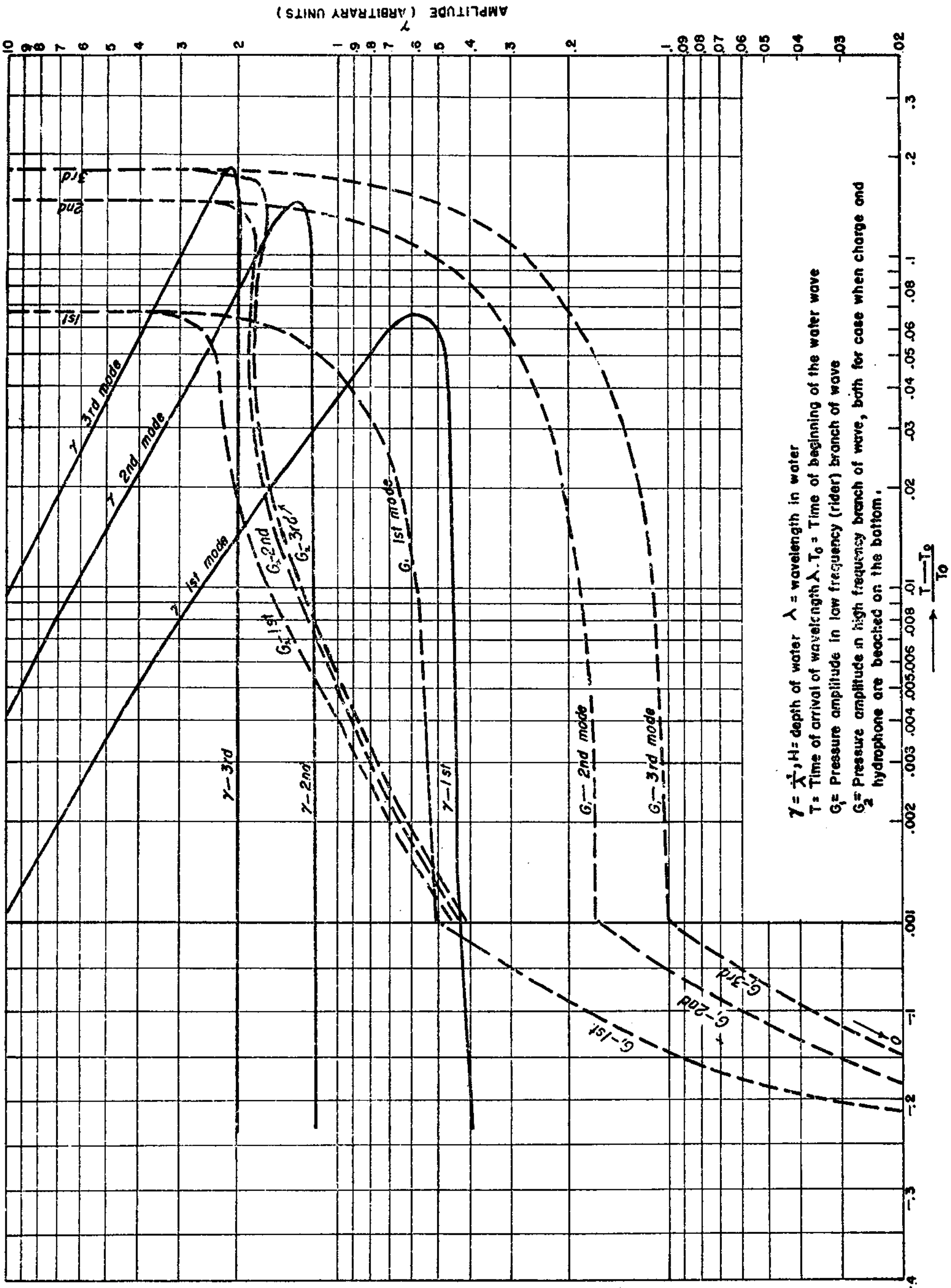


FIGURE 34.—*Theoretical time of arrival and amplitude of the various frequencies in the water wave for the case of (B) a bottom of uniform sound velocity (= 6500 fps) and density (= 2)*

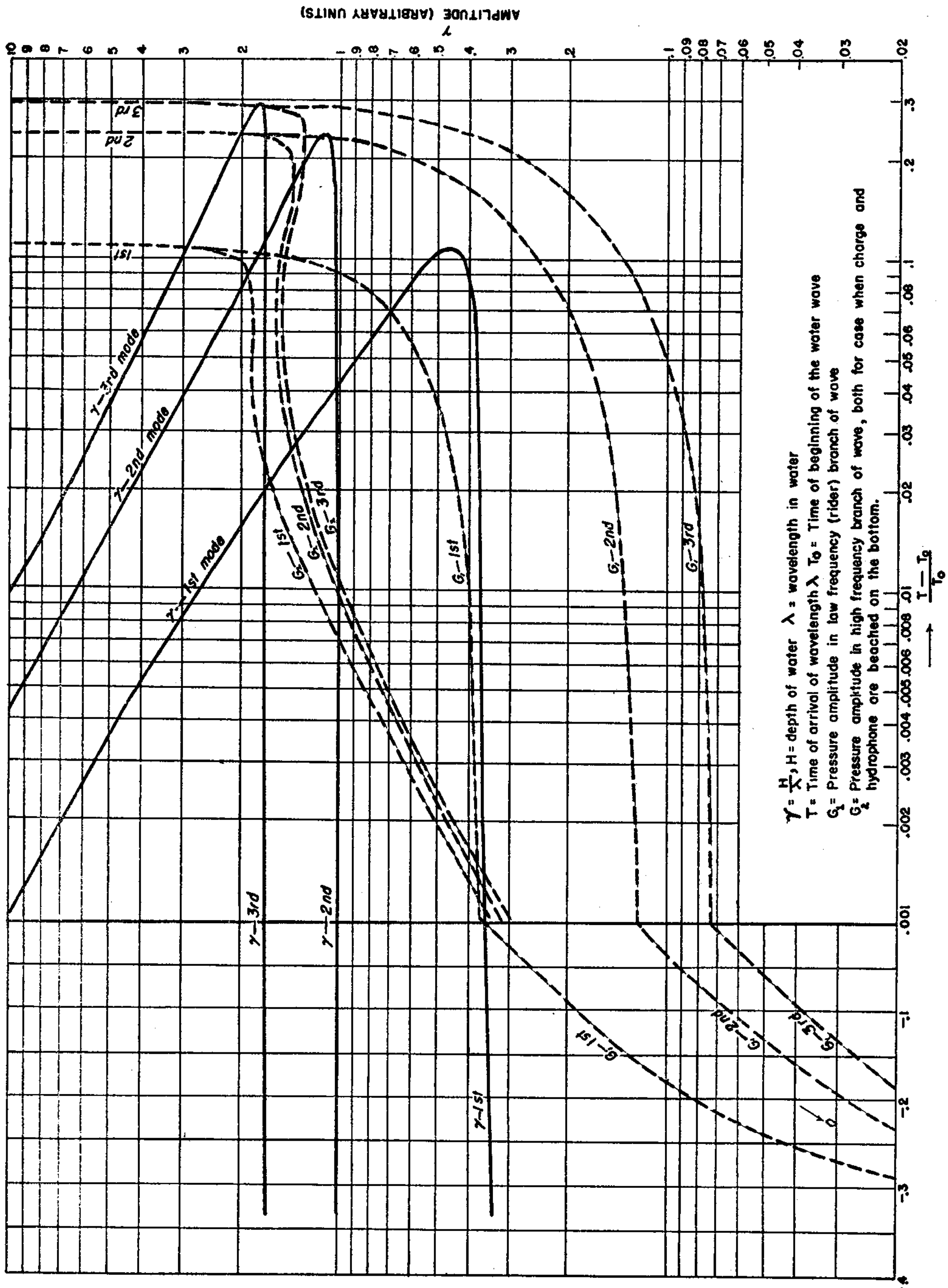


FIGURE 35.—*Theoretical time of arrival and amplitude of the various frequencies in the water wave for the case (C) of a bottom of uniform sound velocity (=7500 fps) and density (=2)*

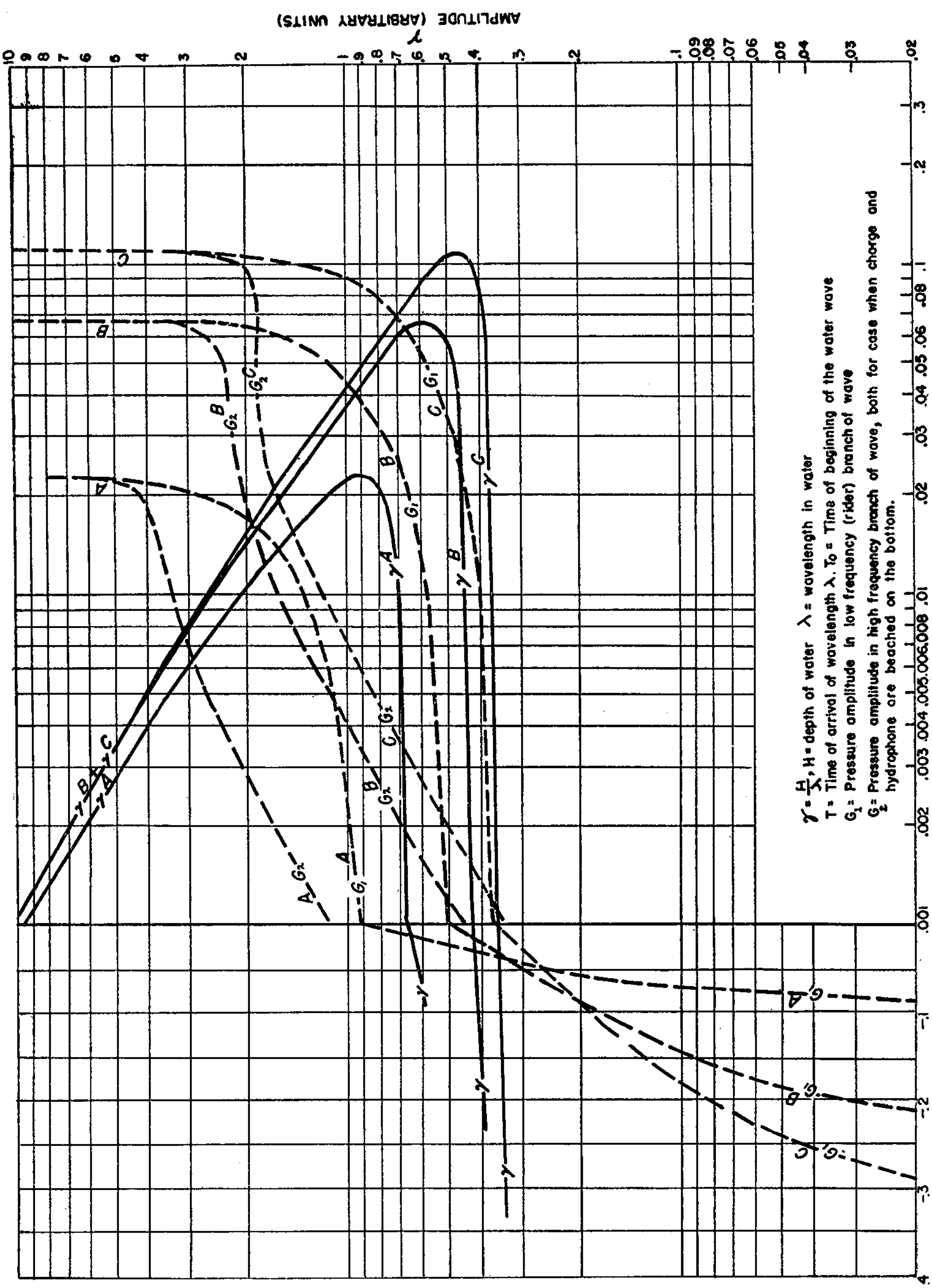


FIGURE 36.—*Theoretical time of arrival and amplitude of the various frequencies in the first mode for uniform bottoms of sound velocity A(5500 fps), B(6500 fps), and C(7500 fps) and density (= 2)*

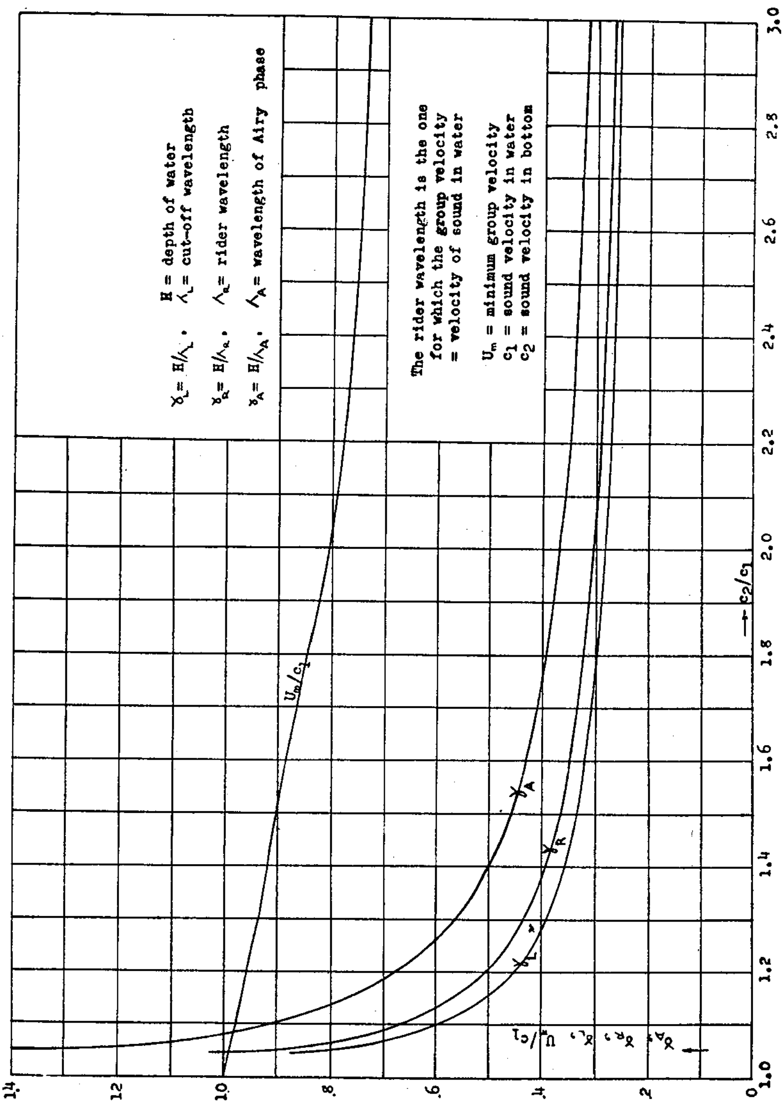


FIGURE 37.—*Dispersion characteristics of the first mode in a two-layered liquid half-space*

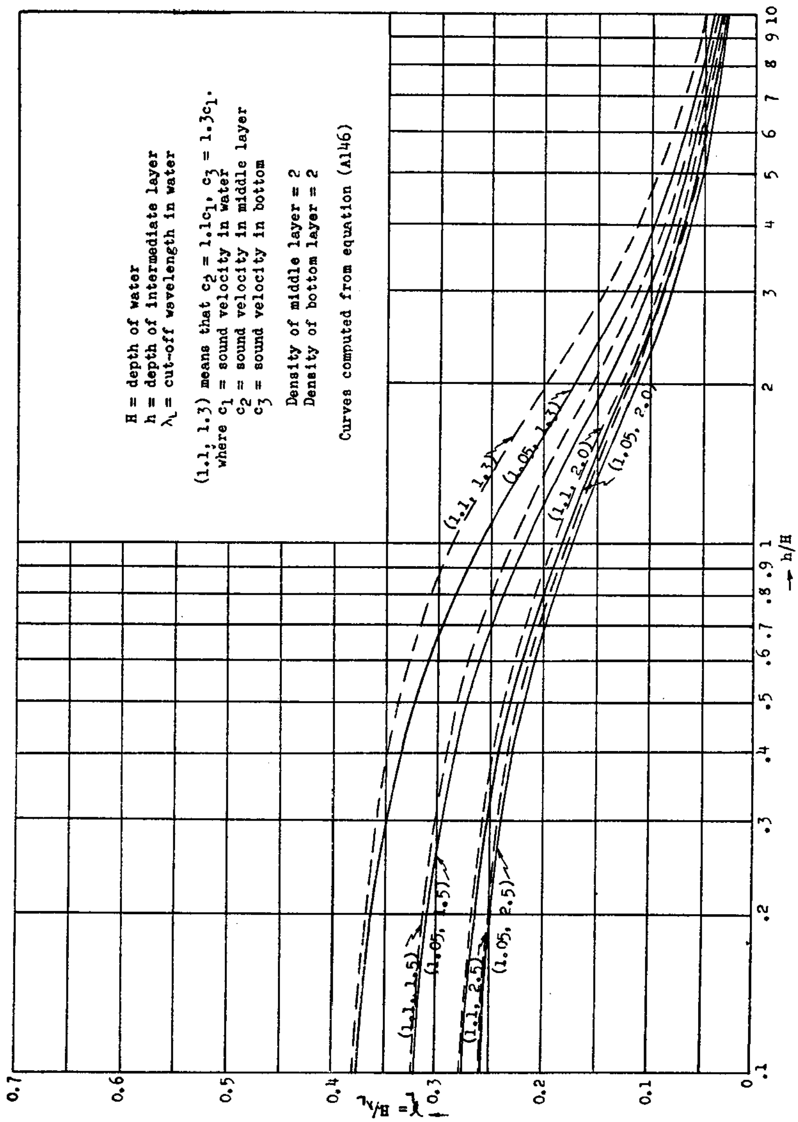


FIGURE 38.—*Cut-off wave length for the first mode in a three-layered liquid half-space*

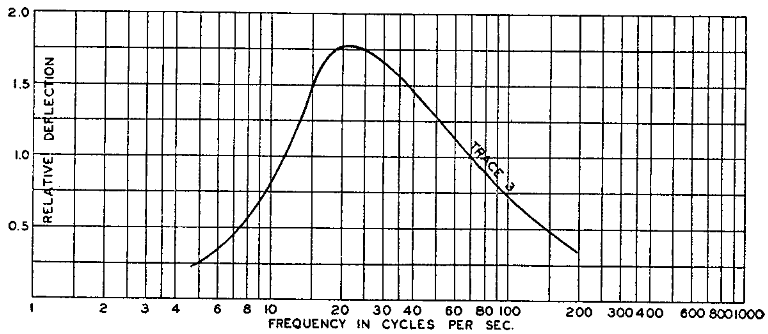


FIGURE 39.—*Overall frequency characteristic geophone system*

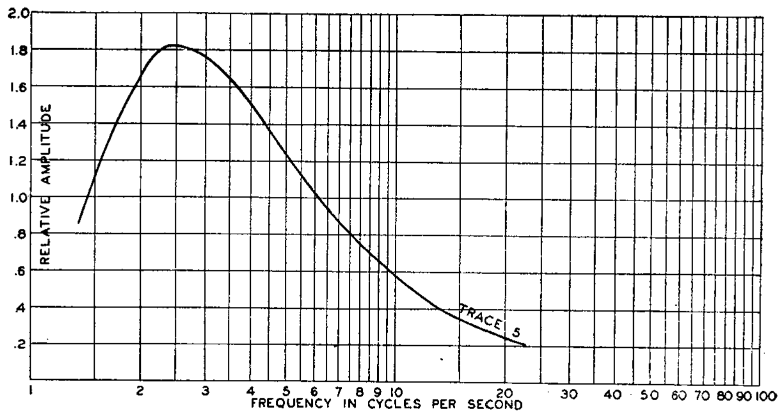


FIGURE 40.—*Mark I system. Overall frequency characteristic*
Calibration of Jan. 1, 1944.

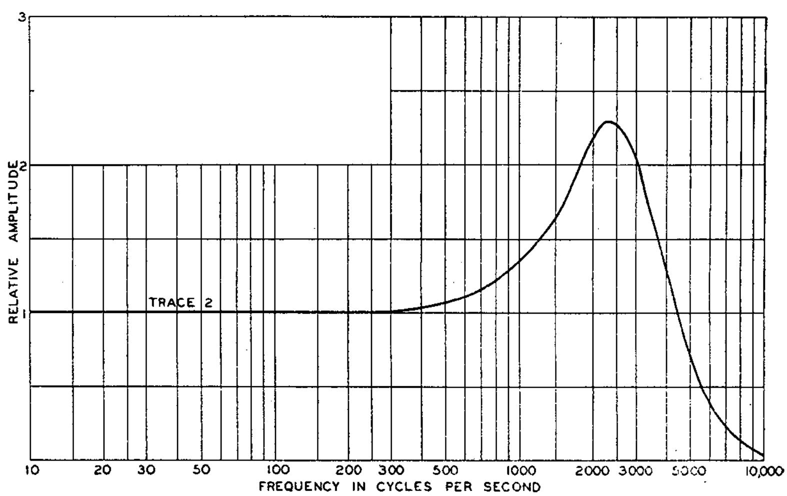


FIGURE 41.—*Mark II system. Overall frequency characteristic*
High-frequency galvanometer. Records previous to 136. Calibration of Dec. 1, 1943

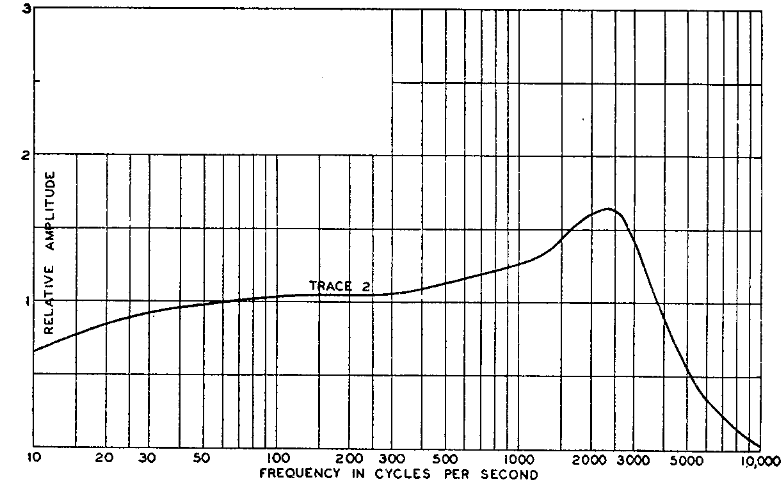


FIGURE 42.—*Mark II system. Overall frequency characteristic*

Calibration of Dec. 7, 1943. High-frequency galvanometer. Record 142 and following

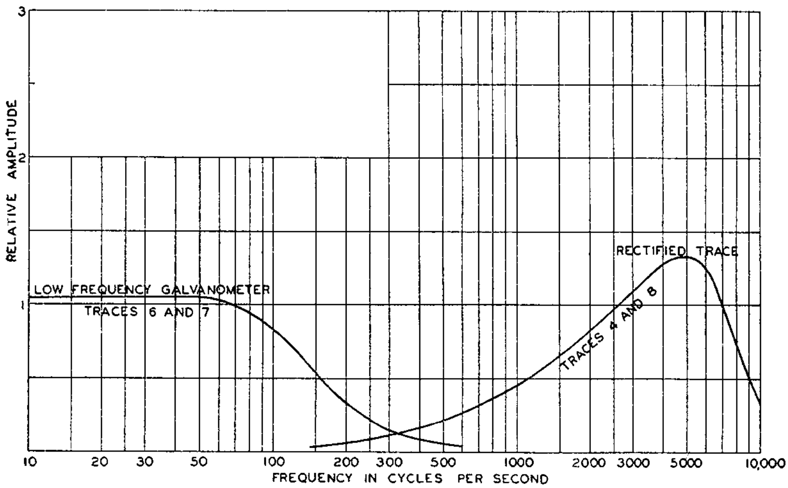


FIGURE 43.—*Mark II system. Overall frequency characteristic*

Calibration of Dec. 1, 1943. Records previous to 136

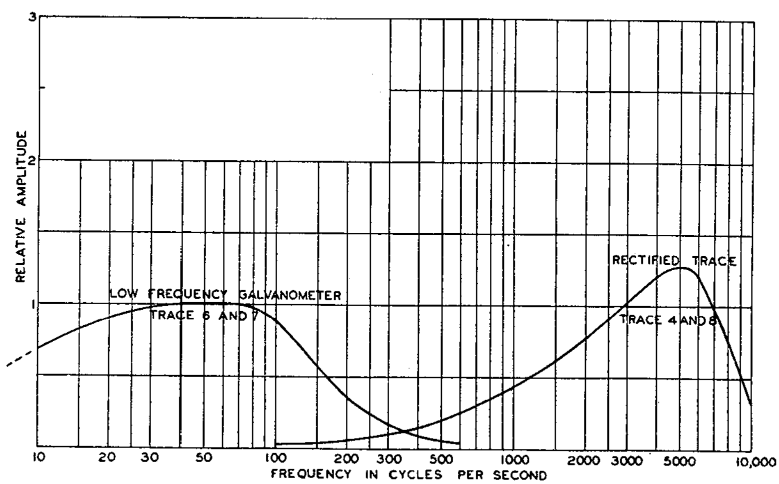


FIGURE 44.—*Mark II system. Overall frequency characteristic*

Calibration of Dec. 7, 1943. Record 142 and following

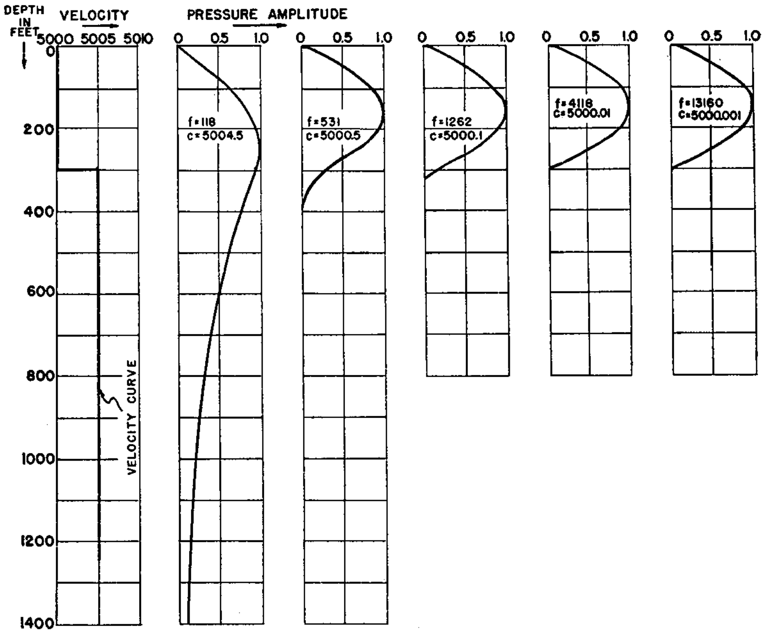


FIGURE 45.—*Vertical distribution of pressure amplitude in the fundamental mode of the free wave*

$f$ = frequency, in cyc/sec
$c$ = velocity of propagation of free wave, in ft/sec
minimum frequency = 93.3 cyc/sec

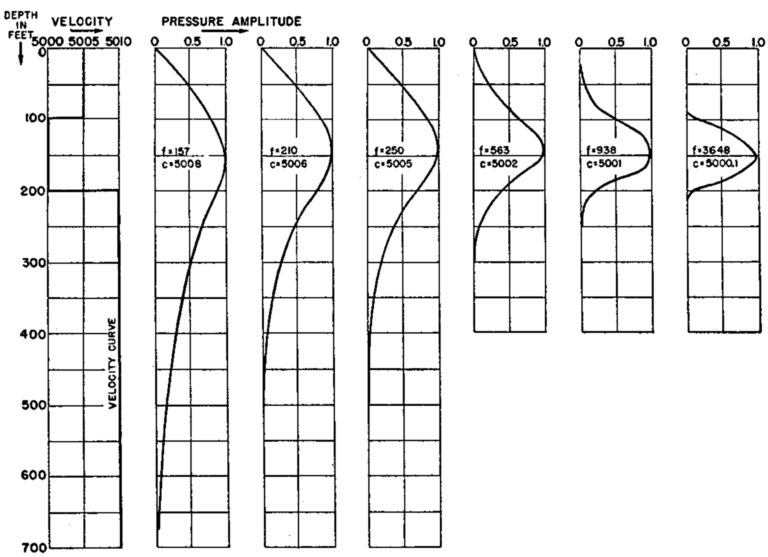


FIGURE 46.—*Vertical distribution of pressure amplitude in the fundamental mode of the free wave*

$f$ = frequency, in cyc/sec
$c$ = velocity of propagation of free wave, in ft/sec
minimum frequency = 103.5 cyc/sec

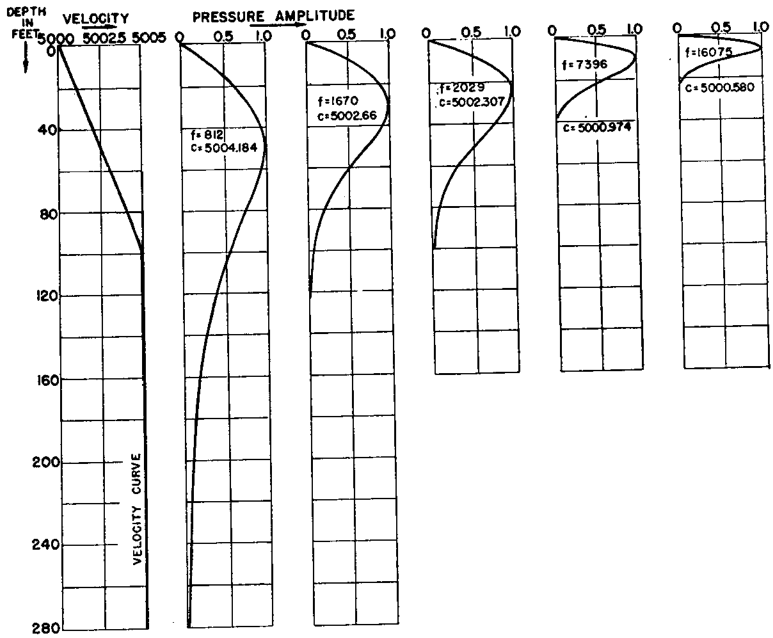


FIGURE 47.—*Vertical distribution of pressure amplitude in the fundamental mode of the free wave*

$f$ = frequency, in cyc/sec
$c$ = velocity of propagation of free wave, in ft/sec
minimum frequency = 498 cyc/sec

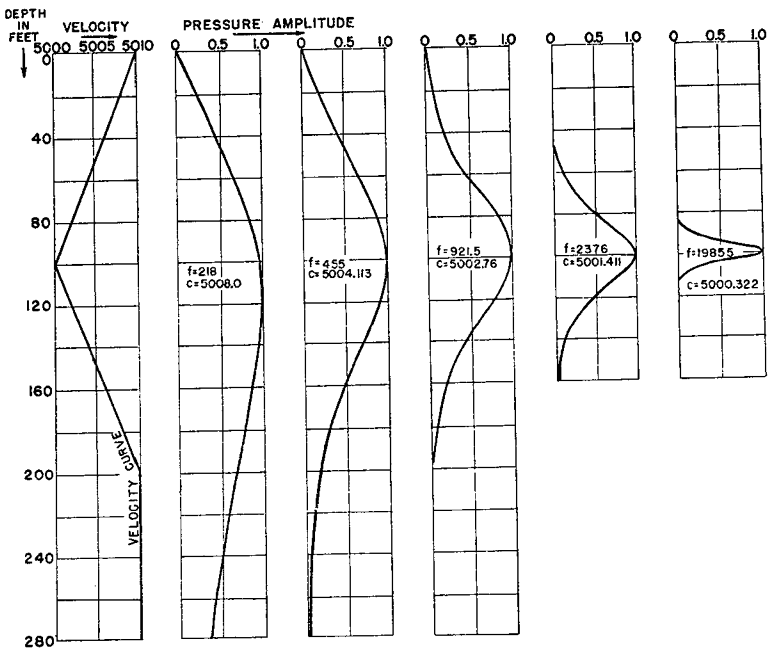


FIGURE 48.—*Vertical distribution of pressure amplitude in the fundamental mode of the free wave*

$f$ = frequency, in cyc/sec
$c$ = velocity of propagation of free wave, in ft/sec
minimum frequency = 138 cyc/sec

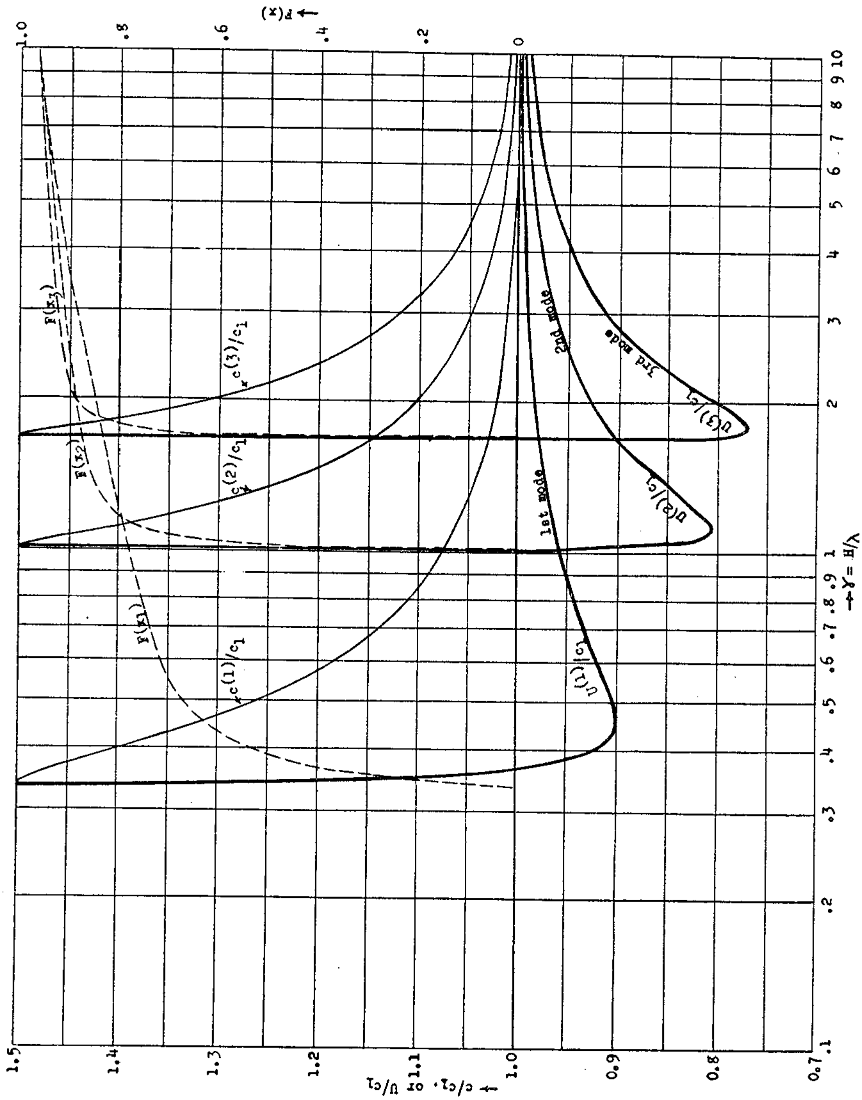


FIGURE 49.—*Variation of the phase velocity $c^{(n)}$ and group velocity $U^{(n)}$ of the nth mode with the wave length $\lambda$ in water*

$F(x_n)$ is the excitation amplitude of the nth mode. Two-layered liquid half-space in which $c_2 = 1.5c_1$

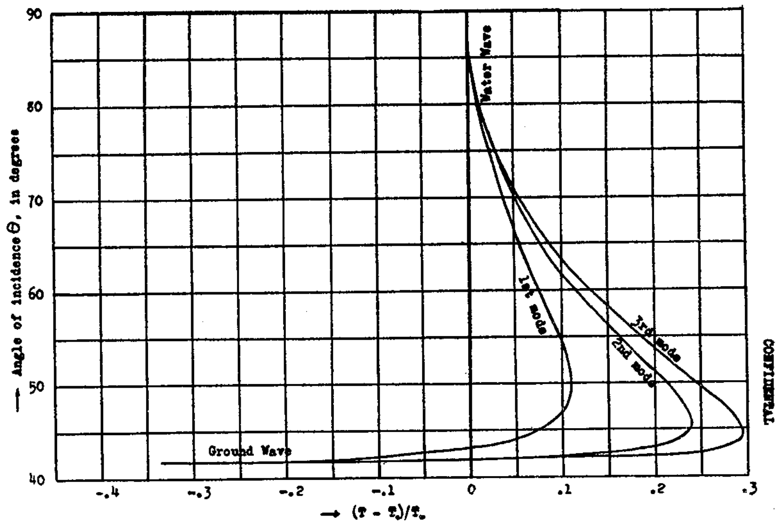


FIGURE 50.—*Angle θ between direction of propagation and the vertical of the component plane waves of the first three modes in a two-layered liquid half-space in which $c_2 = 1.5c_1$, $\theta = \sin^{-1}(c_1/c)$, where c is the phase velocity*

$T$ = time after explosion
$T_0$ = time of arrival of water wave ($= r/c_1$)

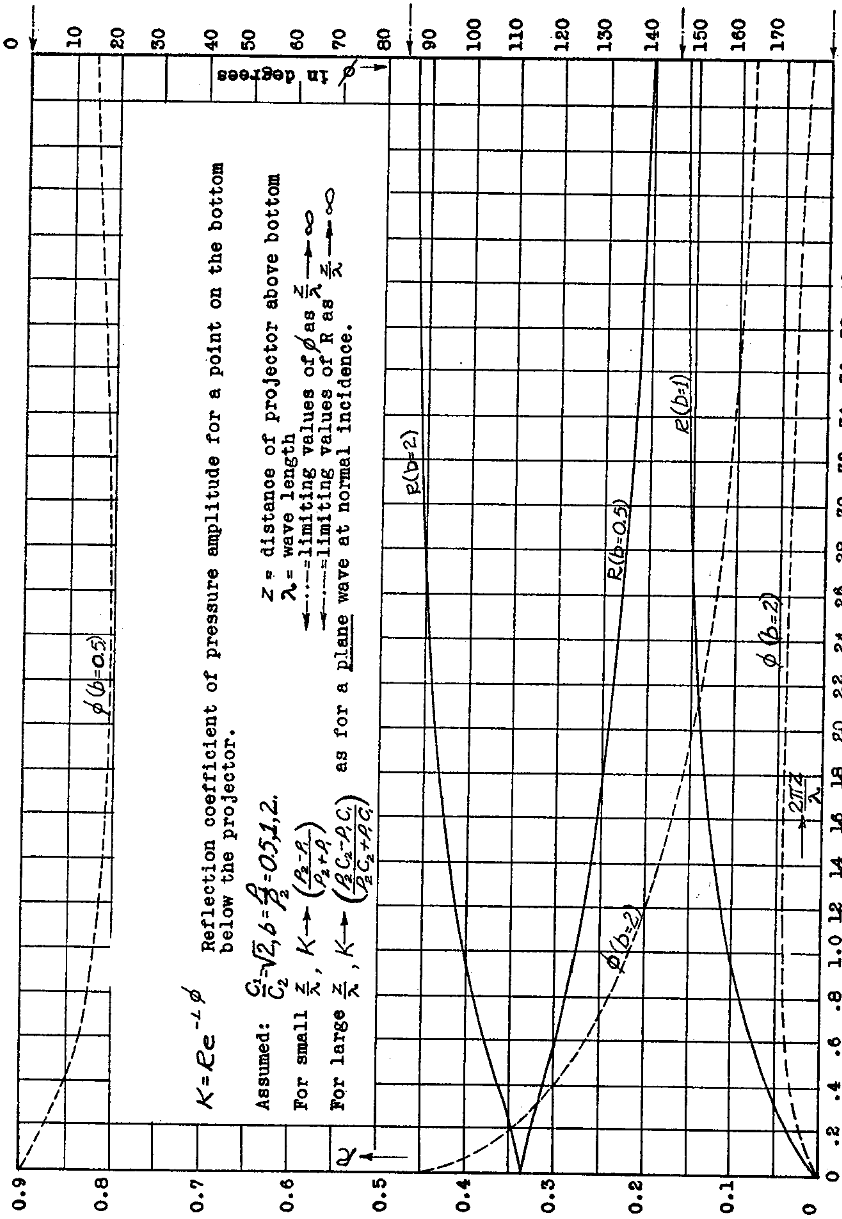


FIGURE 51.—*Magnitude and phase of reflection coefficient for a spherical wave incident on a bottom whose density $\rho_2$ and sound velocity $c_2$ differ from the density $\rho_1$ and sound velocity $c_1$ in water*

# INDEX

Geological Society of America Memoirs

# THEORY OF PROPAGATION OF EXPLOSIVE SOUND IN SHALLOW WATER

C. L. Pekeris

*Geological Society of America Memoirs* 1948;27;1-116
doi: 10.1130/MEM27-2-p1



**Notes**